Hot corinos: molécules pré-biotiques autour des protoétoiles de type solaire

Sandrine Bottinelli

HOT CORINOS: MOLÉCULES PRÉ-BIOTIQUES AUTOUR DES PROTOÉTOILES DE TYPE SOLAIRE

THÈSE PRÉPARÉE EN COTUTELLE ENTRE
L'UNIVERSITÉ JOSEPH FOURIER
ET
L'UNIVERSITÉ D'HAWAÏ

PRÉSENTÉE POUR OBTENIR LE GRADE DE

DOCTEUR
SPÉCIALITÉ: ASTROPHYSIQUE ET MILIEUX DILUÉS

soutenue le 18 octobre 2006

Par
Sandrine Bottinelli

Jury:

Prof. Kim Binsted	Président
Prof. Jean-Louis Monin	co-Président
Dr. Cecilia Ceccarelli	Directeur de thèse
Dr. Jonathan Williams	co-Directeur de thèse
Dr. Françoise Combes	Rapporteur
Prof. Ewine van Dishoeck	Rapporteur
Dr. Roberto Neri	Membre invité

PRE-BIOTIC MOLECULES IN THE HOT CORINOS OF SOLAR-TYPE PROTOSTARS

A DISSERTATION SUBMITTED TO THE GRADUATE DIVISION OF THE UNIVERSITY OF HAWAI'I IN PARTIAL FULFILLMENT OF THE REQUIREMENTS FOR THE DEGREE OF

DOCTOR OF PHILOSOPHY
IN
ASTRONOMY

DECEMBER 2006

By
Sandrine Bottinelli

Dissertation Committee:

Kim Binsted, Chairperson
Jean-Louis Monin, co-Chairperson
Cecilia Ceccarelli
Jonathan P. Williams
Françoise Combes
Ewine van Dishoeck
Roberto Neri

We certify that we have read this dissertation and that, in our opinion, it is satisfactory in scope and quality as a dissertation for the degree of Doctor of Philosophy in Astronomy.

DISSERTATION COMMITTEE

Chairperson

A mes parents, Elisabeth et Louis
A mon frère, Alexandre

Résumé de la thèse

L'un des buts majeurs de l'astrophysique moderne est de comprendre la formation du Système Solaire. Puisque les protoétoiles de faible masse sont des soleils en formation, l'étude de ces objets est un des meilleurs moyens d'étudier le processus de formation du Soleil et de son système planétaire. Dans ma thèse, je me suis concentrée sur la chimie des premières phases d'évolution des protoétoiles de faible masse en étudiant les molécules organiques complexes dans des sources de Classe 0, qui représentent les phases les plus jeunes connues. De telles molécules ont été découvertes dans IRAS16293–2422, le prototype des sources de Classe 0, démontrant l'existence des "hot corinos", des régions où les manteaux des grains subliment. Certaines de ces molécules ont aussi été observées dans des comètes de notre Système Solaire, soulevant la question de savoir si (et auquel cas, comment) la chimie des Classes 0 affecte la composition chimique de la matière du disque protoplanétaire incorporée dans les comètes et autres corps planétaires. Cependant, il est d'abord nécessaire de déterminer si les hot corinos sont omniprésents dans les protoétoiles de faible masse, ou si IRAS16293–2422 est une exception. Ceci était le premier but de ma thèse. L'approche consistait principalement à observer trois sources de Classe 0 pour chercher des molécules organiques complexes. J'ai ainsi découvert et/ou confirmé trois hot corinos de plus. Le second but était de contraindre la taille de la région d'émission des molécules complexes au moyen d'observations interférométriques des deux hot corinos les plus brillants: cette émission est compacte ($\lesssim$150 AU), avec, dans l'un des cas, une composante étendue provenant de l'enveloppe externe. Le troisième but avait pour lieu de confronter les voies de formation possibles des molécules complexes avec les résultats de mes observations pour essayer de distinguer si ces molécules se forment en phase gazeuse ou à la surface des grains. Bien que mes données ne puissent éliminer aucun des deux cas, elles semblent favoriser le second type de formation. De plus, la comparaison entre hot corinos et leurs homologues massifs, les hot cores (qui montre que les molécules complexes sont relativement plus abondantes dans les hot corinos), soutient également la formation à la surface des grains.

Abstract

One of the major goals of modern astrophysics is to understand the formation of our Solar System. Since low-mass protostars are suns in the making, the study of these objects and their environment provides one of the best ways to investigate the Sun's formation process and to peek in the past history of our Solar System. In my thesis, I focused on the chemistry occuring in Class 0 sources (the earliest known phases in the evolutionary scenario of low-mass protostars) by studying complex organic molecules in their envelopes. Such molecules have been discovered in IRAS16293–2422, the prototype of Class 0 sources, proving the existence of hot corinos, the inner regions of the protostellar envelope where the icy grain mantles sublimate. Some of these molecules have also been observed in comets in our Solar System, raising the question of whether (and if so, how) the chemistry of Class 0 objects affects the chemical composition of the protoplanetary disk material from which comets and other planetary bodies form. However, it is first necessary to determine whether hot corinos are ubiquitous in low-mass protostars or if IRAS16293–2422 is an exception. This was the first goal of my thesis. The approach consisted mainly in observing three Class 0 sources to search for complex organic molecules. I thereby discovered and/or confirmed three more hot corinos. The second goal was then to constrain the size of emission of complex molecules. For this, I carried out interferometric observations of the two brightest hot corinos: this emission is compact ($\lesssim$150 AU) with, in one of the sources, an extended component originating from the cooler, less dense outer envelope. The third goal consisted in confronting the possible formation pathways with the results of my observations to try and discriminate whether complex organic molecules form via gas-phase or grain-surface reactions. Although it was not possible to arrive at a definite answer, my data seem to favor the later formation route. Moreover, the comparison of hot corinos and their high-mass analogs, the hot cores (showing that complex molecules are relatively more abundant in hot corinos), also support grain-surface synthesis of these molecules.

Remerciements

Je voudrais tout d'abord remercier mes parents, Elisabeth et Louis, sans qui le riche parcours que j'ai suivi jusqu'à présent n'aurait pu se faire. Ils m'ont toujours soutenue et encouragée (à la fois moralement et financièrement!) à suivre la voie de mon choix. Merci Maman, Papa pour votre aide inestimable, je vous serai éternellement reconnaissante pour tout ce que vous avez fait.
Une mention spéciale pour ma Maman: le soutien logistique qu'elle m'a apporté durant toutes ces années, l'oreille attentive et patiente qu'elle m'a prêtée et les précieux conseils qu'elle m'a donnés aux moments décisifs (dont les toutes dernières phases de rédaction...) ont joué sans conteste un rôle déterminant dans l'achèvement de ma thèse et des étapes qui y ont mené.

Un immense merci également à mon frère, Alexandre qui a aussi toujours cru en moi, et pas seulement sur le plan scientifique. Son "coaching" des vacances de Pâques 2001 m'a aidé à reprendre confiance en moi et a marqué le début d'un renouveau. C'est donc aussi grâce à lui que j'en suis là et j'apprécie toujours autant nos longues conversations téléphoniques puisque nous ne pouvons nous réunir aussi souvent que je le voudrais. Un clin d'œil à Perrine qui trouve toujours la petite carte qui fait chaud au cœur. Alex, Pépé, vos attentions me touchent à chaque fois énormément, et je vous en remercie.

Bien sûr, cette cotutelle a pu démarrer et aboutir grâce au soutien et à la confiance de mes deux directeurs de thèse, Cecilia et Jonathan. Leur passion pour l'astronomie et leur enthousiasme ont été contagieux, et ils ont toujours trouvé les mots pour effacer mes moments de doutes (même si j'ai failli entamer le moral d'acier de Cecilia, elle a tenu bon et n'a pas cessé de m'encourager, et je lui en suis très reconnaissante...). Cecilia, Jonathan, ce fût un grand plaisir de travailler à vos côtés et j'espère que nous continuerons à collaborer de nombreuses années.

Je ne pourrais également jamais assez remercier Valentine pour m'avoir remonté le moral un nombre incalculable de fois, et pour m'avoir stimulée par ses conseils et par nos échanges scientifiques. Valentine, ce fut vraiment (et c'est toujours) un grand réconfort de savoir que je peux compter sur toi.

J'aurais toujours une tendre pensée pour Fred pour m'avoir cueilli une fleur et pour m'en avoir montré tant d'autres plus belles les unes que les autres.

J'ai des pensées particulières pour Isabelle et Anne, mes deux meilleures amies avec qui j'ai partagé mon bureau, mes états d'âme mais surtout mes meilleurs moments pendant toutes ces années de primaire/collège et lycée. Je n'oublierai jamais non plus Sophie (nos devoirs de maths par téléphone et la ballade à cheval près de Lons-le-Saunier), Claire (les joies de l'internat et les vacances à Narbonne-Plage), Émilie (qui m'a aidée à supporter les durs moments de Maths Sup), et Maria-Jo et Marisa (la vie à Londres, les cours, la piscine et les cafés latte à Imperial College). Nous nous sommes un peu perdues de vue mais j'espère qu'on se retrouvera un jour.

Merci à Rita pour avoir écouté mes peines et m'avoir redonné un peu de joie à PPV. J'aurais toujours le sourire en pensant aux fois où toi, Sean et moi sommes allés à Indigo's et au CSO où nous trois avons eu de bonnes parties de rigolade.

Mes amitiés à Sean et Liz pour avoir été de formidables amis et voisins de bureau, pour avoir supporté mes longues conversations téléphoniques en français ;-) et pour les nombreux trajets à l'aéroport.

J'aimerais remercier Nancy pour avoir ouvert sa maison pendant quelques semaines à une pauvre thésarde sans le toit (!) et pour m'avoir montré un beau lever de soleil à Kailua. Merci aussi à elle et Karen T., pour les nombreuses et agréables sessions à la piscine de Mānoa. Merci également à Bob pour avoir toujours eu un mot gentil à mon égard.

Ma vie à Hawai'i n'aurait pas été aussi excitante sans la pirogue que j'ai découverte grâce à Coach Irwin. Je suis toujours aussi triste à l'idée qu'il nous ait quittés si tôt, j'avais encore tellement à apprendre de lui. Merci à tout le Healani Canoe Club pour avoir été comme une deuxième famille. Une pensée particulière pour Sherry et Tracy qui ont toujours été là pour moi, à la fois comme co-équipières mais aussi en dehors de la pirogue.

Cette partie ne serait pas complète sans exprimer ma grande affectuosité pour toute ma famille, en particulier mes grands-parents Mamie Thérèse, Papi Maurice, Grand-Papa Euro et Alice, mes tantes et marraines Cécile et Geneviève, et mon parrain Noël qui j'aimerais soit toujours présent dans nos vies.

J'oublie probablement un certain nombre de personnes qui ont marqué des étapes de ma vie et que j'aurais voulu remercier, j'espère qu'elles me pardonneront les défaillances temporaires de ma mémoire.

Merci à tous du fond du cœur!

Cette thèse a été co-financée par la National Science Fundation, l'Institut de RadioAstronomie Millimétrique, le Centre National de la Recherche Scientifique, et la Région Rhône-Alpes.
J'aimerais également remercier le personnel du Plateau de Bure (en particulier Roberto Neri pour son aide précieuse avec la calibration des données), de l'IRAM-30m, du JCMT, SMA et CSO, non seulement pour leur assistance avec la prise des données, mais aussi pour m'avoir permis d'acquérir une grande expérience observationnelle.

Acknowledgements

I first wish to thank my parents, Elisabeth and Louis, without whom the rich experience I have gained until now would not have been possible. They have always supported and encouraged me (both mentally and financially!) to follow the path of my choice. Thank you Mum and Dad for your invaluable help, I will be forever grateful for all you did.
A special thought for my Mum: the practical support she has provided me for all these years, her careful and patient listening, and the precious advice she has given me at the critical moments (including the last stages of writing...) undoubtedly played a pivotal role in the achievement of my thesis and of the steps that led to it.

A huge thanks as well to my brother, Alexandre, who has also always believed in me, and not just on the scientific level. His coaching during the 2001 Easter holidays helped me to re-gain self-confidence and was the beginning of a new start. It is therefore also owing to him that I am where I am and I still enjoy our long chats over the phone, since we cannot see each other as often as I would like. A wink at Perrine, who always finds the little card that brings warmth to my heart. Alex, Pépé, your thoughtfulness gets me every time and I thank both of you for that.

Of course, the start and completion of this joint supervision thesis was made possible owing to the support from my two advisors, Cecilia and Jonathan, and the trust they placed in me. Their passion for astronomy and enthusiasm were contagious, and they have always found the words to erase the moments of doubts (even if I almost managed to alter Cecilia's morale of steel, she held on tight and never stopped encouraging me, and I am very grateful for that...). Cecilia, Jonathan, it was a great pleasure to work at your sides and I hope that we will keep on collaborating for many years.

I could also never thank Valentine enough for cheering me up a countless number of times and for stimulating me with her advice and with our scientific discussions. Valentine, it was really (and still is) a big comfort to know that I can always count on you.

I will always have a tender thought for Fred, for picking up a flower for me and for showing me so many more, one more beautiful than the other.

I have special thoughts for Isabelle and Anne, my two best friends with whom I shared my desk, my states of mind, but most of all my best times during all those years in primary/secondary and high schools. I will also never forget Sophie (our maths homeworks over the phone and the horse riding near Lons-le-Saunier), Claire (the joy of boarding school and the holidays in Narbonne-Plage), Émilie (who helped making the hard times of "Maths Sup" a bit more bearable), and Maria-Jo and Marisa (the life in London, the lectures, the swimming-pool and the latte coffees at Imperial College). We lost sight of each other, but I hope we will meet again some day.

Many thanks to Rita for listening to my sorrows and for giving me a bit of joy at PPV. I will always smile when thinking about the times you, Sean and I went to Indigo's and to the CSO where the three of us had such good laughs.

My kindest regards to Sean and Liz for having been such wonderful friends and office-mates, for bearing with my long phone conversations in french ;-) and for the numerous pick-up/drop-off at the airport.

I would like to thank Nancy for opening her house to a homeless (!) girl for a few weeks and for showing me a pretty sunrise in Kailua. Thanks to her and Karen T. as well for the numerous and enjoyable trips to the Mānoa swimming-pool. Thank you as well to Bob for always having a kind word for me.

My life in Hawai'i would not have been so exciting without paddling, which I discovered owing to Coach Irwin. I am still so sad when I think that he left us so early, I had so much more to learn from him. Many thanks to the whole Healani Canoe Club for having been like a second family. A special thought for Sherry and Tracy for always being there for me both as teammates, but also outside of the paddling life.

This part would not be complete without me expressing my greatest fondness for my entire family, in particular my grand-parents, Mamie Thérèse, Papi Maurice, Grand-Papa Euro and Alice, my aunts and god-mothers Cécile and Geneviève, and my god-father Noël, who I wish were still present in our lives.

I am probably forgetting a number of persons who impressed upon some stages of my life and whom I would have liked to thank, I hope they will forgive my temporary memory failings.

Thank you all from deep inside!

This thesis work was supported by the National Science Fundation, the Institut de RadioAstronomie Millimétrique, the Centre National de la Recherche Scientifique, and the Région Rhône-Alpes.
I would also like to thank the staff from IRAM Plateau de Bure (in particular Roberto Neri for his precious help with the data calibration), IRAM-30m, JCMT, SMA and CSO, not only for their assistance in acquiring the data presented in this thesis, but also for helping me to gain a large observing experience.

Table of Contents

List of Tables

List of Figures

Chapitre 1
Introduction

Résumé

L'un des moyens de nous aider dans notre quête de la compréhension du passé de notre Système Solaire, est d'étudier la formation d'étoiles de type solaire, c'est-à-dire de faible masse. Bien que les étapes principales de la séquence de formation des protoétoiles de faible masse soient maintenant largement acquises, il reste encore beaucoup à découvrir, en particulier la composition et l'évolution chimique de ces sources.

Pour ma thèse, j'ai observé des objets de Classe 0, qui correspondent au premier stade suivant la naissance d'une protoétoile de faible masse, et dont on a remarqué que la riche composition chimique présentait des ressemblances avec celle des comètes de notre Système Solaire. Cela suggère que la chimie des premières phases de formation d'étoiles de type solaire pourrait avoir un impact sur la composition chimique des matériaux à partir desquels les corps planétaires (planètes, comètes, asteroïdes) se formeront éventuellement. Cependant, avant le début de ma thèse, seulement quelques études s'étaient concentrées sur ce problème, et on avait peu d'informations sur la complexité chimique des protoétoiles de Classe 0. Mon travail a donc consisté à pallier les connaissances manquantes en cherchant des molécules complexes autour des protoétoiles de Classe 0 et en étudiant leur origine.

1.1 Des hot corinos aux comètes (ou: pourquoi s'intéresser aux hot corinos?)

1.1.1 Scénario de formation stellaire et classification des protoétoiles de faible masse: qu'est-ce qu'une Classe 0?

La formation de protoétoiles de faible masse ($\lesssim 2\,M_\odot$) commence dans des nuages moléculaires denses, des régions du milieu interstellaire caractérisées par des densités et des températures de l'ordre de $10^4\,\mathrm{cm}^{-3}$ et 10 K respectivement. Ces nuages moléculaires se fragmentent en plusieurs objets denses ($n \gtrsim 10^6\mathrm{cm}^{-3}$) et froids ($T \lesssim 10\,\mathrm{K}$), appelés cœurs pré-stellaires (Figure 1.1-a). On pense qu'un tel cœur pré-stellaire se contracte lentement jusqu'à ce qu'il atteigne un

état de quasi-équilibre instable, dans lequel seule la pression thermique contre-balance l'auto-gravité du cœur. Pendant cette phase pré-stellaire, les surfaces des grains de poussière sont progressivement enrobées de manteaux de glace. Les molécules telles que le CO se collent facilement à ces manteaux, où elles peuvent mener à la formation de formaldehyde (H_2CO) et méthanol (CH_3OH), par additions successives d'hydrogène atomique.
Lorsque la gravité surpasse la pression thermique, magnétique et de turbulence, le cœur devient gravitationnellement instable, et il subit une phase d'effondrement en "chute libre". Une fois que cette phase dynamique d'effondrement a commencé, un embryon stellaire hydrostatique se forme au centre (une protoétoile) et augmente sa masse en accrétant le gaz de l'envelope en effondrement (e.g. Di Francesco et al. 2006; Ward-Thompson et al. 2006). A partir de là, plusieurs étapes d'évolution d'un objet proto-stellaire de faible masse vers la séquence principale ont été identifiés, basées principalement sur l'étude en continuum de poussière des régions de formation de protoétoiles de faible masse:

- protoétoiles en accrétion (objets de Classe 0, $\lesssim 10^4$ ans): on pense que la phase d'effondrement dynamique décrite ci-dessus est représentée par des sources profondément enfouies, appelées Classe 0 (Figure 1.1-b). Ces objets possèdent une émission dans le continuum submillimétrique étendue mais piquée au centre, traçant la présence d'une large enveloppe de poussière circumstellaire dont la masse, $M_{\rm env}$, est plus large que celle de la protoétoile, $M_\star$. Cette émission est caractéristique d'un corps noir de température $\sim 10-30$ K (Figure 1.1-b'). Ils peuvent également être identifiés par la détection d'une source compacte dans le continuum radio centimétrique et/ou par la présence d'un flot collimaté;

- protoétoiles en accrétion évoluée (objets de Classe I, $\sim 10^4 - 10^5$ ans): ces objets sont entourés d'un disque massif et d'une enveloppe résiduelle ($M_{\rm env} < M_\star$) en effondrement, et ils possèdent des flots faiblement collimatés (Figure 1.1-c). Leur distribution spectrale d'énergie indique que ce sont des environnements plus chauds et ils sont donc observables dans l'infrarouge moyen et lointain. Leur émission correspond à un corps noir avec un excès infrarouge dû à la présence du disque (Figure 1.1-c');

- étoiles T Tauri classiques (objets de Classe II, $\sim 10^5 - 3 \times 10^6$ ans): ces objets ont peu ou pas d'enveloppe mais possèdent un disque circumstellaire développé (Figure 1.1-d) et donc un fort excès infrarouge (Figure 1.1-d'). La transition entre Classe I et Classe II est caractérisée par le début des réactions de fusion du deutérium;

- étoiles T Tauri "weak-lined" (objets de Classe III, $\sim 3 \times 10^6 - 5 \times 10^7$ ans): le disque circumstellaire s'est dissipé (par accrétion et formation de planétésimaux; Figure 1.1-e) et ces objets possèdent donc peu d'excès infrarouge (Figure 1.1-e'). Les objets de Classe III diffèrent des étoiles de la séquence principale par leur émission en rayons X et par la présence résiduelle de lithium (d'où le nom "weak-lined", littéralement "à faible raie").

Alors que le disque se transforme en système planétaire, l'étoile pré-séquence principale continue de se contracter jusqu'à ce que sa température centrale soit suffisamment élevée pour permettre

la fusion d'hydrogène, moment à partir duquel l'étoile appartient à la séquence principale (Figure 1.1-f).

La séquence décrite ci-dessus correspond à l'image "standard", c'est-à-dire le scénario qui obtient actuellement le plus large consensus. Cependant, les paramètres observationnels utilisés pour déterminer la Classe d'une protoétoile ne correspondent pas toujours univoquement à une Classe donnée. En effet, la détermination est souvent faite en évaluant la température bolométrique $T_{\rm bol}$ (c'est-à-dire la température d'un corps noir ayant la même fréquence moyenne pondérée par le flux que celle observée) ou le rapport luminosité submillimétrique sur luminosité bolométrique. Dans les deux cas, il peut y avoir une mauvaise identification de la Classe d'une source: par exemple, la quantité d'émission dans l'infrarouge proche et moyen (influencée par la géométrie) peut faire fortement varier $T_{\rm bol}$ (Evans 1999). Il est donc nécessaire de déterminer plus précisément la structure d'une source, par exemple avec des observations interférométriques. La chimie peut également aider à clarifier la confusion. Par exemple, on peut placer des contraintes sur les profils de densité grâce à l'émission de raies moléculaires (voir Section 2.2), et sur l'âge des protoétoiles de Classe 0 et I en utilisant les espèces soufrées comme horloges chimiques (Buckle & Fuller 2003; Wakelam et al. 2004).

1.1.2 Definition of hot corinos

En analogie avec les hot cores des protoétoiles massives[1], les hot corinos représentent les phases les plus précoces de l'évolution protostellaire, mais pour les étoiles de faible masse au lieu de celles de haute masse.
Les hot corinos sont situés dans les parties internes des enveloppes des protoétoiles de Classe 0 et sont caractérisés d'une manière semblable à celle des hot cores massifs:

- tailles relativement compactes, cependant avec des rayons $r_{\rm hc}$ environ deux ordres de grandeur plus petits que ceux des hot cores ($\lesssim$150 AU et $\lesssim$0.1 pc pour les hot corinos et hot cores respectivement).

- fortes densités: $n \gtrsim 10^7\,{\rm cm}^{-3}$. La détermination des profils de densité de plusieurs protoétoiles de Classe 0 (e.g. Ceccarelli et al. 2000a; Maret et al. 2002; Jørgensen et al. 2002) a montré que les densités des régions centrales de l'enveloppe peuvent atteindre $\sim 10^7\,{\rm cm}^{-3}$ à des rayons de l'ordre de $r_{\rm hc}$ et jusqu'à $10^8 - 10^9\,{\rm cm}^{-3}$ dans les parties les plus au centre (voir bas de la Figure 1.2).

- hautes températures: T$\gtrsim$ 100 K. Comme je l'ai mentionné dans la section précédente, la distribution spectrale d'énergie d'une protoétoile de Classe 0 est dominée par une enveloppe froide (T$\lesssim$30 K). Cependant, la présence de la protoétoile au centre provoque un gradient de température tel que celui montré dans le haut de la Figure 1.2, avec de plus hautes températures à plus petit rayon et plus fortes densités. Eventuellement, la température

[1] Les protoétoiles massives ont des masses $\gtrsim 8\,M_\odot$

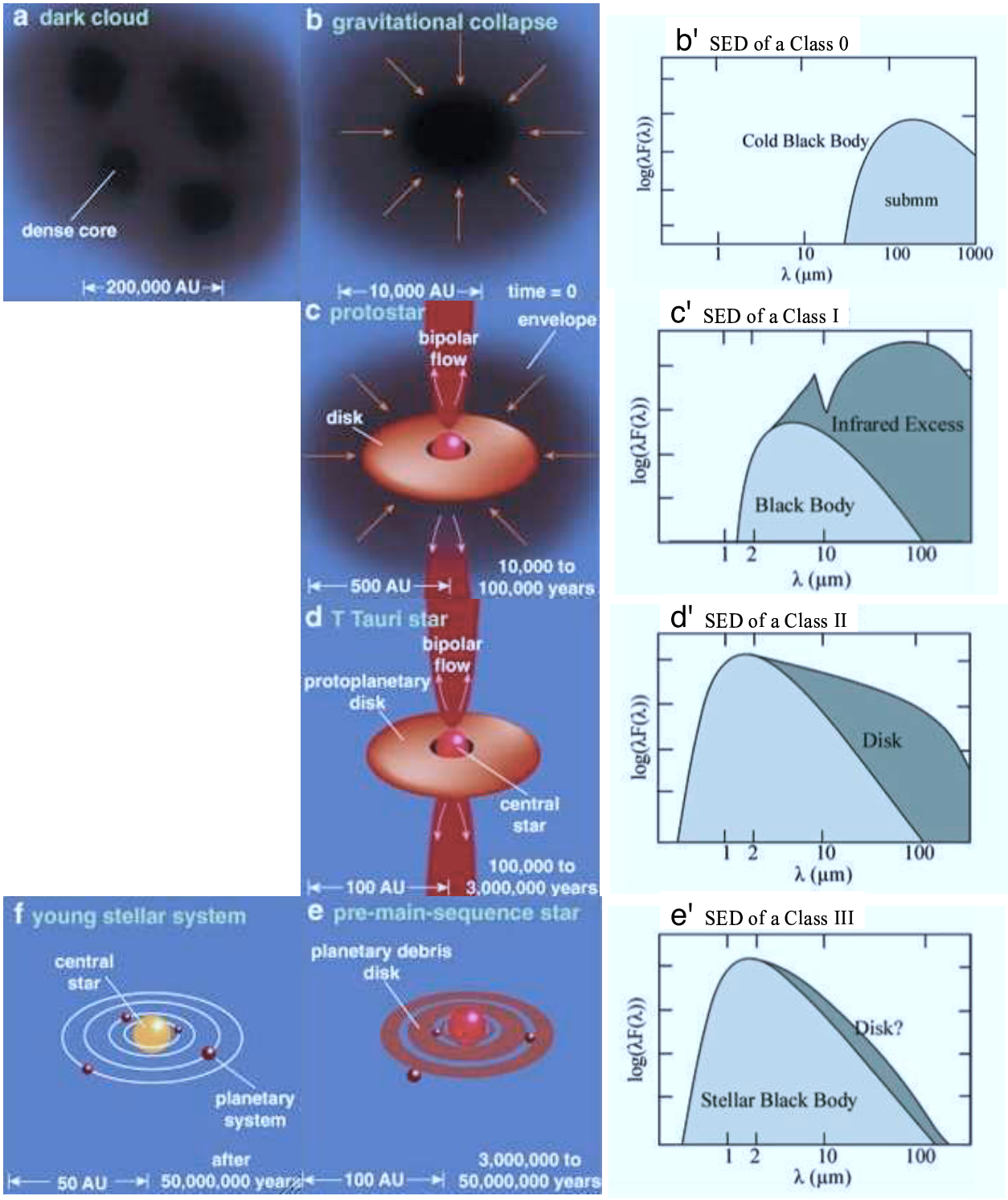

Figure 1.1 Étapes de la formation d'une protoétoile de faible masse (schémas a-f), ainsi que les distributions spectrales d'énergie (SED; schémas b'-e') représentatives des étapes b-e, qui correspondent aux Classes 0, I, II, et III du scénario d'évolution protostellaire. (Adapté de Green 2001; Burton et al. 2005).

peut atteindre une valeur de ∼100 K, à partir de laquelle les manteaux de glace subliment, relâchant dans la phase gazeuse les molécules (H_2CO, CH_3OH, NH_3) qui se sont formées et/ou se sont collées sur la surface des grains pendant la phase pré-stellaire. Les abondances de ces molécules augmentent brusquement à $r < r_{100K}$, où r_{100K} est le rayon où T=100 K[2]. Ceci peut être représenté schématiquement par un saut survenant à r_{100K} avec de faibles abondances à plus large distance (enveloppe externe froide) et des abondances élevées à plus petit rayon (enveloppe interne chaude), comme le montre le trait plein de la Figure 1.3.

- spectres riches en raies émises par des molécules organiques complexes telles que HCOOH, $HCOOCH_3$, CH_3OCH_3, CH_3CN, C_2H_5CN, etc. Ces molécules sont typiques des hot corinos (et des hot cores massifs) car elles reflètent les conditions de haute température de ces objets. En effet, on pense qu'elles se forment soit dans la phase gazeuse à partir d'espèces sublimées (CH_3OH, H_2CO, NH_3) par des réactions nécessitant de hautes températures, soit sur les manteaux de glace des grains d'où elles sont libérées dans la phase gazeuse quand les manteaux subliment.

1.1.3 Hot corinos et molécules pré-biotiques

Pendant plus de deux décennies, les molécules organiques complexes[3] ont été observées vers les plus jeunes protoétoiles massives (les analogues de haute masse des objets de Classe 0). Si ces molécules pouvaient également se former dans les protoétoiles de faible masse et survivre jusqu'à la phase de disque proto-planétaire, elles pourraient être incorporées dans les corps planétaires et amenées sur les planètes telles que la Terre. Une fois là, elles pourraient jouer un rôle dans l'apparition de la vie, par exemple en fournissant les molécules biologiquement actives qui mènent à la formation des premières proto-cellules (Sandford et al. 1998). En effet, les molécules polaires (ou "hydrophiles") telles que H_2CO, HCOOH, la plupart des ketones (e.g. CH_3COCH_3), des ethers (e.g. CH_3OCH_3) et des sucres (e.g. CH_2OHCHO) sont chimiquement réactives et constituent souvent les briques de construction des molécules biologiques, ou bien sont des réactifs menant à ces briques (Pohorille 2002). De plus, beaucoup de ces espèces ont une importance biologique sur Terre: la formaldehyde, les nitriles (c'est-à-dire les molécules organiques azotées telles que CH_3CN et C_2H_5CN, pour lesquelles C et N sont attachés par une liaison triple) et l'éthanol ont toutes été identifiées comme précurseurs indispensables à la production des protéines, des phospholipides, de l'ARN et de l'ADN.

[2]Dans la théorie de formation planétaire, r_{100K} est équivalent à la "limite des neiges" ("snowline" en anglais), le rayon au-delà duquel les glaces d'eau peuvent se former dans le disque proto-planétaire.

[3]Voir Table A.1 pour une liste non-exhaustive.

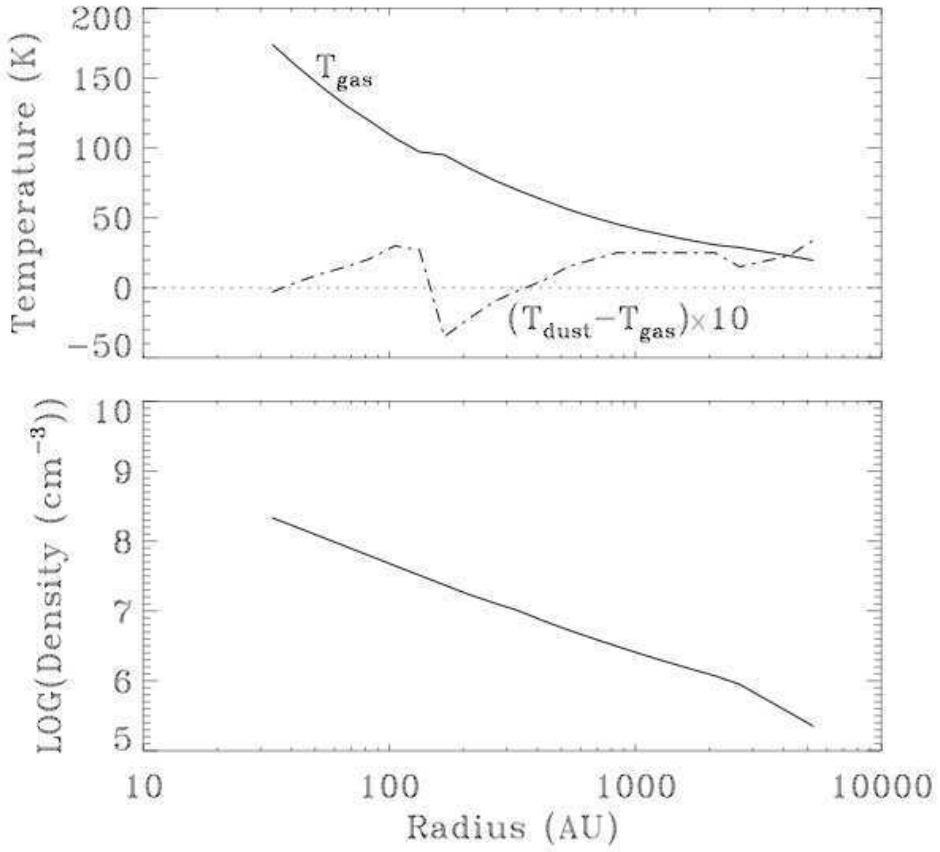

Figure 1.2 Profils de température et densité d'IRAS16293–2422 (Source: Ceccarelli et al. 2000a). — *Haut:* Température du gaz (trait plein) et différence entre la température du gaz et celle de la poussière (trait pointillé) en fonction du rayon. Cette différence montre que les profils de température du gaz et de la poussière sont semblables. Les deux quantités dépassents 100 K à petits rayons ($\lesssim$ 150 AU). — *Bas:* Densité en fonction du rayon sur une échelle log-log. La densité suit une loi de puissance et dépasse 10^7 cm^{-3} pour R$\lesssim$ 150 AU.

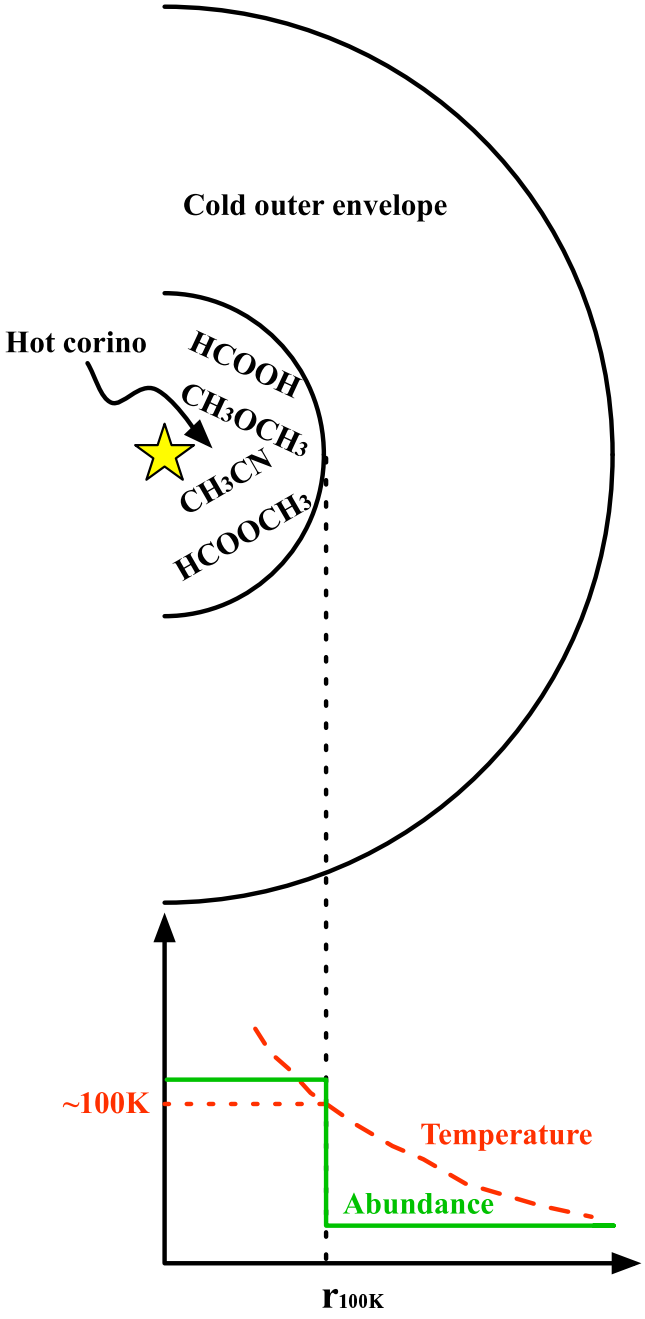

Figure 1.3 Profils de température (trait tirets/rouge) et d'abondances des molécules "parentes" (trait plein/vert) dans un hot corino. $r_{100\mathrm{K}}$ est le rayon où la température atteind 100 K, provoquant la sublimation des manteaux de glaces et la libération dans la phase gazeuse des molécules parentes (H_2CO, CH_3OH, NH_3) qui se sont formées sur les grains pendant la phase pr-́stellaire.

1.2 Précédentes études qui ont motivé cette thèse

1.2.1 Profils d'abondances de H_2O, H_2CO et CH_3OH

H_2O, H_2CO et CH_3OH sont des composants majeurs des manteaux des grains, donc déterminer la présence d'un saut dans leur profil d'abondance fournirait une preuve directe de l'existence d'une région interne chaude où les manteaux de glace subliment. La première étude de la sorte sur une étoile de faible masse a été faite par Ceccarelli et al. (2000a), qui ont modelisé les transitions de l'eau observées avec l'Infrared Space Observatory vers IRAS16293–2422, et ont trouvé une augmentation de l'abondance pour des rayons inférieurs à ∼150 AU. Des modélisations similaires de l'émission des raies de H_2CO dans la même source par Ceccarelli et al. (2000c) et de l'eau dans NGC1333-IRAS4A par Maret et al. (2002) ont montré que les observations pouvaient être reproduites par un saut dans les profils d'abondance de H_2CO et H_2O dans IRAS16293–2422 et NGC1333-IRAS4A respectivement. A la suite de ces travaux pionniers, d'autres études de l'émission des raies de CH_3OH et H_2CO dans un échantillon d'une douzaine de sources de faible masse (Classe 0) par Maret et al. (2004, 2005), ont prédit l'existence d'un saut de H_2CO dans toutes les sources recensées et d'un saut de CH_3OH dans tous les objets sauf un. Cependant, alors que les sauts de CH_3OH ont été confirmés par les modélisations indépendantes de Jørgensen et al. (2005b) et Schöier et al. (2002), et semblent plutôt bien établis, l'existence des sauts de H_2CO est controversée car Jørgensen et al. (2005b) et Schöier et al. (2002) trouvent que, le cas de IRAS16293–2422 mis à part, ces sauts ne sont pas nécessaires pour expliquer l'émission de H_2CO dans les autres objets de Classe 0.

1.2.2 Molécules organiques complexes dans IRAS16293

Dans le passé, les recherches de molécules organiques complexes vers les protoétoiles de faible masse ont été rares et malheureusement sans succès, qu'elles aient été sous forme de recensements (van Dishoeck et al. 1995), ou sous forme de recherche d'une molécule donnée (par exemple la glycine, Ceccarelli et al. 2000b). Néanmoins, il y avait de fortes présomptions de l'existence d'un hot corino dans la Classe 0 IRAS16293–2422, basées sur deux études. D'abord, la modélisation de l'émission des raies de H_2CO dans cette source a montré que les observations ne pouvaient être expliquées par une abondance constante de cette molécule, et qu'un saut était nécessaire, avec une faible abondance dans l'enveloppe externe et élevée dans l'enveloppe interne (Ceccarelli et al. 2000c; Schöier et al. 2002). Ensuite, si la recherche de la glycine dans IRAS16293–2422 par Ceccarelli et al. (2000b) a été infructueuse, les longues intégrations ont toutefois révélé de nombreuses raies d'émission dont les fréquences coïncidaient avec celles de plusieurs grosses molécules. Pris ensemble, l'augmentation de l'abondance de H_2CO et la possible détection de grosses molécules dans IRAS16293–2422 soutiennent la théorie de la sublimation des manteaux de glace des grains là où la température de la poussière dépasse $\sim 100\,K$, justifiant ainsi une recherche plus poussée des molécules organiques complexes. Et en effet, en 2003, Cazaux et al. ont détecté des espèces complexes telles que HCOOH, CH_3COOH, $HCOOCH_3$, CH_3OCH_3, CH_3CN et C_2H_5CN dans IRAS16293–2422, confirmant l'existence d'un hot corino tel qu'il est

défini dans la Section 1.1.2. Simultanément, une étude de l'émission des raies de H_2CO dans un échantillon de protoétoiles de faible masse par Maret et al. (2004) a prétendu que, comme pour IRAS16293–2422, les observations nécessitaient un saut dans l'abondance de H_2CO pour toutes les sources de l'échantillon. Ces sources représentaient donc des cibles adéquates où les molécules complexes avaient des chances d'être trouvées.

Les découvertes de Cazaux et al. (2003), avec l'étude de Maret et al. (2004), ont vraiment stimulé le commencement de ma thèse en Octobre 2003. Des motivations supplémentaires ont été amenées par deux débats, l'un concernant l'origine des molécules organiques complexes dans les hot corinos (e.g. Schöier et al. 2002), et l'autre portant sur l'existence d'un saut dans l'abondance de H_2CO dans les sources de Classe 0 (Section 1.2.1).

1.3 Les quêtes

A partir des éléments présentés dans la section précédente, mon travail de thèse se voulait de répondre aux questions suivantes, qui constituent également le plan de ce manuscript:

- *Y a-t-il un saut dans l'abondance de H_2CO dans les protoétoiles de Classe 0?* (Chapitre 2)
  Puisque H_2CO est un composant principal des manteaux des grains, confirmer l'existence d'un saut dans le profil d'abondance de cette molécule soutiendrait l'existence d'une région chaude où les manteaux de glace subliment, et on trouverait probablement des molécules organiques complexes dans les sources où de tels sauts sont observés. De plus, la quantité de H_2CO dans les régions de sublimation des glaces est un paramètre clé pour comprendre la présence de molécules organiques complexes qui se formeraient à partir de H_2CO.

- *Les hot corinos sont-ils communs parmi les protoétoiles de faible masse?* (Chapitre 3)
  L'existence de molécules organiques complexes dans les enveloppes internes des protoétoiles de Classe 0 pose un défi à la théorie car l'échelle de temps chimique de formation de ces molécules est plus longue que celle de chute libre du gaz (Schöier et al. 2002). Le molécules complexes ne devraient donc pas avoir le temps de se former. Cependant, comme je l'ai dit dans la Section 1.2.2, ces molécules ont néanmoins été observées dans un objet de Classe 0, IRAS16293–2422, et donc la question se pose de savoir si cette source est unique en son genre ou si ce n'est qu'une parmi tant d'autres.

- *Où sont situées les molécules complexes?* (Chapitre 4)
  Le chapitre 3 montrera que les hot corinos semblent omniprésents dans les sources de Classe 0. Il s'ensuit un besoin de caractériser ce nouveau type d'objet, plus précisément de comprendre la présence des molécules organiques complexes qui n'est pas évidente, comme je l'ai mentionné dans l'item précédent. Un paramètre clé est l'origine spatiale de l'émission des molécules complexes que je traiterai dans ce chapitre en présentant des observations à haute résolution de deux hot corinos.

- *Les hot corinos sont-ils semblables aux hot cores?* (Chapitre 5)
  Puisque les hot corinos ont été définis en analogie aux hot cores massifs, il est normal de se demander si ces deux types d'objets sont semblables du point de vue de la chimie: les hot corinos sont-ils des modèles réduits des hot cores ou bien y a-t-il des différences dans les compositions chimiques?

- *Quelle est la voie de formation de ces molécules?* (Chapitre 6)
  Les mécanismes de formation censés intervenir dans les hot cores massifs sont probablement incapables d'expliquer la présence des molécules organiques complexes, puisque l'existence de ces dernières est théoriquement difficile (voir second point). D'autres manières de former ces molécules doivent donc être explorées.

En résumé

Les hot corinos des protoétoiles de Classe 0 sont le point de départ de l'évolution protostellaire, donc la chimie de ces objets affectera ou peut-être même déterminera la composition chimique du futur disque protoplanétaire à partir duquel les comètes, météorites et planètes se forment éventuellement. En trouvant et en caractérisant les hot corinos, cette recherche vise à déterminer les conditions chimiques initiales de la formation planétaire, et ainsi à avancer d'un pas dans notre compréhension de la formation du Système Solaire et plus généralement des protoétoiles de type solaire.

Chapter 1
Introduction

Abstract

One way to help us in the quest of understanding the past of our Solar System, is to study the formation of low-mass, Sun-like stars. Although the main steps in the formation sequence of low-mass protostars are now widely accepted, there is still much to learn, in particular regarding their chemical evolution and complexity.

For my thesis, I looked at Class 0 objects, which correspond to the first stage following the birth of a low-mass protostar and whose rich chemical composition has been noted to present some similarities with that of comets in our Solar System. This suggests that the chemistry of the first phases of solar-type star formation may have an impact on the chemical composition of the material from which planetary bodies (planets, comets, asteroids) will eventually form. However, before the start of my thesis, only a handful of studies had focused on this issue, and little was known about the chemical complexity of Class 0 protostars. My work therefore consisted in beginning to complete this missing information by searching for complex molecules towards Class 0 protostars and studying their origin.

1.1 From hot corinos to comets (or: why do we care about hot corinos?)

1.1.1 Star formation scenario and classification of low-mass protostars: what is a Class 0?

The formation of low-mass ($\lesssim 2\,M_\odot$) protostars starts in dense molecular clouds, which are regions of the interstellar medium (ISM) characterized by densities and temperatures of order $10^4\,\mathrm{cm}^{-3}$ and 10 K respectively. These molecular clouds fragment into dense ($\gtrsim 10^6\,\mathrm{cm}^{-3}$) and cold ($\lesssim 10\,\mathrm{K}$) objects called pre-stellar cores (Figure 1.1-a). It is believed that such a pre-stellar core slowly condenses until it reaches an unstable quasi-equilibrium state in which the thermal pressure alone supports the core against its self-gravity. During this pre-stellar phase, the surface of dust grains are gradually coated by a water-ice mantles. Molecules such as CO easily stick to these grain-mantles, where they can lead to the formation of formaldehyde (H_2CO) and

methanol (CH_3OH) via successive additions of an hydrogen atom.
When gravity overcomes thermal, magnetic and turbulent pressure support, the core becomes gravitationally unstable and undergoes a phase of free-fall collapse. Once this dynamical collapse phase has started, a central hydrostatic stellar embryo (or protostar) begins to build up its mass through the addition of material from the infalling envelope (e.g. Di Francesco et al. 2006; Ward-Thompson et al. 2006). From this point, several stages of the evolution of a low-mass protostellar object to the main sequence have been identified, based mostly on the study of low-mass star forming regions in the dust continuum:

- accreting protostar (Class 0 objects, $\lesssim 10^4$ yr): the dynamic infall phase described above is believed to be represented by the deeply embedded Class 0 sources (Figure 1.1-b). These objects are characterized by possessing an extended submm continuum emission that is centrally condensed, tracing the presence of a large circumstellar dust envelope, whose mass $M_{\rm env}$ is larger than that of the protostar, $M_\star$. This emission is characteristic of a black-body of temperature $\sim 10 - 30$ K (Figure 1.1-b'). They can also be identified by the detection of a compact centimeter radio continuum source and/or the presence of a collimated outflow;

- evolved accreting protostars (Class I objects, $\sim 10^4 - 10^5$ yr): these objects are surrounded by a massive disk and a residual infalling envelope ($M_{\rm env} < M_\star$), and they possess poorly-collimated outflows (Figure 1.1-c). Their energy distribution indicates warmer environments and they are therefore observable in the mid- and far-infrared. The emission corresponds to a black-body with infra-red excess due to the presence of the disk (Figure 1.1-c');

- classical T Tauri stars (Class II objects, $\sim 10^5 - 3 \times 10^6$ yr): these objects have weak, if any, remnants of the envelope, but possess well developed circumstellar disks (Figure 1.1-d) and therefore have strong near-infrared excesses (Figure 1.1-d'). The transition from Class I to Class II is characterized by the onset of deuterium fusion reactions;

- weak-lined T Tauri stars (Class III objects, $\sim 3 \times 10^6 - 5 \times 10^7$ yr): the circumstellar disk has dissipated (by accretion and feeding of planetesimals; Figure 1.1-e) and so these objects show little near-infrared (NIR) excess (Figure 1.1-e'). Class III objects differ from main sequence stars by their X-ray emission and the presence of residual lithium.

While the disk evolves into a planetary system, the pre-main sequence star continues to contract until its temperature is high enough for hydrogen nuclear fusion, at which point it becomes a main sequence star (Figure 1.1-f).

The above sequence corresponds to the "standard" picture, that is, the scenario that currently obtains the largest consensus. However, the observational parameters used to determine the Class of a protostar do not always uniquely corresponds to a given Class. Indeed, this determination is often done by evaluating the bolometric temperature $T_{\rm bol}$ (i.e. the temperature of a black body with the same flux-weighted mean frequency as observed) or the submillimeter-to-bolometric luminosity ratio. In both cases, there can be a misidentification of the Class of a

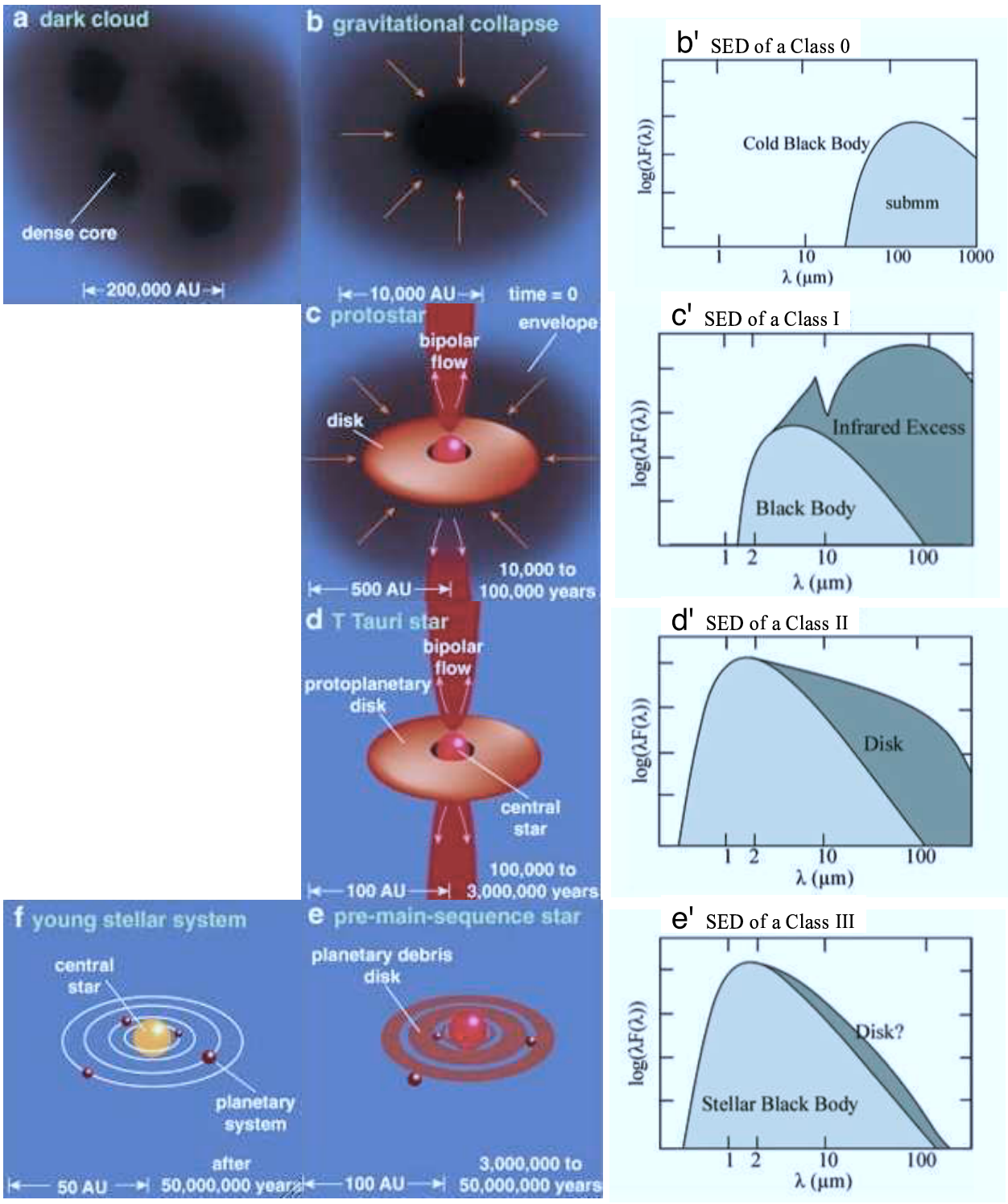

Figure 1.1 Stages of the formation of a low-mass star (panels a-f) along with the spectral energy distributions (SED; panels b'-e') characterizing stages b-e, which correspond to the Class 0, I, II, and III of the protostellar evolutionnary scheme. (From Green 2001; Burton et al. 2005).

source: for example, $T_{\rm bol}$ can be strongly affected by the amount of near- and mid-infrared emission, i.e. by the geometry (Evans 1999). It is therefore necessary to determine more accurately the structure of a source, for example by performing interferometric observations. Chemistry can also help to solve the confusion. For example, constraints can be put on the density profiles from molecular line emission (see Section 2.2), and on the ages of Class 0 and Class I protostars by using sulfur-bearing species as chemical clocks (Buckle & Fuller 2003; Wakelam et al. 2004).

1.1.2 Definition of hot corinos

In analogy with the hot cores of high-mass protostars[1], hot corinos represent the earliest phases of protostellar evolution but for low-mass instead of high-mass stars. They are located in the inner parts of the envelopes of Class 0 protostars and are characterized in a similar way to massive hot cores:

- relatively compact sizes, albeit with absolute radii $r_{\rm hc}$ about two orders of magnitudes smaller than that of hot cores ($\lesssim$150 AU and $\lesssim$0.1 pc for hot corino and hot cores respectively).

- large densities: $n \gtrsim 10^7\,{\rm cm}^{-3}$. The determination of density profiles of several Class 0 protostars (e.g. Ceccarelli et al. 2000a; Maret et al. 2002; Jørgensen et al. 2002) showed that the densities in the central regions of the envelope reach $\sim 10^7\,{\rm cm}^{-3}$at radii of order $r_{\rm hc}$ and up to $10^8 - 10^9\,{\rm cm}^{-3}$ in the most inner parts (see bottom of Figure 1.2).

- high temperatures: T$\gtrsim$ 100 K. As mentioned in the previous section, the SED of a Class 0 protostar is dominated by a cold (T$\lesssim$30 K) envelope. However, the presence of the central protostar will induce a temperature gradient such as the one shown in the top part of Figure 1.2, with larger temperatures at smaller radii and higher densities. Eventually, the temperature can reach $\sim$100 K, at which point the icy mantles sublimate, releasing in the gas-phase the molecules (H_2CO, CH_3OH, NH_3) that formed and/or sticked on the grain surfaces during the pre-stellar phase. The abundances of these molecules increase sharply for $r < r_{\rm 100K}$, where $r_{\rm 100K}$ is the radius at which T=100 K[2]. This can be represented schematically by a jump occurring at $r_{\rm 100K}$ with low abundances at larger radii (cold outer envelope) and high abundances at smaller radii (warm inner envelope) as shown by the solid line in Figure 1.3.

- spectra rich in lines emitted by complex organic molecules such as HCOOH, $HCOOCH_3$, CH_3OCH_3, CH_3CN, C_2H_5CN, etc. These molecules are characteristic of hot corinos (and of massive hot cores) as they reflect the high-temperature conditions of these objects. Indeed, they are thought to form either in the gas-phase from evaporated species (CH_3OH,

[1] High-mass protostars have masses $\gtrsim 8\,M_\odot$

[2] In the planet formation theory, $r_{\rm 100K}$ is analogous to the snowline, the radius beyond which water-ice can form in the protoplanetary disk.

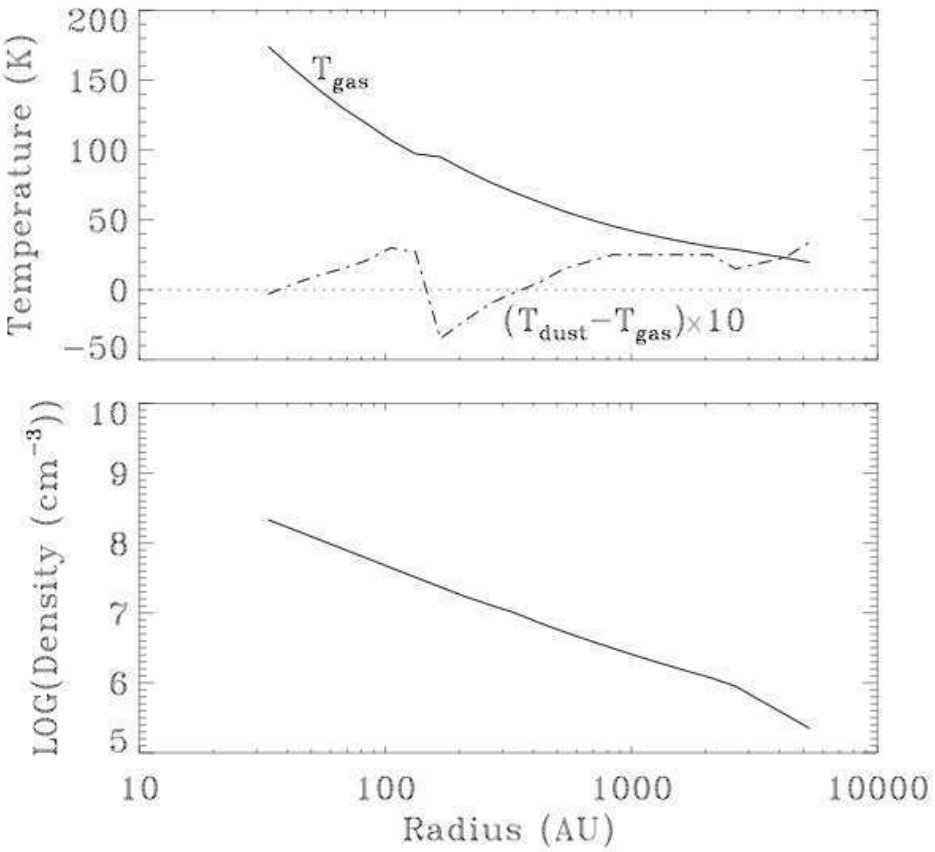

Figure 1.2 Temperature and density profiles of IRAS16293–2422 (from Ceccarelli et al. 2000a). — *Top:* Gas temperature (solid line) and difference between gas and dust temperatures (dotted line) as a function of radius. The later shows that gas and dust temperature profiles are similar. Both quantities exceed 100 K at small radii ($\lesssim$ 150 AU). — *Bottom:* Density as a function of radius on a log-log scale. The density follows a power law and exceeds 10^7 cm^{-3} for R$\lesssim$ 150 AU.

H_2CO, NH_3) via reactions requiring large temperatures, or on the icy grain-mantles from which they are released into the gas-phase when the mantles sublimate.

1.1.3 Hot corinos and pre-biotic molecules

For over two decades, complex organic molecules[3] have been observed towards the youngest massive protostars (the high-mass analogs to Class 0 objects). If these molecules could also form in low-mass protostars and survive until the proto-planetary disk phase, they could be incorporated into planetary bodies and delivered to planets such as the Earth. Once there, they could play a role in the formation of life, for example by providing the biologically active molecules that lead to the formation of the first protocells (Sandford et al. 1998). Indeed, polar (or "hydrophilic") molecules such as H_2CO, HCOOH, most ketones (e.g. CH_3COCH_3), ethers

[3]See Table A.1 for a non-exhaustive list.

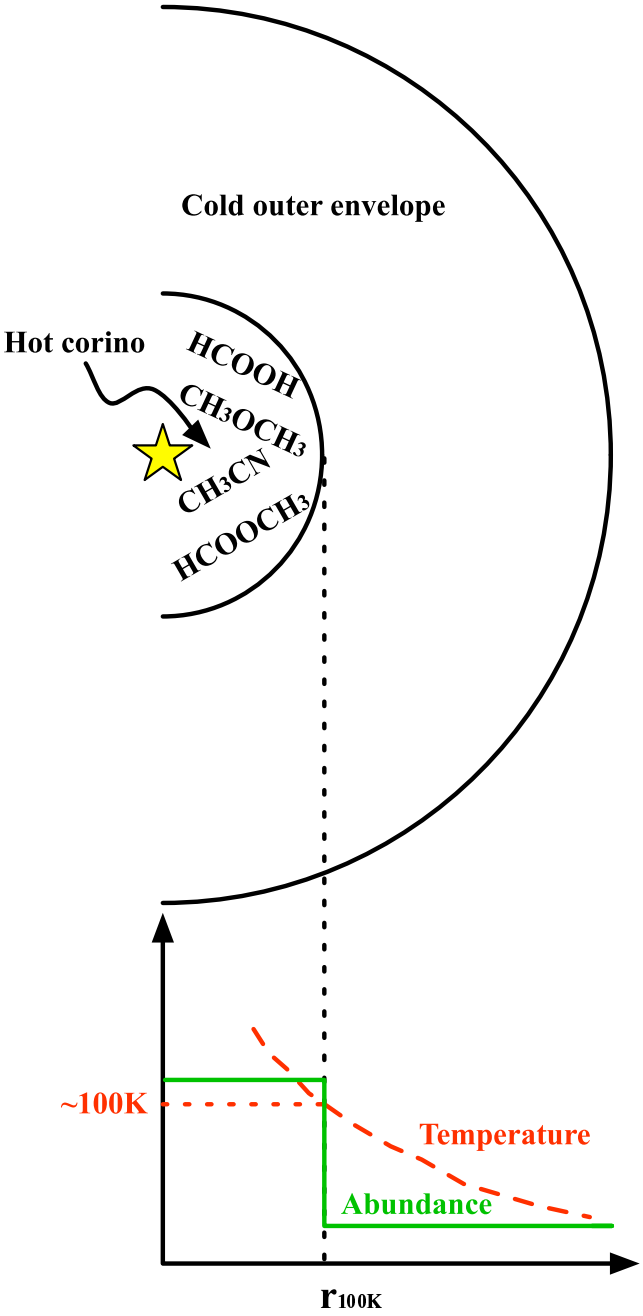

Figure 1.3 Temperature (red/broken line) and parent molecules' abundance (green/solide line) profiles in a hot corino. $r_{100\mathrm{K}}$ is the radius at which the temperature reaches 100 K, leading to the sublimation of ice mantles and the release in the gas-phase of parent molecules (H_2CO, CH_3OH, NH_3) that formed on the grains during the pre-stellar phase.

(e.g. CH_3OCH_3) and sugars (e.g. CH_2OHCHO) are chemically reactive and often constitute building blocks of biological molecules, or are reactants leading to these building blocks (Pohorille 2002). Moreover, many of these species are biologically important on Earth, with formaldehyde, nitriles (i.e. N-bearing organic molecules such as CH_3CN and C_2H_5CN, for which C and N are linked by a triple bond) and ethanol all identified as necessary precursors in the production of proteins, phospholipids, and RNA and DNA.

1.2 Previous studies that drove the start of this thesis work

1.2.1 Abundance profiles of H_2O, H_2CO and CH_3OH

H_2O, H_2CO and CH_3OH are major grain mantle constituents, so that determining the presence of a jump in their abundance profiles would provide direct evidence of the existence of a warm inner region where ices sublimate. The first study of this kind on a low-mass protostar was carried out by Ceccarelli et al. (2000a), who modeled H_2O transitions observed with the Infrared Space Observatory towards IRAS16293–2422, and found an abundance enhancement for radii smaller than $\sim$150 K. A similar modeling of H_2CO line emission in the same source by Ceccarelli et al. (2000c) and of H_2O in NGC1333-IRAS4A by Maret et al. (2002) showed that the observations could be reproduced by a jump in the abundance profiles of H_2CO and H_2O in IRAS16293–2422 and NGC1333-IRAS4A respectively. Following these key works, successive studies of CH_3OH and H_2CO line emission in a sample of about a dozen low-mass, Class 0 sources by Maret et al. (2004, 2005) led to the prediction of the existence of a H_2CO jump in all surveyed sources and of a CH_3OH jump in all but one objects. However, while CH_3OH jumps have been confirmed by the independent modelling of Jørgensen et al. (2005b) and Schöier et al. (2002), and seem therefore fairly well established, the existence of H_2CO jumps is debated as Jørgensen et al. (2005b) and Schöier et al. (2002) find that, except in the case of IRAS16293–2422, they are not necessary to explain H_2CO line emission in other Class 0 objects.

1.2.2 Complex organic molecules in IRAS16293

In the past, searches for complex organic molecules towards low-mass protostars have been sparse and unfortunately unsuccessful, whether they be in the form of surveys (van Dishoeck et al. 1995), or searches for specific molecules (e.g. glycine, Ceccarelli et al. 2000b). Nonetheless, there were strong indications of the existence of a hot corino in the Class 0 IRAS16293–2422, based on two studies. First, the modelling of H_2CO line emission in this source showed that the observations could not be explained by a constant abundance of this molecule, and that a jump was required, with low and high abundances in the outer and inner envelopes respectively (Ceccarelli et al. 2000c; Schöier et al. 2002). Second, if the search for glycine in IRAS16293–2422 by Ceccarelli et al. (2000b) was unfruitful, the deep integrations nonetheless revealed numerous emission lines whose frequencies coincided with that of several large molecules. Altogether, the H_2CO abundance enhancement and the tentative detections of large molecules in IRAS16293–2422 supported the theory of evaporation of the icy grain mantles where the dust temperature

exceeds $\sim 100\,\mathrm{K}$, thereby giving grounds for the presence of a hot corino and for searching further for complex organic molecules. And indeed, in 2003, Cazaux et al. detected complex species such as HCOOH, CH_3COOH, $HCOOCH_3$, CH_3OCH_3, CH_3CN and C_2H_5CN in IRAS16293–2422, confirming the existence of the hot corino as defined in Section 1.1.2. Simultaneously, a study of the H_2CO line emission in a sample of low-mass protostars by Maret et al. (2004) claimed that, as for IRAS16293–2422, the observations required a jump in the H_2CO abundances in all the sources of the sample. Therefore, in view of the Maret et al. (2004) work, these sources constituted targets in which complex molecules were likely to be found.

The findings of Cazaux et al. (2003), along with the Maret et al. (2004) study, really spurred the beginning of this thesis in October 2003. Additional motivations were triggered by the debate concerning the origin of complex organic molecules in hot corinos (e.g. Schöier et al. 2002) and the one regarding the existence of the H_2CO abundance jumps in Class 0 sources (Section 1.2.1).

1.3 The quests

Based on the elements presented in the previous section, my thesis work aimed at answering the following questions, which constitute as well the outline of this manuscript:

- *Is there a H_2CO abundance jump in Class 0 protostars?* (Chapter 2)
  Since H_2CO is a major constituent of grain mantles, confirming the existence of a jump in the abundance profile of this molecule would support the existence of a warm region where icy mantles sublimate, and complex organic molecules would more likely be found in sources where such a jump is observed. In addition, the amount of H_2CO in the ice-sublimation regions is a key parameter for understanding the presence of more complex organic molecules that may form from H_2CO.

- *Are hot corinos common among low-mass protostars?* (Chapter 3)
  The existence of complex organic molecules in the inner envelopes of Class 0 protostars presents a theoretical challenge because the chemical timescale for the formation of these molecules is longer than the gas free-fall time (Schöier et al. 2002). Therefore, the complex molecules should not have time to form. However, as seen in Section 1.2.2, these molecules have nonetheless been observed in one Class 0 object, IRAS16293–2422, so that the question arises as to whether this source is one of a kind or one of many.

- *Where are the complex molecules located?* (Chapter 4)
  Chapter 3 will show that hot corinos seem ubiquitous among Class 0 sources. It follows that there is a need to characterize this new kind of objects, in particular to understand the presence of complex organic molecules which, as mentioned in the previous item, is non-trivial. A key parameter is the spatial origin of the complex molecules' emission which

will be investigated in this chapter by presenting high spatial resolution observations of two hot corinos.

- *Are hot corinos similar to hot cores?* (Chapter 5)
  Since hot corinos have been defined in analogy to massive hot cores, it is only natural to wonder whether the two types of objects are similar on a chemical standpoint: are hot corinos scaled-down versions of hot cores or are there differences in the chemical compositions?

- *What is the formation path of these molecules?* (Chapter 6)
  The formation mechanisms thought to be at play in massive hot cores are unlikely to be able to explain the presence of complex organic molecules, since the existence of the later is theoretically challenging (cf. second item). Therefore, other ways to form these molecules should be explored.

In a nutshell...

The hot corinos of Class 0 protostars are the starting point of the protostellar evolution, so that the chemistry of these objects will affect or maybe even define the chemical composition of the future protoplanetary disk from which comets, meteorites and planets eventually form. By finding and characterizing hot corinos, this research aims at determining the initial chemical conditions of planet formation and hence bringing one step further our understanding of the formation of the Solar System and more generally of solar-type protostars.

Résumé du Chapitre 2
De la sublimation des manteaux de glace

Une des caractéristiques des hot corinos est que ce sont les régions internes de l'enveloppe protostellaire où les manteaux de glace sont sublimés. Ainsi, les protoétoiles pour lesquelles ces régions de sublimation existent sont de bonnes canditates pour être des hot corinos. Une des signatures de la présence de ces régions est l'abondance accrue dans le gaz des composants des manteaux des grains, tels que la formaldehyde (H_2CO) ou le méthanol (CH_3OH). La présence de sauts dans les abondances de H_2CO et CH_3OH a été revendiquée pour plusieurs protoétoiles de Classe 0, mais, alors que les sauts pour le CH_3OH ont été généralement confirmés, les sauts pour le H_2CO sont sujets à discussion. Des observations de transitions à hautes energies de H_2CO telles que $J = 7 - 6$ à 491.9 GHz ($E_{\rm up} = 74\,{\rm cm}^{-1}$), aideraient à résoudre le différent. En utilisant le James Clerke Maxwell Telescope, j'ai observé et detecté cette transition pour cinq objets de Classe 0. Les données apportents un peu plus de soutien pour la présence d'un saut dans l'abondance de H_2CO pour trois des cinq sources, mais pas nécessairement pour les deux restantes. Dans l'ensemble, les données ne sont pas suffisantes pour distinguer avec certitude entre un saut d'abondance et une abondance constante. Des observations de transitions à toujours plus haute energie, ou bien à haute résolution spatiale, seraient nécessaires pour régler la question.

Chapter 2
On the sublimation of ice mantles

Abstract

One of the characteristics of hot corinos, as defined in Section 1.1.2, is that they are inner regions of the protostellar envelope where grain mantles sublimate. Hence, protostars in which these evaporation regions exist would be good hot corino candidates. One signature of the presence of evaporation regions is the enhanced gas-phase abundance of grain mantle constituents such as H_2CO or CH_3OH. The presence of H_2CO and CH_3OH abundance jumps has been claimed in a number of Class 0 protostars, but while the CH_3OH jumps have been mostly confirmed, the H_2CO jumps are debated. Observations of high-energy transitions of H_2CO such as $J = 7 - 6$ at 491.9 GHz ($E_{\rm up} = 74\,{\rm cm}^{-1}$), would help solving the debate. Using the JCMT, I observed and detected this transition in five Class 0 objects. The data bring further support for the presence of a H_2CO abundance jump in three of the five sources, but not necessarily in the remaining two. Overall, the data are not sufficient to firmly discriminate between the jump or constant H_2CO abundances and observations of even higher energy transitions, or with high spatial resolution, would be required to settle the matter.

2.1 Introduction

The claim for the presence or not of a jump in the abundance of the grain mantle constituents relies in part upon the determination of the physical (density and temperature) structure of the envelope surrounding a Class 0 protostar. Therefore, I describe in Section 2.2 how this determination is done in practice. I then move on to the more specific case of constraining the abundance profile of H_2CO, the grain mantle constituent for which the presence of a jump is debated (Section 2.3). Finally in Sections 2.4 and 2.5, I present the JCMT observations and compare the results with the predictions.

2.2 Physical structure of Class 0 protostars

The physical structure of the envelope of a Class 0 protostar is coupled to its chemical structure, both of which are affected by the heat emitted by the central object. Indeed, this heating source

produces gradients in temperature and density. The varying physical conditions will induce modifications in the chemical composition across the envelope, which in turn can affect the physics of the envelope (due to the cooling effect of some molecules). This spatially varying chemistry can be used to constrain the physical structure of Class 0 envelopes. Indeed, for a given molecule, each line will be excited at different temperature and density, so that each line will probe a specific region of the envelope corresponding to these temperature and density. This can be seen by statistical equilibrium considerations. For a given molecule, the densities of an upper and a lower level, n_u and n_l, depend on the balance between the collisional and radiative processes and can be related in the following way:

$$\frac{n_u}{n_l} = \frac{g_u}{g_l} \exp\left(-\frac{h\nu_{ul}}{k_{\rm B}T}\right) \left(1 + \frac{n_{\rm crit}}{n({\rm H_2})}\right)^{-1} \tag{2.1}$$

where g_u and g_l are the statistical weights of the upper and lower levels, ν_{ul} is the frequency of the transition between these levels, $k_{\rm B}$ is Boltzmann's constant, T is the temperature, $n({\rm H_2})$ is the molecular hydrogen density and $n_{\rm crit}$ is the critical density, at which collisional and radiative processes are of equal importance. For transitions in the (sub)millimeter domain, where the Rayleigh-Jeans approximation applies ($h\nu << kT$), this simplifies to:

$$\frac{n_u}{n_l} = \frac{g_u}{g_l} \left(1 - \frac{h\nu_{ul}}{k_{\rm B}T}\right) \left(1 + \frac{n_{\rm crit}}{n({\rm H_2})}\right)^{-1} \tag{2.2}$$

Mathematically, for a two-level system, $n_{\rm crit} = A_{ul}/C_{ul}$, where A_{ul} and C_{ul} are the rate coefficients for radiative and collisional processes respectively. In general, since $A_{ul} \propto \nu^3$, transitions occurring at a higher frequency ν will have a higher critical density, and therefore will probe regions of higher density.

Ideally, using several lines from several molecules (due to the fact that some molecules may be depleted or enhanced in some parts of the envelope) would allow an accurate reconstruction of the temperature and density profiles of the gas in the envelope. However, this method requires a large amount of observations and cannot be applied to all sources. Therefore in practice, an assumption is made about the shape of the density profile and the modeling of some observables allows a determination of the free parameters. Mostly two types of modeling are used:

- *Modelling of line emission using the collapsing Singular Isothermal Sphere (SIS), or "inside-out" hypothesis*
  The SIS model, originally proposed by Shu (1977), assumes that the initial state of the envelope is described by an isothermal sphere in hydrostatic equilibrium with a density $n \propto r^{-2}$. The equilibrium is then perturbed at $r = 0$ where isothermal collapse starts and propagates from the inside to the outside at the speed of sound. In the collapse region, the gas is free-falling, yielding $n \propto r^{-3/2}$, while in the static outer envelope, the density still follows an r^{-2} law (see Figure 2.1). This dynamical model is combined with a radiative transfer code, taking into account heating and cooling of the gas and dust, to predict the line emission, which is then compared with the observations in order to derive

the scaling factors and the radius of the collapse front (Ceccarelli et al. 1996; Maret et al. 2002). Unlike in other models which assume equal gas and dust temperatues, these two parameters are derived independently in the present approach. The model also constrains other parameters such as the mass of the central object and the infall rate.

- *Modelling of the dust continuum emission with a single power-law*
  This method uses spectral energy distributions coupled with maps of the dust continuum emission to trace the H_2 and (dust) temperature distributions. Assuming a single power-law density between an inner and an outer radius (to avoid the central singularity), the fluxes and brightness profiles of the sources are modeled with a radiative transfer code. The modeled parameters are compared to those measured from the observed maps in order to find the best fit. The power-law index for most Class 0 objects is in the range $\sim 1.3-2.0$ (Chandler & Richer 2000; Shirley et al. 2000, 2002; Jørgensen et al. 2002).

The structures derived from both methods are similar and the difference is not significant enough to be distinguished from observations (e.g. Hogerheijde & Sandell 2000). Note however that the inside-out model is supported by evidence of infall observed in a number Class 0 protostars (e.g. Di Francesco et al. 2001; Terebey & Padgett 1997; Ward-Thompson et al. 1996), although non-static initial conditions are more likely than the static initial conditions proposed by Shu (1977), as noted by Whitworth et al. (1996).
For the sources of interest in my thesis, I list in Table B.2 the parameters of the density profile recently published in the literature from one or both methods.

2.3 Constraints on the structure from formaldehyde line emission: the sublimation region.

As mentioned in Sections 1.1.2 and 1.2, determining the presence of a jump in the abundance profile of H_2CO (a major grain mantle constituent) would prove the existence of a warm inner region where icy mantles sublimate. I explained in Section 2.2 that different transitions of a given molecule are emitted in different parts of the envelope, reflecting the local temperature and density. Figure 2.2 illustrates this idea. On the right-hand side, it shows the line intensity predicted by Ceccarelli et al. (2003) for several H_2CO transitions as a function of radius. For low-energy transitions such as the one outlined in blue, the contribution to the line emission mainly comes from the cold outer envelope, whereas for high-energy transitions (e.g. in red), it originates from the warm inner envelope.

Using such modeling of H_2CO line emission, Ceccarelli et al. (2000c) and Maret et al. (2004) claimed the existence of a jump in the H_2CO abundance in IRAS16293 and in seven other Class 0 protostars. Other authors have also carried out analyses of methanol and formaldehyde in low-mass protostars (e.g. Schöier et al. 2002, 2004; Jørgensen et al. 2005b). On the one hand, in contrast with Maret et al. (2004), Jørgensen et al. (2005b) claimed that no jump of formaldehyde abundance is required to model the line intensities in any of the sources except

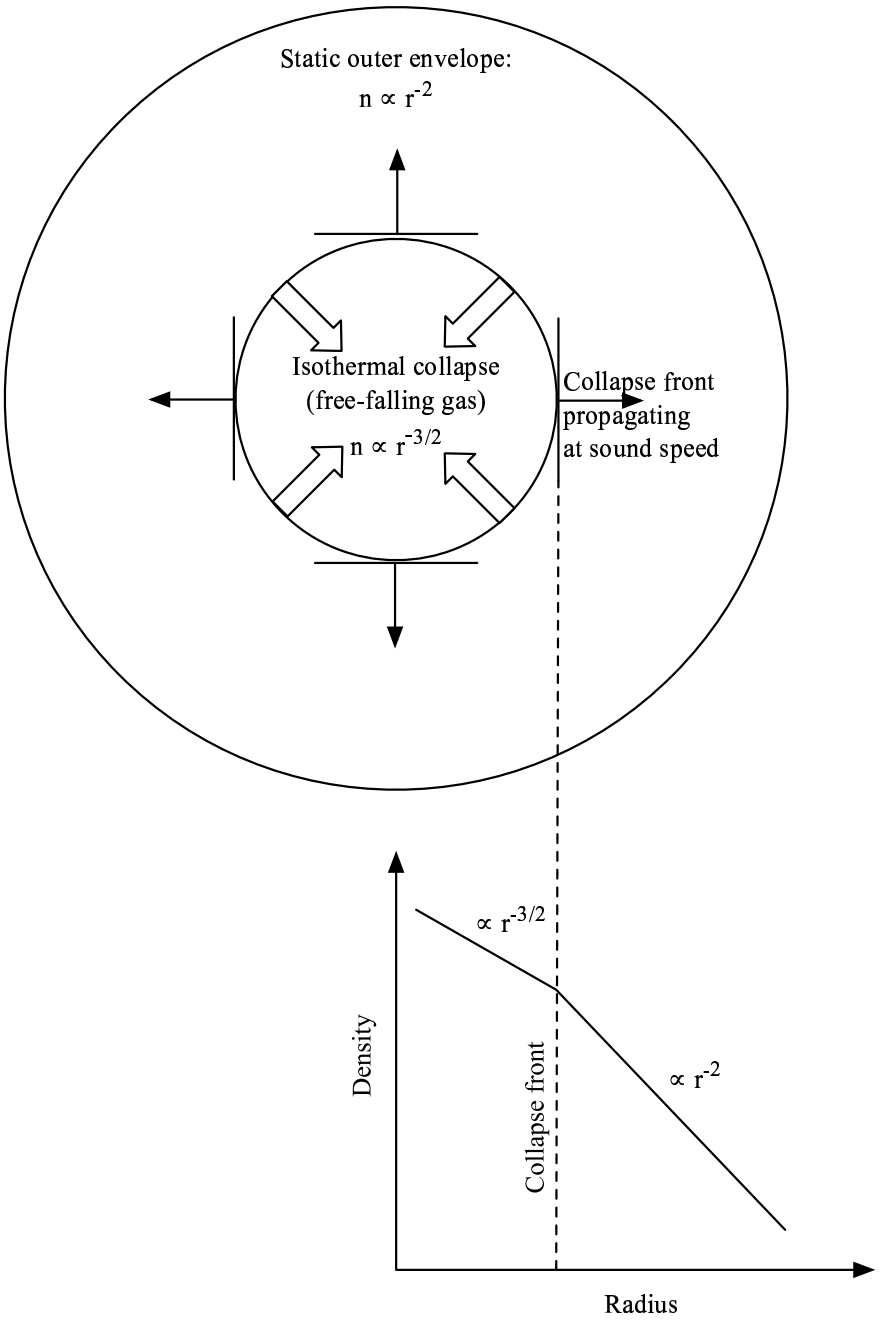

Figure 2.1 Schematic representation of the “inside-out” model.

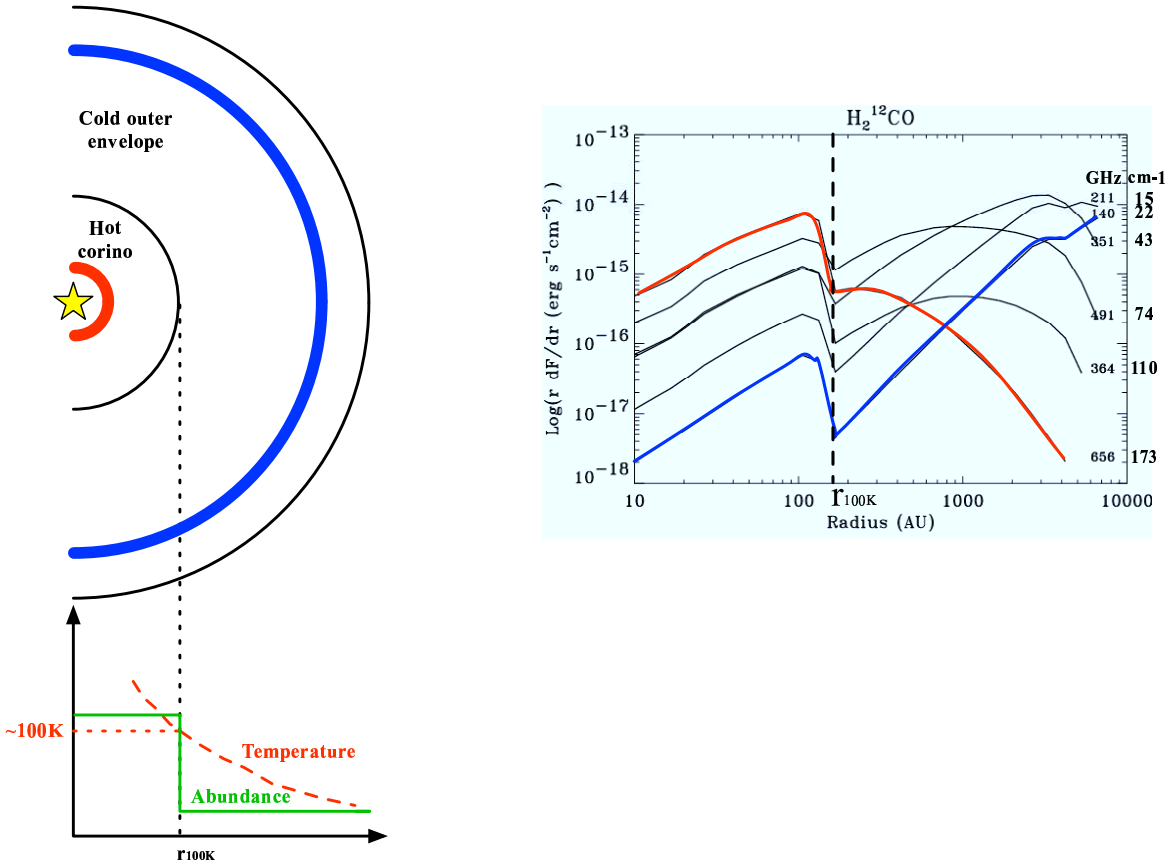

Figure 2.2 *Left:* Schematic view of the envelope of a Class 0 protostar with the temperature and parent molecules' abundance profiles (as in Figure 1.3). The red and blue areas are examples of regions where most of the emission of respectively high and low energy transitions (shown in the right-hand side diagram) originates. — *Right:* Modeled line intensities as a function of distance from the central object for six H_2CO transitions, whose frequencies (in GHz) and energy of the upper level (in cm^{-1}) are indicated next to each line (form Ceccarelli et al. 2003). — r_{100K} is the radius at which $T = 100\,K$.

Table 2.1 Formaldehyde and methanol abundances in hot corinos and hot corino candidates.

Source	$L_{\rm bol}$[a]	$X_{\rm hc}(H_2CO)$		$X_{\rm hc}(CH_3OH)$	
	($L_\odot$)	M04[b]	J05[d]	M05[c]	J05[d,e]
NGC1333-IRAS4A	6	2×10^{-8}	3×10^{-9}	$< 1 \times 10^{-8}$	$\leq 3.5 \times 10^{-9}$
NGC1333-IRAS4B	6	3×10^{-6}	1×10^{-8}	7×10^{-7}	9.5×10^{-8}
NGC1333-IRAS2A	16	2×10^{-7}	8×10^{-10}	3×10^{-7}	1.5×10^{-7}
L1448-MM	5	6×10^{-7}	1×10^{-8}[f]	5×10^{-7}	1×10^{-9}
L1448-N	6	1×10^{-6}	–	$< 4 \times 10^{-7}$	–
L1157-MM	11	1×10^{-8}	1×10^{-10}	$< 3 \times 10^{-8}$	$< 3 \times 10^{-10}$
L1527	2	6×10^{-6}	2×10^{-9}	–	$< 6 \times 10^{-10}$
IRAS16293–2422	27	1×10^{-7}	6×10^{-8}[f]	1×10^{-7}	1×10^{-7}

NOTE — A dash indicates that the source was not observed.
[a] From Jørgensen et al. (2002).
[b] Maret et al. (2004).
[c] Maret et al. (2005).
[d] Jørgensen et al. (2005b).
[e] Methanol abundances averaged over A- and E-types.
[f] From Schöier et al. (2002).

IRAS16293[1] (Schöier et al. 2002). On the other hand, like Maret et al. (2005), Jørgensen et al. (2005b) and Schöier et al. (2002) found a methanol abundance jump in IRAS4B, IRAS2A and IRAS16293, but not necessarily in IRAS4A. The hot corino abundances of formaldehyde and methanol found by the two groups are summarized in Table 2.1.

The difference in the determination of the H_2CO abundance profiles could be due to the different assumptions used by the authors:

- velocity structure: Maret et al. (2004) assume a non-turbulent, infalling envelope to match the accretion process occuring in Class 0 protostars, whereas Jørgensen et al. (2005b) use a constant turbulent broadening over the whole envelope based on the assumption that most of the mass of the envelop is not infalling.

- ortho-para ratio (o/p): considering that the o/p is badly defined in IRAS16293, the source which has the highest number of observed transitions, Maret et al. (2004) adopted the canonical value of 3; Jørgensen et al. (2005b) on the other hand attempted to derive the o/p by determining independently the abundances of the ortho and para forms of H_2CO from the few number of lines, which yielded o/p = 1.6. In fact, it is possible that the o/p varies across the envelope.

Figure 2.3 shows the ratios of modeled to observed H_2CO line fluxes as a function of the upper energy of the lines, in the Class 0 IRAS2 (Maret et al. 2004), in the cases of a jump and a

[1] Schöier et al. (2004) obtained a better fit to the H_2CO data with a depletion region for radii between R_1 (where T is equal to the sublimation temperature) and R_2 (where $n(H_2) = 10^5\,{\rm cm}^{-3}$), instead of a jump at R_1. However, since the value for R_2 that these authors obtained from modeling is larger than the outer envelope radius, the model effectively corresponds to a jump model.

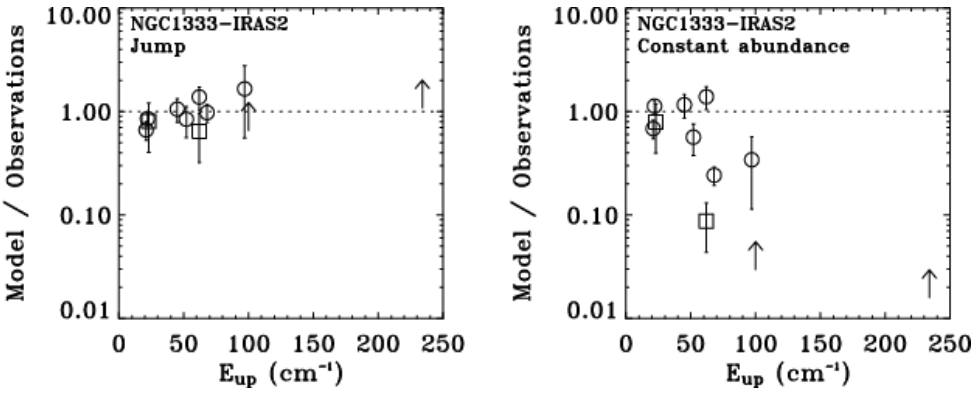

Figure 2.3 Ratios of modeled to observed H_2CO line fluxes as a function of the upper energy of the lines, in the Class 0 NGC1333-IRAS2 (Maret et al. 2004). The left panel shows the results when the model is run assuming a jump in the H_2CO abundance profile whereas in the right panel, a constant abundance was used. Circles and squares represent $H_2^{12}CO$ and $H_2^{13}CO$ respectively, and arrows indicate lower limits.

constant abundance profiles. While the predictions do not differ much for the low-energy transitions ($E_{up} \lesssim 50 cm^{-1}$), there are substantial differences for high-energy transitions. Therefore, observations of the later are critical to discriminate for the presence of a H_2CO abundance jump. Three such transitions, which have not been observed so far and which have the best possible atmospheric transmission in the frequency ranges currently attainable with ground-based facilities, are: $J = 7-6$ at 491.9 GHz ($E_{up} = 74$ cm^{-1}), $J = 9-8$ at 656.4 GHz ($E_{up} = 173$ cm^{-1}) and $J = 11-10$ at 823.0 GHz ($E_{up} = 183$ cm^{-1}). I chose to start with the $J = 7-6$ transition, which had the best atmospheric transmission of the three and therefore would be the easiest to target, and I describe the observations in the next section.

2.4 Observations with the JCMT

The $7-6$ transition of H_2CO at 491.9 GHz was observed in NGC1333-IRAS4A, NGC1333-IRAS4B, NGC1333-IRAS2A, L1448-MM, L1448-N and IRAS16293–2422. These sources, described in Appendix B, are the brightest ones for which predictions of the line intensity have been made by Maret et al. (2004) and Ceccarelli et al. (2000c). Positions and physical parameters are given in Tables B.1 and B.2. The first three sources and the last one are thereafter referred to IRAS4A, IRAS4B, IRAS2A and IRAS16293 respectively.

The observations were performed with the JCMT in December 2004 and March 2005 in beam-switching mode, with the C-band of receiver W (RxW_C) operating in single-side band and with the Digital Autocorrelation Spectrometer (DAS). The spectral resolution and typical system temperatures were 0.2 km s^{-1} and 900-2800 K respectively. The antenna temperatures T_A^* were converted into main beam temperatures T_{mb} using $T_{mb} = T_A^*/\eta_{mb}$, where η_{mb} is the

main beam efficiency and is equal to 52%[2].

2.5 Results

H_2CO $7-6$ was detected towards all sources but IRAS2A, for which the data were not useable and therefore nothing can be said about the transition in this source. Figure 2.4 shows the observed spectra and measured integrated intensities are given in Table 2.2 The last three columns of that table also give the ratios (R1, R2 and R3) of the measured fluxes to those predicted by the models found in the literature. In R1 and R2, the modeled fluxes are taken from (Maret et al. 2004), assuming, respectively, a jump and a constant profile for the H_2CO abundance. In R3, the modeled fluxes were kindly provided by J. K. Jørgensen (priv. comm.), and were obtained using a constant H_2CO abundance and the model presented in Jørgensen et al. (2005b)[3].

For L1448-MM, L1448-N and IRAS16293, the abundance jump model predicts values that are within a factor two of the observed values. On the other hand, for IRAS4A, the constant abundance models provide slightly better fits (by a factor 2 to 3). Finally, regarding IRAS4B, R3 is the closest to one, but still a factor three away. However, single-dish observations of IRAS4A and IRAS4B (Chapter 3), as well as interferometric observations in the case of IRAS4A, require the presence of a sublimation region to explain the presence of the detected complex organic molecules.

Overall, the constant abundance model of Maret et al. (2004) overestimates (and in one case underestimates) the observed abundances by at least a factor three and can therefore probably be excluded to represent most sources (in particular IRAS4B), but the difference produced by the two other models (at most a factor three) is not significant enough to discriminate between them.

Conclusion

Considering that H_2CO is an important grain-mantle constituent and that its gas-phase abundance in the sublimation regions is a critical parameter to understand the formation of complex organic molecules, I tried in this Chapter to determine whether the abundance profile of this so-called parent molecule possesses a jump or if it is constant. To do this, I presented observations of the high-energy H_2CO (7-6) transition obtained with the JCMT toward five Class 0 protostars. Comparison of measured and modeled fluxes favors the jump model in three sources, IRAS16293, L1448-MM and L1448-N, but does not allow to exclude the constant abundance model, and observations of still higher energy transitions ($J = 9-8$ and $J = 11-10$ which have

[2]From `http://docs.jach.hawaii.edu/JCMT/HET/GUIDE/het_guide/`.

[3]The two constant abundance models yield different results due to the different assumptions mentioned in §2.3.

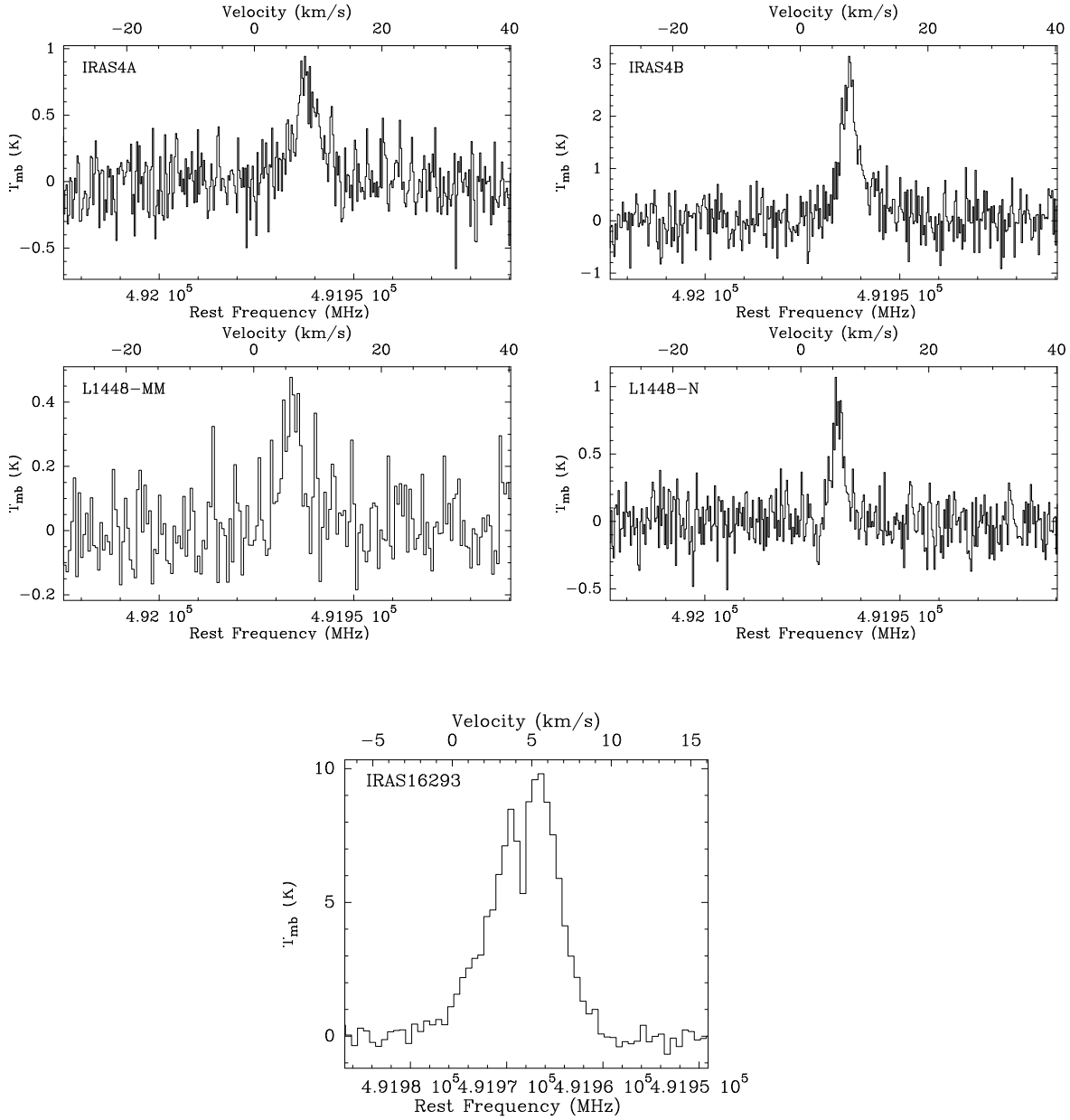

Figure 2.4 Observed spectra towards NGC1333-IRAS4A, NGC1333-IRAS4B, L1448-MM, L1448-N and IRAS16293–2422. rms and spectral resolution are given in Table 2.2.

Table 2.2 Observed parameters and ratios to predicted line fluxes for H_2CO $7-6$

Source	rms (K)	δV^a (km s^{-1})	$\int T_{\rm mb}{\rm dV}^b$ (K km s^{-1})	$F_{\rm obs}/F_{\rm m04,j}$ (R1)^c	$F_{\rm obs}/F_{\rm m04,c}$ (R2)^c	$F_{\rm obs}/F_{\rm j05}$ (R3)^d
IRAS4A	0.2	0.2	3.2±0.2	0.4	0.7	1.2
IRAS4B	0.3	0.2	8.8±0.3	6.0	18.9	3.0
L1448-MM	0.1	0.4	1.4±0.1	1.1	3.1	2.3
L1448-N	0.2	0.2	1.9±0.2	1.7	4.9	–
IRAS16293	0.3	0.4	46.5±0.7	1.2	3.6	2.6

[a] Spectral resolution.
[b] Measured integrated intensity in K km s^{-1}.
[c] R1 and R2 are the ratios of observed to modeled flux where $F_{\rm m04,j}$ and $F_{\rm m04,c}$ are the fluxes predicted by the jump and constant models respectively of Maret et al. (2004) (except for IRAS16293 for which the predicted values are taken from Ceccarelli et al. 2000c).
[d] R3 is th ratio of observed to modeled flux where $F_{\rm j05}$ is the flux predicted by the model of Jørgensen et al. (2005b) (J. K. Jørgensen, priv. comm.). A dash indicates that the source was not modeled.

$E_{\rm up}$=173 and 183 cm^{-1} respectively) would be required. Alternatively, high-resolution interferometric observations would yield the determination of the H_2CO abundances in the inner $\sim 1''$ and hence would allow to discriminate between the two models.

Résumé du Chapitre 3
La chasse aux hot corinos

La découverte de molécules organiques complexes autour de la protoétoile IRAS16293–2422 a démontré l'existence des hot corinos. La seconde question (mais en fait un des buts majeurs de ma thèse) que je traite dans ce travail, est de savoir si d'autres sources de Classe 0 abritent des hot corinos. La chasse aux hot corinos a commencé avec une sélection de sources pour former un échantillon de Classes 0 qui sont devenues les cibles d'une étude menée à l'aide d'un télescope à antenne unique (l'IRAM-30m[1]). Cette étude visait à chercher des molécules organiques complexes, que j'ai effectivement détectées vers trois autres protoétoiles de type solaire. J'ai utilisé la méthode dite du diagramme rotationnel pour analyser les données de l'IRAM-30m et pour calculer les densités de colonnes et les abondances. Je trouve que les rapports des abondances des molécules complexes aux abondances de CH_3OH ou H_2CO sont proches de l'unité et ne dépendent pas des abondances de CH_3OH ou de H_2CO dans les hot corinos, ce qui indique que les molécules complexes sont formées efficacement. Les résultats de ce chapitre ont été publiés dans Bottinelli et al. (2004a) et Bottinelli et al. (2006).

[1]IRAM = Institut de RadioAstronomie Millimétrique. L'IRAM est financé par l'INSU/CNRS (France), le MPG (Allemagne) et l'IGN (Espagne).

Chapter 3
Hunting for hot corinos

Abstract

The discovery of complex organic molecules towards IRAS16293–2422 proved the existence of hot corinos. The second question I address in this work (but in fact one of the major goals of my thesis) is whether other Class 0 sources harbored hot corinos. The hunt for hot corinos started with selecting sources to constitute a sample of Class 0 that would be the targets of a single-dish survey (carried out with the IRAM-30m[1]) aiming at looking for complex organic molecules, which I indeed detected in three more solar-type protostars (Sections 3.1 and 3.2). I used the so-called rotational diagram method to analyze the single-dish data and calculate column abundances (Section 3.3). I found that the ratios of complex molecule abundances to CH_3OH or H_2CO abundances are close to unity and do not depend on the CH_3OH nor the H_2CO abundances in the hot corinos, which indicates that the complex molecules form efficiently. These results are presented in Sections 3.4 and discussed in Section 3.5. Results from this chapter have been published in Bottinelli et al. (2004a) and Bottinelli et al. (2006).

3.1 Source selection

The building of my source sample is based on two criteria:

1. due to their distance and luminosity, they are expected to have brighter lines compared to other Class 0 sources (e.g. from the André et al. 2000 sample);

2. the presence, claimed by Maret et al. (2004, 2005), of a warm ($\gtrsim$100 K) inner region where grain mantles sublimate.

The second criterion is based on the modeling of multi-transition observations of H_2CO and CH_3OH which required jumps in the abundance profiles of these molecules across the envelope: low abundances in the outer, cold envelope where formaldehyde and methanol are still frozen onto grain surfaces, and high abundances in the inner, warm envelope where the heat from the

[1]IRAM = Institut de RadioAstronomie Millimétrique. IRAM is supported by INSU/CNRS (France), MPG (Germany) and IGN (Spain).

central object causes the desorption of formaldehyde and methanol into the gas-phase. The choice of this criterion is justified by the fact that such jumps are indicators of grain mantles sublimation, the sine qua non condition for the presence of complex molecules in the gas-phase. Moreover, these jumps were also found for IRAS16293–2422 (Maret et al. 2005; Ceccarelli et al. 2000c), the first Class 0 source towards which complex organic molecules were detected, so that sources having H_2CO and/or CH_3OH abundance jumps are the best candidates where to search for complex molecules.
These criteria yielded a sample of seven Class 0 protostars, described in Appendix B: NGC1333-IRAS4A, NGC1333-IRAS4B, NGC1333-IRAS2A, L1448-MM, L1448-N, L1157-MM, and L1527. The first three sources will be thereafter referred to as IRAS4A, IRAS4B and IRAS2A respectively.

It should be noted that other authors have carried out analyses of methanol and formaldehyde in low-mass protostars (e.g. Schöier et al. 2002, 2004; Jørgensen et al. 2005b). These works have been presented in Chapter 2 and I refer the reader to this chapter for a more detailed discussion of the differences between the Maret et al. and other studies. Jørgensen et al. (2005b) and Schöier et al. (2002) The hot corino abundances of formaldehyde and methanol found by the two groups are summarized in Table 2.1. In the following we will adopt the Maret et al. (2004, 2005) framework, but we will also discuss the results in the light of the Jørgensen et al. (2005b) analysis.

3.2 Observations and data reduction

The observations were carried out in June 2003 with the 30-meter telescope of the Institut de RadioAstronomie Millimétrique (IRAM). With four receivers, this telescope provided the largest bandwidth and the highest flexibility of setups that we needed in order to look for as many complex molecules' transitions as possible. The positions used for pointing were those given in Table B.1.

Based on the observations of IRAS16293 by Cazaux et al. (2003), we targeted the following complex molecules: methyl formate ($HCOOCH_3$-A and -E), formic acid (HCOOH), dimethyl ether (CH_3OCH_3), methyl cyanide (CH_3CN), and ethyl cyanide (C_2H_5CN). Different telescope settings were used in order to include as many transitions as possible for each molecule. Table 3.1 shows the observed frequency ranges, the molecules that have transition(s) in these ranges, and for each source, the rms reached in the low resolution spectra. Spectroscopic parameters for the targeted transitions (such as frequency and energy of the upper level)can be found in Table C.1.

All lines were observed with a low resolution, 1 MHz filter bank of 4×256 channels split between different receivers, providing a velocity resolution of $\sim$ 3, 2, and 1 km s^{-1} at 3, 2, and 1 mm, respectively. Each receiver was simultaneously connected to a unit of the autocorrelator, with spectral resolutions of 20, 80 or 320 kHz and bandwidths between 40 and 240 MHz, equiv-

Table 3.1 Frequency ranges covered during the observations of the sample of solar-type protostars.

Frequency range (GHz)	Molecules[a]	rms[b] (mK)					
		I4A	I4B	I2A	L1448	L1157	L1527
90.07 – 90.32	$HCOOCH_3$-A/E, HCOOH (C_2H_5OH)	2	2	2	2	2	2
98.50 – 98.75	$HCOOCH_3$-A/E, C_2H_5CN (C_2H_5OH)	1	2	3	2	2	7
110.29 – 110.43	CH_3CN (C_2H_5OH)	5	5	–	–	7	10
135.62 – 135.86	HCOOH (CH_3CHO-A, C_2H_5OH)	2	–	–	–	–	–
146.56 – 146.92	CH_3OCH_3, C_2H_5CN (C_2H_5OH)	8	–	–	–	–	–
223.17 – 223.42	CH_3OCH_3, C_2H_5CN	9	13	34	9	18	32
226.50 – 227.00	$HCOOCH_3$-A/E (CH_3CHO-A, C_2H_5OH)	11	11	15	10	13	10
240.95 – 241.40	HCOOH, CH_3OCH_3	15	–	–	–	–	–
257.35 – 257.55	CH_3CN	6	22	28	14	10	82

NOTE. – Abbreviations for the sources are: I4A = IRAS4A, I4B =IRAS4B, I2A = IRAS2A, L1448 = L1448-MM, L1157 = L1157-MM. Due to time constraints, L1448-N was not observed.

[a] Species in parenthesis were not the primary targeted molecules but were of interest since they were also detected by Cazaux et al. (2003).

[b] rms reached in the low resolution spectra. A dash indicates that no data were taken in the corresponding frequency range.

alent to a (unsmoothed) velocity resolution of 0.1–0.4 km s^{-1}. At 3, 2 and 1 mm, the angular resolution is 24, 16 and 10″ and typical system temperatures were 100–200 K, 180–250 K and 500–1500 K, respectively.

Two observation modes were used: position switching with the OFF position at an offset of $\Delta\alpha$ = –100″, $\Delta\delta$ = +300″, and wobbler switching with a 110″ throw in azimuth. Pointing and focus were regularly checked using planets or strong quasars, providing a pointing accuracy of 3″.

For a set of spectra with the same settings (frequency range and resolution), the data reduction consisted in the following steps:

- Examine the individual spectra in order to eliminate the bad ones (e.g. those containing standing waves).
- Determine the continuum from line-free frequency windows and substract it.
- Convert the antenna temperature T_A to main-beam temperature T_{mb} by $T_{mb} = T_A \frac{F_{eff}}{B_{eff}}$, where F_{eff} is the forward efficiency (95, 93, and 88% at 3, 2 and 1 mm respectively), and B_{eff} the main beam efficiency (76, 69 and 50% at 3, 2 and 1 mm respectively).
- Sum the spectra to obtain the final spectrum.

Figures 3.1, 3.2 and 3.3 show the spectra obtained towards sources where complex organic molecules have been detected: IRAS4A, IRAS4B and IRAS2A respectively.

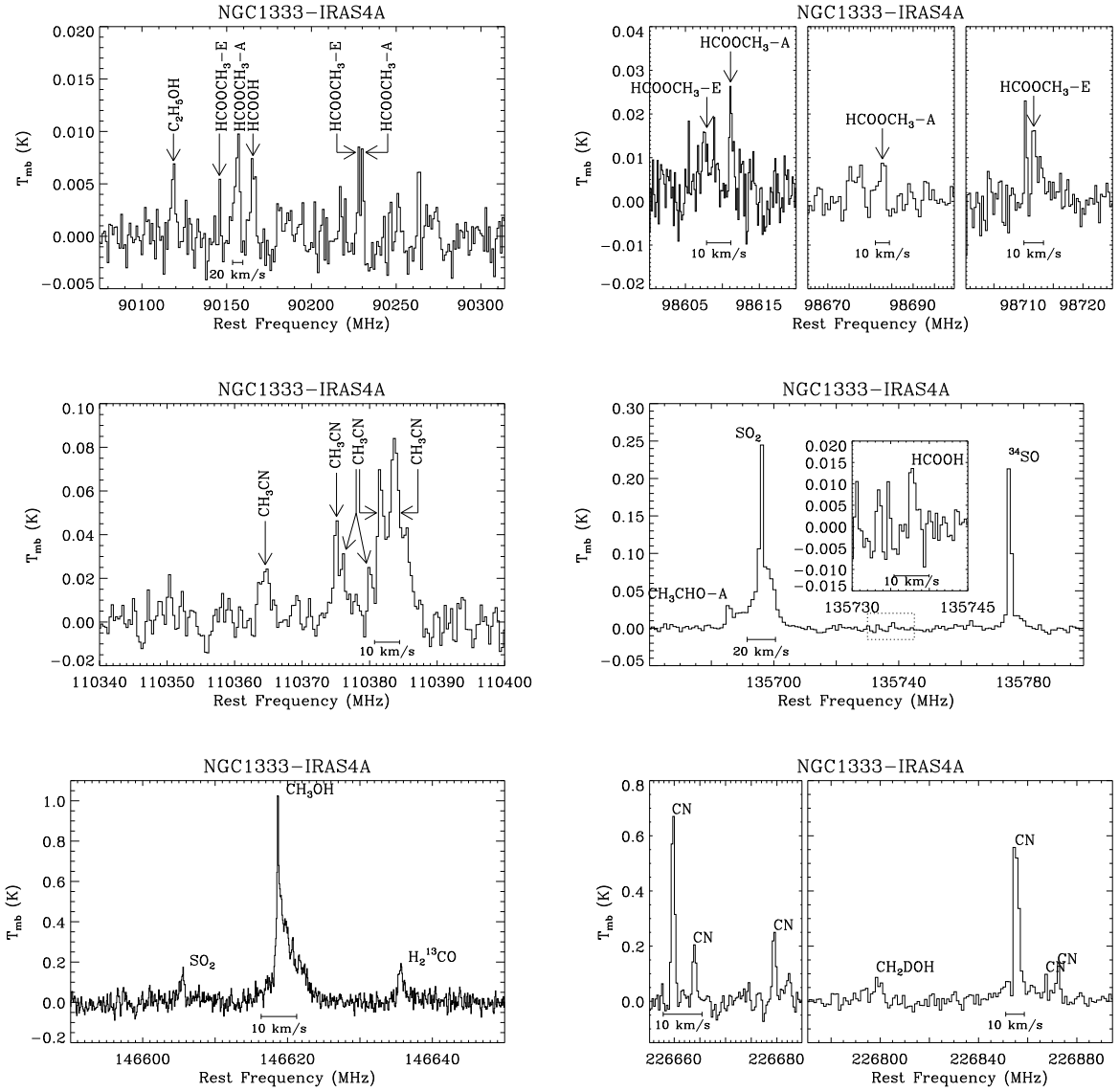

Figure 3.1 Observed spectra towards NGC1333-IRAS4A. From left to right, top to bottom, the rms are 2, 5, 2, 4, 6, 3 (insert 5), 31, 28, 19, 26, 19, 26, 12 mK, and spectral resolutions are 3.3, 0.5, 1.9, 0.9, 0.8, 2.2 (insert: 0.7), 0.2, 0.4, 1.3, 0.4, 0.8, 1.2 and 1.2 km s^{-1}. — NOTE: Known transitions are indicated but not all of them are detections, e.g., $HCOOCH_3$ at 90.145 GHz for IRAS4A is not considered as such, but the upper limit derived from it is consistent with the rotational diagram of Fig. 3.5(a). Unlabeled lines are unidentified.

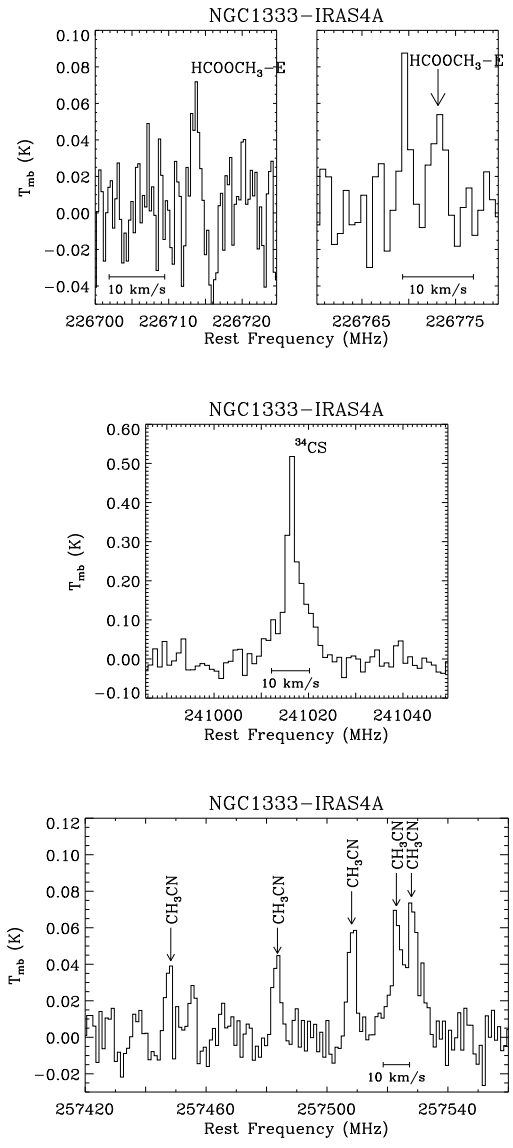

Figure 3.1 *(Continued)*

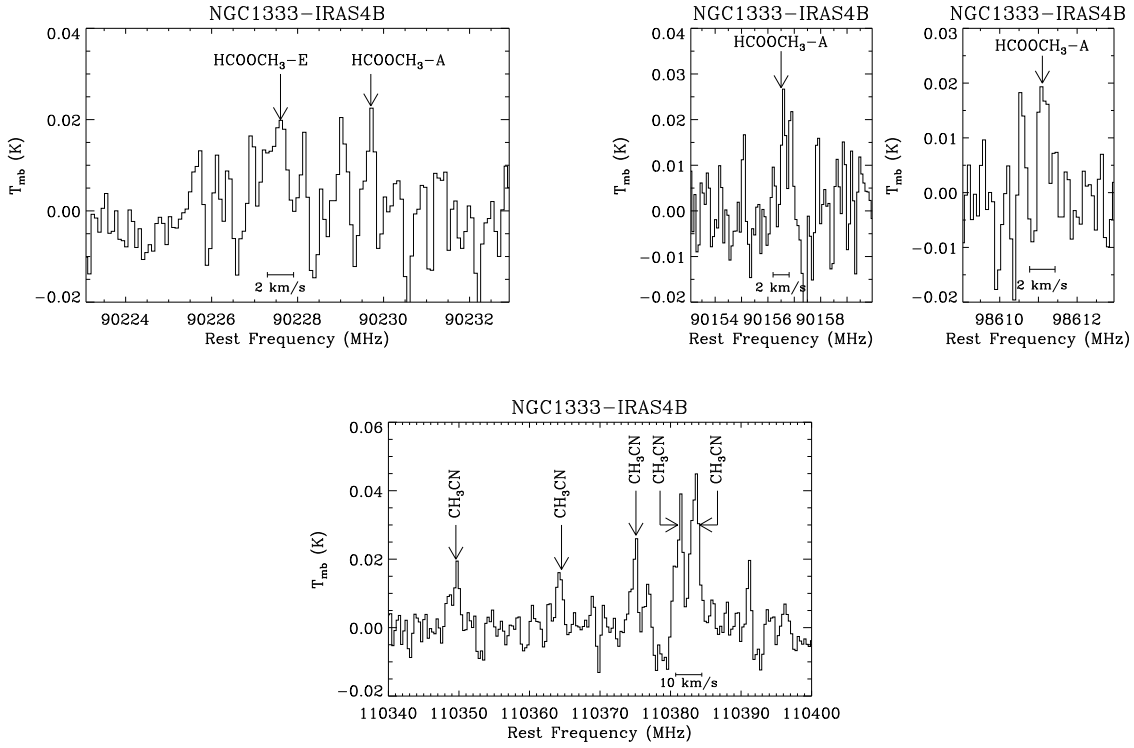

Figure 3.2 Observed spectra towards NGC1333-IRAS4B. The rms are 7, 7 and 5 mK, and the spectral resolutions are 0.2, 0.3, 0.8 km s^{-1}, at 90, 98 and 110 GHz respectively.

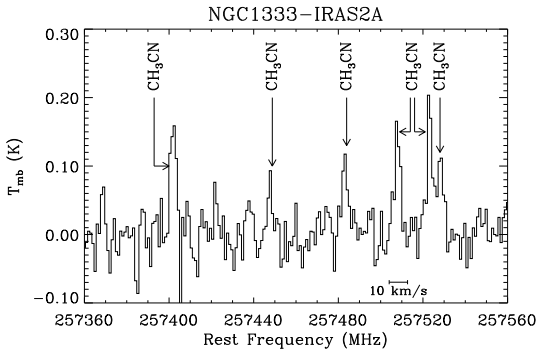

Figure 3.3 Observed spectrum towards NGC1333-IRAS2A. The rms and spectral resolution are 28 mK and 1.2 km s^{-1}.

3.3 Rotational diagram method

Rotational diagrams allow us to calculate the rotational temperature T and the column density N of a molecule, from the observed integrated intensities $\int T_{\rm mb} dv$. Section 3.3.1 details the general method while Section 3.3.2 explains how multiplets were dealt with.

3.3.1 Singlets

In the approximation of an optically thin line-emission of a transition from an upper (u) to a lower (l) state, the column density in the upper state is given by:

$$N_u = \frac{8\pi k \nu^2 \int T_{\rm mb} {\rm dv}}{hc^3 A_{ul}}$$

where k = Botzmann constant = $1.38{\times}10^{-16}$ erg K^{-1},
ν = frequency of the transition (Hz),
$\int T_{\rm mb}$dv is the integrated intensity,
h = Planck constant = $6.27{\times}10^{-27}$ erg s,
c = speed of light = $3{\times}10^{10}$ cm s^{-1},
A_{ul} = Einstein A-coefficient for the transition (or probability of emission, s^{-1}).

The rotational diagram method I describe here will allow me to derive column densities in a single beamsize. However, the observations were made at different frequencies, so that the measured integrated intensities (see Tables 3.2, 3.3 and 3.4 in Section 3.4) refer to the beamsizes corresponding to the frequencies at which the transitions were detected. For the sources I observed, the size of emission region (θ_s) is smaller than the beamsize (θ_b). Indeed, interferometric observations of IRAS16293 (Section 4.3.1, Kuan et al. 2004; Bottinelli et al. 2004b; Chandler et al. 2005), IRAS4A (Section 4.3.2) and NGC1333-IRAS2A (Jørgensen et al. 2005a) show that the bulk of the emission is $\lesssim 1''$, which is much smaller than the smallest beamsize achievable with the IRAM-30m. Therefore, for a given molecule, I can correct the integrated intensities observed at lower frequencies (i.e. in a larger beam) for beam dilution with respect to $\theta_{\rm b,min}$, the smallest beamsize in which a transition of that molecule was detected. Hence:

$$\begin{aligned} N_u &= \frac{8\pi k \nu^2 \int T_{\rm mb} dv \left(\frac{\theta_b}{\theta_{b,\rm min}}\right)^2}{hc^3 A_{ul}} \\ &= \frac{8\pi k}{hc^3} \times \frac{\nu^2 I}{A_{ul}} \end{aligned} \quad (3.1)$$

where I is the integrated intensity corrected for beam dilution.

Dividing both sides by the degeneracy of the upper level, g_u, and plugging in numbers yields:

$$\frac{N_u}{g_u} = C \frac{(\nu[{\rm GHz}])^2 \ I[{\rm K\ km\ s^{-1}}]}{A_{ul} g_u} \quad (3.2)$$

where C = constant = 1937.5.

Assuming local thermal equilibrium (LTE, which occurs when the density is larger than the critical density), the level populations follow the Boltzmann distribution:

$$N_u = \frac{N}{Z(T)} g_u \; e^{-E_u/kT} \tag{3.3}$$

where:
$Z(T)$ (also called $Q(T)$) is the partition function of the molecule at temperature T and is given by:

$$\sum_i \; g_i \; e^{-E_i/kT} \tag{3.4}$$

E_u = energy of the upper level[2].

Taking the natural logarithm, we have:

$$\ln\left(\frac{N_u}{g_u}\right) \;=\; \ln\left(\frac{N}{Z(T)}\right) - \frac{E_u}{kT} \;=\; -\frac{1}{T}\;\frac{E_u[\mathrm{erg}]}{k} + ln\left(\frac{N}{Z(T)}\right) \tag{3.5}$$

$$\underbrace{\ln\left(\frac{N_u}{g_u}\right)}_{y} = \underbrace{-\frac{1}{T}}_{a} \;\; \underbrace{E_u[\mathrm{K}]}_{x} + \underbrace{\ln\left(\frac{N}{Z(T)}\right)}_{b} \tag{3.6}$$

From observations, we know I, hence using equation 3.2, we can plot $y = \ln\left(\frac{N_u}{g_u}\right)$ vs $x = E_u$ (in K), as shown schematically on Figure 3.4.

The best line fit to the data points yields:

1. the slope $a = -\frac{1}{T}$, i.e. T=$-1/a$

2. the intercept $b = \ln\left(\frac{N}{Z(T)}\right)$, i.e. $N = Z(T)e^b$

In principle, the partition function can be computed from Equation 3.4 since the E_i's and g_i's are known and tabulated in molecular databases such as the one from the JPL[3]. In practice however, it was obtained by interpolating from the values given by the JPL molecular database at a number of temperatures.
Hence we can calculate N, the column density averaged over $\theta_{b,\mathrm{min}}$. We can then obtain the column density of the molecule in a hot corino of size $\theta_{\mathrm{hc}} < \theta_{b,\mathrm{min}}$:

$$N_{\mathrm{hc}} = N \times \left(\frac{\theta_{\mathrm{hc}}}{\theta_{b,\mathrm{min}}}\right)^2 \tag{3.7}$$

[2]A note on units for E_u: in equation 3.3, E_u is in erg, but in the JPL molecular database, E_u is given in cm^{-1}. However, as can be seen from what follows equation 3.6, the most useful unit for E_u is K (1 K = 1.44 cm^{-1}).

[3]http://spec.jpl.nasa.gov/

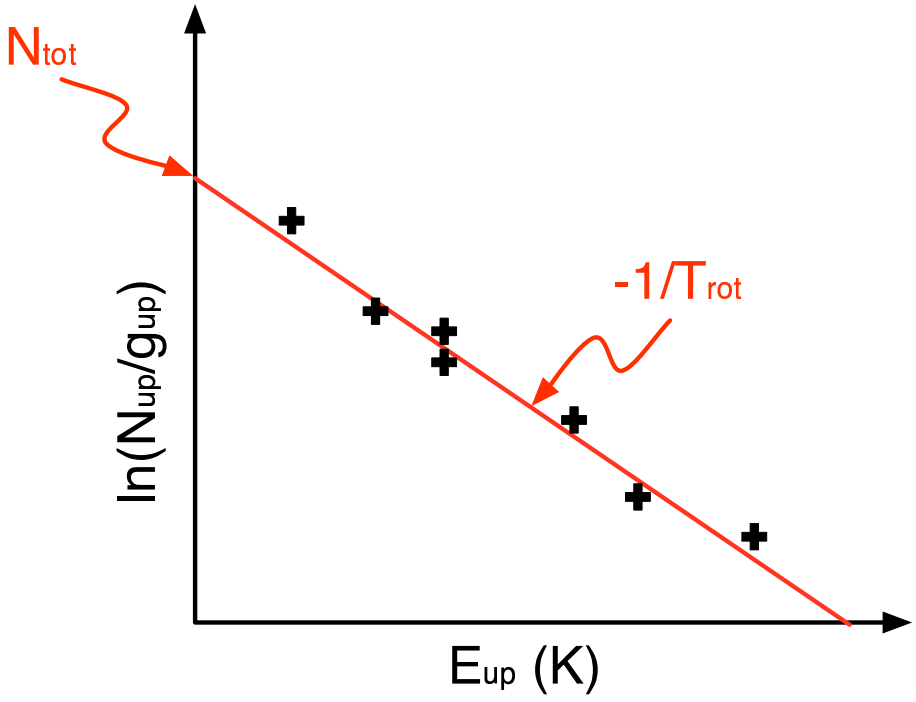

Figure 3.4 Schematic view of a rotational diagram.

and finally the abundance of the molecule in the hot corino:

$$x_{\rm hc} = \frac{N_{\rm hc}}{N_{\rm H_2}} \tag{3.8}$$

where $N_{\rm H_2}$ is the hydrogen column density in the hot corino.

3.3.2 Multiplets

Unresolved multiplets require a specific treatment in the rotational diagram method. Indeed in this case, only one line is observed, but it consists in several individual transitions i with the same (or very close) frequency ν and the same upper energy E_u, but different Einstein coefficients $A_{ul}(i)$ and degeneracies $g_u(i)$.
The general method described in Section 3.3.1 can be applied to each transition i, i.e. I want to plot $\ln(N_u(i)/g_u(i))$ vs E_u. However, since the transitions are unresolved, the individual $I(i)$ cannot be measured, so Equation 3.2 cannot be used directly to determine $\ln(N_u(i)/g_u(i)$. Instead, the latter needs to be related to the observable, I, in order to draw the rotational diagram.
On the one hand, I, the observed integrated intensity (corrected for beam dilution), is the sum

of the integrated intensity for each transition i:

$$I = \sum_i I(i) \tag{3.9}$$

On the other hand, Equation 3.2 becomes:

$$N_u(i) = C\frac{\nu^2 I(i)}{A_{ul}(i)} \tag{3.10}$$

$$\Rightarrow I(i) = \frac{A_{ul}(i)}{C\nu^2} N_u(i) \tag{3.11}$$

Therefore:

$$I = \sum_i \left(\frac{A_{ul}(i)}{C\nu^2} N_u(i)\right) = \frac{1}{C\nu^2} \sum_i \left(A_{ul}(i)\ g_u(i)\ \frac{N_u(i)}{g_u(i)}\right) \tag{3.12}$$

Now, from Equation 3.2, we have:

$$\frac{N_u(i)}{g_u(i)} = \frac{N}{Z(T)}\ \exp\left(-\frac{E_u}{kT}\right) \tag{3.13}$$

i.e. $N_u(i)/g_u(i)$ is a constant since, as mentioned above, the multiplets have the same E_u. Hence:

$$I = \frac{1}{C\nu^2}\ \frac{N_u(i)}{g_u(i)}\ \sum_i (A_{ul}(i)\ g_u(i))$$

$$\Rightarrow \frac{N_u(i)}{g_u(i)} = C\ \frac{\nu^2\ I}{\sum_i (A_{ul}(i)\ g_u(i))} \tag{3.14}$$

Using Equation 3.14, I can plot $\ln(N_u(i)/g_u(i))$ vs E_u; the rotational temperature and column density can then be determined in the same way as for the singlets (Equations 3.6, 3.7 and 3.8).

3.4 Results

3.4.1 Detections

Most of the complex molecules I searched for in IRAS4A were detected (transitions are listed in Table 3.2). In IRAS4B and IRAS2A, only $HCOOCH_3$ and/or CH_3CNwere detected (Tables 3.3 and 3.4 respectively), but overall, *my observations confirm the presence of complex molecules and hence of hot corinos in these three sources.*

I considered as good identifications only lines with a 3-σ detection and a $V_{\rm LSR}$=7.0±0.4 km s^{-1}. For each molecule, I also list in the aforementionned tables, the transition lines, their corresponding frequencies and energies of the upper levels, as well as the parameters (peak temperature, full-width at half-maximum, and integrated intensity) determined from a gaussian fit. Other parameters necessary to apply the rotational diagram method, namely the Einstein

A-coefficients A_{ul} and degeneracy of the upper level g_u, can be found in Table C. A_{ul}s are derived from the parameter $\log(I)$ listed in that table by:

$$A_{ul} = \frac{2.7964 \times 10^{-10}\ I\ \nu^2\ Q_{300}}{g_u\ (e^{-E_l/300} - e^{-E_u/300})} \tag{3.15}$$

where ν is the frequency in GHz, Q_{300} is the partition function at 300 K, and E_l and E_u are the energies of the lower and upper levels, respectively, of the transition.

Remarks

- There were a couple of tentative detection of C_2H_5OH: $4_{1,4} - 3_{0,3}$ at 90.118 GHz in IRAS4A and $10_{2,9} - 9_{1,8}$ at 226.661 GHz in IRAS4B. Although the $10_{2,9} - 9_{1,8}$ transition has a greater probability of occuring than the $4_{1,4} - 3_{0,3}$ transition ($\log(I)$=-3.9 vs -4.8), it was not seen in IRAS4A, which could be due to the fact that it also has a higher energy (28 vs 3.5 cm^{-1}).
- No observations were made at 110 GHz for IRAS2A (see Table 3.1).
- The rms reached at 257 GHz for IRAS4B is too high to detect the CH_3CN transitions at this frequency, if the line ratios are similar to those in IRAS4A.

3.4.2 Rotational diagrams, column densities and abundances

Following the method described in Section 3.3, I plotted rotational diagrams for the molecules with at least 2 detected transitions:

- in IRAS4A: $HCOOCH_3$-A and $HCOOCH_3$-E (Figure 3.5(a)), and HCOOH and CH_3CN (Figure 3.5(b));
- in IRAS4B: $HCOOCH_3$-A and CH_3CN (Figure 3.5(c));
- in IRAS4B: CH_3CN (Figure 3.5(d)).

The derived rotational temperatures and beam-averaged column densities are listed in Tables 3.5. This table also gives the hot corino abundances which were calculated using Equations 3.7 and 3.8 and the hot corino sizes and H_2 column densities derived from Maret et al. (2004).

Upper limits

No transitions were detected for the following molecules:

- HCOOH in IRAS4B and IRAS2A;
- $HCOOCH_3$ in IRAS2A;

Table 3.2 Molecular lines detected toward NGC1333-IRAS4A.

Molecule	Transition line	Frequency (MHz)	E_u [a] (cm^{-1})	$T_{mb} \pm$ rms (mK)	ΔV [b] $\pm \delta V$ [c] (km s^{-1})	$\int T_{mb} dV$ (K km s^{-1})
$HCOOCH_3$-A	$7_{2,5} - 6_{2,4}$	90156.5	13.7	22 ± 5	1.5 ± 0.5	0.036 ± 0.008
	$8_{0,8} - 7_{0,7}$	90229.7	13.9	16 ± 5	2.5 ± 0.5	0.041 ± 0.009
	$8_{3,6} - 7_{3,5}$	98611.1	18.9	28 ± 7	1.2 ± 0.2	0.036 ± 0.006
	$8_{4,5} - 7_{4,4}$	98682.8	22.2	95 ± 2	4.2 ± 1.9	0.042 ± 0.015
$HCOOCH_3$-E	$7_{2,5} - 6_{2,4}$	90145.7	13.7	14 ± 5	1.3 ± 0.5	0.019 ± 0.007
	$8_{0,8} - 7_{0,7}$	90227.8	14.0	16 ± 5	3.1 ± 0.5	0.055 ± 0.008
	$8_{3,6} - 7_{3,5}$	98607.8	18.9	13 ± 4	3.8 ± 0.9	0.054 ± 0.017
	$8_{4,5} - 7_{4,4}$	98711.7	22.2	22 ± 7	1.4 ± 0.2	0.034 ± 0.009
	$20_{2,18} - 19_{2,18}$	226713.1	83.6	61 ± 26	1.6 ± 0.8	0.099 ± 0.038
	$20_{3,18} - 19_{3,17}$	226773.3	83.6	54 ± 19	2.1 ± 0.8	0.121 ± 0.040
HCOOH	$4_{2,2} - 3_{2,1}$	90164.5	16.4	16 ± 5	0.8 ± 0.5	0.015 ± 0.008
	$6_{2,4} - 5_{2,3}$	135737.7	24.6	15 ± 5	1.8 ± 1.4	0.029 ± 0.008
CH_3CN [d]	$6_{3,0} - 5_{3,0}$	110364.6	57.6	24 ± 6	4.8 ± 0.8	0.110 ± 0.055
	$6_{2,0} - 5_{2,0}$	110375.1	32.8	46 ± 6	2.3 ± 0.8	0.112 ± 0.012
	$6_{1,0} - 5_{1,0}$	110381.5	17.9	67 ± 6	3.1 ± 0.8	0.241 ± 0.033
	$6_{0,0} - 5_{0,0}$	110383.6	12.9	83 ± 6	4.0 ± 0.8	0.347 ± 0.008
	$14_{4,0} - 13_{4,0}$	257448.9	143.9	40 ± 12	3.3 ± 1.2	0.141 ± 0.008
	$14_{3,0} - 13_{3,0}$	257482.7	109.1	53 ± 19	2.6 ± 0.4	0.150 ± 0.008
	$14_{2,0} - 13_{2,0}$	257507.9	84.3	59 ± 19	3.1 ± 0.4	0.195 ± 0.008
	$14_{1,0} - 13_{1,0}$	257522.5	69.4	74 ± 19	2.2 ± 0.4	0.172 ± 0.008
	$14_{0,0} - 13_{0,0}$	257527.4	64.4	68 ± 12	3.8 ± 1.2	0.274 ± 0.008

[a] Energy of the upper level of the transition.
[b] Width of the observed line (full-width at half-maximum of the fitted gaussian).
[c] Spectral resolution of the observation (when possible, the integrated intensity was derived from the high resolution data).
[d] All the CH_3CN lines are (unresolved) triplets. The quoted signal is the integral over each triplet. Larger linewidths could be due to the larger spacing between the components of the triplets.

Table 3.3 Molecular lines detected toward NGC1333-IRAS4B.

Molecule	Transition line	Frequency (MHz)	E_u (cm^{-1})	T_{mb} ± rms (mK)	$\Delta V^a \pm \delta V^b$ (km s^{-1})	$\int T_{mb} dV$ (K km s^{-1})
$HCOOCH_3$-A	$7_{2,5} - 6_{2,4}$	90156.5	13.7	26 ± 7	0.6 ± 0.3	0.017 ± 0.004
	$8_{0,8} - 7_{0,7}$	90229.7	13.9	23 ± 7	0.5 ± 0.3	0.013 ± 0.004
	$8_{3,6} - 7_{3,5}$	98611.1	18.9	21 ± 7	0.7 ± 0.2	0.016 ± 0.004
$HCOOCH_3$-E	$8_{0,8} - 7_{0,7}$	90227.8	14.0	18 ± 6	1.8 ± 0.5	0.035 ± 0.005
CH_3CN[d]	$6_{4,0} - 5_{4,0}$	110349.7	92.3	18 ± 5	2.3 ± 0.8	0.045 ± 0.009
	$6_{3,0} - 5_{3,0}$	110364.6	57.6	17 ± 5	2.8 ± 0.8	0.049 ± 0.011
	$6_{2,0} - 5_{2,0}$	110375.1	32.8	24 ± 5	2.5 ± 0.8	0.062 ± 0.013
	$6_{1,0} - 5_{1,0}$	110381.5	17.9	33 ± 5	3.4 ± 0.8	0.119 ± 0.014
	$6_{0,0} - 5_{0,0}$	110383.6	12.9	42 ± 5	3.8 ± 0.8	0.171 ± 0.015

[a] Energy of the upper level of the transition.
[b] Width of the observed line (full-width at half-maximum of the fitted gaussian).
[c] Spectral resolution of the observation (when possible, the integrated intensity was derived from the high resolution data).
[d] All the CH_3CN lines are unresolved triplets, except at 110349.7 MHz which is an unresolved doublet. The quoted signal is the integral over each triplet or doublet.

Table 3.4 Molecular lines detected toward NGC1333-IRAS2A.

Molecule	Transition line	Frequency (MHz)	E_u[a] (cm^{-1})	T_{mb} ± rms (mK)	$\Delta V^b \pm \delta V^c$ (km s^{-1})	$\int T_{mb} dV$ (K km s^{-1})
CH_3CN[c]	$14_{5,0} - 13_{5,0}$	257403.6	188.5	169 ± 28	3.8 ± 1.2	0.692 ± 0.091
	$14_{4,0} - 13_{4,0}$	257448.9	143.9	111 ± 43	1.6 ± 0.4	0.190 ± 0.046
	$14_{3,0} - 13_{3,0}$	257482.7	109.1	113 ± 28	3.4 ± 1.2	0.413 ± 0.044
	$14_{2,0} - 13_{2,0}$	257507.9	84.3	145 ± 32	2.7 ± 0.7	0.411 ± 0.055
	$14_{1,0} - 13_{1,0}$	257522.5	69.4	198 ± 28	3.1 ± 1.2	0.662 ± 0.087
	$14_{0,0} - 13_{0,0}$	257527.4	64.4	115 ± 28	3.8 ± 1.2	0.470 ± 0.068

[a] Energy of the upper level of the transition.
[b] Width of the observed line (full-width at half-maximum of the fitted gaussian).
[c] Spectral resolution of the observation (when possible, the integrated intensity was derived from the high resolution data).
[d] All the CH_3CN lines are unresolved triplets. The quoted signal is the integral over each triplet.

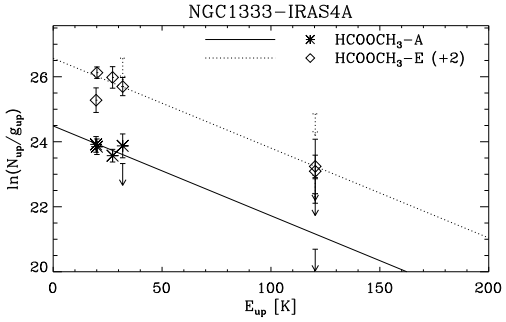

(a) Rotational diagram for $HCOOCH_3$-A and $HCOOCH_3$-E in IRAS4A.

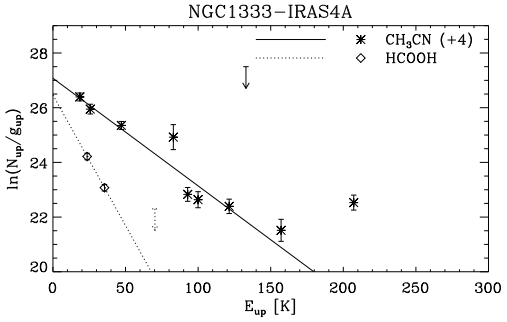

(b) Rotational diagram for HCOOH and CH_3CN in IRAS4A.

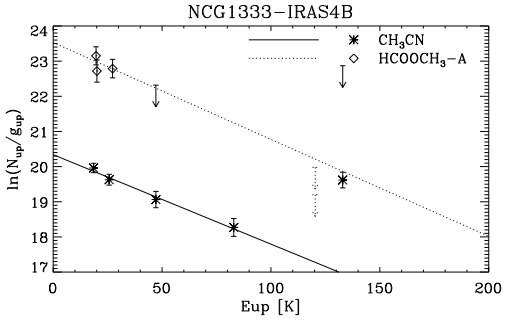

(c) Rotational diagram for $HCOOCH_3$-A and CH_3CN in IRAS4B. The excess of emission of the CH_3CN transition at 135 K is probably due to contamination from unknown line(s) and this point is not included in the fit.

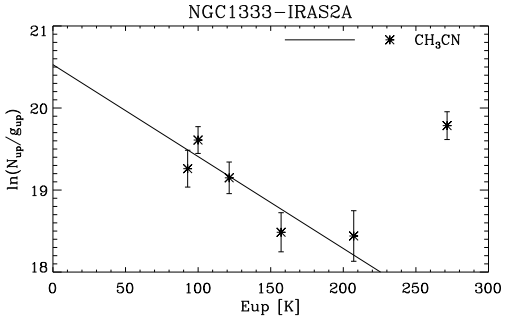

(d) Rotational diagram for CH_3CN in IRAS2A. The excess of emission of the transition at 270 K is probably due to contamination from CH_3OH $18_{3,16} - 18_{2,17}$ and this point is not included in the fit.

Figure 3.5 Rotational diagrams of the detected complex molecules in NGC1333-IRAS4A, NGC1333-IRAS4B and NGC1333-IRAS2A, corrected for beam dilution at lower frequencies. The arrows show the upper limits for undetected transitions. Lines represent the best fit to the data. Error bars are derived assuming a calibration uncertainty of 10% on top of the statistical error.

- CH_3OCH_3 and C_2H_5CN in all sources

For these molecules, I calculated the upper limits on the integrated intensities as:

$$2\sigma\ (1+\alpha)\ \delta V\ \sqrt{N_{\rm c}}\ =\ 2\sigma\ (1+\alpha)\ \sqrt{\Delta V\ \delta V} \tag{3.16}$$

where σ is the rms per channel, α is the calibration uncertainty (10%), $N_{\rm c} = \Delta V/\delta V$ is the number of channels, ΔV is the line width estimated from detected lines and δV is the channel width. Regarding the rotational temperatures, I assumed the same values as what found for detected molecules of the same type (i.e. either O-bearing or N-bearing) and in the same source, whenever possible. More specifically, I took:

- In IRAS4A, $T_{\rm rot}(CH_3OCH_3) = T_{\rm rot}(HCOOCH_3\text{-A}) = T_{\rm rot}(HCOOCH_3\text{-E})$
- In IRAS4B, $T_{\rm rot}(CH_3OCH_3) = T_{\rm rot}(HCOOH) = T_{\rm rot}(HCOOCH_3\text{-A})$
- In IRAS2A, $T_{\rm rot}(CH_3OCH_3) = T_{\rm rot}(HCOOH) = T_{\rm rot}(HCOOCH_3\text{-A}) = T_{\rm rot}(HCOOCH_3\text{-A}$, IRAS4B)
- In each source, $T_{\rm rot}(C_2H_5CN) = T_{\rm rot}(CH_3CN)$

I then used equations 3.1 and 3.3 to obtain upper limits for the beam-averaged column densities.

Remarks to Table 3.5

- The rotational temperature of $HCOOCH_3$-A in IRAS4B is poorly constrained due to the absence of points at higher energies.
- The derived CH_3CN abundance is consistent with the value obtained by Jørgensen et al. (2005b) for an inner ($T > 90$ K) region.
- The upper limit derived for the CH_3OCH_3 abundance in IRAS2A ($x < 4.2 \times 10^{-7}$) is consistent with the value quoted in Jørgensen et al. (2005a) (3×10^{-8} in an inner, $T > 90$ K region).
- Jørgensen et al. (2005a) also report a tentative detection of $HCOOCH_3$ but do not give an estimate of the abundance of this molecule.

3.5 Discussion

Since low-mass protostars were thought to have insufficient luminosities to develop a hot core-type region, I start by investigating the potential dependence of the complex molecules' abundances on the luminosity. I then look at how these abundances relate to those of major grain mantle constituents, namely CH_3OH and H_2CO.

Table 3.5 Results from the rotational diagrams and upper limits for NGC1333-IRAS4A, -IRAS4B and -IRAS2A.

Molecule	$T_{\rm rot}$ (K)	$\theta_{\rm min}$ ($''$)	$N_{\rm beam}$ [b] ($\rm cm^{-2}$)	$X_{\rm hc}$ [c]
IRAS4A — $N(\rm H_2) = 1.6 \times 10^{24}$ $\rm cm^{-2}$, $\theta_{\rm hc} = 106$ AU $= 0.48''$ [d]				
$\rm HCOOCH_3$-A	36	11	$(1.1 \pm 0.6)\times10^{14}$	$(3.4 \pm 1.7)\times10^{-8}$
$\rm HCOOCH_3$-E	36 ± 5	11	$(1.2 \pm 0.2)\times10^{14}$	$(3.6 \pm 0.7)\times10^{-8}$
HCOOH	10 ± 2	10	$(1.8 \pm 0.7)\times10^{13}$	$(4.6 \pm 1.9)\times10^{-9}$
$\rm CH_3OCH_3$	36	11	$< 5.0\times10^{13}$	$< 1.5\times10^{-8}$
$\rm CH_3CN$	27 ± 1	10	$(7.4 \pm 1.0)\times10^{12}$	$(1.6 \pm 0.2)\times10^{-9}$
$\rm C_2H_5CN$	27	11	$< 3.8\times10^{12}$	$< 1.2\times10^{-9}$
IRAS4B — $N(\rm H_2) = 8.1 \times 10^{22}$ $\rm cm^{-2}$, $\theta_{\rm hc} = 54$ AU $= 0.25''$ [d]				
$\rm HCOOCH_3$-A	38 ± 49	10	$(4.7 \pm 3.6)\times10^{13}$	$(1.1 \pm 0.8)\times10^{-6}$
HCOOH	38	22	$< 1.0\times10^{13}$	$< 1.0\times10^{-6}$
$\rm CH_3OCH_3$	38	10	$< 6.8\times10^{13}$	$< 1.2\times10^{-6}$
$\rm CH_3CN$	39 ± 3	22	$(9.7 \pm 1.0)\times10^{11}$	$(9.5 \pm 0.2)\times10^{-8}$
$\rm C_2H_5CN$	39	10	$< 4.2\times10^{13}$	$< 7.5\times10^{-7}$
IRAS2A — $N(\rm H_2) = 2.1 \times 10^{23}$ $\rm cm^{-2}$, $\theta_{\rm hc} = 94$ AU $= 0.43''$ [d]				
$\rm HCOOCH_3$-A	38	10	$< 2.9\times10^{14}$	$< 6.7\times10^{-7}$
HCOOH	38	25	$< 7.4\times10^{12}$	$< 1.2\times10^{-7}$
$\rm CH_3OCH_3$	38	10	$< 1.8\times10^{14}$	$< 4.2\times10^{-7}$
$\rm CH_3CN$	87 ± 17	10	$(3.7 \pm 1.0)\times10^{12}$	$(8.7 \pm 2.4)\times10^{-9}$
$\rm C_2H_5CN$	87	10	$< 4.3\times10^{13}$	$< 1.0\times10^{-7}$

[a] Smallest beam size for which a transition was detected (see text for details).
[b] Column density averaged over $\theta_{\rm min}$.
[c] Abundances in the hot corino using the $\rm H_2$ column densities, $N(\rm H_2)$, and hot corino sizes, $\theta_{\rm hc}$, taken from Maret et al. (2004) and given in the header of each source.
[d] At 220 pc.

3.5.1 Luminosity dependence

Before the discovery of a hot corino around IRAS16293, it was believed impossible to have chemically rich regions following mantle evaporation around low-mass protostars. The argument was that, given the low luminosity of these objects, the regions where the ices sublimate would be so small that the gas crossing-time would be shorter than the time required to form complex organic molecules in the gas-phase (e.g. Schöier et al. 2002). This is in fact not the case since several hot corinos have now been discovered (Cazaux et al. 2003; Jørgensen et al. 2005a, this work). But the question remains regarding the impact of the luminosity on the abundances of complex organic molecules in hot corinos.

Table 3.6 summarizes the measured abundances and upper limits for the four hot corinos. In order to remove the uncertainty on the sizes of the hot corinos, I choose to look at abundance ratios, in particular with respect to formaldehyde and methanol since these molecules have been proposed to be the parent molecules for complex oxygen-bearing species, if they are formed in the gas-phase. These abundance ratios are plotted on Figure 3.6 as a function of the bolometric luminosity of the low-mass protostars. For information, the abundance ratio for CH_3CN is also plotted (C_2H_5CN was not included due to the number of upper limits), although formaldehyde and methanol are not thought to be the parent molecules of nitrogen-bearing species (see Section 6.3.4).
Note that the abundance ratios of CH_3OCH_3 with respect to both H_2CO and CH_3OH in IRAS2A seem to be "outliers" compared to the other protostars and to other O-bearing molecules. However, recall that the CH_3OCH_3 abundance was taken from Jørgensen et al. (2005a) where it was derived from only one detected transition. Apart from the CH_3OCH_3 points and taking into account the uncertainties pertaining to abundance determination, one can see from Figure 3.6 that the abundance ratios of complex molecules with respect to H_2CO or CH_3OH do not depend on the luminosity, in the range $\sim 5 - 30$ $L_\odot$. Since the abundances of H_2CO or CH_3OH are not themselves a function of luminosity (see Maret et al. 2004, 2005), then *the absolute abundances of the complex species do not depend on the luminosity of the protostar*. Whatever the formation mechanism, either in the gas phase or on the grain surfaces, the efficiency in forming complex organic molecules is largely constant in the range of studied luminosities. Since the luminosity, together with the density, defines the radius at which ices sublimate, this also implies that this efficiency is rather constant in the inner 200 AUs or so of the studied sources, despite the different involved densities (from 10^6 to 10^9 cm^{-3}, Maret et al. 2004).

I also investigated the possible dependence of the abundance ratios on the ratio of submillimeter to bolometric luminosity, L_{smm}/L_{bol}, since it has been suggested as an indicator of evolutionary stage. I find that the abundance ratios do not depend on this parameter either. Maret et al. (2004) found an apparent anti-correlation between the inner abundance of H_2CO and L_{smm}/L_{bol} and proposed that this could be explained if L_{smm}/L_{bol} depends on the initial conditions of the protostars rather than their evolutionary stage. Indeed, more atomic hydro-

Table 3.6 Abundances of parent and daughter molecules in my sample of four low-mass protostars.

Molecule	IRAS16293	IRAS4A	IRAS4B	IRAS2A	Ref.
H_2CO	1×10^{-7}	2×10^{-8}	3×10^{-6}	2×10^{-7}	1,2,3
CH_3OH	1×10^{-7}	$<1\times10^{-8}$	7×10^{-7}	3×10^{-7}	4
$HCOOCH_3$-A	1.7×10^{-7}	3.4×10^{-8}	1.1×10^{-6}	$<6.7\times10^{-7}$	5,2,6
HCOOH	6.2×10^{-8}	4.6×10^{-9}	$<1.0\times10^{-6}$	$<1.2\times10^{-7}$	5,2,6
CH_3OCH_3	2.4×10^{-7}	$<2.8\times10^{-8}$	$<1.2\times10^{-6}$	3.0×10^{-8}	5,2,6,7
CH_3CN	1.0×10^{-8}	1.6×10^{-9}	9.5×10^{-8}	8.7×10^{-9}	5,2,6
C_2H_5CN	1.2×10^{-8}	$<1.2\times10^{-9}$	$<7.5\times10^{-7}$	$<1.0\times10^{-7}$	5,2,6

References – (1) Ceccarelli et al. (2000c). (2) Bottinelli et al. (2004a). (3) Maret et al. (2004). (4) Maret et al. (2005). (5) Cazaux et al. (2003). (6) This work. (7) Jørgensen et al. (2005a).

gen is available in less dense (i.e. with a higher L_{smm}/L_{bol}) environments, which leads to the formation of more H_2CO and CH_3OH. If I plot the inner CH_3OH abundance as a function of L_{smm}/L_{bol}, I also notice an apparent anti-correlation. Since the abundance ratios are roughly constant with different L_{smm}/L_{bol}, then the absolute abundances of complex molecules should also be anti-correlated with this parameter. Following a similar line of thought as Maret et al. (2004) and assuming that complex O-bearing molecules form on grain surfaces via H, O, OH and/or CH_3 additions, this anti-correlation could be indicative of these species being more readily available in less dense environments.

3.5.2 Dependence on methanol and formaldehyde hot corino abundances

Since CH_3OH and H_2CO are major grain-mantle constituents, they appear as key molecules. It is therefore interesting to investigate the abundance ratios of complex molecules to CH_3OH and H_2CO as a function of CH_3OH and H_2CO abundances themselves. I plot these quantities for hot corinos in Figures 3.7 and 3.8 respectively. From these figures, one can see that:

(i) The complex molecules in hot corinos have comparable abundance ratios, apparently independent of the CH_3OH and H_2CO abundances.

(ii) These abundance ratios are close to unity.

This implies that, whatever the formation mechanism (which will be investigated in chapter 6), complex molecules are produced efficiently.

Note that, using the methanol abundances derived by Jørgensen et al. (2005b) does not change the shape of Figure 3.7 since their values are comparable to the ones derived by Maret et al. (2005). However, if I take formaldehyde abundances from Jørgensen et al. (2005b), I obtain abundance ratios that are larger than those plotted in Figure 3.8 (as expected since Jørgensen et al. do not model any H_2CO abundance jump), and that the abundance ratios are scattered

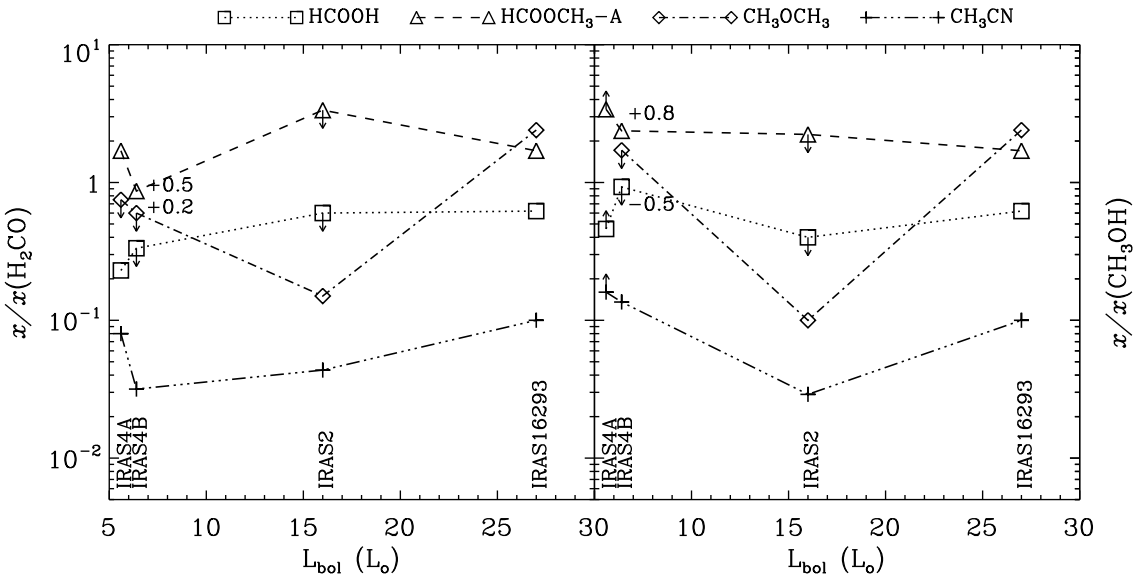

Figure 3.6 The abundances of the observed species normalized to the formaldehyde (left) and methanol (right) abundances, plotted as a function of bolometric luminosity. Square, triangles, diamonds and plus signs represent HCOOH, $HCOOCH_3$, CH_3OCH_3 and CH_3CNrespectively. The abundance for CH_3OCH_3 in IRAS2A was taken from Jørgensen et al. (2005a) and is likely underestimated (see text). Note that I only have an upper limit on the CH_3OH abundance in the hot corino of IRAS4A, therefore, I did not plot the point corresponding to CH_3OCH_3 for which only an upper limit is available in that source. Also, I do not show C_2H_5CN since only upper limits are available in three of the four sources.

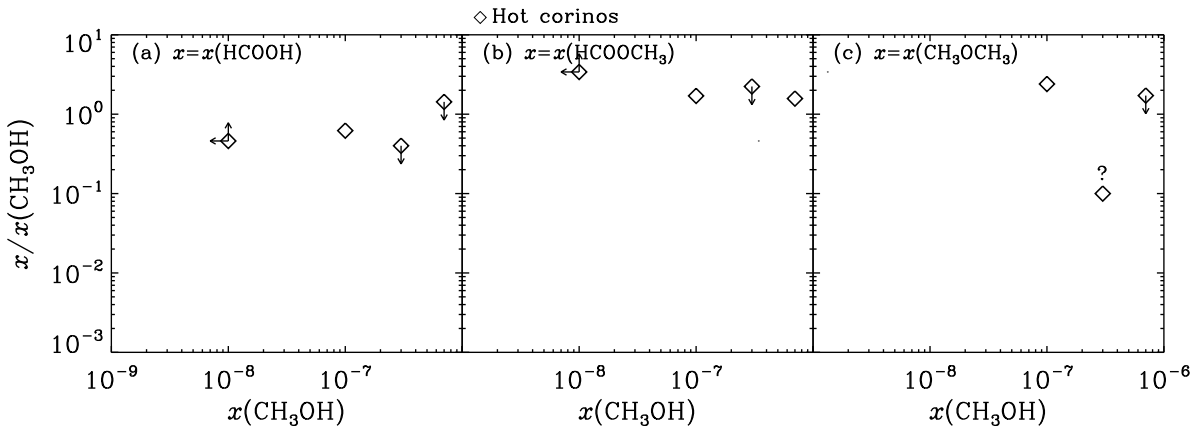

Figure 3.7 Abundance ratios of complex O-bearing molecules to methanol in hot corinos, plotted as a function of the methanol abundance in hot corinos. The point corresponding to CH_3OCH_3 in IRAS4A is not represented due to both CH_3OCH_3 and CH_3OH abundances being upper limits in this source. The question mark refers to the ratio in IRAS2A and indicates that the CH_3OCH_3 abundance is likely underestimated in this source (see Section3.5.1).

by up to two orders of magnitude.

Conclusion

In this chapter, I presented the detections of formic acid, methyl formate and/or methyl cyanide in the low-mass protostars IRAS4A, IRAS4B and IRAS2A, confirming the presence of a hot corino in their inner envelope. Note that the detections were obtained in all the sources where the complex organic molecules were searched for. It is unlikely that this is an observational bias because the selected sources are representative of Class 0 objects as they sample a range of values for a number of physical parameters (see Table B.1 and B.2).

The conclusions arising from the analysis of these observations combined with data on IRAS16293 (the first and only other hot corino discovered so far) are:

- *Hot corinos are a common phase in the formation of solar-type protostars* and complex organic molecules are ubiquitous in Class 0 protostars.

- The absolute abundances of complex molecules in hot corinos do not depend on the bolometric luminosity.

- Absolute abundances are apparently anti-correlated with L_{smm}/L_{bol}, which, in the case of grain-surface formation, could be indicative of H, O, OH and/or CH_3 being more readily available in less dense environments.

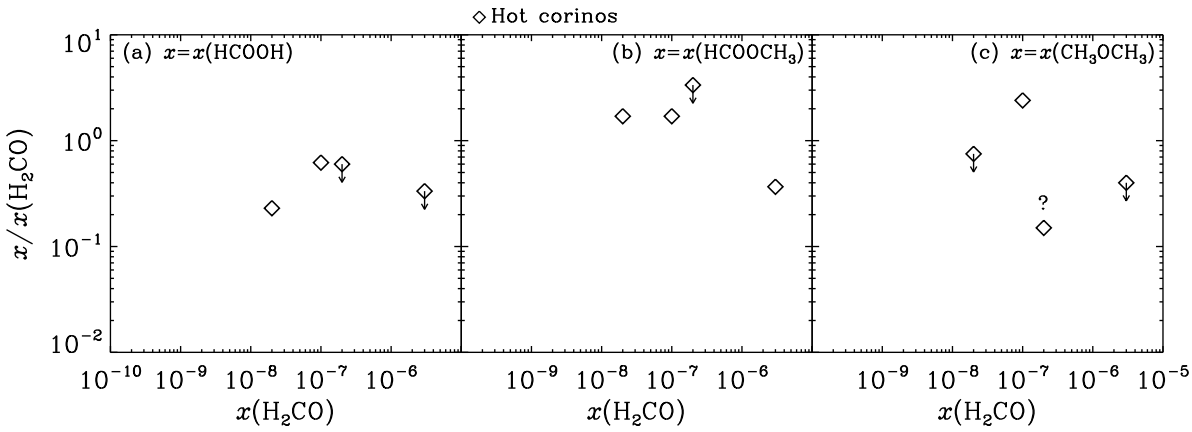

Figure 3.8 Abundance ratios of complex O-bearing molecules to formaldehyde in hot corinos, plotted as a function of the formaldehyde abundance in hot corinos.

- Abundance ratios with respect to CH_3OH and H_2CO are of order unity and do not depend on CH_3OH nor H_2CO abundances, indicating that complex molecules are formed efficiently.

Résumé du Chapitre 4
"Pister" la taille des hot corinos

Les observations décrites dans le Chapitre 3, faites avec l'IRAM-30m, un télescope à antenne unique, ont permis la détection de molécules complexes dans plusieurs protoétoiles de Classe 0, montrant ainsi que les hot corinos sont communs dans ces objets. Un paramètre clé pour la compréhension de la présence de ces molécules complexes est leur distribution spatiale. Puisque leur émission a été prédite de provenir des $\sim 1-1,5$ secondes d'arc internes (de diamètre, correspondant à $\sim 50-200$ AU, suivant la distance de la source), des observations interférométriques sont nécessaires pour atteindre cette résolution spatiale et vérifier les prédictions. J'ai donc utilisé l'interféromètre du Plateau de Bure (PdB) de l'IRAM pour observer le $HCOOCH_3$ et/ou le CH_3CN vers IRAS16293–2422 (IRAS16293) et NGC1333-IRAS4A (IRAS4A), les deux hot corinos les plus brillants. En comparant les flux mesurés avec le PdB et le 30m, je montre que l'émission des molécules complexes dans IRAS16293 provient uniquement de deux régions de taille $\lesssim 0.8-1''$, centrées sur les deux composantes de ce système binaire. Une composante compacte est aussi présente dans IRAS4A, mais en plus, une partie de l'émission est étendue. Les résultats des observations interférométriques de IRAS16293 ont été publiés dans Bottinelli et al. (2004b), et un article comportant les observations de IRAS4A est en préparation.

Chapter 4
"Tracking" the size of hot corinos

Abstract

The single-dish observations described in chapter 3 showed that hot corinos are common in Class 0 protostars, as revealed by the detection of several complex molecules. A key parameter in understanding the presence of these complex molecules is their spatial distribution. Since the emission has been predicted to originate from the inner $\sim 1-1.5''$ (in diameter, corresponding to $\sim 50-200$ AU depending on the source's distance), interferometric observations are required to reach this spatial resolution and verify the prediction. I therefore used the IRAM Plateau de Bure (PdB) Interferometer to observe $HCOOCH_3$ and/or CH_3CN in IRAS16293–2422 (IRAS16293) and NGC1333-IRAS4A (IRAS4A), the two brightest hot corinos. By comparing the fluxes measured with the PdB and the 30m, I show that the complex molecules' emission in IRAS16293 solely originates from two $\lesssim 0.8-1''$ regions centered on the two components of this proto-binary system. A compact component is also present in IRAS4A, but additionnally, some of the emission is extended.
The results of the interferometric observations of IRAS16293 have been reported in Bottinelli et al. (2004b) and an article dealing with the observations of IRAS4A is in preparation.

4.1 Introduction

Ever since the first survey of IRAS16293 by van Dishoeck et al. (1995), there has been a debate, not only about the existence of hot corinos, but also regarding the location and origin of complex organic molecules. The first debate was solved with the discovery of complex molecules in several Class 0 objects (Cazaux et al. 2003; Bottinelli et al. 2004a, 2006; Chapter 3), but the second one is still ongoing. In the hot corino definition (section 1.1.2) and in the previous chapters, I had implicitly assumed that the presence of complex organic molecules was due to thermal evaporation of the icy grain mantles across the hot corino. However, several authors have challenged this theory and other mechanisms have been suggested for the nature of complex molecule emission:

- the emission could be due to an interaction between an outflow and the inner envelope: discussing the case of IRAS16293, van Dishoeck et al. (1995) proposed that, in turbulent

shear zones where the outflow interacts with the envelope, grain-grain collisions could be effective at removing icy mantles. For the same source, Chandler et al. (2005) also invoke the passage of a jet and its shock interaction with the dense gas to account for their observed abundance enhancement.

- the complex organic molecules could be located in a circumstellar disk: for example, from their analysis of the continuum emission in IRAS2A, Jørgensen et al. (2005a) claim the presence of a disk in this source and raise the possibility that (at least some of) the complex organic molecule emission comes from this disk, whose gas would have been heated by accretion shocks (Schöier et al. 2004).

- alternatively, the interaction of UV or X-rays with the cavities excavated by the outflow would be the cause of the presence of the complex molecules (Schöier et al. 2002, 2004).

The combination of interferometric and single-dish observations can help solve the issue, as both the small and large scales of the envelopes of low-mass protostars can be sampled. The high sensitivity and high spatial resolution achievable by the PdB made it a particularly well suited instrument to investigate the small scales. I describe in section 4.2 the PdB observations of some of the transitions that had been dectected with the IRAM-30m towards IRAS16293 and IRAS4A. Discussions of the interferometric data presented in section 4.3 can be found in section 4.4.

4.2 Observations

4.2.1 IRAS16293

Observations of IRAS16293 (see Appendix B.1) were carried out at the PdB on February 1st and March 25th 2004 in the B and C configurations of the array. Five CH_3CN transitions at 110.4 GHz and 4 $HCOOCH_3$ transitions at 226.4 GHz were obtained simultaneously, along with the continuum emission at 3 mm and 1.3 mm. The receivers were tuned single side band at 3 mm and double side band at 1.3 mm. CH_3CN and $HCOOCH_3$ transitions were covered with two correlator units, each of 40 and 80 MHz bandwidth respectively. Typical system temperatures were 250 K (USB) at 3 mm and 500 K (DSB) at 1.3 mm. Phase and amplitude calibrations were obtained by observing the nearby point sources 1514-241 and NRAO 530 every 20 minutes. Bandpass calibration was carried out on 3C273 and 0851+202 and the absolute flux density scale was derived from MWC349, 3C345 and 0923+392. Data calibration was performed in the antenna based manner and uncertainties are less than 10% at 3 mm and less than 20% at 1.3 mm.

4.2.2 IRAS4A

This source, described in B.2, was observed on January 29th 2005 with the PdB in the A configuration, which is the most extended, giving the highest spatial resolution. 3 and 1.3 mm

continuum emission and five CH_3CN transitions at 110.4 GHz were obtained simultaneously. At 3 and 1.3 mm respectively, the receivers were tuned single side band and double side band, and typical system temperatures were ∼400 K (USB) and ∼300 K (DSB). CH_3CN transitions were covered with two correlator units of 40 MHz bandwidth each. Bandpass, phase and amplitude calibrations were obtained by observing the nearby point sources 3C84 and 0234+285 every 20 minutes. Data calibration was performed in the baseline based manner and uncertainties are less than 10%.

4.2.3 Data reduction

Flux densities were obtained from visibilities using standard IRAM procedures. Continuum images were produced by averaging line-free channels. Line maps were obtained by cleaning line images after subtraction of the continuum directly from the visibilities.

4.3 Results

4.3.1 IRAS16293

Figures 4.1-a and 4.1-c show the integrated line emission of CH_3CN and $HCOOCH_3$, averaged over all the transitions listed in Table 4.1 for each molecule. Continuum emission at 3 and 1.3 mm is displayed in Figures 4.1-b and 4.1-d respectively . These maps show two components which are spatially coincident with the centimeter wavelength emission regions A and B mapped by Wootten (1989) and with the millimeter wavelength emission regions MM1 and MM2 mapped by Mundy et al. (1990, 1992). As already noted in the previously mentioned works (see also Looney et al. 2000; Schöier et al. 2004), the south-east region ("source A" or "MM1") is the weakest in the continuum but brightest in line emission. On the contrary, the north-west region ("source B" or "MM2") is the brightest in the continuum and weakest in line emission. Table 4.1 gives the intensities and sizes of the line and continuum emissions. Note that the energy of the upper level of the CH_3CN transitions decreases with frequency, but that maps which were averaged over each individual transition do not show any significant difference. This means that the emitting region does not depend on the energy of the transition, i.e. on the excitation conditions (but rather on a jump of the molecular abundances). Within the errors, we recover all the line emission measured by the IRAM 30m (Cazaux et al. 2003).

Finally, the spectra at 1.3 and 3 mm of emission regions A and B are shown in Figures 4.2 and 4.3, assuming a $V_{\rm LSR}$=3.9 (panels a) and 2.7 km s^{-1} (panels b) respectively (see discussion in Section 4.4.1). Again, note that the sums of A and B (panels c of Figure 4.2 and 4.3) reproduce very well the features in the spectra obtained for the same transitions at the IRAM 30m (Cazaux et al. 2003).

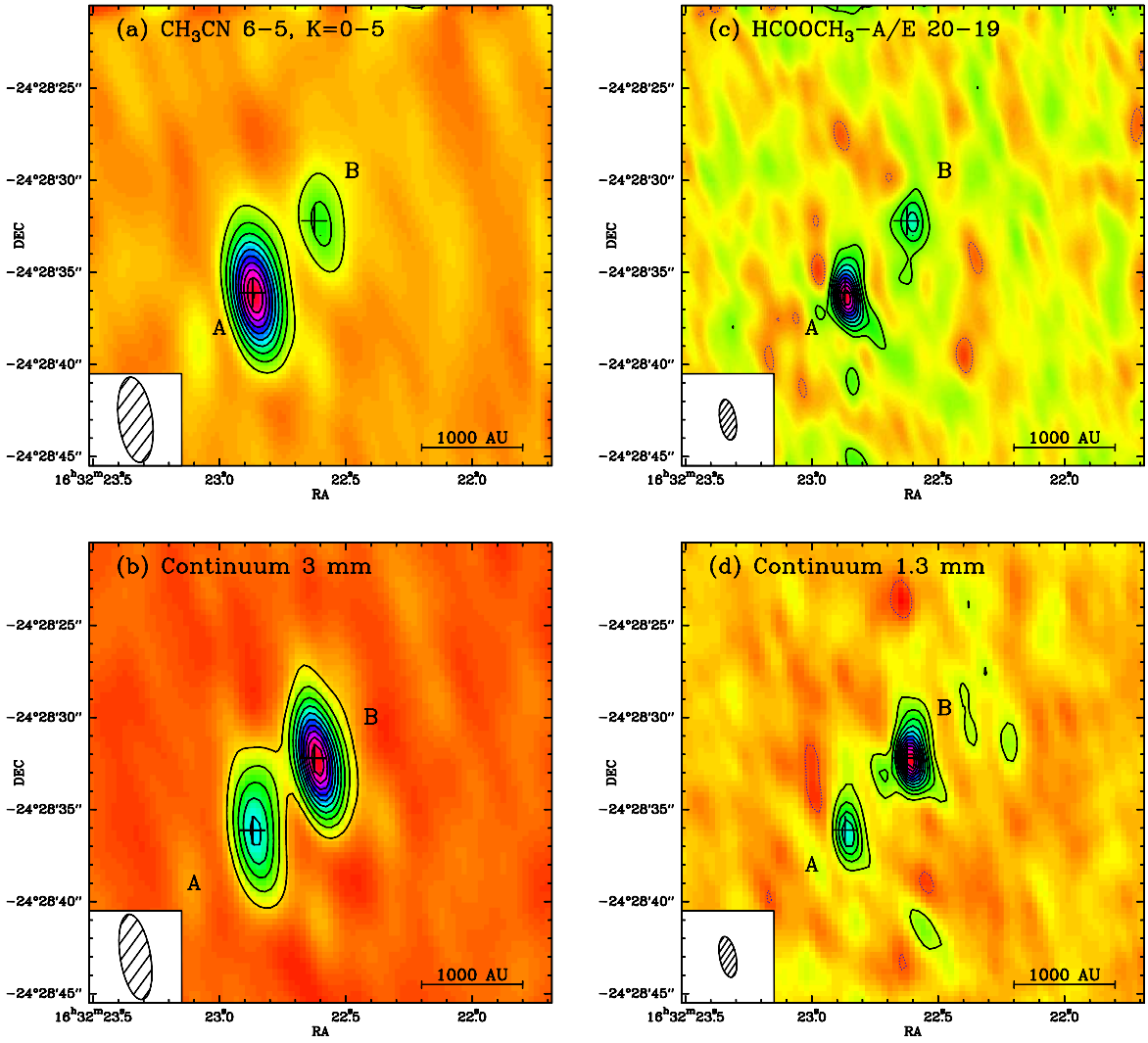

Figure 4.1 Line and continuum Plateau de Bure maps of IRAS16293–2422 — (a) Line map of CH_3CN, averaged over the five transitions listed in Table 1; the rms is 3 mJy beam^{-1}and contours range from 15 to 150 mJy beam^{-1} in steps of 15 mJy beam^{-1}. (b) Continuum emission at 3 mm, with an rms of 3 mJy beam^{-1}; contour levels range from 20 to 220 mJy beam^{-1} in steps of 20 mJy beam^{-1}. (c) Line map of $HCOOCH_3$-A and -E, averaged over the four transitions listed in Table 1; the rms is 8 mJy beam^{-1}and contour levels range from 20 to 200 mJy beam^{-1} in steps of 20 mJy beam^{-1}. (d) Continuum emission at 1.3 mm, with an rms of 15 mJy beam^{-1}; contour levels range from 50 to 600 mJy beam^{-1} in steps of 50 mJy beam^{-1}. Beam sizes are $4\farcs7 \times 1\farcs6$ and $2\farcs2 \times 0\farcs9$ at 3 and 1.3 mm respectively.

Table 4.1 Line and continuum emission measured with the Plateau de Bure in IRAS16293–2422

Molecule	Transition	E_{up}[a] (cm^{-1})	Frequency (GHz) or Wavelength	(Integrated) intensity A	(Integrated) intensity B	Size (″)[b] A	Size (″)[b] B
CH_3CN	$6_{5,0} - 5_{5,0}$	137.1	110.330	1.39(0.09)	0.51(0.06)	0.8(0.2)	< 0.8
	$6_{4,0} - 5_{4,0}$	92.4	110.350	1.70(0.08)	0.38(0.06)	0.8(0.2)	< 0.8
	$6_{3,0} - 5_{3,0}$	57.6	110.364	2.75(0.08)	0.67(0.05)	0.9(0.1)	< 0.8
	$6_{2,0} - 5_{2,0}$	32.8	110.375	2.56(0.08)	0.51(0.05)	1.2(0.1)	< 0.8
	$6_{1,0} - 5_{1,0}$	17.9	110.381	5.26(0.10)	1.05(0.07)	0.9(0.1)	< 0.8
	$6_{0,0} - 5_{0,0}$	12.9	110.383				
$HCOOCH_3$-E/A	$20_{2,19} - 19_{2,18}$	83.5	226.713/226.718	6.44(0.41)	3.36(0.36)	1.4(0.2)×0.7(0.1)	0.8(0.2)
	$20_{1,19} - 19_{1,18}$	83.5	226.773/226.778	11.13(0.49)	4.05(0.39)	1.6(0.1)×0.8(0.1)	0.8(0.1)
continuum			3 mm	0.17	0.26	3.4×1.4	1.5×0.8
continuum			1.3 mm	0.77	1.02	3.7×1.2	1.5×0.8

NOTES — The line intensity is in units of Jy km s^{-1}, while the continuum is in Jy. Errors are given in parentheses.
[a] Energy of the upper level of the transition.
[b] FWHM of gaussian fit.

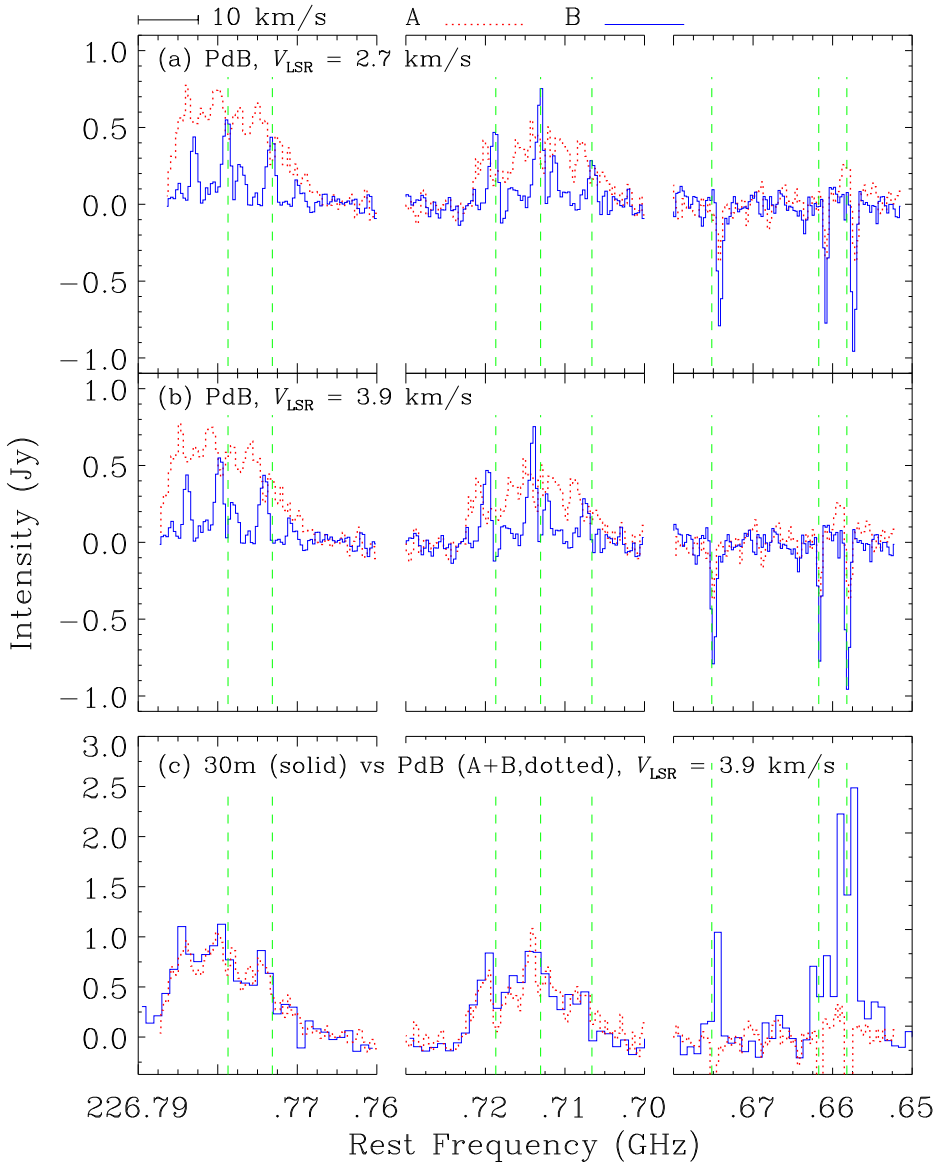

Figure 4.2 1 mm spectra of IRAS16293–2422 — (a) Spectra at 1 mm averaged over the emission regions of sources A (dotted line) and B (solid line), and displayed for $V_{\rm LSR}$=2.7 km s^{-1}. The velocity resolution is 0.4 km s^{-1} and rms are 0.08 and 0.06 Jy for A and B respectively. (b) Same as (a) but with $V_{\rm LSR}$=3.9 km s^{-1}. (c) The solid line represents the spectrum obtained at the IRAM 30m (Cazaux et al. 2003) with a velocity resolution of 1.3 km s^{-1}and rms of 0.11 Jy. Overlayed in dotted line is the sum of the Plateau de Bure spectra of sources A and B (rms=0.10 Jy). Vertical lines indicate the frequencies of $HCOOCH_3$-A, $HCOOCH_3$-E and CH_3OD lines (emission) and CN lines (absorption). Right to left are CN $2_{\frac{3}{2},\frac{5}{2}} - 1_{\frac{1}{2},\frac{3}{2}}$, $2_{\frac{3}{2},\frac{1}{2}} - 1_{\frac{1}{2},\frac{1}{2}}$, $2_{\frac{3}{2},\frac{3}{2}} - 1_{\frac{1}{2},\frac{1}{2}}$, CH_3OD $5_{2,4} - 4_{2,3}$, $HCOOCH_3$-E and -A $20_{2,19} - 19_{2,18}$, $HCOOCH_3$-E and -A $20_{1,19} - 19_{1,18}$.

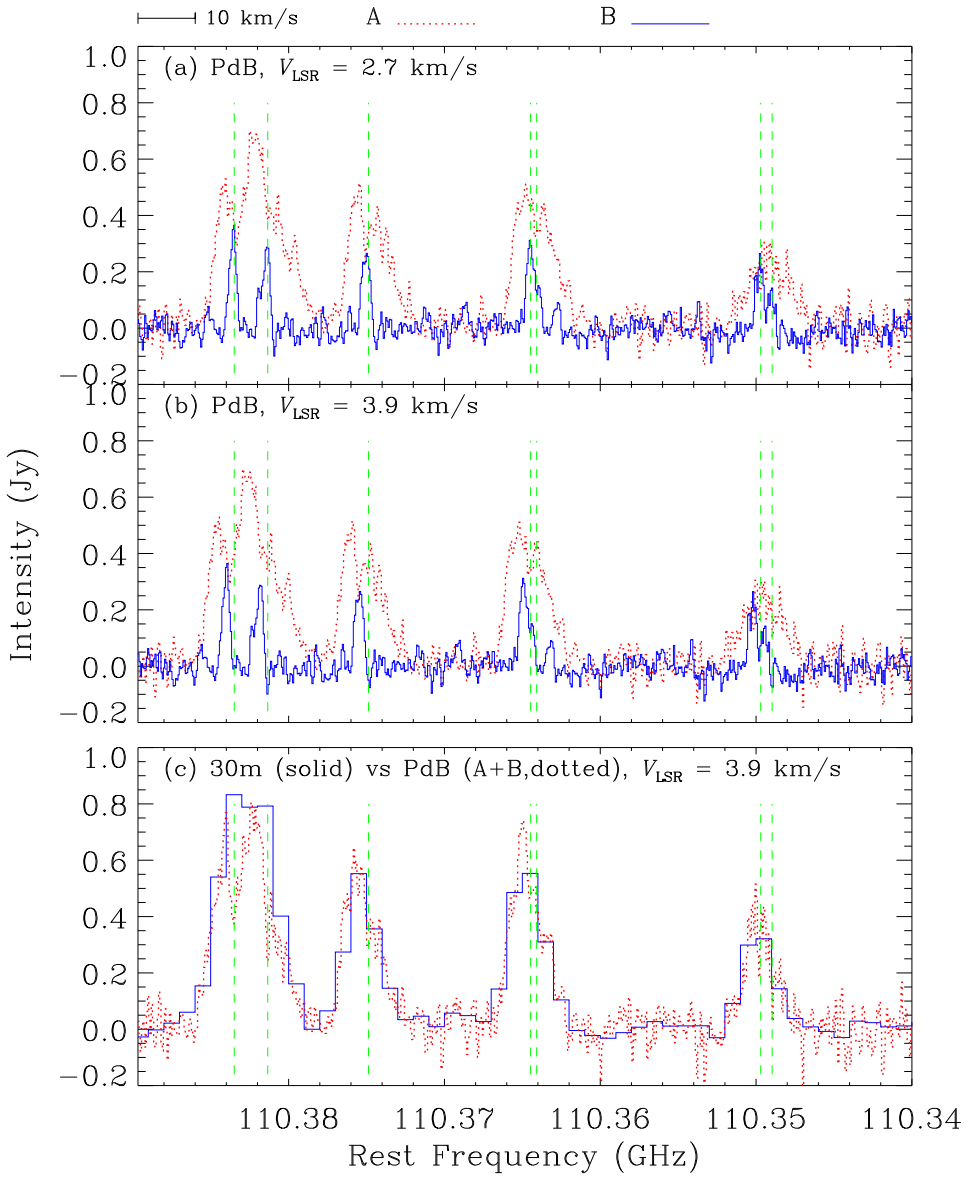

Figure 4.3 3 mm spectra of IRAS16293–2422 — (a) Spectra at 3 mm averaged over the emission regions of sources A (dotted line) and B (solid line), and displayed for $V_{\rm LSR}$=2.7 km s^{-1}. The velocity resolution is 0.2 km s^{-1} and rms are 0.05 and 0.04 Jy for A and B respectively. (b) Same as (a) but with $V_{\rm LSR}$=3.9 km s^{-1}. (c) The solid line represents the spectrum obtained at the IRAM 30m (Cazaux et al. 2003) with a velocity resolution of 2.7 km s^{-1}and rms of 0.03 Jy. Overlayed in dotted line is the sum of the Plateau de Bure spectra of sources A and B (rms=0.06 Jy). Vertical lines indicate the frequencies of CH_3CN $6-5$, $K=0-4$ (left to right); these transitions are triplets which are partly resolved for K=3 and 4.

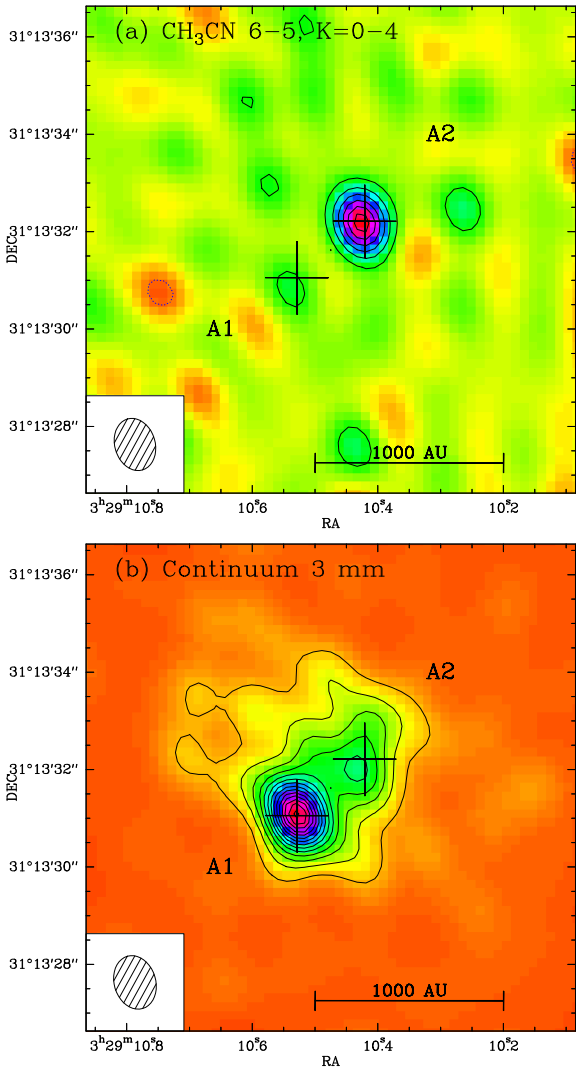

Figure 4.4 Line and continuum Plateau de Bure maps of NGC1333-IRAS4A — (a) Line map of CH_3CN, averaged over the transitions listed in Table 4.2; the rms and contour levels are 2 and 5 mJy beam^{-1} respectively. — (b) Continuum emission at 3 mm; the rms and contour levels are 1 and 10 mJy beam^{-1} respectively. — (c) Continuum emission at 1.3 mm; the rms and contour levels are 6 and 25 mJy beam^{-1} respectively. — Beam sizes are $1''.1 \times 0''.8$ in (a) and (b) and $0''.7 \times 0''.5$ in (c).

Table 4.2 Line and continuum emission measured with the Plateau de Bure in NGC1333-IRAS4A.

Molecule	Transition	E_{up}[a] (cm^{-1})	Frequency (GHz) or Wavelength	(Integrated) intensity A1	(Integrated) intensity A2	Size (″)[b] A1	Size (″)[b] A2
CH_3CN	$6_{3,0} - 5_{3,0}$	57.6	110.364	–	0.58(0.07)	< 0.6	0.9(0.1)
	$6_{2,0} - 5_{2,0}$	32.8	110.375	–	0.17(0.02)	< 0.6	< 0.6
	$6_{1,0} - 5_{1,0}$	17.9	110.381	–	0.32(0.05)	< 0.6	0.6(0.2)
	$6_{0,0} - 5_{0,0}$	12.9	110.383	–	0.40(0.06)	< 0.6	0.7(0.1)
continuum			3 mm	0.35	0.18	1.2×0.9	2.0×1.1
continuum			1.3 mm	2.07	0.92	1.3	1.2

NOTES — The line intensity is in units of Jy km s^{-1}, while the continuum is in Jy. Errors are given in parentheses.
[a] Energy of the upper level of the transition.
[b] FWHM of gaussian fit.

4.3.2 IRAS4A

Figure 4.4-a shows the integrated line emission of CH_3CN averaged over all the transitions listed in Table 4.2, while the 3 mm continuum is displayed in Figure 4.4-b. The continuum maps show two components whose peak positions and separation (1.″8 ∼ 390 AU at 220 pc) are consistent with that found in other (sub)millimeter works (Lay et al. 1995; Looney et al. 2000), as well as in the centimeter regime (Reipurth et al. 2002). The line emission map is, however, new and shows that the component that is the weakest in the continuum (the north-west region, A2) possesses CH_3CN emission, whereas the brightest continuum region (A1 in the south-east) does not have any counterpart in the line map, down to 2 mJy $beam^{-1}$. This line-continuum contrast is reminiscent of what was found for IRAS16293 in section 4.3.1.

Table 4.2 gives the intensities and sizes of the line and continuum emission, and Figure 4.5 shows the CH_3CN spectrum averaged over the emission region around A2 overlaid with the spectrum obtained at the IRAM-30m by Bottinelli et al. (2004a). For the K=3, all the emission measured by the IRAM-30m is recovered by the PdB (within the errors), whereas only ∼25% of the single-dish emission is recovered for the lower-energy transitions (K=0–2).

4.4 Discussion

4.4.1 IRAS16293

The most important result of the presented observations is that the complex molecules observed by Cazaux et al. (2003) originate in two compact regions, whose diameters are about 1.5″ (A) or less (B), as shown in Figure 4.1 (and Table 4.1). This goes along with the fact that the images do not show any evidence of emission associated with the molecular outflows seen at larger scales (see below for the discussion on the line profiles). Also, following the remark in section 4.1, the

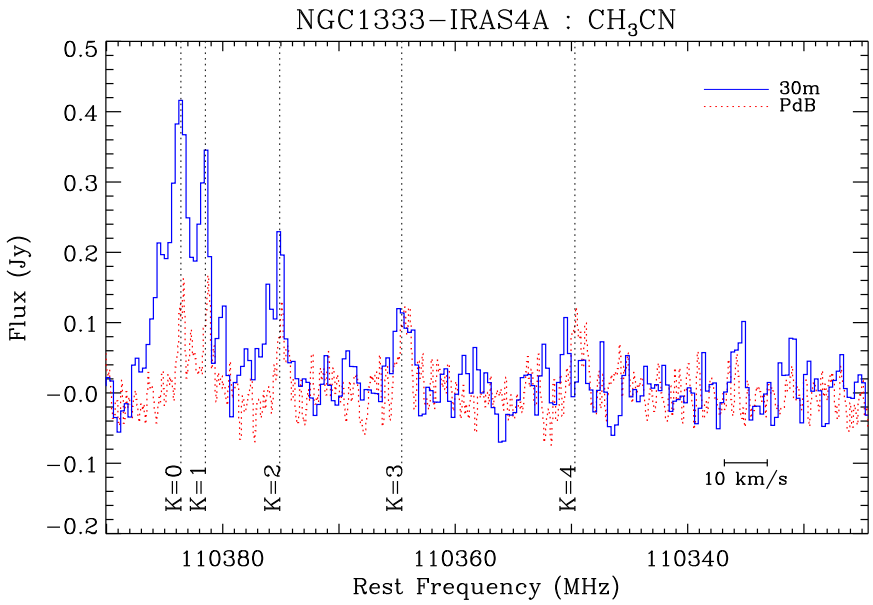

Figure 4.5 CH_3CN spectra towards NGC1333-IRAS4A. — The solid blue line represents the spectrum obtained at the IRAM 30m (Bottinelli et al. 2004a) with a velocity resolution of 0.8 km $s^{-1}$and rms of 0.03 Jy. Overlayed in dotted red line is the Plateau de Bure spectrum averaged over the emission region of IRAS4A2 (velocity resolution=0.2 km s^{-1}, rms=0.03 Jy). Vertical dashed lines indicate the frequencies of the CH_3CN transitions.

Plateau de Bure images do not reveal any evidence of emission from cavities excavated from the outflows either. Indeed, the cavities are typically $\sim$ 20" in size, located $\sim$ 30" away from the source along the ^{12}CO outflow (see e.g. Arce & Sargent 2004), which would have been easily detected by the Plateau de Bure. The two regions where the molecular emission comes from, are compact, and while source A is barely resolved in the 1mm images, source B is unresolved. The measured sizes (1.5″ at 160 pc correspond to a radius of about 120 AU) are remarkably consistent with the emission coming from a region where the dust temperature exceeds 100 K in source A (150-200 AU: based on multi-frequency single dish observations: Ceccarelli et al. 2000a,c; Schöier et al. 2002), and therefore, where the grain mantles sublimate. Thus, these observations support the basic prediction (from the modeling of the single dish observations; Ceccarelli et al. 2000a,c; Cazaux et al. 2003) that a hot corino with a radius of about 150 AU exists inside the cold envelope of IRAS16293, and that in that region, complex molecules are formed because of grain mantle evaporation.

In addition to that, the Plateau de Bure observations confirm that the two sources A and B are different, as noted by previous authors (Wootten 1989; Mundy et al. 1990, 1992). They differ in line intensities and extent (Fig. 4.1), and this may correspond to a difference in their chemical composition. But, before discussing this point, it is necessary to address the second most striking difference in the two sources: their line profiles (Figures 4.2 and 4.3). Source A has clearly broadened spectra (FWHM $\sim$ 8 km s^{-1}), while source B shows apparently much

narrower profiles (FWHM $\sim$ 2 km s^{-1}). Furthermore, the lines of source B seem to peak at $V_{\rm LSR}$=2.7 km s^{-1}, whereas the parent cloud velocity is at $V_{\rm LSR}$=3.9 km s^{-1} (compatible with the spectra of source A, although given the broad profiles it is difficult to precisely determine the $V_{\rm LSR}$ of source A). Note that the cloud's $V_{\rm LSR}$ (3.9 km s^{-1}) is very nicely measured by the three CN absorption lines [1] in the observed band of Figure 4.2. As said, no evidence of outflowing gas is seen in the images, and also the broad line profiles of source A are consistent with gas *infalling* towards a $\sim$1 M$_\odot$ object (Ceccarelli et al. 2000a,c; Schöier et al. 2002). Therefore, both the images and line profiles of source A are fully consistent with the hot corino hypothesis.

The case of source B is less obvious: why does this source have narrower lines and why do they peak at 2.7 km s^{-1}? But is this true? A very careful look at the B spectra raises doubts. Indeed, all the B lines have a second small peak —more visible in Figure 4.2, but even there, sometimes at the limit of the noise— on the red-shifted side of the spectrum. This second peak could indeed be part of the line itself, which would be strongly self-absorbed at $V_{\rm LSR}$=3.9 km s^{-1}. If this is the case, the linewidths of source B would be $\sim$ 4-6 km s^{-1} (Fig. 4.2), similar to the linewidths measured towards source A. Note that the blue peak is expected to be brighter than the red peak in the case of optically thick lines from infalling gas (Leung & Brown 1977; Zhou 1992, 1995; Choi et al. 1995), so it would be consistent with the $\sim$ 1 M$_\odot$ hot corino hypothesis of source B too. This alternative explanation, optically thick lines in source B, is therefore very appealing and worth exploring in some detail. Using the LTE approximation, the required column densities for the CH_3CN and $HCOOCH_3$ lines to be optically thick are $N \sim 10^{16}$ cm^{-2} and $N \sim 10^{17}$ cm^{-2} respectively. These values are about one order of magnitude larger than the column density derived in B from the emission lines, assuming that the lines are optically thin, LTE populated and that the emission region fills up the Plateau de Bure synthesized beam (see below). Considering that the three adopted assumptions all underestimate the true column density, it is indeed possible, but not firmly established, that the lines in source B are optically thick. Unfortunately, "physical" considerations do not help either to distinguish between the two possible interpretations, optically thin or thick lines in source B. In the first case (B has $V_{\rm LSR}$=2.7 km s^{-1} and FWHM $\sim$ 2 km s^{-1}), source B would be less massive than A and would revolve around it at 1.2 km s^{-1} (multiplied by the inclination of the orbit), at a distance of 800 AU, which is fully consistent with $M_{\rm A} \sim 1 M_\odot$ (unless the orbit is in the sky plane). In the second case (B also has $V_{\rm LSR}$=3.9 km s^{-1} and FWHM $\sim$ 4-6 km s^{-1}), A and B have comparable masses (similar FWHM), but B is more compact. Note that the possible identification of CH_3OD in the spectrum of source B would support the case of $V_{\rm LSR}$(B)=2.7 km s^{-1}, but future high resolution observations of optically thin lines are required to definitely settle the question.

As said, the nature of source B affects the determination of the molecular abundances in this source, and hence, how much the chemical composition of the A and B hot corinos differ.

[1] The absorption originates in the foreground (envelope + cloud) cold gas, which absorbs the photons emitted in the hot corino regions (the CN emission component, being extended, is filtered out by the interferometric observations).

Using the relation between column density and observed continuum flux density, and using a dust opacity κ_ν of 0.8 cm^2 g^{-1} at 1.3 mm and a dust temperature T_d of 40 K (e.g. Walker et al. 1986), we derive molecular hydrogen column densities from the 1.3 mm continuum emission equal to $N(\mathrm{H_2, A}) = 3.5 \times 10^{24}$ cm^{-2} in A and $N(\mathrm{H_2, B}) = 1.7 \times 10^{25}$ cm^{-2} in B (consistent with the values of Mundy et al. 1992). Using these values and the CH_3CN total column densities derived from the rotational diagram method ($N_\mathrm{A} = 1.7 \times 10^{15}$ cm^{-2} and $N_\mathrm{B} = 3.9 \times 10^{14}$ cm^{-2}), we get CH_3CN abundances of 4.8×10^{-10} and 2.3×10^{-11} for A and B respectively, i.e. CH_3CN is ~ 20 times more abundant in A than in B. A rotational diagram could not be drawn for the $HCOOCH_3$ transitions as they have similar upper energy levels, but assuming T_rot ∼60 K (Cazaux et al. 2003) we get $HCOOCH_3$ column densities of $N_\mathrm{A} = 2.6 \times 10^{16}$ cm^{-2} and $N_\mathrm{B} = 8.4 \times 10^{15}$ cm^{-2}, i.e $HCOOCH_3$ abundances of 7.5×10^{-9} and 4.9×10^{-10} for A and B respectively, a factor 15 difference[2]. Note, however, that since B is unresolved in the line emission, and the lines could be optically thick (see above discussion), the molecular abundances quoted for B may be underestimated by about an order of magnitude (note also that the region of molecular emission could be more compact than the continuum emission region). Therefore, resolving the problem of the nature of the observed line emission in source B is crucial, not only to determine the dynamical state of this source, but also to correctly assess the difference in the chemical composition of sources A and B.

4.4.2 IRAS4A

There are two important outcomes from the PdB observations of this source:

1. the CH_3CN emission is concentrated in a compact region of size $\lesssim 0\farcs8$ (∼200 AU assuming a distance of 220 pc for IRAS4A) centered on the north-west component, IRASA2.

2. the comparison with the IRAM-30m observations shows that there is some extended emission arising in the low-energy transitions, whereas the high-energy ones are solely emitted in the compact region.

The modelling of H_2CO single-dish observations (Maret et al. 2004) predicted that, in IRAS4A, the dust reaches ∼100 K (the sublimation temperature of icy mantles) at a radius of about 50 AU (∼0.″23). Since the measured size is consistent with this prediction, the first result supports the theory of the presence of complex organic molecules being due to grain mantle sublimation, as in the case of IRAS16293.

In the second point, the fact that not all the flux is recovered is due to the way interferometers work. Because the observations are made with a finite number of antennas over a finite amount of time, only a portion of the paramater space (the *uv* plane) corresponding to the physical field of view can be covered. The further apart the antennas are, the less coverage there is at small *uv* distances (see Figure 4.6), which corresponds to large physical scales. Therefore,

[2]Note that the abundances quoted in Cazaux et al. differ from those derived here because of the different estimate of the H_2 column density.

extended emission is not properly sampled and does not appear on interferometric maps, i.e. interferometers are insensitive to (or resolve out) extended emission. In principle, it is possible to overcome this problem by combining interferometric and single-dish observations the later being used to "fill the central hole". However, in the case of IRAS4A, the PdB array was used in a very extended configuration so that even medium scales are poorly sampled as shown on Figure 4.6. In fact, for these observations, the array was insensitive to structures on scales larger than about $4''$ (e.g. Wilner & Welch 1994) whereas the beamsize of the IRAM-30m observations at 110 GHz was $22''$, and the missing information at intermediate scales prevents from combining the interferometric and single-dish data. Therefore, it is not possible at this stage to conclude on the spatial distribution of the extended emission. Nonetheless, the molecule's abundance profile can be determined by modeling the single-dish emission in a similar way as has been done for H_2CO and CH_3OH, i.e. with a jump from a low abundance in the cold, outer envelope to a high value in the hot corino. Assuming that about half of the single-dish emission originates from the outer envelope and an excitation temperature of $\sim 10 - 20$ K, the CH_3CN column density in an $18''$ beam is $2{\times}10^{12}$ cm^{-2}. Using the density profile derived by Jørgensen et al. (2002) yields a corresponding H_2 column density of $8{\times}10^{22}$ cm^{-2} such that the abundance in the cold envelope is $2{\times}10^{-11}$, two orders of magnitude lower than the hot corino abundance (Table 3.5, Bottinelli et al. 2004a). This abundance is somewhat lower than what has been found in the dark molecular cloud TMC-1 ($3 - 5 \times 10^{-10}$, Matthews & Sears 1983; Minh et al. 1993), a situation similar to that of H_2CO and CH_3OH for which the abundances in dark molecular clouds such as TMC-1 and L134N (e.g. Brown 1981; Pratap et al. 1997; Wootten et al. 1978; Dickens et al. 2000) are about an order of magnitude higher than the abundances in the outer envelopes of Class 0 protostars (Maret et al. 2005, 2004; Jørgensen et al. 2004). This difference is likely due to the fact that these molecules suffer depletion onto the grain mantles during the collapse phase that marks the transition between dark molecular cloud and Class 0 (e.g. Ceccarelli et al. 2006).

4.4.3 Continuum emission, complex molecules and outflows

The similarity among the features of IRAS16293 and IRAS4A are striking as demonstrated by the schemcatic view of these two source in Figure 4.7:

1. the strong continuum sources (IRAS16293B and IRAS4A1) have little or no emission from complex molecules whereas the weakest continuum sources (IRAS16293A and IRAS4A2) are the strongest in line emission from these molecules;

2. strong, highly-collimated outflows are driven by the weak continuum sources;

3. poorly collimated outflows aligned with the strong continuum sources, which are either weak (IRAS4A1) or show no indication of high-velocity gas in the vincinity of the source (IRAS16293B).

In IRAS16293, the complex morphology of outflows and the difference with the continuum have been noted for many years (e.g. Wootten 1989; Walker et al. 1993; Stark et al. 2004) but it

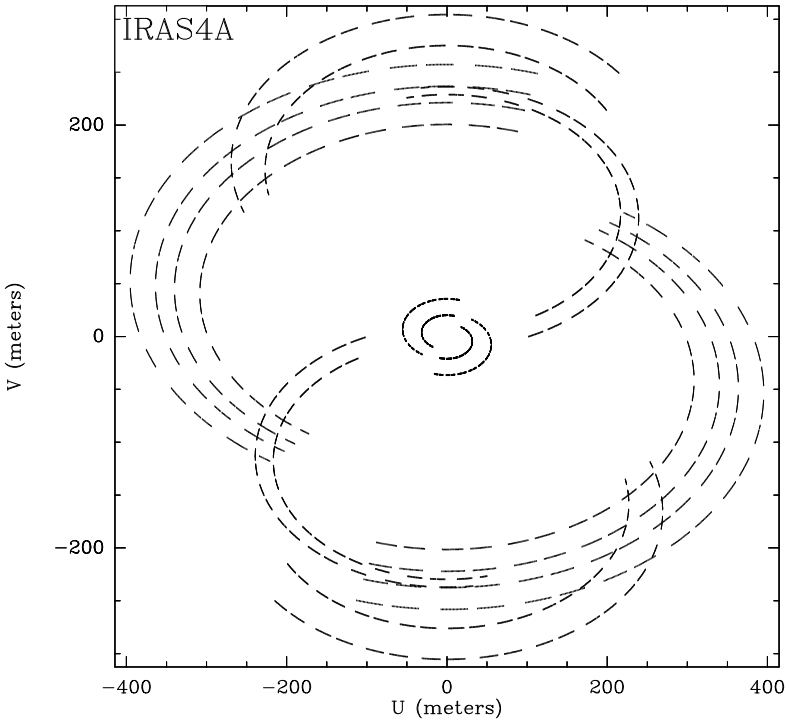

Figure 4.6 Coverage of the *uv* plane for the Plateau de Bure observations of NGC1333-IRAS4A. The coverage is poor for *uv* distances $\lesssim$150 m, so that emission on scales $\gtrsim 4''$ is resolved out.

is only recently that more information on the driving sources of the outflows in IRAS4A has been available (Choi 2005). The interferometric observations of this thesis are the first to show the stronger emission from complex organic molecules in the sources driving the collimated outflows (see also Kuan et al. 2004 for similar results obtained simultaneously in IRAS16293 with respect to Bottinelli et al. 2004b).

Initially, it was thought that there was no outflow associated with IRAS16293B, which was attributed to the fact that this source may be in an earlier evolutionary phase than IRAS16293A (e.g. Wootten 1989). This was supported by the higher H_2 column density in IRAS16293B, as traced by the stronger dust emission (i.e. the protostar has not yet accreted/blown away most of its envelope; e.g. Walker et al. 1993). But Walker et al. (1993) also suggested that the morphology of the outflow could be dual, i.e. a collimated one driven by A and a larger one that would have been driven in the past by B (hence the lack of activity in the vincinity of B). Higher-resolution observation confirmed the quadrupolar nature of the outflows with source A actively driving the NE-SW outflow, whereas the E-W outflow was driven by source B in the past and is now "fossilized", as noted by Stark et al. (2004). In this case, source B would be interpreted as being "older". Choi (2005) also suggested the interpretation of a different evolutionary stage between IRAS4A1 and 4A2, but proposed the strong continuum source, IRAS4A1, to be "younger", thereby driving a shorter, weaker outflow.

Note that the adjectives "older" and "younger" are not to be taken in their absolute meaning, which does not make sense for a binary system in which the formation of the components is

coeval by definition (consistent with the fact that, in the case of IRAS16239, similar dynamical times have been derived for the two outflows). I use them here to indicate that some of the observed features are representative of a more/less advanced evolutionary phase, i.e. one of the protostellar components would have reached a certain phase of evolution faster/slower than the other one, due to physical and/or dynamical differences.

Another interesting interpretation for the difference in outflow morphology is that of Walker et al. (1993) who proposed the presence of time variable outflows generated by FU Orionis-type outbursts in source B to explain the fossil state of the E-W outflow associated with this source. However, it is not clear what would trigger these outbursts and why they would occur in one of the components only. Nonetheless, a possible implication is that the two components have a different mass.

Regarding the difference in emission from complex molecules, two factors can increase the size of the region where the dust temperature, $T_{\rm d}$, is larger than $\sim$100 K (and hence increase the emission's strength):

- the luminosity of the central object: the higher it is, the further away the sublimation front is located.
- the density of the inner regions: when these regions are optically thick to the dust, $T_{\rm d}$ becomes higher than in the case of optically thin dust, so that at a given radius, $T_{\rm d}$ is larger than in the optically thin case, or equivalently, the radius where $T_{\rm d}$ reaches 100 K is larger.

Let us consider the case of IRAS16293. The hot corino in source A is (barely) resolved and larger than the hot corino in source B, which is unresolved. In principle, from the above points, this implies either that protostar A[3] is more luminous than protostar B, or that the inner regions in source A are denser than in source B (or both). Since the continuum in source A is weaker than in source B, then the envelope around source A is less massive and less dense than that surrounding source B, so that we are left with the first possibility, that is the central object in source A being more luminous. This could be due to protostar A being either more massive or subject to a higher accretion rate (or both). This could mean that the pre-stellar core that gave birth to the IRAS16293 system fragmented in an inhomogeneous way with the clump prior to source A being more massive but undergoing a larger accretion rate, hence leading to the smaller present envelope mass and larger protostellar luminosity. Note that the possibility of the central object in source A being more massive than the one in source B was already evoked in Section 4.4.1 and in Bottinelli et al. (2004b) as one of the potential explanation for the apparent difference in the systemic velocities of the complex organic molecular lines.

In IRAS4A, a similar reasoning could hold with the only difference that the protostar surrounded by the more massive envelope, A1, would have such a low luminosity that either the

[3]In this discussion, I ignore the multiple components of source A evidenced by Wootten (1989) and Chandler et al. (2005), and I use the terms "protostar" and "central object" interchangeably.

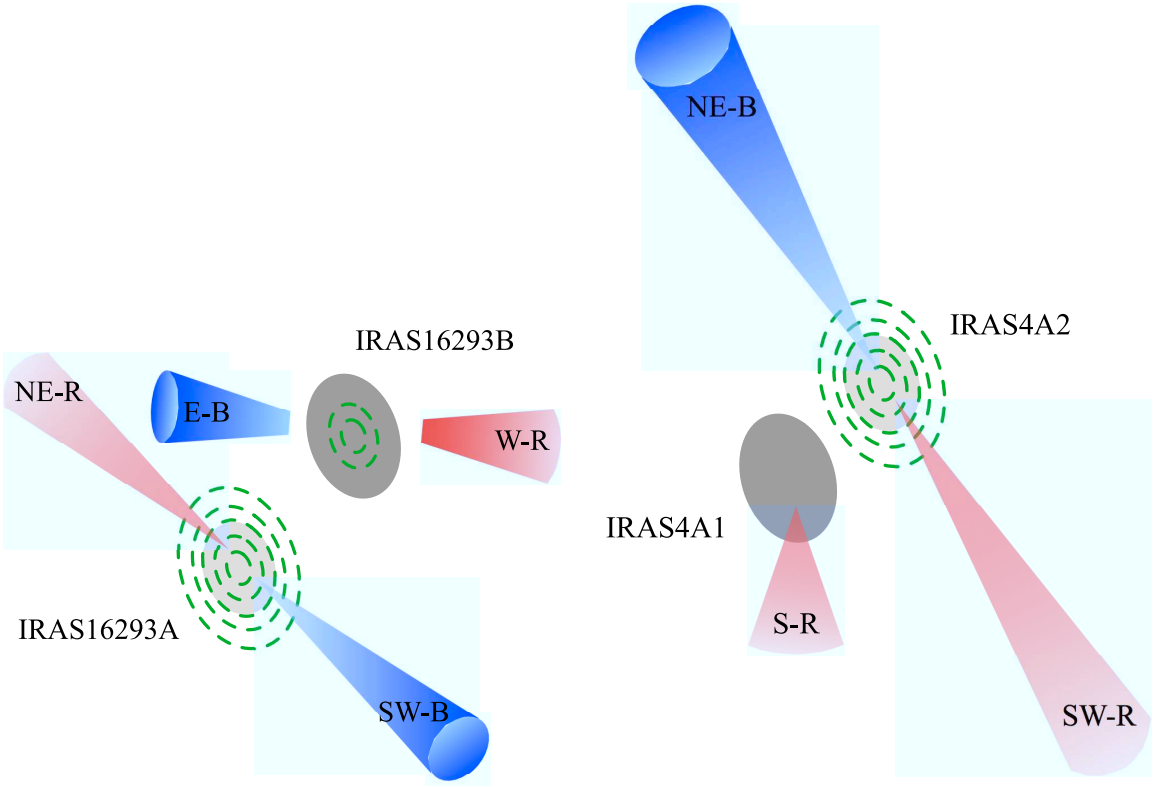

Figure 4.7 Schematic views of IRAS16293–2422 (left) and NGC1333-IRAS4A (right). The continuum emission is represented by grey blobs (dark and light grey indicate strong and weak continuum respectively). The green dashed contours represent the emission from complex organic molecules with the number of contours increasing with the emission's strength. The blue and red cones show the outflows with the labels indicating the direction and velocity range, e.g. NE-R = northeast red (sources: Stark et al. 2004; Walker et al. 1993, 1988 for IRAS16293, Choi 2005 for IRAS4A). Note that the blue counterpart of the S-R outflow from IRAS4A1 is not observed in Choi (2005). Features' strengths and extent are not to scale.

hot corino is too small to be detected, or complex molecules are not present in the gas phase.

Conclusion

The interferometric observations of IRAS16293 and IRAS4A with the Plateau de Bure show unambiguously that at least some, if not all, of the emission from the observed complex organic molecules originates from compact ($\lesssim 1.5''$) regions, which is consistent with grain mantle evaporation hypothesis. No indication was found in support of other formation mechanisms for these molecules.

Two scenarii have been proposed to explain the observed differences in line profile and systemic velocities in IRAS16293A and IRAS16293B. I also tried to draw conclusions from the

striking similarities in the line and continuum emissions of IRAS16293 and IRAS4A. However, the available data are insufficient to fully understand how and why the two components in each object differ in their dynamical and chemical state. More interferometric observations of the present sources (e.g. of optically thin lines) and of other (somewhat close, i.e. with separation $\lesssim 1000$ AU) binary systems are needed in order to solve the issues raised in the discussion.

Résumé du Chapitre 5
Hot cores: les grands frères des hot corinos?

A chaque fois que des découvertes sont faites concernant un aspect de la formation d'étoiles de faible masse, nous essayons de rechercher des propriétés similaires pour la formation d'étoiles massives, et vice versa. Les hot cores des étoiles massives n'ont pas échappé à la règle puisque des analogues de faible masse ont été cherchés et trouvés: les hot corinos. Mais quel est le degré de similitude de ces analogues? Les hot corinos sont-ils simplement de petits hot cores, ou bien y a-t-il une différence dans la chimie de ces objets? Dû aux différences physiques entre les hot corinos et les hot cores (telles que masse et luminosité), la comparaison de ces deux types d'objets pourrait permettre d'identifier les paramètres influençant la formation et l'évolution des molécules complexes. Puisque les hot cores massifs ont été étudiés depuis plus de 25 ans, une large quantité de données a été publiée. J'ai donc fait une recherche bibliographique pour rassembler des informations sur les molécules qui m'intéressent (HCOOH, $HCOOCH_3$, CH_3OCH_3, CH_3CN and C_2H_5CN), et sur le CH_3OH et H_2CO. Dans ce chapitre, je présente les résultats de cette recherche, ainsi que des observations complémentaires obtenues avec le JCMT. J'utilise les densités de colonne des molécules complexes pour montrer que les hot corinos sont à la hauteur des hot cores puisque les molécules organiques complexes sont relativement plus abondantes dans les hot corinos.

Chapter 5
Hot cores: hot corinos' bigger brothers?

Abstract

Whenever findings are made about some features of low-mass star formation, we try to search for the similar properties for massive star formation, and vice versa. Hot cores did not escape the rule since analogs were searched for and found in hot corinos. But how similar are these analogs? Are hot corinos simply small hot cores, or is there a difference in the chemistry of these objects? Due to the physical differences between hot corinos and hot cores (such as mass and luminosity), comparing these two types of objects could help to pinpoint the parameters influencing the formation and evolution of complex molecules. Since massive hot cores have been studied for over 25 years, a large amount of data has been published. I therefore reviewed the literature to gather information on the complex organic molecules I am interested in (HCOOH, $HCOOCH_3$, CH_3OCH_3, CH_3CN and C_2H_5CN), and on CH_3OH and H_2CO. In this chapter, I present the results of this search, as well as some complementary observations taken with the JCMT. I use the complex molecules' column densities to show that hot corinos are living up to hot cores since complex organic molecules are relatively more abundant in hot corinos.

5.1 Introduction

Hot cores associated with massive protostars have been defined as regions with diameters $\lesssim$0.1 pc, densities $\gtrsim 10^7$ cm^{-3}, temperatures $\gtrsim$100 K, large molecular line optical depths, high line brightness temperatures and the presence of complex organic species (see e.g. Kurtz et al. 2000). The term "hot core" was originally coined in 1979. The first hot core was discovered in the Orion Kleinmann-Low nebula (Orion KL or OMC-1) and was named so because observations and analysis of ammonia lines with high energies above the ground state ("hot ammonia") revealed the presence of a hot ($\gtrsim$220K) and dense ($\gtrsim 5 \times 10^7$ cm^{-3}) component (e.g. Morris et al. 1980). Since such warm and dense regions were believed to be the cradles for very young massive protostars, the use of molecular line emission to derive the physical parameters of these cradles quickly spread. Hence, following the discovery of the Orion hot core, many more were detected from observation of hot ammonia or CH_3CN. A list of known hot cores (to the best of my knowledge) is given in Table 5.1. At the time, motivations for the hot core search included

finding information on the efficiency and mechanics of star formation and on the composition of icy mantles (Walmsley & Schilke 1993). These incentives are still very topical, but others were added along the way.

For example, there has been some debate about the nature of their heating source (Kurtz et al. 2000). The current consensus is that hot cores are heated internally by massive (O or B) protostars. Indeed, observationally, hot cores are usually near (but not associated with — see e.g. Minier et al. 2003; Walsh et al. 1998) ultra-compact H II regions (UCHIIs) (Kurtz et al. 2000; Churchwell 2002). Moreover, some of them could be short-lived ($\lesssim 10^5$yr) precursors to UCHIIs (Churchwell 2002), in which case they would represent the earliest phase of massive star formation. Cesaroni et al. (1994) found that some hot cores were coincident with groups of water masers, which are known signposts of massive star formation. Finally, there is evidence for rotation and collapse in a number of hot cores (Kurtz et al. 2000), providing further support for star formation at the center of these cores.

But more relevant to this work, early observations of the Orion hot core (e.g. Sutton et al. 1985; Blake et al. 1987) also revealed a wealth of more or less complex molecules, whether C-, N-, O- and/or S-bearing (see Table A.1), and with them came the questions of how complex molecules could get and of how they formed. To answer the first question, more and more sensitive observations have been carried out, including deep searches for the amino acid glycine (CH_2NH_2COOH; Combes et al. 1996; Hollis et al. 2003). Regarding the second question, the presence of deuterated molecules, for example, was puzzling since these species were known to form rather in cold dark clouds via mechanisms that are inefficient at the high temperatures of hot cores, and surface reactions and/or freeze-out processes were already invoked (Gerin et al. 1992; Walmsley & Schilke 1993 and Millar 1993, and references therein).

The presence of complex organic molecules in massive hot cores has been imputed to gas-phase reactions, triggered by the high temperatures of these regions, among evaporated grain mantle components such as H_2CO, CH_3OH and NH_3. This gas-phase chemistry was thought to occur rapidly as it could reproduce some of the observed abundances in $\sim 10^4$ yr (e.g. Charnley et al. 1992; Nomura & Millar 2004). As mentioned in Section 1.3, this timescale is longer than the gas free-fall time in the inner envelopes of low-mass protostars (several hundred years – Schöier et al. 2002). The question is therefore whether the same chemistry occurs in both types of objects, and whether comparing them could tell us about the parameters influencing the formation and evolution of complex molecules.

To do this comparison, I describe in Section 5.2 the literature review that I did in search of measurements of complex molecules' abundances in known massive hot cores. In Section 5.3, I present some observations I carried out with the JCMT on a couple of sources. In Section 5.5, I assess the relevance of the gathered data for the comparison with hot corinos. Finally, the comparison itself is presented in Section 5.4.

5.2 Literature review

I performed this literature review on the massive hot cores listed by Kurtz et al. (2000), as well as three additional sources, all of which are reported in Table 5.1. I searched for the abundances of the complex molecules I detected in hot corinos (HCOOH, $HCOOCH_3$, CH_3OCH_3, CH_3CN and C_2H_5CN), as well as that of H_2CO and CH_3OH, since these are needed to calculate abundance ratios. I report the results of this search in Table 5.2, for sources for which I found column densities (or a limit) for at least two complex molecules. For a given source, the different rows correspond to the values taken from different authors, which are listed in column (11). These column densities are beam-averaged over the beam size given in column (10).

For the comparison, my main focus was on the O-bearing molecules, but I consider the N-bearing ones here as well for completeness. From Table 5.2, there are only five hot cores (Sgr B2(N), Orion hot core, Orion compact ridge, G327.30−0.60 and W3(H_2O)) for which data on all five O-bearing molecules studied here (H_2CO, CH_3OH, HCOOH, $HCOOCH_3$ and CH_3OCH_3) are available[1]. However, there are another six sources (Sgr B2(M), G10.47+0.03, G31.41+0.31, G34.26+0.15, W51 e1/e2 and NGC6334) for which CH_3OH and at least two of the complex molecules molecules (HCOOH, $HCOOCH_3$ and CH_3OCH_3) have measured abundances. These detections are summarized in Table 5.3.

As can be seen from Table 5.2, the dataset is very inhomogeneous. However, in most cases, column densities derived by different authors are consistent within a factor three, taking into account the (usually small) different beamsizes. Nonetheless, there are some discrepancies that I could not understand. For example, in the case of G34.26+0.15, Ikeda et al. (2001) find a $HCOOCH_3$ column density roughly one order of magnitude lower than MacDonald et al. (1996), whereas the two authors have similar column densities for C_2H_5CN. Similarly for W3(H_2O), Ikeda et al. find a $HCOOCH_3$ column density significantly lower than Helmich & van Dishoeck (1997) did. To try and check whether there might be an observational bias, I carried out observations of a couple of sources to search for the same complex molecules (Section 5.3). A more important issue in my opinion is the differences in the CH_3OH abundances, which can reach up to almost two orders of magnitude. I look in Section 5.5 how this difference may impact the comparison with hot corinos.

[1]The reported HCOOH abundance in W3(H_2O) is an upper limit (Liu et al. 2001), and H_2CO abundances in Sgr B2 (N) and G327.30−0.60 are lower limits (Gibb et al. 2000a; Nummelin et al. 2000)

Table 5.1 Massive hot cores reported in the literature (adapted from Kurtz et al. 2000).

Source	Other name	RA (2000) $h\ m\ s$	Dec (2000) $^\circ\ '\ ''$	$L_{\rm IR}$ $L_\odot$
W3(H_2O)		02 27 04.6	+61 52 25	1.0×10^5
Orion-KL HC[a]	OMC-1 HC[a]	05 35 14.5	−05 22 30	1.5×10^5
Orion-KL CR[b]	OMC-1 CR[b]	05 35 13.4	−05 23 07	1.5×10^5
Sgr B2 (N)		17 47 20.0	−28 22 17	6.5×10^6
Sgr B2 (M)		17 47 20.5	−28 23 06	6.5×10^6
G5.89−0.39	IRAS 17574−2403, W 28A2	18 00 30.4	−24 04 00	7.1×10^5
G9.62+0.19	IRAS 18032−2032	18 06 13.9	−20 31 44	4.4×10^5
G10.47+0.03		18 08 38.4	−19 51 52	5.0×10^5
G10.62−0.38		18 10 28.8	−19 55 41	1.1×10^6
G19.62−0.23		18 27 38.1	−11 56 36	1.6×10^5
G29.96−0.02		18 46 03.9	−02 39 22	1.4×10^6
G31.41+0.31	IRAS 18449−0115	18 47 34.6	−01 12 43	2.1×10^5
G34.26+0.15	IRAS 18507+0110	18 53 18.5	+01 14 58	6.3×10^5
G45.07+0.13	IRAS 19110+1045	19 13 22.1	+10 50 53	1.1×10^6
G45.12+0.13	IRAS 19111+1048	19 13 27.9	+10 53 37	1.3×10^6
G45.47+0.05	IRAS 19120+1103	19 14 20.8	+11 09 04	1.1×10^6
W51 e1		19 23 43.8	+14 30 26	1.5×10^6
W51 e2		19 23 43.9	+14 30 35	1.5×10^6
W51 e8		19 23 44.2	+14 30 28	1.5×10^6
W51 d		19 23 39.9	+14 31 06	1.5×10^6
IRAS 20126+4104		20 14 25.1	+41 13 32	1.3×10^4
DR 21(OH) MM 1		20 39 01.1	+42 22 49	5.0×10^4
G327.30−0.60		15 53 05.0	−54 35 24	1.0×10^5
NGC 6334(I)	NGC 6334(F)	17 20 53.4	−35 47 01	2.6×10^5
NGC 7538 IRS1		23 13 45.3	+61 28 10	8.7×10^4

NOTE — This is a non-exhaustive list. The last three sources were not lised in Kurtz et al. (2000).

[a] Hot core component, $v_{\rm LSR} = 5$ km s^{-1}.

[b] Compact ridge component, $v_{\rm LSR} = 7.5$ km s^{-1}.

Table 5.2 Column densities for selected species and hot cores.

Source	H_2	H_2CO	CH_3OH	HCOOH	$HCOOCH_3$	CH_3OCH_3	CH_3CN	C_2H_5CN	θ_b[a]	Ref.
(1)	(2)	(3)	(4)	(5)	(6)	(7)	(8)	(9)	(10)	(11)
W3(H_2O)	9.6(22)	4.0(14)	8.8(15)	–	6.7(14)	2.0(15)	2.7(13)	–	15	h97
	9.6(22)	–	3.9(15)	–	<9.3(13)	–	–	<1.9(13)	17	i01
	–	–	–	<4.1(15)	–	–	–	2.1(15)	7×6	l01
	–	5.0(14)	7.5 (15)	–	–	–	–	–	15	v00
	–	–	–	–	**8.8(14)**	**3.0(15)**	**4.0(13)**	–	14,20	This work
Orion-KL HC[b]	8.0(23)	5.5(15)	1.1(17)	6.0(14)	1.1(16)	6.0(15)	3.1(15)	2.4(15)	14	s95
	1.0(23)	–	1.4(17)	–	9.4(15)	–	–	1.5(15)	17	i01
Orion-KL CR[b]	8.0(23)	2.9(16)	3.0(17)	1.1(15)	2.5(15)	1.5(16)	3.8(15)	4.0(15)	14	s95
	3.0(23)	–	4.9(16)	–	1.7(15)	–	–	9.1(14)	17	i01
Sgr B2 (N)	3.0(24)	>1.5(15)	1.0(16)[c]	4.2(14)	5.6(15)	7.9(15)	6.3(17)[e]	1.6(15)	23	n00
	5.0(24)	–	8.3(16)	7.1(13)	2.6(15)	3.5(15)	–	5.2(15)	17	i01
Sgr B2 (M)	2.0(24)	>1.5(15)	1.0(16)[d]	–	1.6(15)	3.4(15)	3.1(17)[e]	2.2(14)	23	n00
G10.47+0.03	–	–	2.7(16)	1.5(14)	–	4.4(15)	–	–	20	i01
G31.41+0.31	–	–	1.4(16)	1.6(14)	–	3.7(15)	–	–	20	i01
G34.26+0.15	5.3(23)	>1.7(14)	1.8(16)	<9.1(14)	1.6(16)	–	2.4(14)	<4.7(14)	14	m96
	3.0(23)	–	2.6(14)	–	1.4(15)	3.7(15)	–	4.1(14)	20	i01
	–	–	–	<7.7(15)	2.6(16)	–	–	2.1(15)	9×5	l01
W51 e1/e2	3.6(23)	–	1.0(17)	–	1.2(16)	–	–	7.0(14)	17	i01
	–	–	–	**9.2(14)**	**1.4(16)**	**1.1(16)**	**3.9(14)**	–	14,20	This work
W51 e1	–	–	–	1.8(16)	1.0(17)	–	–	4.7(15)	7×6	l01
W51 e2	–	–	–	1.8(16)	1.9(17)	–	–	4.1(15)	7×6	l01
W51 d	–	–	–	1.3(16)	1.8(15)	–	–	4.6(16)	7×6	l01
	–	–	–	–	**1.6(15)**	–	**3.4(14)**	–	20	This work
G327.3	3.2(23)	>2.2(15)	1.7(16)	8.5(13)	1.6(16)	1.2(16)	1.0(16)	–	23	g00
	2.0(23)	–	2.1(16)	1.7(14)	–	6.4(15)	–	–	17	i01
NGC6334	2.0(23)	–	3.4(16)	1.9(14)	–	7.5(15)	–	–	20	i01
	–	1.6(15)	3.8(16)	–	–	–	–	–	15	v00
NGC7538-IRS1	7.2(22)	–	<2.6(14)	–	<6.3(13)	–	–	<1.3(13)	17	i01
	–	–	–	<4.5(15)	–	–	–	–	11×7	l01
	–	1.9(14)	2.2(15)	–	–	–	–	–	15	v00

NOTE — $a(b) = a \times 10^b$; column densities are in cm^{-2}; bold-faced values are derived from my observations (Section 5.3).
References: g00 = Gibb et al. (2000a) h97 = Helmich & van Dishoeck (1997); i01 = Ikeda et al. (2001); l01 = Liu et al. (2001); m96 = MacDonald et al. (1996); n00 = Nummelin et al. (2000); s95 = Sutton et al. (1995); t99 = Thompson & MacDonald (1999); v00 = van der Tak et al. (2000b).
[a] Beam size in arcsec over which listed column densities are averaged, except where noted.
[b] HC = hot core, CR = compact ridge (see Table 5.1).
[c] CH_3OH column density in a 2″ hot core is 5.0×10^{18} cm^{-2} (Nummelin et al. 2000).
[d] CH_3OH column density in a 1″ hot core is 7.9×10^{18} cm^{-2} (Nummelin et al. 2000).
[e] CH_3CN column density is given for a 2.″7 and 1.″6 source in Sgr B2 (N) and (M) respectively (Nummelin et al. 2000).

Table 5.3 Summary of detected complex and mantle molecules for selected species and hot cores.

Source	Mantle		Complex O-bearing			Complex N-bearing	
	H_2CO	CH_3OH	HCOOH	$HCOOCH_3$	CH_3OCH_3	CH_3CN	C_2H_5CN
W3(H_2O)	✓	✓	<	✓	✓	✓	✓
Orion-KL HC[b]	✓	✓	✓	✓	✓	✓	✓
Orion-KL CR[b]	✓	✓	✓	✓	✓	✓	✓
Sgr B2 (N)	>	✓	✓	✓	✓	✓	✓
G327.3	>	✓	✓	✓	✓	✓	
Sgr B2 (M)	>	✓		✓	✓	✓	✓
G10.47+0.03		✓	✓		✓		
G31.41+0.31		✓	✓		✓		
G34.26+0.15	>	✓	<	✓	✓	✓	✓
W51 e1/e2		✓	✓	✓			✓
W51 d			✓	✓			✓
NGC6334	✓	✓	✓		✓		
NGC7538-IRS1	✓	✓	<	<			<

NOTE — A checkmark indicates that a "firm" column density (i.e. not an upper or a lower limit, represented as < and > signs respectively) has been found in the literature (see Table 5.2 for values and references; lower limits were obtained in cases when the column densities were underestimated due to optically thick transitions). I gathered in the top part of the table the sources for which column densities or limits are available on all the O-bearing and mantle species. The bottom part lists the other sources used in Section 5.4.

5.3 New observations with the JCMT and their results

The JCMT observations of W3(H_2O), W51 e1/e2 and W51 d (see Table 5.1 for positions) were performed in March, April, June and August 2005 in beam-switching mode, with receivers A (RxA) and B (RxB), operating in double-side and single-side band respectively, associated to Digital Autocorrelation Spectrometer (DAS). Beamsizes, spectral resolutions, bandwidths and system temperatures for each receiver are listed in Table 5.4. This table also gives the main-beam efficiencies, $\eta_{\rm mb}$, which were used to convert the antenna temperatures $T_{\rm A}^*$ into main beam temperatures $T_{\rm mb}$, the two quantities being related by $T_{\rm mb} = T_{\rm A}^*/\eta_{\rm mb}$.
Table 5.5 shows the central frequencies of the 500 MHz bands over which the sources were observed, and the rms reached in each band.

The detected transitions are shown in Table 5.6. I built rotational diagram following, as in Chapter 3, the method outlined in Section 3.3. Figure 5.1 shows the diagrams for which the rotational temperature, $T_{\rm rot}$, could be derived. I summarize in Table 5.7 the obtained rotational temperatures and beam-averaged column densities. When $T_{\rm rot}$ could not be derived, I assumed a value based on the literature and reported it in square brackets in Table 5.7.

I also reported in Table 5.2 the column densities I derived. For W3(H_2O), the values I obtained are consistent with those of Helmich & van Dishoeck (1997), who also used the JCMT. Unfortunately, my observations were not sensitive enough to detect HCOOH and C_2H_5CN and compare them with other published values. Regarding W51 e1/e2, the values I derive for HCOOH and $HCOOCH_3$ are consistent with those of Liu et al. (2001), taking into account the beam dilution. Ikeda et al. (2001) had found a $HCOOCH_3$ column density similar to the one I obtained.

My observations are certainly too scarse to determine whether the column densities of complex molecules found in the literature are consistent. Attempts to measure the column densities that are missing in Table 5.2 would, in any case, probably also yield column densities for the complex molecules that were already observed, thereby providing means to check the consistency of the results. However, such attempts would require a methodical study which is beyond the scope of my thesis. The upside is that other researchers are aware of this issue as can be seen by the recent work of Bisschop et al. (2006). These authors performed a partial survey of seven massive hot cores (five of which are not included in Table 5.3), and detected HCOOH, $HCOOCH_3$ and CH_3OCH_3 in most of them. It will therefore be very interesting to include their more uniform dataset in a future comparison.

Table 5.4 Observing parameters for the JCMT data of the W51 e1/e2, W51d and W3(OH/H_2O) hot cores.

	RxA	RxB
Beamsize θ_b ($''$)	20	14
Spectral resolution δf (MHz)	0.3	0.6
Spectral resolution δv (km s^{-1})	$\sim$0.4	$\sim$0.6
Bandwidth (MHz)	500	500
System temperature T_{sys} (K)	$\sim$600-700[a]	$\sim$600[b],$\sim$700[c]
Main-beam efficiency[d] η_{mb} (%)	69	63

[a] Apart for W51 e1/e2 for which $T_{sys} \sim$ 900 K due to a larger sky opacity during the RxA observation of this source ($\tau \sim 0.3$ vs ~ 0.2 for the other sources).
[b] T_{sys} for W3(OHH_2O) for which sky opacity was low ($\tau \lesssim 0.1$).
[c] T_{sys} for W51 e1/e2 for which $\tau \sim 0.1$.
[d] From `http://docs.jach.hawaii.edu/JCMT/HET/GUIDE/het_guide/`.

Table 5.5 Tuning frequencies and rms reached during the JCMT observations of W51 e1/e2, W51d and W3(OH/H_2O).

Source	RxA[a]			RxB[b]			
[c]	220.6	225.6	232.0	332.6	338.3	339.1	344.5
W51 e1/e2	0.11	0.11	0.15	0.18	0.35	0.11	0.13
W51 d	0.10	0.10	0.12	–	–	–	–
W3(OH/H_2O)	0.12	0.12	0.11	0.10	0.09	0.07	0.07

NOTE — A dash indicates that the source was not observed at that frequency.
[a] Rms in K in 0.4 km s^{-1}channels.
[b] Rms in K in 0.6 km s^{-1}channels.
[c] This line gives the frequencies in GHz on which the 500 MHz bandwith was centered.

Table 5.6 Transitions detected with the JCMT in W51 e1/e2, W51d and W3(OH/H_2O).

Molecule	Transition line	Frequency (MHz)	E_u [a] (cm^{-1})	$T_{mb} \pm$ rms (mK)	ΔV [b] $\pm \delta V$ [c] (km s^{-1})	$\int T_{mb} dV$ (K km s^{-1})
			W51 e1/e2			
HCOOH	$15_{3,13} - 14_{3,12}$	338201.8	98.8	0.581 ± 0.354	7.5 ± 0.6	4.631 ± 14.42
	$15_{4,11} - 14_{4,10}$	338248.7	114.2	0.547 ± 0.354	8.4 ± 0.6	4.891 ± 9.278
$HCOOCH_3$-A	$19_{3,17} - 18_{3,16}$	225618.7	73.6	0.598 ± 0.113	7.7 ± 0.4	4.895 ± 1.013
	$18_{4,14} - 17_{4,13}$	233777.5	71.7	0.684 ± 0.113	6.4 ± 0.4	4.642 ± 1.025
	$19_{11,9} - 18_{11,8}$	233854.2	125.9	0.867 ± 0.083	8.6 ± 0.8	7.897 ± 5.291
	$13_{7,7} - 12_{6,6}$	339186.0	48.6	0.314 ± 0.108	3.5 ± 0.6	1.180 ± 0.519
	$13_{7,6} - 12_{6,7}$	339196.4	48.6	0.867 ± 0.108	7.3 ± 0.6	6.701 ± 1.631
$HCOOCH_3$-E	$19_{3,16} - 18_{3,15}$	225608.8	73.6	0.596 ± 0.113	6.5 ± 0.4	4.134 ± 0.867
	$18_{5,13} - 17_{5,12}$	228628.8	74.9	0.893 ± 0.113	8.3 ± 0.4	7.861 ± 4.819
	$19_{13,7} - 18_{13,6}$	233524.6	148.0	0.513 ± 0.083	9.6 ± 0.8	5.256 ± 1.356
	$19_{11,8} - 18_{11,7}$	233845.3	125.9	0.704 ± 0.083	6.5 ± 0.8	4.902 ± 4.117
	$27_{15,13} - 26_{15,12}$	332352.6	247.6	0.435 ± 0.134	4.9 ± 1.1	2.272 ± 1.745
	$27_{14,14} - 26_{14,13}$	332626.0	234.3	0.665 ± 0.134	8.4 ± 1.1	5.953 ± 1.509
	$13_{7,7} - 12_{6,7}$	339129.3	48.6	0.711 ± 0.082	10.9 ± 1.1	8.289 ± 1.876
	$13_{7,6} - 12_{6,6}$	339152.7	48.6	0.443 ± 0.082	4.9 ± 1.1	2.299 ± 0.913
	$28_{17,12} - 27_{17,11}$	344347.8	288.1	0.278 ± 0.131	3.3 ± 0.5	0.964 ± 1.194
CH_3OCH_3	$12_{1,12} - 11_{0,11}$	225599.1	41.0	1.623 ± 0.113	7.4 ± 0.4	12.763 ± 0.891
	$19_{1,19} - 18_{0,18}$	344358.1	104.7	1.435 ± 0.131	7.4 ± 0.5	11.357 ± 1.720
CH_3CN [d]	$12_{7,0} - 11_{7,0}$	220539.1	283.6	0.291 ± 0.078	6.4 ± 0.8	1.971 ± 1.142
	$12_{6,0} - 11_{6,0}$	220594.3	219.2	0.790 ± 0.113	8.3 ± 0.4	7.092 ± 3.957
	$12_{5,0} - 11_{5,0}$	220641.1	164.6	0.918 ± 0.113	10.6 ± 0.4	10.339 ± 1.187
	$12_{4,0} - 11_{4,0}$	220679.3	119.9	1.017 ± 0.113	7.7 ± 0.4	8.355 ± 5.037
	$12_{3,0} - 11_{3,0}$	220709.1	85.2	1.599 ± 0.113	9.8 ± 0.4	16.659 ± 1.575
	$12_{2,0} - 11_{2,0}$	220730.3	60.4	1.518 ± 0.113	9.3 ± 0.4	15.030 ± 1.477
	$12_{1,0} - 11_{1,0}$ [e]	220743.0	45.5	2.090 ± 0.113	13.7 ± 0.4	30.497 ± 1.825
	$12_{0,0} - 11_{0,0}$ [e]	220747.2	40.5			

Table 5.6 — *Continued.*

			W51 d			
HCOOH	$10_{3,7} - 9_{3,6}$	225512.6	53.7	0.571 ± 0.104	10.2 ± 0.4	6.192 ± 3.020
$HCOOCH_3$-A	$19_{3,17} - 18_{3,16}$	225618.7	73.6	0.254 ± 0.072	8.0 ± 0.8	2.162 ± 3.380
$HCOOCH_3$-E	$19_{3,16} - 18_{3,15}$	225608.8	73.6	0.255 ± 0.072	5.3 ± 0.8	1.433 ± 2.081
CH_3OCH_3	$12_{1,12} - 11_{0,11}$	225599.1	41.0	0.455 ± 0.072	7.5 ± 0.8	3.634 ± 2.565
	$13_{0,13} - 12_{1,12}$	231987.8	48.5	0.484 ± 0.115	4.5 ± 0.4	2.316 ± 0.694
CH_3CN[d]	$12_{7,0} - 11_{7,0}$	220539.1	283.6	0.275 ± 0.100	6.2 ± 0.3	1.831 ±
	$12_{6,0} - 11_{6,0}$	220594.3	219.2	0.508 ± 0.100	10.7 ± 0.3	5.767 ± 1.188
	$12_{5,0} - 11_{5,0}$	220641.1	164.6	0.591 ± 0.100	13.3 ± 0.3	8.331 ± 1.639
	$12_{4,0} - 11_{4,0}$	220679.3	119.9	1.082 ± 0.100	8.0 ± 0.3	9.269 ± 6.769
	$12_{3,0} - 11_{3,0}$	220709.1	85.2	1.148 ± 0.100	8.4 ± 0.3	10.282 ± 6.905
	$12_{2,0} - 11_{2,0}$	220730.3	60.4	1.056 ± 0.100	8.4 ± 0.3	9.424 ± 7.014
	$12_{1,0} - 11_{1,0}$[e]	220743.0	45.5	1.429 ± 0.100	12.8 ± 0.3	19.472 ± 8.600
	$12_{0,0} - 11_{0,0}$[e]	220747.2	40.5			
			W3(H_2O)			
$HCOOCH_3$-A	$19_{3,17} - 18_{3,16}$	225618.7	73.6	0.286 ± 0.077	2.2 ± 0.8	0.675 ± 1.326
	$18_{4,14} - 17_{4,13}$	233777.5	71.7	0.199 ± 0.077	2.7 ± 0.8	0.579 ± 0.245
$HCOOCH_3$-E	$18_{2,16} - 17_{2,15}$	233753.9	71.7	0.258 ± 0.077	2.2 ± 0.8	0.614 ± 0.218
CH_3OCH_3	$12_{1,12} - 11_{0,11}$	225599.1	41.0	0.615 ± 0.117	3.9 ± 0.4	2.540 ± 1.249
	$13_{0,13} - 12_{1,12}$	231987.8	48.5	0.613 ± 0.111	4.6 ± 0.4	2.969 ± 0.508
	$16_{2,15} - 15_{1,14}$	330406.5	78.3	0.712 ± 0.062	6.4 ± 0.1	4.842 ± 2.933
	$19_{1,19} - 18_{0,18}$	344358.1	104.7	0.675 ± 0.074	4.3 ± 0.5	3.063 ± 3.007
CH_3CN[d]	$12_{4,0} - 11_{4,0}$	220679.3	119.9	0.244 ± 0.073	5.4 ± 0.8	1.403 ± 0.253
	$12_{3,0} - 11_{3,0}$	220709.1	85.2	0.512 ± 0.073	6.3 ± 0.8	3.452 ± 0.274
	$12_{2,0} - 11_{2,0}$	220730.3	60.4	0.442 ± 0.073	7.6 ± 0.8	3.589 ± 0.295
	$12_{1,0} - 11_{1,0}$	220743.0	45.5	0.521 ± 0.073	4.3 ± 0.8	2.401 ± 0.563
	$12_{0,0} - 11_{0,0}$	220747.2	40.5	0.729 ± 0.073	7.1 ± 0.8	5.521 ± 0.640

[a] Energy of the upper level of the transition.
[b] Width of the observed line (full-width at half-maximum of the fitted gaussian).
[c] Spectral resolution of the observation.
[d] All the CH_3CN lines are unresolved triplets.
[e] The $K = 0$ and $K = 1$ CH_3CN triplets are blended.

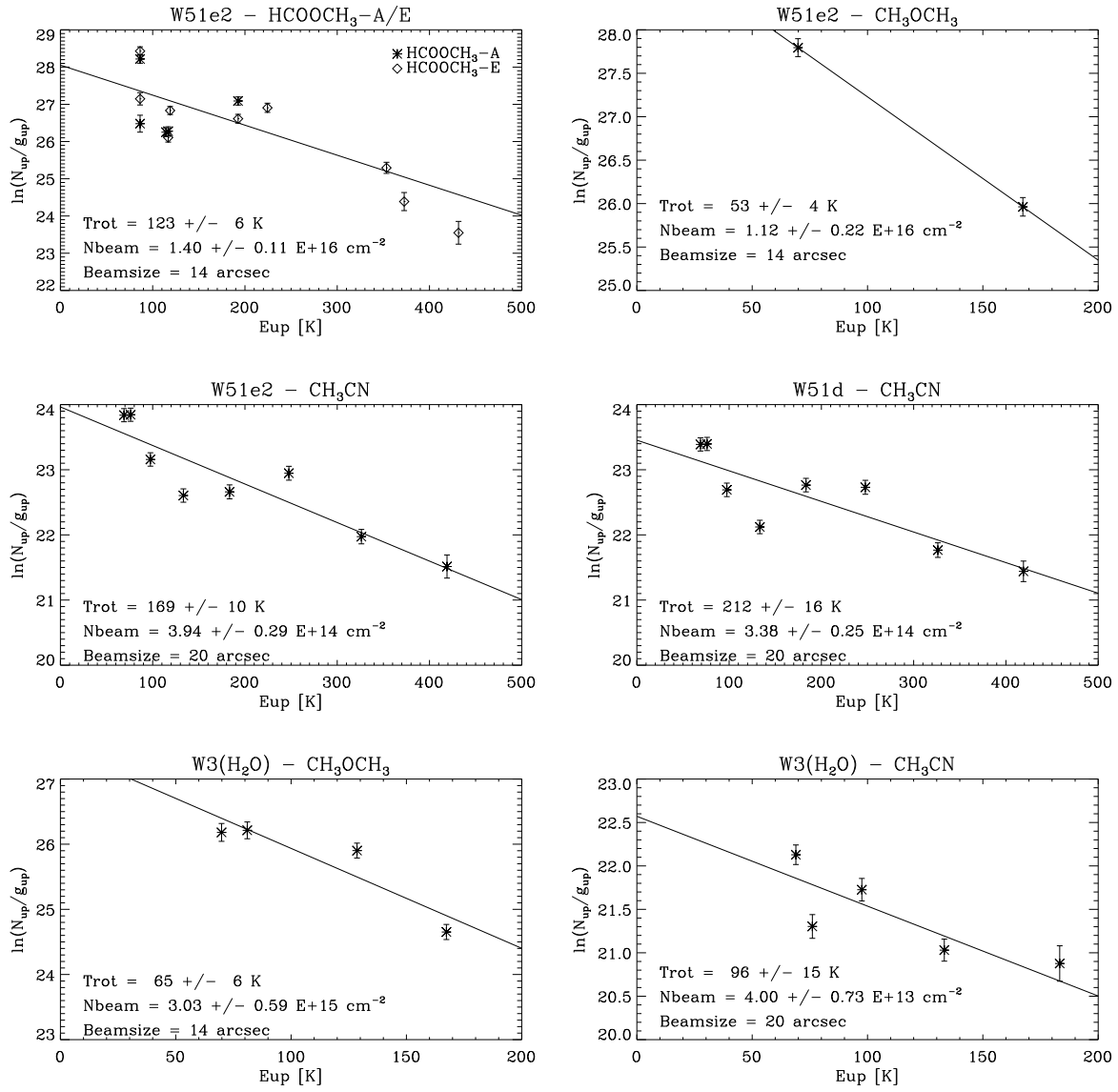

Figure 5.1 Rotational diagrams of some complex molecules towards the massive hot cores W51 e1/e2, W51 d and W3 (OH/H_2O).

Table 5.7 Results from the rotational diagrams for the massive hot cores W51 e1/e2, W51d and W3(OH/H_2O).

Molecule	$T_{\rm rot}$ (K)	$\theta_{\rm beam}$ [a] ($''$)	$N_{\rm beam}$ ($\rm cm^{-2}$)
	W51 e1/e2		
HCOOH	[200] [b]	14	$9.2\pm6.5\times10^{14}$
$HCOOCH_3$	123±6	14	$1.4\pm0.1\times10^{16}$
CH_3OCH_3	53±6	14	$1.1\pm0.3\times10^{16}$
CH_3CN	169±10	20	$3.9\pm0.3\times10^{14}$
	W51 d		
$HCOOCH_3$	[200] [b]	20	$1.6\pm1.1\times10^{15}$
CH_3CN	212±16	20	$3.4\pm0.3\times10^{14}$
	W3 (H_2O)		
$HCOOCH_3$	[140] [c]	14	$8.8\pm5.1\times10^{14}$
CH_3OCH_3	65±6	14	$3.0\pm0.6\times10^{15}$
CH_3CN	96±15	20	$4.0\pm0.7\times10^{13}$

[a] Beam size over which the column density was averaged.
[b] From Liu et al. (2001).
[c] From Ikeda et al. (2001).

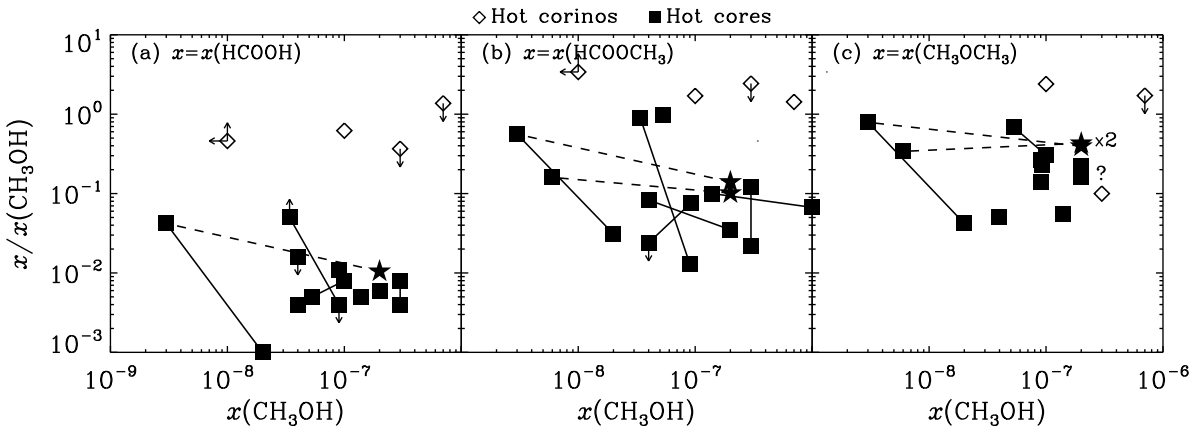

Figure 5.2 Abundance ratios of complex O-bearing molecules to methanol, plotted as a function of the methanol abundance in hot cores, plotted over the hot corino data (from Figure 3.7). Open diamonds represent hot corinos. Filled squares represent abundances ratios of hot cores, derived from beam-averaged column density analysis. Squares linked by a solid line represent abundance determinations from different authors. Stars represent the hot cores of SgrB2 (N) and (M), where an analysis of the methanol emission similar to what done in the hot corinos has been carried out (Nummelin et al. 2000). The dotted lines connect the SgrB2 (N) and (M) hot cores (stars) to the squares corresponding to the cold envelopes of these sources. See the text for further details. The point corresponding to CH_3OCH_3 in IRAS4A is not represented due to both CH_3OCH_3 and CH_3OH abundances being upper limits in this source. The question mark refers to the ratio in IRAS2A and indicates that the CH_3OCH_3 abundance is likely underestimated in this source (see Section3.5.1).

5.4 Comparison with hot corinos

Figures 5.2 and 5.3 plot the abundance ratios of complex O-bearing molecules to CH_3OH and H_2CO respectively, for massive hot cores and as derived from the literature (Section 5.2). For a given complex molecule, if a given source had two column densities reported by different authors, then two abundance ratios were derived and reported in in Figure 5.2, linked with a solid line. In Figure 5.2, I also report the results obtained from the hot core + outer envelope analysis of CH_3OH emission in SgrB2 (N) and (M), to show the uncertainty associated with the different methods of abundance ratios' determinations (see Section 5.5).

The abundance ratios with respect to CH_3OH and H_2CO were noticed to be roughly constant for hot corinos. Regarding hot cores, the ratios seem to decrease with increasing CH_3OH or H_2CO abundance, but the data are also consistent with a constant ratio with a larger scatter. In any case, it is clear from these figures that *the abundance ratios with respect to methanol in hot cores are lower than in hot corinos* by 1–2 orders of magnitude, whereas abundance ratios with respect to formaldehyde are comparable in hot corinos and hot cores. One also notices that the HCOOH abundance ratios in hot cores are about one order of magnitude lower than the $HCOOCH_3$ and CH_3OCH_3 abundance ratios, whereas they are lower by only about a factor four

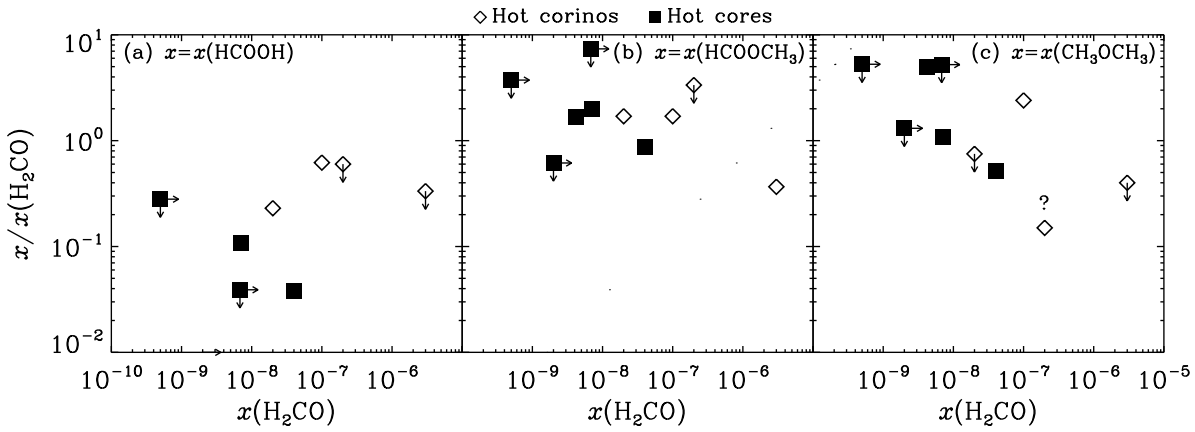

Figure 5.3 Abundance ratios of complex O-bearing molecules to formaldehyde, plotted as a function of the formaldehyde abundance in hot cores, plotted over the hot corino data (from Figure 3.8). Open diamonds represent hot corinos. Filled squares represent abundances ratios of hot cores, derived by beam-averaged column density analysis.

in hot corinos. For completeness, I considered how Figures 5.2 and 5.3 would change if I were to use beam-averaged abundances ratios in hot corinos, as in hot cores. In this case, abundance ratios in hot corinos would be smaller by a factor $\lesssim 10$: ratios for $HCOOCH_3$ and CH_3OCH_3 would become comparable in the two types of objects, while HCOOH ratios would still be larger in hot corinos than in hot cores. This is very likely due to the relative larger contribution of methanol and formaldehyde emission in the cold envelope in low mass with respect to high mass protostars. Indeed, high energy transitions are more easily detected in high than low mass protostars (e.g. Comito et al. 2005; Schilke et al. 2001, 1997; Blake et al. 1995), which support the above interpretation.

5.5 Relevance

The question of the relevance of the comparison arises because abundance ratios were determined in a different way in hot corinos and in hot cores.

In hot corinos, the CH_3OH and H_2CO hot core abundances were available from the analysis of these molecules' emission (Chapter 2.3; Maret et al. 2004, 2005). Assuming that the emission of the complex molecules comes from the same region (an assumption supported by the interferometric observations), the hot corino abundances of the complex species were derived from the beam-averaged values taking into account the beam dilution.

In most hot cores, however, only beam-averaged CH_3OH and H_2CO column densities are available, so that abundance ratios were taken as beam-averaged column density ratios. However, as I will discuss a bit further, the generally high rotational temperatures derived for CH_3OH (and for some of the complex molecules) indicate that the observed CH_3OH emission is dominated by the hot cores.

There are a few exceptions to the fact that only beam-averaged values could be found. Indeed, in some sources, it was possible to find an analysis of the methanol emission similar to what has been done for the hot corinos, namely disentangling the hot core from the cold outer envelope contribution in the beam, by means of a two-component LTE model. This was the case for SgrB2 (N) and (M) (Nummelin et al. 2000), and for G10.47+0.03, G31.41+0.31 and G34.26+0.15 (Hatchell et al. 1998). The only analysis I could find in the literature which combined radiative transfer and temperature, density and abundance profiles, is that of van der Tak et al. (2000a). Unfortunately, the sources for which they find a jump are not part of the sample I use in the comparison.

Considering the cases of SgrB2 (N) and (M), and assuming, as for hot corinos, that the complex molecules' emission originate from the $2''$ and $1''$ hot cores inferred by Nummelin et al. (2000), I estimated the abundance ratios of complex O-bearing molecules to CH_3OH in the hot cores. The values are plotted with star symbols in Figure 5.2, which shows that there is only a factor 4 difference in the abundance ratios if the hot core or the outer envelope abundance of methanol is used. I also performed the same calculation for the sources analyzed by Hatchell et al. (1998), and found similar results, but did not plot the values for clarity.

In principle, the different methods used to derive the abundance ratios in hot cores (beam-averaged column density) and corinos (full density and chemical structure analysis) may lead to such a different result that the comparison may be meaningless. However, while this would certainly be the case for the absolute values of the abundances, the abundance ratios suffer much less from the different methods, as shown by the "small" factor 4 in the SgrB2 (N) and (M) sources (Nummelin et al. 2000). In practice, the beam-averaged abundance ratios are very different from the reality only if the spatial distributions of the different molecules in the considered source are different, and/or if there is a large contribution from the outer envelope with respect to the hot core. While a direct measure of the molecular emission extent would require carrying out interferometric observations, the available data can give a good hint on where the emission originates from, by looking at the rotational temperature, $T_{\rm rot}$. As a matter of fact, the $T_{\rm rot}$ of the hot cores considered in this study (with the possible exception of the H_2CO and HCOOH) are implying that the emission is dominated indeed by the hot cores rather than the cold envelope (which may also be due to an observational bias, that is if the observed transitions are probing warm rather than cold gas). In this respect, therefore, I think that the comparison between hot corinos and hot cores shown in Figures 5.2 is reliable. There is, however, more uncertainty associated with the hot cores' abundance ratios reported in Figure 5.3, since H_2CO emission could have an important contribution from the cold envelope.

Conclusion

Whether considering beam-averaged ratios in all objects or not, Figure 5.2 (and to a lesser extent Figure 5.3) show that *hot corinos are not just scaled versions of hot cores* and that in fact, complex molecules are relatively more abundant in hot corinos than in hot cores. This conclusion would still be valid if I assume CH_3OH and H_2CO abundances from Jørgensen et al. (2005b) since, as mentioned in the previous section, the abundance ratios with respect to CH_3OH and H_2CO would be similar and higher respectively, so in any case, higher than the abundance ratios in massive hot cores. The possible explanations for the difference between hot cores and hot corinos will be investigated in Section 6.4.

Résumé du Chapitre 6
La chimie des hot corinos/cores

Dans ce chapitre, je passe en revue les concepts majeurs intervenant dans la chimie des hot corinos et hot cores. Je décris les différents types de réactions ayant lieu, d'une manière générale, dans le milieu interstellaire, et porte une attention particulière aux processus prenant place lors de la phase pré-stellaire. En effet, c'est durant cette phase que les manteaux des grains se forment, donc ces processus ont un fort impact sur la chimie ayant lieu par la suite dans les hot corinos/cores. J'en viens ensuite au cœur du sujet en détaillant les chemins de formation possibles pour certaines molécules organiques complexes, typiques des hot corinos/cores. Enfin, j'analyse les résultats des chapitres 3 à 5 dans le contexte des éléments présentés dans les premières parties du présent chapitre, pour montrer que, bien qu'on ne puisse éliminer aucun des mécanismes de formation, il semblerait que la formation sur la surface des grains soit favorisée. Cette analyse fait partie de Bottinelli et al. (2006).

Chapter 6
Chemistry of hot corinos/cores

Abstract

I review in this section the major concepts intervening when dealing with the chemistry of hot cores and corinos. I start with a description of the different types of reactions taking place in the ISM (Section 6.1) and bring special attention to the processes occuring during the pre-stellar phase (Section 6.2). Indeed, it is during this phase that the grain mantles are formed, so these processes have a strong impact on the subsequent chemistry taking place in hot cores/corinos. I then move on to the heart of the issue by detailing the possible formation pathways of some complex organic molecules typically found in hot cores/corinos. Finally I put the results found in Chapters 3 to 5 in the context of the elements presented in the first sections of this chapter to show that, even though no formation mechanism can be discriminated against, there seems to be more support in favor of grain-surface formation.
The analysis presented in this chapter is part of Bottinelli et al. (2006).

6.1 Interstellar chemistry: general considerations

Since the identification of the first interstellar molecule in 1940 by McKellar, over 120 molecules have been discovered (see `http://www.ph1.uni-koeln.de/vorhersagen/` for an up-to-date list). These range from the simple diatomic molecules to a thirteen-atom carbon chain, which shows that the ISM possesses sites of a very rich chemistry. Many models have been developed to try and reproduce the chemistry leading to the formation of the detected molecules. Complex chemical networks of up to 4000 reactions among several hundred species have been built. Gas-phase chemistry has been successful in explaining several observational aspects of interstellar chemistry, but it has become clear that it is not sufficient to understand all the data and that grain-surface chemistry is necessary. I therefore describe here the types of reactions occurring in the ISM for the two broad classes (gas-phase and grain-surface), including, in the case of grain-surface chemistry, the desorption mechanisms that return the species in the gas-phase.

6.1.1 Gas-phase reactions

Gas-phase reactions are generally constrained by the low densities and cold temperatures of the ISM. Low densities imply that only binary (also called bimolecular, i.e. involving two reactants) reactions can take place. Cold temperatures require that only exothermic reactions with a very low or no activation barrier are possible in the gas-phase, because the rate coefficient k obey the Arrhenius rate law (e.g. Herbst 1995):

$$k(T) = A(T) \exp(-E_{\rm a}/k_{\rm B}T) \tag{6.1}$$

where $A(T)$ is the pre-exponential factor, $E_{\rm a}$ is the activation energy and $k_{\rm B}$ is Boltzmann's constant. Hence at low temperature, reactions are too slow to be competitive if the activation barrier is too high.

The different types of reactions that can occur are detailed in a number of publications (e.g. Tielens 2005; Lequeux 2002; Herbst 1995). They are briefly described below and summarized in Table 6.1:

- *Ion-molecule reactions* A + B^+ $\rightarrow$ C + D^+: these reactions have no activation barrier and can occur at very low temperatures provided that they are exothermic. The rate coefficients are in the range $\sim 10^{-9} - 10^{-7}$ cm^3 s^{-1} at 10 K (Herbst 1995).

- *Radiative association* A + B $\rightarrow$ AB + hν: the direct combination of the two reactants with emission of a photon. For this kind of reaction to occur, the product must form in a state that has permitted transitions with the fundamental state in order to get rid of excess energy by emission of a photon. This is a slow process (rate coefficient $k \sim 10^{-17}$ cm^3 s^{-1}; Lequeux 2005), unless one of the reactants is abundant (H or H_2), in which case, $k \sim 10^{-9}$ cm^3 s^{-1} (Gerlich & Horning 1992).

- *Dissociative recombination* $AB^+ + e^-$ $\rightarrow$ A + B: formation of neutral species by reaction between a molecular ion and an electron. These tend to be quite rapid with rate coefficients at room temperature from 10^{-7} to 10^{-6} cm^3 s^{-1} and a small inverse dependence on temperature (Herbst 1995).

- *Neutral-neutral reactions* A + B $\rightarrow$ C + D: reactions between stable neutral atoms or molecules. Many possess an activation barrier so that they do not happen in cold regions of the ISM, due to the temperature dependence in equation (6.1). They are however fundamental in regions with warm temperatures. Reactions between radicals (molecules with one or several unpaired electrons) or between a radical and an atom generally do not have an activation barrier and can occur at low temperatures at rate coefficients larger than 10^{-10} cm^3 s^{-1} (Herbst 1995; Smith et al. 2004, and references therein).

- *Photodissociation and photo-ionization* AB + hν $\rightarrow$ A + B and CD + hν $\rightarrow$ CD^+: destruction of molecules by one of the following: (i) UV radiation, (ii) cosmic rays (CR),

Table 6.1 Types of gas-phase reactions

Name	Equation	Rate coefficient ($cm^3\ s^{-1}$)
Ion-molecule reactions	$A + B^+ \rightarrow C + D^+$	$\sim 10^{-9} - 10^{-7}$
Radiative association	$A + B \rightarrow AB + h\nu$	$\sim 10^{-17} - 10^{-9}$
Dissociative recombination	$AB^+ + e^- \rightarrow A + B$	$\sim 10^{-7} - 10^{-6}$
Neutral-neutral reactions	$A + B \rightarrow C + D$	$\sim 10^{-10}$
Photodissociation	$AB + h\nu \rightarrow A + B$	$\sim 10^{-17} - 10^{-9}\ s^{-1}$
Photo-ionization	$CD + h\nu \rightarrow CD^+$	$\sim 10^{-17} - 10^{-9}\ s^{-1}$
Charge transfer	$A^+ + B \rightarrow A + B^+$	$\sim 10^{-9}$

(iii) secondary UV radiation produced by collisional excitation of H_2 or He by CR followed by radiative de-excitation. The rate at which this type of reaction occurs is expressed by the ionization rate, which ranges from $10^{-9}\ s^{-1}$ in environments suffering no extinction, down to $10^{-17}\ s^{-1}$ in dense regions.

6.1.2 Grain-surface reactions

Dust particle surfaces are assumed to start out as mixtures of silicates and graphitic material, and gradually covered by mantles of water-ice via accretion of atomic oxygen followed by hydrogenation (Tielens & Hagen 1982; Jones & Williams 1984). The production of molecules on grain surfaces requires the reactants to stick. This adsorption process is known to occur with high efficiency at low temperatures and for large ($\sim 0.2\mu$m in diameter) grains (Herbst 1995). However, due to the low density of dust particles, it is slow: for example, for CO molecules in a molecular cloud of density $10^4\ cm^{-3}$and assuming a standard dust-to-gas ratio of 1:100, the adsorption time scale is of order 10^5 years.

Following adsorption, the reactants need to be be mobile and/or reactive. It is generally assumed that when exothermic reactions between adsorbed species are possible, then, whenever the species approach each other, the reaction occurs (Williams 1993). The mobility, or diffusion, can be achieved via the classical "thermal hoping" mechanism or via quantum tunneling (the so-called Langmuir-Hinshelwood mechanism — see top of Figure 6.1), the later being faster for light species such as atomic hydrogen. Alternatively, a gas-phase species can adsorb on a site that is already occupied (Eley-Rideal mechanism, bottom of Figure 6.1), in which case only exothermicity is required for the reaction to occur.

The most important grain-surface reaction is the formation of H_2, which cannot be formed in the gas-phase (e.g. Hollenbach & Salpeter 1971; Cazaux & Tielens 2004; Cuppen & Herbst 2005; Cuppen et al. 2006). It is also generally accepted that heavy atoms such as C, N, and O striking and sticking to the grains will be hydrogenated efficiently to saturated forms (CH_4, NH_3, H_2O), unless intermediate radicals are desorbed before they can react with another H (Tielens & Hagen 1982; Herbst 1995).
Several desorption mechanisms have been proposed (Williams 1993; Tielens 2005):

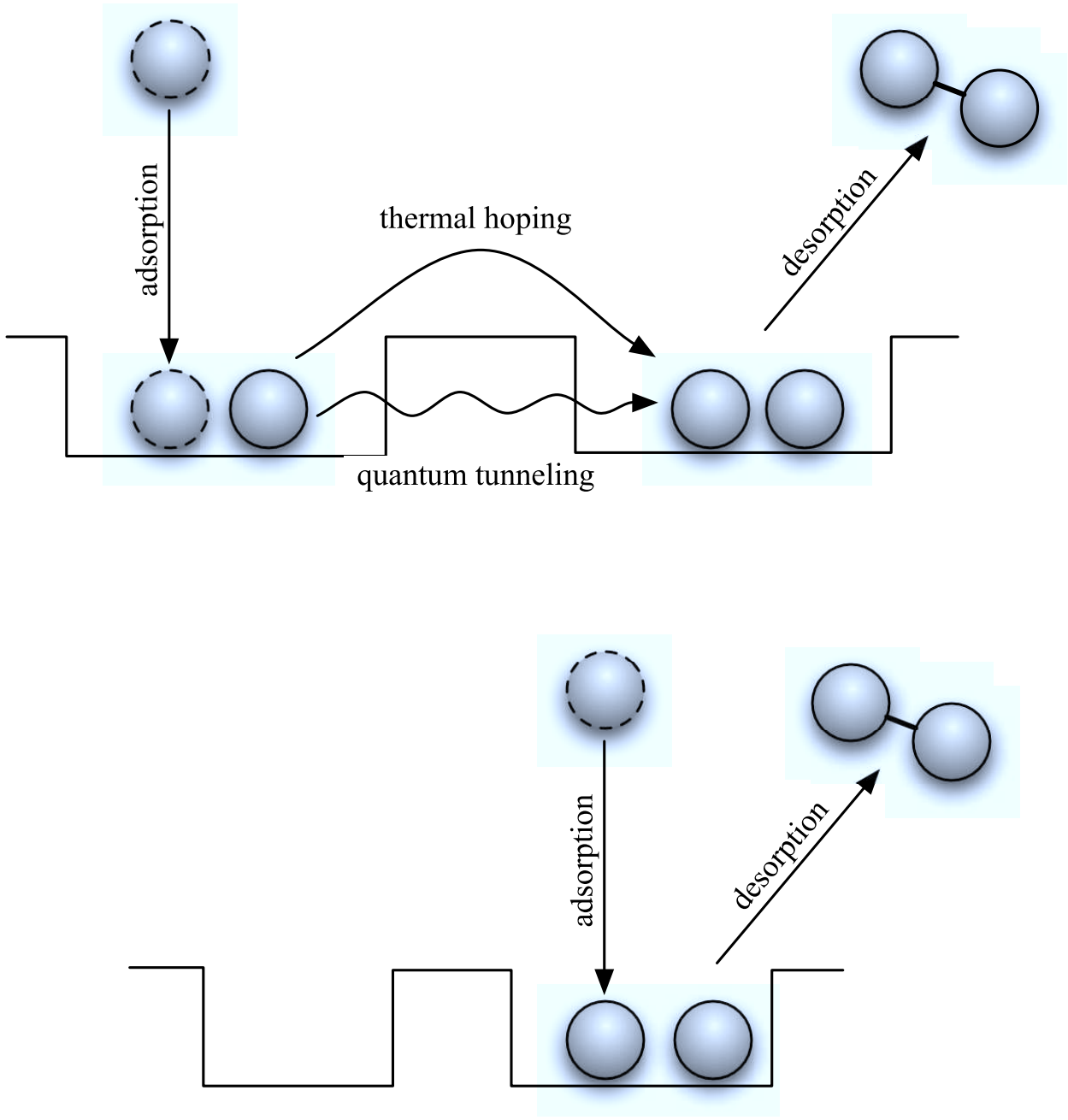

Figure 6.1 Reaction mechanisms on grain surfaces – **Langmuir-Hinshelwood mechanism (top):** Two species adsorb on different sites of the grain surface and one of them diffuse via thermal hoping or quantum tunneling. **Eley-Rideal mechanism (bottom):** One species adsorb on a site already occupied by another one.

- *Thermal desorption*: in the vicinity of a star, the grains can heat to a point at which the vapor pressure of the mantle causes substantial sublimation of the icy material. For water-ice mantle, this occurs around 100 K (Tielens & Allamandola 1987).
- *Cosmic-ray heating*: the passage of cosmic rays through dust deposits energy in each dust grain, causing the evaporation of loosely bound species like CO (Leger et al. 1985).
- *Chemical desorption*: the energy released in exothermic reaction between adsorbed species can lead directly to the ejection of the product, and even possibly of neighboring species, as it is the case for H_2 formation (e.g. Greenberg 1973).
- *Sputtering of dust*: when interstellar gas is shocked (e.g. by a stellar jet), there is substantial gas flow around the dust (leading to h, H_2 and He impacts on the grains), followed by high post-shock temperatures. These cause sputtering of the dust and return of mantle material to the gas (e.g. Pineau des Forets et al. 1993).

6.2 Chemistry of pre-stellar cores

The chemical mechanisms at play during the pre-stellar core phase are important for understanding the chemistry of Class 0 protostars, so I describe in this section several key processes that characterize the chemistry in pre-stellar cores (PSCs): depletion (or freeze-out) of gas-phase species, high deuterium fractionation and grain-surface reactions.

6.2.1 Depletion

Depletion is the process by which molecules stick onto grain surfaces, thereby lowering their abundance with respect to ISM values. It occurs as a direct result of the increase in density with evolution. Freeze-out has been expected due to the fact that, for typical H_2 densities of $10^4 - 10^5$ cm^{-3}, the timescale for a gaseous CO to be deposited onto a dust grain (or depletion timescale) is $\sim 10^5 - 10^4$ yr, comparable to dynamical time-scales of PSCs (Caselli et al. 1999, and references therein).

The amount of depletion of a given molecule is a function of the strength of the physical adsorption bond between that species and the grain surface (i.e. its binding energy to the grain surface), the cross section and number density of the grains, and the velocity of the molecule. Bergin & Langer (1997) modeled the chemistry of evolving and collapsing low-mass protostellar cores. Their models predict that at the middle to late stages of dynamical evolution of a cold dense core, prior to the formation of a protostar, various species will selectively deplete from the gas phase. For example, tightly bound sulfur-bearing molecules such as CS, SO and C_2S, are sensitive to the density increase and exhibit larger and larger depletions as the PSC evolves (these species virtually disappear from the gas-phase for $n(H_2) \sim 3 \times 10^4$ cm^{-3}, corresponding to $t \sim 10^7$ yr in the models presented by Bergin & Langer 1997). On the contrary, due to the assumed low binding energy of the precursor molecule N_2, both NH_3 and N_2H^+ only deplete at

the highest densities ($\sim$ 10^6 cm^{-3}, Tafalla et al. 2002).
Observationally, freeze-out has been seen in several cores with depletion factors 4–1000 (Caselli et al. 1999; Bacmann et al. 2002; Bergin et al. 2002; Pagani et al. 2005; see Di Francesco et al. 2006; Ceccarelli et al. 2006 for reviews). This process has direct consequences on deuterium fractionation and grain-surface reactions as described below. It can also affect the dynamical evolution since depletion affects the ionization fraction, and thereby the coupling of the cloud to the magnetic field. Indeed, in a magnetized cloud, neutral particles contract relative to the ionized species, which are bound to the magnetic field lines (this is the ambipolar diffusion process; Mestel & Spitzer 1956). An increased abundance of ionized particles (i.e. a higher ionization fraction) will counteract the contraction, and so reduce the collapse speed Since electron fraction tends to increase with freezing-out of CO and other neutrals (due to the fact that the destruction rate of H_2D^+ and H_3^+ is reduced, leading to an increase in the abundance of H_2D^+, the main agent of ionization — Caselli 2002), then depletion lengthens star formation timescales.

6.2.2 Deuterium fractionation

High deuterium fractionation is the enhancement of deuterated isotopologues beyond levels expected from the elemental D/H ratio of $\sim 1.5\times10^{-5}$. Deuteration is initiated by the formation of H_2D^+ from HD (the main deuterium reservoir in cold molecular gas, such as PSCs and molecular clouds), via:

$$H_3^+ \ + \ HD \ \rightarrow \ H_2D^+ \ + \ H_2 \qquad (6.2)$$

H_2D^+ can then transfer deuterium to other molecules. However, H_3^+ and H_2D^+ are mainly destroyed by CO. This is why CO depletion plays a role in deuteration as mentioned above. Indeed, for large enough densities ($\gtrsim$ 10^5 cm^{-3}) and low enough temperatures ($\lesssim$ 20 K), CO depletes onto grain surfaces, i.e. the main destruction agent of H_3^+ and H_2D^+ disappears, allowing reaction 6.2 to become the dominant destruction route of H_3^+. Subsequently, the increased abundance of H_2D^+ leads to a more efficient propagation of the deuterium to other molecules, i.e. a higher deuterium fractionation. In fact, H_2D^+ is not the only molecule allowing deuterium transfer from HD to other species. Indeed, further reactions of H_2D^+ with HD in a similar way as in 6.2, will lead to the formation of HD_2^+ and D_3^+. For large CO depletion factors, D_3^+ becomes the most abundant deuterated form of H_3^+ (Roberts et al. 2003; Walmsley et al. 2004; Ceccarelli & Dominik 2005).

Observationally, the role of CO in the large deuteration of PSCs has been demonstrated by Bacmann et al. (2003) and Crapsi et al. (2005), who found that the D/H ratio increases as the CO depletion factor increases (see also Ceccarelli et al. 2006). Quantitatively, D/H ratios are found to be between 0.05 and 0.4 in a sample of dense cores (Crapsi et al. 2005). Observations of PSCs also revealed abundance enhancements of multiply deuterated species, such as D_2CO (Bacmann et al. 2003), ND_3 (Roueff et al. 2005) and D_2H^+ (Vastel et al. 2004, 2006).

6.2.3 Grain-surface reactions

Another important process in PSCs are grain-surface reactions. Grain-surface reactions play a crucial role in many astrophysical environment. The most notable example is the formation of molecular hydrogen in the ISM. Due to the high abundance of this molecule, a high-efficiency process is needed and none of the considered gas-phase reactions satisfy this condition (e.g. Herbst et al. 2005). Grain-surface formation of H_2 has therefore been invoked for many years (as early as 1963 by Gould & Salpeter) and has recently been confirmed by laboratory work (Hornekaer et al. 2003; Roser et al. 2002). Apart from reacting with itself, atomic hydrogen is also thought to react with heavier, slower-moving species that stick to dust particles (e.g. Tielens & Hagen 1982; Hasegawa et al. 1992). In these so-called association reactions, the product formed by the two reactants is stabilized by a third body (here, the grain). This process leads to the formation of another key component of the ISM, water ice, via:

$$\mathrm{O} \xrightarrow{+\mathrm{H}} \mathrm{OH} \xrightarrow{+\mathrm{H}} \mathrm{H_2O} \tag{6.3}$$

or via a set of reactions where O_2 acts as a catalyzer:

$$\mathrm{O} + \mathrm{O_2} \rightarrow \mathrm{O_3} \tag{6.4}$$

$$\mathrm{O_3} + \mathrm{H} \rightarrow \mathrm{O_2} + \mathrm{OH} \tag{6.5}$$

$$\mathrm{OH} + \mathrm{H_2} \rightarrow \mathrm{H_2O} + \mathrm{H} \tag{6.6}$$

which has the net effect: $\mathrm{O} + \mathrm{H_2} \rightarrow \mathrm{H_2O}$.
Other important molecules formed in such a way include NH_3 (from atomic nitrogen) and CH_4 (from atomic carbon).

In PSCs, grain-surface reactions are believed to be responsible, in particular, for the formation of formaldehyde and methanol. Indeed, enhanced methanol (and formaldehyde) abundances are observed in several environments (such as in hot corinos as described in Section 1.2.1, and in outflows associated with some low-mass protostars), and gas-phase models are unable to reproduce these abundances. For example, the methanol abundances observed in Orion are underestimated by up to four orders of magnitude (Menten et al. 1988). This is one of the reasons why this molecule is thought to form on the grains. As early as 1982, Tielens & Hagen proposed a grain-surface route proceeding via successive hydrogenation of CO (a species that is known to freeze-out onto grains in PSCs as mentioned above), leading to the formation of H_2CO and ultimately of CH_3OH :

$$\mathrm{CO} \rightarrow \mathrm{HCO} \rightarrow \mathrm{H_2CO} \rightarrow \mathrm{H_2COH} \rightarrow \mathrm{CH_3OH} \tag{6.7}$$

This process has been studied experimentally by several groups and, although Hiraoka et al. (2002) could not form any CH_3OH in this way, experiments by Watanabe et al. (2003) and Hidaka et al. (2004) found that this process could form methanol efficiently at low temperatures.

Surface chemistry in PSCs also includes deuteration via atomic deuterium, which is produced in the gas by dissociative recombination of deuterated ions, for example:

$$H_2D^+ + e^- \rightarrow D + H + H \quad (6.8)$$

$$D_3^+ + 3e^- \rightarrow D + D + D \quad (6.9)$$

As hydrogen atoms, deuterium atoms diffuse rapidly on grain surface and are highly reactive so that they can produce deuterated species via successive D additions. The relative abundances of the different isotopologues[1] and isotopomers[2] depends on the flux ratio between H and D landing on the grains (Tielens 1983; Charnley et al. 1997). Alternatively, D atoms can substitute H atoms in the main isotopologue: experiments by Nagaoka et al. (2005) showed that methanol could be deuterated in this way.

6.3 Theories of formation paths of selected complex organic molecules

In this section, we review the different reactions that have been proposed for the formation of some complex species. For all the moleules considered here, these reactions can occur in the gas-phase or on grain surfaces. Gas-phase reactions usually involve H_2CO or CH_3OH as precursors, or parents. These are supposed to form on grain surfaces (e.g. Charnley et al. 1995) and evaporate in the gas-phase where they undergo further reaction to form more complex, or daughter, molecules. Grain-surface reactions generally consist in H or O additions and radical-radical reactions.

6.3.1 Formic acid

In the gas-phase model of Leung et al. (1984), the precursor ion of HCOOH, $HCOOH_2^+$, is produced via the radiative association

$$H_2O + HCO^+ \rightarrow HCOOH_2^+ + h\nu \quad (6.10)$$

followed by dissociative electron recombination to produce HCOOH. But Irvine et al. (1990) mention that this reaction is believed not to occur due to a competitive exothermic reaction to form H_3O^+ and CO. Instead, they attribute the gas-phase formation of HCOOH via an ion-molecule reaction followed again by a dissociative electron recombination

$$CH_4 + O_2^+ \rightarrow HCOOH_2^+ + H \quad (6.11)$$

$$HCOOH_2^+ + e^- \rightarrow HCOOH + H \quad (6.12)$$

[1]Isotopologue: species where one or several H atom(s) has/have been replaced by D atom(s); e.g. CH_3OH (the main isotopologue, where no H atoms have been replaced by D atoms) $\rightarrow$ CH_3OD.

[2]Isotopomers: molecules with the same chemical composition but different arrangements of the atoms; e.g. CH_3OD, CH_2DOH.

Reaction (6.12) has been measured in the laboratory and found to be rapid at low temperature (Rowe et al. 1984). Moreover, the calculated HCOOH abundance agrees with the values observed by Irvine et al. (1990) in the dark cloud L134 N.

On grain surfaces, Tielens & Hagen (1982) proposed the formation of HCOOH through successive additions of H, O, and H to solid-state CO:

$$\mathrm{CO} \xrightarrow{\pm\mathrm{H}} \mathrm{HCO} \xrightarrow{\pm\mathrm{O}} \mathrm{HCOO} \xrightarrow{\pm\mathrm{H}} \mathrm{HCOOH} \tag{6.13}$$

The models of Hasegawa & Herbst (1993) are able to reproduce the abundances observed in massive hot cores for ages larger than $10^5 - 10^6$ yr. Moreover, radiolysis experiments (simulating the processing of interstellar ices by cosmic rays) by Hudson & Moore (1999) showed that HCOOH could form in H_2O–CO mixed ices via the above sequence. Finally, the grain-surface formation of HCOOH is supported by the interferometric observations of Sgr B2 and W51 by Liu et al. (2001), and would also be consistent with observations of this molecule in the ices surrounding the massive protostar W33A (Schutte et al. 1999; Gibb et al. 2000b).

6.3.2 Methyl formate

The commonly accepted formation path for $HCOOCH_3$ starts with the reaction between protonated methanol and formaldehyde to form protonated methyl formate and molecular hydrogen:

$$[\mathrm{CH_3OH_2}]^+ + \mathrm{H_2CO} \rightarrow [\mathrm{HC(OH)OCH_3}]^+ + \mathrm{H_2} \tag{6.14}$$

followed by dissociative recombination of $[HC(OH)OCH_3]^+$ with electrons to form $HCOOCH_3$ (Blake et al. 1987). However, laboratory and theoretical work by Horn et al. (2004) indicates the existence of a very large activation energy for reaction (6.14), so that the later cannot lead to the formation of protonated methyl formate. Therefore, the formation of methyl formate in hot cores cannot occur via this reaction. Horn et al. searched for more favorable transitions between the reactants and products of reaction (6.14), but were unsuccessful. These authors also investigated reactions involving other abundant species in hot cores, such as protonated formaldehyde and CO. They show that none of the studied processes produces enough methyl formate to explain the observed abundances. However, they also state that one possibility for producing more methyl formate is that formic acid would be synthesized on grain surfaces and desorbed into the gas phase, in which case the reaction:

$$\mathrm{CH_3^+} + \mathrm{HCOOH} \rightarrow \mathrm{HC(OH)OCH_3^+} + h\nu \tag{6.15}$$

would play a significant role.
As pointed out in section 6.3.1, there are indeed evidences in favor of HCOOH being synthesized on grain surfaces. The downfall is that Horn et al. (2004) find that even if HCOOH is injected with an abundance one order of magnitude higher than observed in OMC-1, their model still

predicts a $HCOOCH_3$ abundance between one and two orders of magnitude below the observed value in this source. In the light of their work, they conclude that $HCOOCH_3$ should be produced at least in part on grain surfaces.

Two schemes for grain-surface formation of $HCOOCH_3$ have been proposed, but none of them has undergone laboratory investigation yet:

- Formation from precursors CO, O, C, and H landing on grain (Herbst 2005):

$$CO + H \rightarrow HCO \tag{6.16}$$

$$C \xrightarrow{+H} CH \xrightarrow{+H} CH_2 \xrightarrow{+H} CH_3 \xrightarrow{+O} CH_3O \tag{6.17}$$

$$CH_3O + HCO \rightarrow HCOOCH_3 \tag{6.18}$$

  Charnley & Rodgers (2005) mention that many radicals (like CH_3O and HCO) could form in close proximity via the hot secondary electron generated by the passage of a cosmic ray through the ice. In this case, it would ensues that radical-radical reactions such as (6.18) could occur efficiently.

- Sorrell (2001) proposed a model in which the photoprocessing of grain mantles by UV starlight creates a high concentration of radicals in the bulk interior of mantles. Grain-grain collisions then provide excess heat causing radical-radical reactions to occur and form large organic molecules. In this scheme, $HCOOCH_3$ would be produced from the reaction between the carboxyl acid (COOH) and the methyl group (CH_3) in the following way:

$$CO + OH \rightarrow COOH \quad \text{or} \quad HCO + HCO \rightarrow COOH + CH \tag{6.19}$$

$$CH \xrightarrow{+H} CH_2 \xrightarrow{+H} CH_3 \tag{6.20}$$

$$COOH + CH_3 \rightarrow HCOOCH_3 \tag{6.21}$$

  However, any grain-surface chemistry preceding the hot core/corino phase would occur in a very dense and highly visually extinct environment, hence well shielded from UV starlight. Therefore, such a UV photolysis of grains is unlikely to happen, as pointed out by Peeters et al. (2006). Nevertheless, the radical-radical reaction (6.21) could still be a possible formation path for $HCOOCH_3$ via cosmic ray processing.

6.3.3 Dimethyl ether

CH_3OCH_3 was proposed by Blake et al. (1987) to form in the gas-phase by methyl cation transfer to methanol, followed by electron dissociative recombination:

$$CH_3OH_2^+ + CH_3OH \rightarrow CH_3OCH_4^+ + H_2O \tag{6.22}$$

$$CH_3OCH_4^+ + e^- \rightarrow CH_3OCH_3 + H \tag{6.23}$$

Peeters et al. (2006) claim that their models support such a gas-phase route if the methanol abundance is of the order 10^{-6} or more, as it is the case for the OMC-1 hot core (recall that for hot corinos, $X(CH_3OH) \leq 3 \times 10^{-7}$). However, Ceccarelli et al. (2006) note that experimental measurements of the neutral products of dissociative recombination reactions show that two-body products such as in reaction (6.23) are often minor channels. Therefore, gas-phase formation of CH_3OCH_3 is plausible but not demonstrated.

On the grains, CH_3OCH_3 could be produced by a similar scheme as for $HCOOCH_3$, that is cosmic ray processing followed by the radical-radical reaction $CH_3 + CH_3O \rightarrow CH_3OCH_3$ (Allen & Robinson 1977). As in the case of $HCOOCH_3$, this reaction has not been validated by laboratory studies.

6.3.4 Methyl and ethyl cyanide

For completeness, I mention here the possible formation routes of these two molecules. However, I will not discuss them any further in this work, due to the lack of data on potential parents such as NH_3.

Two substantially different formation routes for CH_3CN have been proposed in the literature: either in the gas-phase or on grain surfaces.

- In the Rodgers & Charnley (2001) chemical model of massive hot cores, CH_3CN is synthesized in the gas-phase from NH_3 in the following way: HCN is synthesized from the reaction between NH_3 and C^+ (yielding $HCNH^+$, reaction (6.24)), followed by electron recombination or proton transfer to ammonia (6.25). CH_3CN is then formed from the radiative association between the methyl ion and HCN (6.26), again followed by electron recombination (6.27):

$$NH_3 + C^+ \rightarrow HCNH^+ \tag{6.24}$$

$$HCNH^+ + e^- \rightarrow HCN + H \text{ or } HCNH^+ \rightarrow HCN + NH_4^+ \tag{6.25}$$

$$CH_3^+ + HCN \rightarrow CH_3CNH^+ + h\nu \tag{6.26}$$

$$CH_3CNH^+ + e^- \rightarrow CH_3CN + H \tag{6.27}$$

  Comparisons between the results from this model and observations suggest that a grain-surface formation of CH_3CN is not required.

- On grain surfaces, CH_3CN can be formed by successive hydrogenation of C_2N or by recombination between CN and CH_3:

  - $C_2N \xrightarrow{+H} HCCN \xrightarrow{+H} CH_2CN \xrightarrow{+H} CH_3CN$. This set of reactions, used in Caselli et al. (1993), underestimates the CH_3CN abundance by a factor about 50 compared to the

Table 6.2 Summary of gas-phase and grain-surface reactions for the formation of selected complex organic molecules.

Molecule	Gas-phase	Grain-surface
HCOOH	$CH_4 + O_2^+ \rightarrow HCOOH_2^+ + H$ $HCOOH_2^+ + e^- \rightarrow HCOOH + H$	$CO \xrightarrow{+H} HCO \xrightarrow{+O} HCOO \xrightarrow{+H} HCOOH$
$HCOOCH_3$	$H_2COH^+ + H_2CO \rightarrow H_2COHOCH_2^+ + h\nu$	$CH_3O + HCO \rightarrow HCOOCH_3$ $COOH + CH_3 \rightarrow HCOOCH_3$
CH_3OCH_3	$CH_3OH_2^+ + CH_3OH \rightarrow CH_3OCH_4^+ + H_2O$ $CH_3OCH_4^+ + e^- \rightarrow CH_3OCH_3 + H$	$CH_3 + CH_3O \rightarrow CH_3OCH_3$
CH_3CN	$CH_3^+ + HCN \rightarrow CH_3CNH^+ + h\nu$ $CH_3CNH^+ + e^- \rightarrow CH_3CN + H$	$C_2N \xrightarrow{+H} HCCN \xrightarrow{+H} CH_2CN \xrightarrow{+H} CH_3CN$ $CN + CH_3 \rightarrow CH_3CN$

abundance observed in the Orion hot core. This could be explained by the fact that HCCN formation is in competition with C_3N formation and the former is indicated by the authors as a less important pathway.

– $CN + CH_3 \rightarrow CH_3CN$ (Hasegawa & Herbst 1993), which yield a CH_3CN abundance in good agreement with the Orion hot core value for an age of 10^5 yr.

Regarding C_2H_5CN, some studies point towards grain-surface formation of this molecule by hydrogenation of HC_3N (Blake et al. 1987; Charnley et al. 1992; Caselli et al. 1993). Observations by Liu & Snyder (1999) are consistent with this theory. However, the abundance ratio of CH_3CN to C_2H_5CN predicted by Caselli et al. (1993) is at least two orders of magnitude smaller than the ratio observed in hot cores and hot corinos. Therefore, it seems unlikely that both CH_3CN and C_2H_5CN form via the surface reactions proposed by Caselli et al.

6.3.5 Summary

For all the complex molecules considered here, grain-surface formation is a possible alternative to gas-phase formation. So far, we implicitly implied that grain-surfaces processes were taking place during the cold phase preceding the heat-up of the dust by the newly born star. However, during the warm-up phase, it is improbable that the dust temperature suddenly jumps from ∼10 to ∼100 K. Instead, there is more likely a temperature gradient leading to a gradual heating of the grains (e.g. Viti et al. 2004; Garrod & Herbst 2006). The effect of this gradient on grain-surface and gas-phase chemistry can be quite substantial. Indeed, the modeling by Garrod & Herbst (2006) shows that gas-phase and grain-surface chemistries are strongly coupled during the warm-up phase: molecules formed on the grain can evaporate and affect the gas-phase chemistry whose products can re-accrete and change in turn the grain-surface chemistry. In particular, Garrod & Herbst (2006) find that $HCOOCH_3$, HCOOH and CH_3OCH_3 are formed via both gas-phase and grain-surface chemistry, although surface processes are dominant for slower onset of the central object.

Note that for some molecules, grain-surface formation is not only an alternative, but also apparently the only choice. This is the case for $HCOOCH_3$ and even more so for HCOOH since it has been detected in the ices of star forming regions (e.g. Schutte et al. 1999; Keane et al. 2001), as well as of quiescent molecular clouds (Knez et al. 2005). In particular, the detection of icy HCOOH in quiescent clouds would indicate, not only that HCOOH formation occurs on grain-surface, but also that it would pre-date the first phase of the star formation mechanism, supporting the theory of formation in the cold, rather than warm-up phase. Whether the other complex organic molecules could also follow the same pattern cannot be commented upon since, to our knowledge, no other complex molecule has been detected in ices. This is because unfortunately, the infrared spectra of complex organic molecules are not well known in this medium. The difficulty in determining the presence of these molecules lies in the fact that they may produce only slight shifts and broadenings, and that the peak positions are characteristic of functional groups not molecular species (Tielens, priv. comm.). Hence, specific identifications are always somewhat ambiguous. The carbonyl (C=O) group is probably best to search for and Keane et al. (2001) attributed an absorption feature at 5.8 μm to this group in H_2CO and HCOOH.

Overall, it also stands out from the above sections that more experiments on thermal surface chemistry at low temperatures are needed to check the feasibility of the outlined reactions. Also, since cosmic ray processing of icy grain mantles seems able to produce complex molecules, quantitative models are also necessary to determine the expected amount of specific molecules from this process.

6.4 Implications

In this section, I refer to the ratios of complex molecules' abundances to CH_3OH and H_2CO abundances that were derived in Chapters 3 and 5, and plotted in Figures 3.7, 3.8, 5.2 and 5.3. Since the later two figures summarized the data for both hot corinos and hot cores, I show them again here as Figures 6.2 and 6.3, for pratical purposes.

6.4.1 Abundance ratios in hot corinos

In sections 3.5.2, I showed that the abundance ratios of complex organic molecules to H_2CO or CH_3OH in hot corinos (i) are of order unity and (ii) do not seem to depend on the CH_3OH or H_2CO abundances, as can be seen from Figures 6.2 and 6.3. The implications are:

- *In the case of gas-phase formation from methanol or formaldehyde:* (i) and (ii) mean that, in all the hot corinos, the formation of complex molecules uses up a significant fraction of the parent molecules sublimated from the mantles. However, gas-phase chemistry does not seem able to reproduce this behavior. For example, the collapsing envelope model of Rodgers & Charnley (2003; see also Rodgers & Charnley 2001) predicts CH_3OCH_3

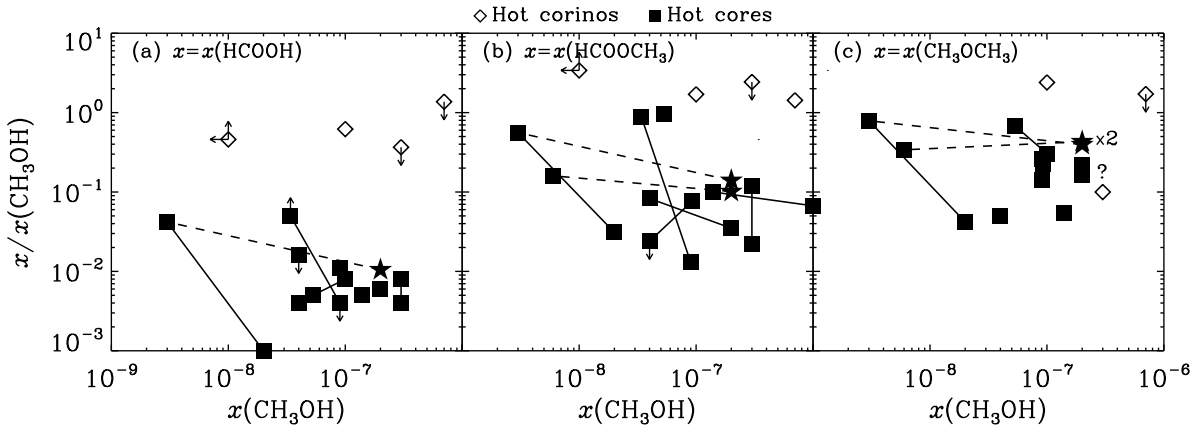

Figure 6.2 Abundance ratios of complex O-bearing molecules to methanol, plotted as a function of the methanol abundance, in hot corinos and in hot cores. Open diamonds represent hot corinos. Filled squares represent abundances ratios of hot cores, derived from beam-averaged column density analysis. See Figure 5.2 for details.

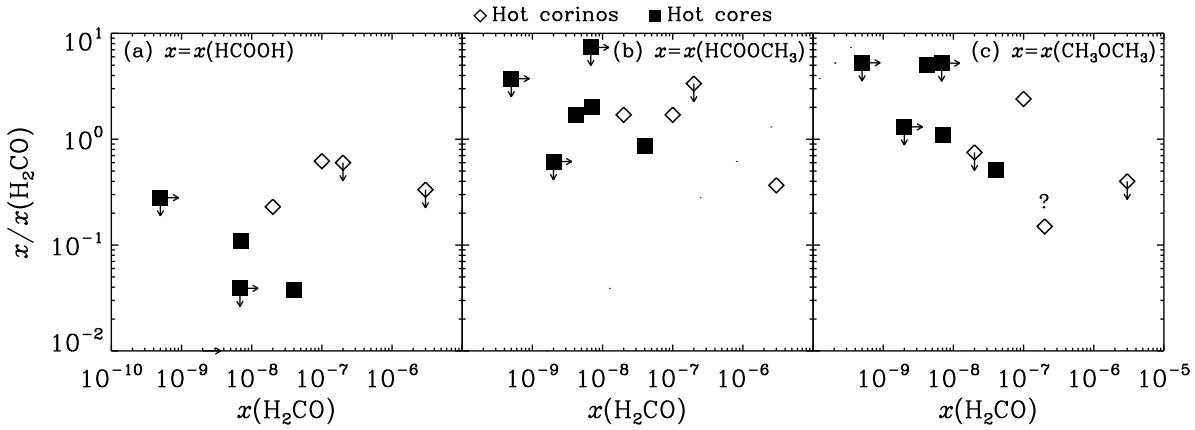

Figure 6.3 Abundance ratios of complex O-bearing molecules to formaldehyde, plotted as a function of the formaldehyde abundance, in hot corinos and in hot cores. Open diamonds represent hot corinos. Filled squares represent abundances ratios of hot cores, derived by beam-averaged column density analysis.

to CH_3OH abundance ratios of only $10^{-2} - 10^{-1}$. Similarly, Rodgers & Charnley (2001) predicted $HCOOCH_3$ to CH_3OH abundance ratios $< 7 \times 10^{-3}$, and we now know that they used too high a formation rate coefficient for $HCOOCH_3$, so that the actual prediction should be even smaller (Horn et al. 2004). Therefore, either gas-phase models are not adequate, or complex molecules are not formed in the gas phase.

- *In the case of grain-surface formation:* (i) and (ii) show that complex molecules are as important mantle constituent as CH_3OH and H_2CO. Observations of solid HCOOH and CH_3OH along quiescent lines of sight by Knez et al. (2005) and in protostars (Keane et al. 2001) support this idea since the quoted HCOOH and CH_3OH abundances yield abundance ratios of order unity, as I find for the hot corinos. No observations of other complex molecules in the ices are available, but their presence cannot be excluded considering, as mentioned in section 6.3.5, the difficulty of identifying their signature in infrared spectra.

Note that gas-phase reactions proposed in section 6.3.1 for the formation of HCOOH do not involve CH_3OH or H_2CO. Therefore the conclusion mentioned for gas-phase formation do not apply to this molecule, whereas the analysis regarding grain-surface formation is still valid.

Overall, in the Maret et al. (2004, 2005) framework, the hot corino data presented in my thesis are consistent with either gas-phase or grain-surface formation of complex molecules in hot corinos, with nonetheless more support for the later route. However, other scenarios could be considered. For example, complex molecules could form in the ISM, deplete onto grain mantles during the accretion phase and desorb as the protostar heats up its environment. If this formation in the ISM were true, we should be able to observe their low-energy transitions in dark clouds or in the cold envelopes of the protostars. For example, Remijan & Hollis (2006) observed a transition of HCOOH with E_u=3.2 K around IRAS16293B for which the spatial distribution is around (and not peaking at) the position determined from the continuum. I also showed in Section 4.4.2 that there was some extended CH_3CN emission, i.e. from the cold outer envelope, in IRAS4A. I cannot therefore rule out this theory, but more observations are needed to support it.

6.4.2 Comparison with abundance ratios in hot cores

In Section 5.4, I found that the abundance ratios of complex molecules to CH_3OH in hot corinos were larger than in hot cores (see Figure 6.2), i.e. that the complex molecules were relatively more important in hot corinos.
This could be due to a difference in the chemistry, since the later depends on environmental parameters such as the density and temperature of the gas. For example, the model of Rodgers & Charnley (2001) shows that the predicted abundances are more or less important at 100 or 300 K, depending on whether O- or N-bearing species are considered. In any case, since high-mass protostars are several orders of magnitude more luminous than low-mass ones, the sublimation region is expected to be larger in the former, so that overall, complex organic

molecules would be relatively more abundant in hot cores if formed in the gas-phase. However, I observe the opposite, which seems to favor grain-surface formation. A number of processes presented in Sections 6.2 and 6.3 would support this interpretation:

- *Deuterium fractionation* (§6.2.2)
  It is already known that the levels of deuteration differ in low-mass and high-mass protostars, more specifically that extreme deuteration occurs in low-mass but not in high-mass protostars (e.g. Ceccarelli et al. 2006 and references therein). So a possible explanation for the difference between hot cores and hot corinos could lie in the overall grain mantle composition. Indeed, Boogert et al. (2004) summarize the abundances of some mantle constituents (H_2O, CO, CO_2, CH_3OH, OCN^-) in two low-mass and high-mass embedded protostars and there also large differences can be seen. It would therefore not be surprising that this would also be the case for complex molecules if they formed on the grain surfaces.

- *Grain-surface reactions in the PSC phase* (§6.2.3)
  Hot corinos are preceded by a longer cold phase than hot cores are. During this phase, grain-surface reactions are at play, building up the icy mantles. Therefore, in the case of grain-surface synthesis, complex molecules in hot cores would not have time to become as important a grain-mantle constituent as in hot corinos.

- *UV/X/cosmic-ray processing* (§6.3)
  Recall that all the proposed grain-surface formation routes of complex molecules involved (secondary) UV, X-ray or cosmic-ray processing. Hot cores/corinos are shielded from external UV radiation fields, but low-mass protostars, unlike massive ones, are known to be powerful X-ray sources (e.g. Feigelson & Montmerle 1999). X-rays have already been proposed to be the reason for the presence of calcite in the low-mass protostars (Chiavassa et al. 2005; Ceccarelli et al. 2002b). In our case, X-rays emitted by Class 0 objects could provide the necessary energy to produce a large number of radicals and hence a large amount of complex molecules on the grain surfaces, thereby explaining the larger abundance ratios observed in hot corinos compared to hot cores.

- *Gradual warm-up* (§6.3.5)
  Considering for example the methyl formate, the gas-grain model in the warm-up phase presented in Garrod & Herbst (2006) shows that the gas-phase formation of this molecule is more efficient at low temperatures, and that the grain-surface pathway leads to higher abundances the longer the dust temperature remains in the $40 - 60$ K range. Either way, formation of complex molecules during the warm-up stage of the protostar would be more efficient in low- than in high-mass environments.

Note that due to the low number statistics of hot corinos, the explanations proposed to account for the apparent difference with hot cores are only pathways to explore, and further observations are needed to increase the number of known hot corinos and hence to understand better any variation between the two types of objects.

6.4.3 Comparison with abundance ratios in Galactic Center clouds

Hot corinos/cores are not the only objects where complex molecules have been observed. Indeed, Requena-Torres et al. (2006) have carried out a survey of complex O-bearing molecules in Galactic Center (GC) clouds. These clouds are known to possess a warm (> 100 K) and not too dense ($\sim 10^4$ cm^{-3}) gas (Hüttemeister et al. 1993; Rodríguez-Fernández et al. 2000; Ceccarelli et al. 2002a). This warm component is probably caused by shocks (e.g. Flower et al. 1995; Rodríguez-Fernández et al. 2004) arising from cloud-cloud collisions (Hüttemeister et al. 1993, 1998). These shocks are thought to be at the origin of the enhanced NH_3 (Flower et al. 1995), SiO (Martín-Pintado et al. 1997) and C_2H_5OH (Martín-Pintado et al. 2001) abundances. Surprisingly enough, considering the very different physical environments between GC clouds and hot corinos, Requena-Torres et al. (2006) found, as I did in Chapter 3 for hot corinos (see also Bottinelli et al. 2006), that the ratios of the abundances with respect to CH_3OH (which are comparable to those reported in Figure 6.2 for hot cores) are approximately constant and do not depend on the CH_3OH abundance. The authors conclude that the gas-phase abundances of the organic molecules they observed in GC clouds are likely due to the formation of these molecules on the grain surfaces and their release in the gas-phase from sputtering/erosion of the grain mantles by the shocks, as it is the case for ammonia, silicon oxide and ethanol.

These observations have some implications for two of the processes already approached in the previous section:

- *X-ray processing*
  There is evidence for the presence of X-rays in these GC clouds as noted by Martín-Pintado et al. (2000) who suggest that X-rays could contribute to the formation of molecules on grain surfaces and evaporate small dust grains. This theory adds some support to the possible role played by X-rays in the formation of complex organic molecules on the grains.

- *Gradual warm-up*
  Since GC clouds are not subject to a warm-up phase, it would seem at first that the observations of complex molecules in these sources are acting against the gradual warm-up theory. However, recall as well that the abundance ratios in GC clouds are comparable to those in hot cores, i.e. *smaller* than in hot corinos. Therefore it may be possible that complex molecules are solely formed on grain-surfaces in GC clouds, while they are formed via the gradual warm-up schemes in hot corinos, and the (small) interaction with the gas-phase would make the complex molecules formation more efficient, thereby accounting for the difference between GC clouds and hot corinos.

Conclusion

The overview of the chemical processes intervening at different stages leading to the observation of complex organic molecules show that explaining their existence is far from straightforward

due to the many (interacting) factors potentially involved. Nethertheless, I believe that it will be possible, via a combination of larger observational datasets, (increasingly more) accurate models, and more laboratory experiments, to disentangle these factors. Until then, I tried to answer one of the long-standing questions regarding the formation of complex molecules, namely whether they are synthesized in the gas-phase or on grain-surfaces. As often in physics, it might not be a "black-or-white" issue, as it has been suggested that the observed abundances could be the result of a coupling between gas-phase and grain-surface reaction. But overall, although there is no absolute proof, there is circumstantial evidence for the formation of complex organic molecules on grain surfaces, either in the cold phase preceding the begin of the star formation process, or in the warm-up phase following the birth of the protostar. In these scenarios, there is also a possibility that X-rays emitted by low-mass protostars participate in the formation of these complex molecules.

Chapitre 7
Conclusions et perspectives

7.1 Conclusions

Dans la section 1.3, j'ai présenté l'ébauche du contenu de ma thèse sous la forme de cinq questions auxquelles mon travail se voulait de répondre. Je réitère ces questions ci-dessous, avec les résultats apportés par mes observations et la façon dont ces dernières aident à construire la route menant aux réponses des quêtes posées.

1. *Y a-t-il un saut dans l'abondance de H_2CO dans les protoétoiles de Classe 0?* (Chapitre 2)

   Dans ce chapitre, j'ai rappelé le rôle essentiel de la détermination des profils d'abondance de H_2CO, un composant principal des manteaux des grains. En effet, la présence d'un saut dans ce profil indiquerait la présence de régions internes chaudes dans les enveloppes des protoétoiles de Classe 0, où les manteaux des grains subliment. De plus, puisque H_2CO est très probablement un réactif menant à la formation de molécules complexes dans la phase gazeuse, il est crucial de connaître son abondance. Le saut de H_2CO a été proclamé et débattu dans la littérature et des observations de transitions à hautes energies de H_2CO devraient fournir les informations nécessaires pour résoudre la controverse. En utilisant le JCMT, un télescope à antenne unique de 15 mètres, j'ai donc observé la transition $J = 7 - 6$ de H_2CO ($E_{\rm up} = 74$ cm^{-1}) dans cinq protoétoiles de faible masse, et je l'ai détectée dans toutes les sources. La comparaison des flux observés et prédits montre que le modèle de sauts semble plus approprié qu'un modèle constant pour IRAS16293, L1448-MM et L1448-N, alors que ce pourrait être l'inverse pour IRAS4A et IRAS4B. Dans tous les cas, les données présentées sont encore insuffisantes pour confirmer ou exclure l'une des deux hypothèses.

2. *Les hot corinos sont-ils communs parmi les protoétoiles de faible masse?* (Chapitre 3)

   La découverte d'un hot corino dans IRAS16293 a montré que, malgré le défi théorique posé par leur présence, les molécules organiques complexes peuvent se former dans l'enveloppe

interne d'un objet de Classe 0. Une question naturelle était donc de savoir si IRAS16293 est une exception ou si ces molécules sont omniprésentes dans les environnements chauds des protoétoiles de type solaire. J'ai donc cherché des molécules organiques complexes dans trois autres sources de Classe 0 (IRAS4A, IRAS4B et IRAS2A) avec l'IRAM-30m, et j'ai effectivement trouvé certaines des molécules visées dans ces trois objets, indiquant que les hot corinos sont probablement des objets répandus. Comparé à IRAS16293, un plus petit nombre de molécules a été trouvé, ce qui est probablement dû au fait que mes cibles ont une plus faible luminosité (et donc une région de sublimation plus petite) et sont plus éloignées que IRAS16293. Par contre, les abondances relatives (par rapport à un composant majeur des manteaux des grains, tel que CH_3OH) sont comparables dans les quatre sources, ce qui pourrait signifier que la chimie est semblable d'une Classe 0 à une autre.

3. *Où sont situées les molécules complexes?* (Chapitre 4)

   À l'origine, la présence des molécules organiques complexes a été proposée comme étant due au chauffage thermique des manteaux de glace des grains dans l'enveloppe interne, mais d'autres scenarios ont été suggérés: la désorption des molécules piégées dans les manteaux de glace pourrait être provoquée par les chocs occasionnés par les flots, la turbulence ou le chauffage des murs d'une cavité par rayons UV ou X, plutôt que par chauffage thermique. Il a également été proposé que les molécules pouvaient être situées à la surface d'un disque circumstellaire, au lieu d'être réparties dans toute l'enveloppe interne. La région d'émission des molécules complexes est donc un facteur clé pour mieux comprendre leur formation et leur présence dans la phase gazeuse. La taille de cette région ayant été prédite d'être de l'ordre de $1''$, l'utilisation d'un interféromètre est nécessaire. J'ai fait des observations de IRAS16293 et IRAS4A avec le Plateau de Bure de l'IRAM, qui ont montré que l'émission des molécules complexes est compacte et de taille $\lesssim 0.8''$, et qu'une composante étendue est présente dans IRAS4A mais pas dans IRAS16293. Aucune preuve de l'interaction du flot ou de la présence de cavités n'a été trouvée et mes données soutiennent donc la théorie du chauffage thermique.

4. *Les hot corinos sont-ils semblables aux hot cores?* (Chapitre 5)

   Puisque les molécules organiques complexes ont d'abord été découvertes dans hot cores des protoétoiles massives, j'ai pensé que des informations pouvaient ressortir de la comparaison de ces deux types d'objets. Pour les hot cores massifs, j'ai utilisé les données trouvées dans la littérature et j'ai fait des observations complémentaires avec le JCMT pour montrer que les molécules organiques complexes sont relativement plus abondantes dans les hot corinos que dans les hot cores. Les facteurs possibles expliquant cette différence sont la composition des manteaux des grains, l'efficacité des réactions chimiques ayant lieu dans la phase

gazeuse et/ou à la surface des grains, ou la quantité de rayons X émanant de l'objet central.

5. *Quelle est la voie de formation de ces molécules?* (Chapitre 6)

   A l'exception de la molécule $HCOOCH_3$, pour laquelle des données récemment obtenues en laboratoire ont montré que la formation en phase gazeuse de cette molécule est fortement improbable, des chemins de réaction à la fois en phase gazeuse et à la surface des grains ont été suggérés pour la formation des molécules complexes détectées dans les hot corinos. Bien que mes observations n'excluent aucun des deux procédés, les abondances relativement plus élevées des molécules complexes trouvées dans les hot corinos, comparées aux hot cores, soutiennent la formation à la surface des grains. En effet, au moins deux paramètres pourraient donner aux hot corinos l'opportunité de développer des manteaux plus riches en molécules complexes: d'une part, l'échelle de temps de la phase pré-stellaire (pendant laquelle les manteaux des grains se forment) est plus longue pour les protoétoiles de faible masse que pour celles de haute masse, d'autre part, le rayonnement X émis par les protoétoiles de faible masse est relativement plus important que celui émis par les protoétoiles massives, ce qui pourrait diversifier les réactions de surface et/ou augmenter leur efficacité.

7.2 Perspectives

Continuer la chasse aux hot corinos: IRAM-30m, Effelsberg et GBT

Le fait d'avoir trouvé trois hot corinos sur trois sources ciblées est très encourageant. Cependant, bien que j'ai essayé de chercher des tendances dans les abondances de molécules complexes que j'ai calculées, les faibles statistiques ne permettent pas des conclusions sûres. Il est donc nécessaire de détecter plus d'objets et de déterminer leur composition chimique afin de confirmer les résultats présentés. Plusieurs antennes sont idéales pour poursuivre cette recherche. L'IRAM-30m permet d'obtenir la plus haute sensibilité et couverture spectrale dans le domaine millimétrique et ces caractéristiques ont fait leurs preuves comme le montrent les détections que j'ai présentées dans le chapitre 3. Puisque de l'émission étendue provenant de l'enveloppe froide a été déduite dans IRAS4A, une autre façon de chercher les hot corinos est d'utiliser le télescope d'Effelsberg ou le Green Bank Telescope (GBT): ils fonctionnent à des fréquences plus basses que l'IRAM-30m, permettant ainsi la détection de transitions de plus basses energies. Ces observations peuvent être ensuite combinées avec des données interférométriques du Very Large Array pour déterminer la taille de la composante compacte.

Continuer à pister: ALMA

L'interféromètre du Plateau de Bure (PdB) de l'IRAM est actuellement le plus sensible pour faire des observations à haute résolution de l'émission des molécules organiques complexes dans les hot corinos. Il y a cependant deux problèmes dûs aux faibles luminosités des protoétoiles de

Classes 0: (i) avec les observations d'IRAS4A, j'ai atteint la plus haute résolution dont le PdB est capable ($\sim$0.″8 à 3 mm), mais ces données montrent aussi que la taille du hot corino est plus petite que cela; (ii) il paraît difficile de faire, dans un laps de temps raisonnable, un recensement interférométrique des molécules complexes dans ces sources.
Un tel projet (c'est-à-dire, mesurer la taille d'émission des molécules complexes dans plusieurs hot corinos) sera faisable avec l'instrument de prochaine génération, l'Atacama Large Millimeter Array (ALMA), qui aura les plus hautes sensibilités et résolutions requises: seulement une heure d'intégration sur la source, au lieu de sept, pour atteindre la même sensibilité et résolution spectrale que pour les observations d'IRAS4A, mais avec une résolution spatiale de 0.″1. Les résultats de ce recensement interférométrique devraient fournir des informations capitales pour contraindres les modèles chimiques des hot corinos.
En attendant, on peut encore en apprendre beaucoup avec le PdB (grâce notamment aux nouveaux récepteurs et aux lignes de bases étendues) en choisissant avec soin les molécules et sources ciblées.

Travail théorique et en laboratoire

Les modèles chimiques des hot cores et hot corinos sont limités par la précision des réseaux chimiques et des coefficients de réactions (e.g. Aikawa et al. 2003; Wakelam et al. 2004, 2005). Ainsi, comme l'ont montré des études récentes (e.g. Garrod & Herbst 2006; Horn et al. 2004), le travail en laboratoire est indispensable pour améliorer la précision des modèles chimiques et notre compréhension des observations. Quelques pistes pourraient être suivies dans ce domaine:

- les coefficients de réaction de surface sont mal connus et seulement une poignée d'études ont essayé de s'attaquer à ce problème. Des nouveaux réseaux de réactions sont actuellement en train d'être développés pour inclure des procédés tels que la photolyse et les réactions entre radicaux (Widicus Weaver et al. 2005). Ce travail permettra d'avoir une base de données plus complète à utiliser dans les modèles chimiques.

- peu de modèles prennent en compte la dynamique de l'enveloppe protostellaire. Un travail notoire à cet égard est celui de Ceccarelli et al. (1996), mais le réseau chimique de ce modèle n'inclue pas de molécules complexes. La modélisation de Rodgers & Charnley (2003) a pallié ce manque, mais utilise seulement un réseau de réactions en phase gazeuse alors qu'il est maintenant clair que les procédés à la surface des grains doivent être pris en compte. Des recherches sont en cours (Aikawa et al. en préparation), sur le couplage des chimies en phase gazeuse et à la surface des grains dans une enveloppe en effondrement, afin de sonder les effets de la dynamique sur la formation et la localisation des molécules complexes. Des observations interférométriques actuelles et à venir sont/seront tout à fait adéquates pour contraindre ce type de modélisation.

- il y a tellement de raies non identifiées dans les spectres observés qu'il est possible que des molécules clés manquent dans les réseaux menant aux molécules complexes. Par exemple,

ainsi que Hollis (2005) l'a récemment dit, "l'isomérisme est-il la clé" des molécules complexes? Hollis suggère que les isomères tels que celui de H_2CO, t-HCOH, pourraient avoir un rôle important dans la formation des molécules complexes. Afin d'établir si cet isomère et d'autres sont présents dans l'espace, il est nécessaire de déterminer leur spectres, rotationnels, ce qui peut être fait par des modèles "ab initio" de chimie quantique ou par des mesures en laboratoire (Hollis 2005).

"Molecular Universe" est un réseau européen financé par le "Sixth Framework Programme" (FP6) de l'Union Européenne. Le but de ce réseau, dans lequel le Laboratoire d'AstrOphysique de Grenoble (LAOG) est impliqué, est de fournir des expériences en laboratoire clés et des calculs de chimie quantique pour des molécules simples. Malheureusement, le sujet des molécules organiques complexes n'est pas couvert par ce réseau, mais, dans le cas où des hypothèses de simplification peuvent être faites pour les molécules complexes, j'espère que certains résultats pourront être utilisés pour mieux comprendre la chimie de ces espèces ou pour renforcer l'argumentation de la nécessité d'expériences et de calculs dédiés.

Avancer sur le chemin de l'évolution

Le devenir des molécules organiques complexes observées dans les hot corinos est bien sûr d'un intérêt particulier puisque certaines de ces espèces sont aussi observées dans les comètes de notre Système Solaire. Ces molécules sont-elles détruites et reformées dans la nébuleuse proto-planétaire? Se peut-il qu'elles se (re)collent sur les grains de poussière, si bien que le matériau circumstellaire garderait une "mémoire chimique" des phases précoces de formation? Avec nos connaissances et instruments actuels, il paraît difficile de savoir si on peut répondre à ces questions. Cependant, j'espère que les hautes sensibilités et résolutions d'ALMA permettront d'obtenir des observations révolutionnaires d'objets plus évolués. Par exemple, Lahuis et al. (2006) ont trouvé du gaz chaud dans les régions internes (<6 AU) d'un objet de Classe I, et on peut donc se demander quelle genre de chimie a lieu dans ce gaz. Toujours plus loin sur le chemin d'évolution, les molécules complexes pourraient se former sur les grains dans le plan médian, froid et dense, d'un disque proto-planétaire, comme elles l'ont fait dans le cœur pré-stellaire, également froid et dense. Si les couches du disque pouvaient se mélanger, alors la désorption des molécules pourrait survenir lorsque les grains atteignent la surface ou le bord interne du disque (suivant si le mélange est radial ou vertical), auquel cas il y aurait une possibilité d'observer leur émission.

7.3 Le mot de la fin

Les observations et études des hot cores ont mené à la recherche et découverte des hot corinos. Cela a ouvert de nouvelles perspectives sur le premier type d'objets, notamment en ce qui concerne les processus chimiques en place. Les hot corinos sont des objets très intéressants en eux-mêmes. En effet, leur chimie pourrait affecter la composition chimique des materiaux à partir desquels les planétésimaux se forment éventuellement. Il est également possible que les molécules

organiques complexes se reforment dans le plan médian, froid et dense, du disque protoplanétaire de la même manière que pendant l'effondrement précédant la phase de Classe 0. Dans un cas comme dans l'autre, ces esp'eces pourraient jouer un rôle majeur dans notre compréhension de la composition des corps planétaires. Incidemment, les hot corinos peuvent aussi nous aider à mieux comprendre leur homologues massifs. Au cours des 20 dernières années, nous sommes partis des hot cores pour arriver aux hot corinos. Je me suis principalement concentrées sur les hot corinos, une nouvelle classe d'objets pour laquelle j'ai trouvé et commencé à caractériser les quelques premiers membres. J'espère que cette thèse aidera à indiquer le chemin, non seulement pour de futurs travaux qui continueront la quête de la compréhension de cette phase critique de l'évolution de protoétoiles de type solaire, mais aussi pour les études qui retourneront vers les hot cores!

Finalement, il ressort clairement de ce travail que non seulement plus de données (antenne simple, interférométrie et transitions à hautes énergies) sont requises, mais aussi que des études en laboratoire des réactions à la surface des grains sont nécessaires afin de répondre aux questions quelles, pourquoi, où et comment les molécules complexes se forment.

Chapter 7
Conclusions and perspectives

7.1 Conclusions

In section 1.3, I outlined the content of my thesis in the form of five questions that this work aimed at answering. I list here these questions again, along with the findings that came from my observations and how they helped to pave the road leading to the answers to the quests exposed in the outline.

1. *Is there a H_2CO abundance jump in Class 0 protostars?* (Chapter 2)

   In this chapter, I recalled the pivotal role of determining the abundance profile of H_2CO, a major grain mantle constituent. Indeed, the presence of a jump in this profile would indicate the presence of warm inner regions in the envelopes of Class 0 protostars, where grain mantles sublimate. Moreover, since H_2CO is likely to be a reactant leading to the formation of complex molecules in the gas-phase, it is crucial to know its abundance. The H_2CO jump has been claimed and debated in the literature and observations of high-energy transitions of H_2CO should provide the necessary information to solve the controversy. Using the 15-meter single-dish of the JCMT, I therefore targeted the $J = 7 - 6$ transition of H_2CO ($E_{\rm up} = 74$ cm^{-1}) in five low-mass and detected it in all of them. Comparison of the observed and predicted fluxes show that the jump model seems more adequate than a constant model for IRAS16293, L1448-MM and L1448-N, whereas it might be the opposite for IRAS4A and IRAS4B. In any case, the present data are still insufficient to confirm or exclude either hypothesis.

2. *Are hot corinos common among low-mass protostars?* (Chapter 3)

   The discovery of a hot corino in IRAS16293 showed that, despite the theoretical challenged posed by their presence, complex organic molecules can be formed in the inner envelope of a Class 0 object. A natural question was whether IRAS16293 was an exception or if

these molecules were ubiquitous in the warm environments of sun-like protostars. I therefore looked for complex organic molecules towards three other Class 0 sources (IRAS4A, IRAS4B and IRAS2A) with the IRAM-30m and did find some of the targeted molecules in all three objects, indicating that hot corinos are likely common. A smaller number of molecules was found compared to IRAS16293, but this is likely due to the fact that my targets have a lower luminosity (hence a smaller sublimation region) and are located further away than IRAS16293. Indeed, relative abundances (with respect to a major ice mantle constituent such as CH_3OH) are comparable in all four sources, which could mean that the chemistry is similar from one Class 0 to another.

3. *Where are the complex molecules located?* (Chapter 4)

   Originally, the presence of complex organic molecules has been proposed to be due to the thermal heating of icy grain mantles in the inner envelope, but alternative scenarios have been suggested: the molecules could be located at the surface of a circumstellar disk, molecules trapped in icy mantles could be desorbed by shocks from outflows, turbulence or UV/X-ray heating of cavity walls, rather than thermal heating. The region of emission of complex molecules is therefore a key factor to better understand their formation. In any case, such region had been predicted to be of the order of $1''$ so that the use of an interferometer was required. I carried out IRAM Plateau de Bure observations of IRAS16293 and IRAS4A, which showed that the emission from complex molecules is compact with sizes $\lesssim 0.8''$ and that an extended component is present in IRAS4A but not in IRAS16293. No evidence was found for outflow interaction or the presence of cavities and my data supports the thermal heating theory.

4. *Are hot corinos similar to hot cores?* (Chapter 5)

   Since complex organic molecules were first discovered in the hot cores of massive protostars, I thought that information could be gained by comparing the two types of objects. I therefore used literature data and carried out complementary JCMT observations of some massive hot cores to show that complex organic molecules are relatively more abundant in hot corinos than in hot cores. Possible factors to explain this difference are the composition of grain mantles, the gas-phase and/or grain-surface chemical reactions taking place, or the amount of X-ray radiation from the central object.

5. *What is the formation path of these molecules?* (Chapter 6)

   With the exception of $HCOOCH_3$, for which recent laboratory data have shown that gas-phase formation of this molecule is highly unlikely, both gas-phase and grain-surface routes have been suggested for the formation of the complex molecules detected in hot corinos.

Although my observations do not rule out either of the two processes, the relatively higher abundance of complex molecules found in hot corinos compared to hot cores is supportive of grain-surface formation. Indeed, the time scale for the pre-stellar phase, during which grain mantles form, is longer for low-mass than for high-mass protostars, giving the former the opportunity to develop richer mantles.

7.2 Perspectives

Keep hunting for hot corinos: IRAM-30m and GBT

The fact that I found three hot corinos out of three targeted sources is very encouraging. However, although I tried to look for trends in the derived abundances of complex molecules, the low-number statistics do not allow for firm conclusions. Therefore it is necessary to detect more of these objects and determine their chemical composition in order to confirm the present results. Two single-dish antennas are ideally suited to pursue this search. The IRAM-30m allows for the highest sensitivity and bandwidth coverage in the millimeter range and these characteristics have proved themselves as shown by the detections I presented in Chapter 3. Since extended emission from the cold envelope was inferred in IRAS4A, another way to look for hot corinos is to use the Green Bank Telescope (GBT): it operates at lower frequencies than the IRAM-30m, thereby allowing the detection of lower-energy transitions. These observations can then be combined with interferometric data from the Very Large Array to determine the size of the compact component.

Keep tracking: ALMA

The IRAM Plateau de Bure (PdB) interferometer is currently the most sensitive facility to carry out the high-resolution observations of the emission from complex organic molecules in hot corinos. There are however two issues inherent to the low luminosities of Class 0 protostars: (i) with the observations of IRAS4A, I have reached the highest resolution that the PdB is capable of ($\sim$0.″8 at 3 mm), but these data also show that the size of the hot corino is smaller than that; (ii) it appears difficult to carry out, in a reasonable amount of time, an interferometric survey of complex molecules in these sources.
Such a project (that is, measure the size of the complex molecules' emission in several hot corinos) will be feasible with the next generation instrument, the Atacama Large Millimeter Array (ALMA), which will provide the higher sensitivity and resolution needed: only one hour, instead of seven, of on-source integration to reach the same sensitivity and spectral resolution as in the IRAS4A observations, but with a spatial resolution of 0.″1. The results of this interferometric survey would provide invaluable information to constrain chemical models of hot corinos.
In the meantime, much can be learnt with the PdB by carefully choosing the targeted molecules and sources.

Theoretical and laboratory work

Chemical models of hot cores and hot corinos are limited by the accuracy of chemical networks and rate coefficients (e.g. Aikawa et al. 2003; Wakelam et al. 2004, 2005) Hence, as shown by recent studies (e.g. Garrod & Herbst 2006; Horn et al. 2004), laboratory work is critical to improve the accuracy of chemical models and our understanding of observations. A couple of leads could be pursued in this area:

- rate coefficients for surface reactions are poorly known and only a handful studies have tried to tackle this issue. New reactions networks are being developped to include processes such as photolysis and radical-radical reactions (Widicus Weaver et al. 2005). This work will allow more complete reaction databases to be input in the chemical models.

- few models take into account the dynamics of the protostellar envelope. An important work in this regard is that of Ceccarelli et al. (1996), but the chemical network of this model did not include complex molecules. The modelling of Rodgers & Charnley (2003) palliated this lack, but only made used of a gas-phase reaction network whereas it has become clear that grain-surface processes need to be taken into account. Investigations are currently under way (Aikawa et al. in prep), looking at the coupling of gas-phase and grain-surface chemistries in an infalling envelope in order to probe the effects of the dynamics on the formation and location of complex molecules. Current and future interferometric observations are/will be perfectly suited to constrain this type of modelling.

- there are so many unidentified lines in the observed spectra that it may be that we are missing some critical molecules in the networks leading to complex molecules. For example, as Hollis (2005) recently put it, "is isomerism the key" to complex molecules? Hollis suggests that isomers such as the one for H_2CO, t-HCOH, may have an important role in the formation of complex molecules. In order to establish whether this and other isomers are present in space, it is necessary to determine their rotational spectra, which could be done via ab initia quantum chemical models or via laboratory measurements. (Hollis 2005).

The Molecular Universe is a european network financed by Sixth Framework Programme (FP6) of the European Union. The goal of this network, in which the Laboratoire d'AstrOphysique de Grenoble (LAOG) is involved, is to provide some key laboratory experiments and quantum chemical computations for simple molecules. Unfortunately, the issue of the complex organic molecules is not covered by this network, but, in the cases where simplifying assumptions can be made about complex molecules, I am hoping that some of the results may be of use either to better understand the chemistry of these species or to make a stronger case for the need of dedicated experiments/computations.

Move up the evolutionary path

The fate of the complex organic molecules observed in hot corinos is of course of particular interest since some of these species are also observed in the comets of our Solar System. Are these molecules destroyed and reformed in the protoplanetary nebula? Could they (re)freeze onto dust grains so that the circumstellar material would keep a "chemical memory" of the early stages of formation? With our current knowledge and instrumentation, it seems uncertain whether these questions could be answered. However, I hope that the high sensitivity and resolution of ALMA will allow for some ground-breaking observations of more evolved objects. For example, Lahuis et al. (2006) found hot gas in the inner regions (<6 AU) of a Class I object, and one can wonder what kind of chemistry is taking place in this gas. Further up still on the evolutionary path, complex molecules could form on the grains in the cold, dense, mid-plane of a proto-planetary disk, as they did in the cold, dense prestellar core. If some mixing of the disk's layers could occur, then the molecules could desorb as the grains reach the disk's surface or inner edge (depending on whether mixing is radial or vertical), in which case there might be a chance we could observe their emission.

7.3 Final words

Observations and studies of hot cores led to the search and finding of hot corinos. This opened new perspectives on the first class of objects, especially regarding the chemical processes at play. Hot corinos are very interesting objects in themselves. Indeed their chemistry might affect the chemical composition of the material from which planetesimals eventually form. It may also be possible that complex organic molecules are reformed in the cold, dense mid-plane of a proto-planetary disk in the same way they may have been during the collapse prior to the Class 0 stage. Either way, they could play a crucial role in our understanding of the composition of planetary bodies. Incidentally, they can also help us to better understand their massive counterparts. In the past 20 years we have gone from hot cores to hot corinos. I primarily focused on hot corinos, a new class of objects for which I found and started characterizing the first few members. I hope this thesis will help pave the road not only for subsequent work that will pursue the quest of understanding this critical phase in the evolution of sun-like protostars, but also for studies that will go back to hot cores!

Finally, it clearly stands out from this work that not only more data (single-dish, interferometric and high-energy transitions) are needed, but also that laboratory studies of grain-surface reactions are necessary in order to answer of the question of which, why, where and how complex molecules are formed.

References

Aikawa, Y., Ohashi, N., & Herbst, E. 2003, ApJ, 593, 906

Allen, M. & Robinson, G. W. 1977, ApJ, 212, 396

André, P., Ward-Thompson, D., & Barsony, M. 2000, Protostars and Planets IV, 59

Arce, H. G. & Sargent, A. I. 2004, ApJ, 612, 342

Bachiller, R., Martin-Pintado, J., Tafalla, M., Cernicharo, J., & Lazareff, B. 1990, A&A, 231, 174

Bachiller, R. & Perez Gutierrez, M. 1997, ApJ, 487, L93+

Bacmann, A., Lefloch, B., Ceccarelli, C., Castets, A., Steinacker, J., & Loinard, L. 2002, A&A, 389, L6

Bacmann, A., Lefloch, B., Ceccarelli, C., Steinacker, J., Castets, A., & Loinard, L. 2003, ApJ, 585, L55

Barsony, M., Ward-Thompson, D., André, P., & O'Linger, J. 1998, ApJ, 509, 733

Bergin, E. A., Alves, J., Huard, T., & Lada, C. J. 2002, ApJ, 570, L101

Bergin, E. A. & Langer, W. D. 1997, ApJ, 486, 316

Bisschop, S. E., Jørgensen, J. K., & van Dishoeck, E. F. 2006, A&A

Blake, G. A., Sandell, G., van Dishoeck, E. F., Groesbeck, T. D., Mundy, L. G., & Aspin, C. 1995, ApJ, 441, 689

Blake, G. A., Sutton, E. C., Masson, C. R., & Phillips, T. G. 1987, ApJ, 315, 621

Boogert, A. C. A., Pontoppidan, K. M., Lahuis, F., Jørgensen, J. K., Augereau, J.-C., Blake, G. A., Brooke, T. Y., Brown, J., Dullemond, C. P., Evans, N. J., Geers, V., Hogerheijde, M. R., Kessler-Silacci, J., Knez, C., Morris, P., Noriega-Crespo, A., Schöier, F. L., van Dishoeck, E. F., Allen, L. E., Harvey, P. M., Koerner, D. W., Mundy, L. G., Myers, P. C., Padgett, D. L., Sargent, A. I., & Stapelfeldt, K. R. 2004, ApJS, 154, 359

Bottinelli, S., Ceccarelli, C., Lefloch, B., & Williams, J. P. 2006, A&A, submitted

Bottinelli, S., Ceccarelli, C., Lefloch, B., Williams, J. P., Castets, A., Caux, E., Cazaux, S., Maret, S., Parise, B., & Tielens, A. G. G. M. 2004a, ApJ, 615, 354

Bottinelli, S., Ceccarelli, C., Neri, R., Williams, J. P., Caux, E., Cazaux, S., Lefloch, B., Maret, S., & Tielens, A. G. G. M. 2004b, ApJ, 617, L69

Brown, R. L. 1981, ApJ, 248, L119

Buckle, J. V. & Fuller, G. A. 2003, A&A, 399, 567

Burton, M. G., Lawrence, J. S., Ashley, M. C. B., Bailey, J. A., Blake, C., Bedding, T. R., Bland-Hawthorn, J., Bond, I. A., Glazebrook, K., Hidas, M. G., Lewis, G., Longmore, S. N., Maddison, S. T., Mattila, S., Minier, V., Ryder, S. D., Sharp, R., Smith, C. H., Storey, J. W. V., Tinney, C. G., Tuthill, P., Walsh, A. J., Walsh, W., Whiting, M., Wong, T., Woods, D., & Yock, P. C. M. 2005, Publications of the Astronomical Society of Australia, 22, 199

Caselli, P. 2002, Planet. Space Sci., 50, 1133

Caselli, P., Hasegawa, T. I., & Herbst, E. 1993, ApJ, 408, 548

Caselli, P., Walmsley, C. M., Tafalla, M., Dore, L., & Myers, P. C. 1999, ApJ, 523, L165

Cazaux, S. & Tielens, A. G. G. M. 2004, ApJ, 604, 222

Cazaux, S., Tielens, A. G. G. M., Ceccarelli, C., Castets, A., Wakelam, V., Caux, E., Parise, B., & Teyssier, D. 2003, ApJ, 593, L51

Ceccarelli, C., Baluteau, J.-P., Walmsley, M., Swinyard, B. M., Caux, E., Sidher, S. D., Cox, P., Gry, C., Kessler, M., & Prusti, T. 2002a, A&A, 383, 603

Ceccarelli, C., Caselli, P., Herbst, E., Tielens, A. G. M. M., & Caux, E. 2006, in Protostars and Planets V

Ceccarelli, C., Castets, A., Caux, E., Hollenbach, D., Loinard, L., Molinari, S., & Tielens, A. G. G. M. 2000a, A&A, 355, 1129

Ceccarelli, C., Caux, E., Tielens, A. G. G. M., Kemper, F., Waters, L. B. F. M., & Phillips, T. 2002b, A&A, 395, L29

Ceccarelli, C. & Dominik, C. 2005, A&A, 440, 583

Ceccarelli, C., Hollenbach, D. J., & Tielens, A. G. G. M. 1996, ApJ, 471, 400

Ceccarelli, C., Loinard, L., Castets, A., Faure, A., & Lefloch, B. 2000b, A&A, 362, 1122

Ceccarelli, C., Loinard, L., Castets, A., Tielens, A. G. G. M., & Caux, E. 2000c, A&A, 357, L9

Ceccarelli, C., Maret, S., Tielens, A. G. G. M., Castets, A., & Caux, E. 2003, A&A, 410, 587

Cesaroni, R., Churchwell, E., Hofner, P., Walmsley, C. M., & Kurtz, S. 1994, A&A, 288, 903

Chandler, C. J., Brogan, C. L., Shirley, Y. L., & Loinard, L. 2005, ApJ, 632, 371

Chandler, C. J. & Richer, J. S. 2000, ApJ, 530, 851

Charnley, S. B., Kress, M. E., Tielens, A. G. G. M., & Millar, T. J. 1995, ApJ, 448, 232

Charnley, S. B. & Rodgers, S. D. 2005, in IAU Symposium, 262–+

Charnley, S. B., Tielens, A. G. G. M., & Millar, T. J. 1992, ApJ, 399, L71

Charnley, S. B., Tielens, A. G. G. M., & Rodgers, S. D. 1997, ApJ, 482, L203+

Chiavassa, A., Ceccarelli, C., Tielens, A. G. G. M., Caux, E., & Maret, S. 2005, A&A, 432, 547

Choi, M. 2005, ApJ, 630, 976

Choi, M., Evans, II, N. J., Gregersen, E. M., & Wang, Y. 1995, ApJ, 448, 742

Choi, M., Panis, J.-F., & Evans, II, N. J. 1999, ApJS, 122, 519

Churchwell, E. 2002, ARA&A, 40, 27

Combes, F., Q-Rieu, N., & Wlodarczak, G. 1996, A&A, 308, 618

Comito, C., Schilke, P., Phillips, T. G., Lis, D. C., Motte, F., & Mehringer, D. 2005, ApJS, 156, 127

Crapsi, A., Caselli, P., Walmsley, C. M., Myers, P. C., Tafalla, M., Lee, C. W., & Bourke, T. L. 2005, ApJ, 619, 379

Cuppen, H. M. & Herbst, E. 2005, MNRAS, 361, 565

Cuppen, H. M., Morata, O., & Herbst, E. 2006, MNRAS, 367, 1757

Di Francesco, J., Evans, N. J., I., Caselli, P., Myers, P. C., Shirley, Y., Aikawa, A., & Tafalla, M. 2006, in Protostars and Planets V

Di Francesco, J., Myers, P. C., Wilner, D. J., Ohashi, N., & Mardones, D. 2001, ApJ, 562, 770

Dickens, J. E., Irvine, W. M., Snell, R. L., Bergin, E. A., Schloerb, F. P., Pratap, P., & Miralles, M. P. 2000, ApJ, 542, 870

Estalella, R., Anglada, G., Rodriguez, L. F., & Garay, G. 1991, ApJ, 371, 626

Evans, II, N. J. 1999, ARA&A, 37, 311

Feigelson, E. D. & Montmerle, T. 1999, ARA&A, 37, 363

Flower, D. R., Pineau des Forets, G., & Walmsley, C. M. 1995, A&A, 294, 815

Garrod, R. T. & Herbst, E. 2006, A&A, submitted

Gerin, M., Combes, F., Wlodarczak, G., Jacq, T., Guelin, M., Encrenaz, P., & Laurent, C. 1992, A&A, 259, L35

Gerlich, D. & Horning, S. 1992, Cosmic Res., 92, 1509

Gibb, E., Nummelin, A., Irvine, W. M., Whittet, D. C. B., & Bergman, P. 2000a, ApJ, 545, 309

Gibb, E. L., Whittet, D. C. B., Schutte, W. A., Boogert, A. C. A., Chiar, J. E., Ehrenfreund, P., Gerakines, P. A., Keane, J. V., Tielens, A. G. G. M., van Dishoeck, E. F., & Kerkhof, O. 2000b, ApJ, 536, 347

Girart, J. M. & Acord, J. M. P. 2001, ApJ, 552, L63

Gould, R. J. & Salpeter, E. E. 1963, ApJ, 138, 393

Green, T. 2001, Am. Scientist, 89, 316

Greenberg, J. M. 1973, in Molecules in the Galactic Environment, ed. M. A. Gordon & L. E. Snyder, 93–+

Gueth, F., Guilloteau, S., & Bachiller, R. 1996, A&A, 307, 891

—. 1998, A&A, 333, 287

Hasegawa, T. I. & Herbst, E. 1993, MNRAS, 261, 83

Hasegawa, T. I., Herbst, E., & Leung, C. M. 1992, ApJS, 82, 167

Hatchell, J., Thompson, M. A., Millar, T. J., & MacDonald, G. H. 1998, A&AS, 133, 29

Helmich, F. P. & van Dishoeck, E. F. 1997, A&AS, 124, 205

Herbst, E. 1995, Ann. Rev. Phys. Chem., 46, 27

—. 2005, J. Phys. Chem. A, 109, 4017

Herbst, E., Chang, Q., & Cuppen, H. M. 2005, Journal of Physics Conference Series, 6, 18

Hidaka, H., Watanabe, N., Shiraki, T., Nagaoka, A., & Kouchi, A. 2004, ApJ, 614, 1124

Hiraoka, K., Sato, T., Sato, S., Sogoshi, N., Yokoyama, T., Takashima, H., & Kitagawa, S. 2002, ApJ, 577, 265

Hogerheijde, M. R. & Sandell, G. 2000, ApJ, 534, 880

Hollenbach, D. & Salpeter, E. E. 1971, ApJ, 163, 155

Hollis, J. M. 2005, in IAU Symposium, ed. D. C. Lis, G. A. Blake, & E. Herbst, 227–236

Hollis, J. M., Pedelty, J. A., Snyder, L. E., Jewell, P. R., Lovas, F. J., Palmer, P., & Liu, S.-Y. 2003, ApJ, 588, 353

Horn, A., Møllendal, H., Sekiguchi, O., Uggerud, E., Roberts, H., Herbst, E., Viggiano, A. A., & Fridgen, T. D. 2004, ApJ, 611, 605

Hornekaer, L., Baurichter, A., Petrunin, V. V., Field, D., & Luntz, A. C. 2003, Science, 302, 1943

Hudson, R. L. & Moore, M. H. 1999, Icarus, 140, 451

Hüttemeister, S., Dahmen, G., Mauersberger, R., Henkel, C., Wilson, T. L., & Martín-Pintado, J. 1998, A&A, 334, 646

Hüttemeister, S., Wilson, T. L., Bania, T. M., & Martín-Pintado, J. 1993, A&A, 280, 255

Ikeda, M., Ohishi, M., Nummelin, A., Dickens, J. E., Bergman, P., Hjalmarson, Å., & Irvine, W. M. 2001, ApJ, 560, 792

Irvine, W. M., Friberg, P., Kaifu, N., Matthews, H. E., Minh, Y. C., Ohishi, M., & Ishikawa, S. 1990, A&A, 229, L9

Jiménez-Serra, I., Martín-Pintado, J., Rodríguez-Franco, A., & Marcelino, N. 2004, ApJ, 603, L49

Jones, A. P. & Williams, D. A. 1984, MNRAS, 209, 955

Jørgensen, J. K., Bourke, T. L., Myers, P. C., Schöier, F. L., van Dishoeck, E. F., & Wilner, D. J. 2005a, ApJ, 632, 973

Jørgensen, J. K., Hogerheijde, M. R., Blake, G. A., van Dishoeck, E. F., Mundy, L. G., & Schöier, F. L. 2004, A&A, 415, 1021

Jørgensen, J. K., Schöier, F. L., & van Dishoeck, E. F. 2002, A&A, 389, 908

—. 2005b, A&A, 437, 501

Keane, J. V., Tielens, A. G. G. M., Boogert, A. C. A., Schutte, W. A., & Whittet, D. C. B. 2001, A&A, 376, 254

Knee, L. B. G. & Sandell, G. 2000, A&A, 361, 671

Knez, C., Boogert, A. C. A., Pontoppidan, K. M., Kessler-Silacci, J., van Dishoeck, E. F., Evans, N. J., Augereau, J.-C., Blake, G. A., & Lahuis, F. 2005, ApJ, 635, L145

Kuan, Y.-J., Huang, H.-C., Charnley, S. B., Hirano, N., Takakuwa, S., Wilner, D. J., Liu, S.-Y., Ohashi, N., Bourke, T. L., Qi, C., & Zhang, Q. 2004, ApJ, 616, L27

Kurtz, S., Cesaroni, R., Churchwell, E., Hofner, P., & Walmsley, C. M. 2000, Protostars and Planets IV, 299

Lahuis, F., van Dishoeck, E. F., Boogert, A. C. A., Pontoppidan, K. M., Blake, G. A., Dullemond, C. P., Evans, II, N. J., Hogerheijde, M. R., Jørgensen, J. K., Kessler-Silacci, J. E., & Knez, C. 2006, ApJ, 636, L145

Lay, O. P., Carlstrom, J. E., & Hills, R. E. 1995, ApJ, 452, L73+

Lefloch, B., Castets, A., Cernicharo, J., & Loinard, L. 1998, ApJ, 504, L109+

Leger, A., Jura, M., & Omont, A. 1985, A&A, 144, 147

Lequeux, J. 2002, Le Milieu Interstellaire (Le Milieu Interstellaire, James Lequeux, Avec le comcours d'Edith Falgarone et Charles Ryter. EDP Sciences et CNRS Editions.)

—. 2005, The interstellar medium (The interstellar medium, Translation from the French language edition of: Le Milieu Interstellaire by James Lequeux, EDP Sciences, 2003 Edited by J. Lequeux. Astronomy and astrophysics library, Berlin: Springer, 2005)

Leung, C. M. & Brown, R. L. 1977, ApJ, 214, L73

Leung, C. M., Herbst, E., & Huebner, W. F. 1984, ApJS, 56, 231

Liu, S.-Y., Mehringer, D. M., & Snyder, L. E. 2001, ApJ, 552, 654

Liu, S.-Y. & Snyder, L. E. 1999, ApJ, 523, 683

Loinard, L., Rodríguez, L. F., D'Alessio, P., Wilner, D. J., & Ho, P. T. P. 2002, ApJ, 581, L109

Looney, L. W., Mundy, L. G., & Welch, W. J. 2000, ApJ, 529, 477

MacDonald, G. H., Gibb, A. G., Habing, R. J., & Millar, T. J. 1996, A&AS, 119, 333

Maret, S., Ceccarelli, C., Caux, E., Tielens, A. G. G. M., & Castets, A. 2002, A&A, 395, 573

Maret, S., Ceccarelli, C., Caux, E., Tielens, A. G. G. M., Jörgensen, J. K., van Dishoeck, E., Bacmann, A., Castets, A., Lefloch, B., Loinard, L., Parise, B., & Schöier, F. L. 2004, A&A, 416, 577

Maret, S., Ceccarelli, C., Tielens, A. G. G. M., Caux, E., Lefloch, B., Faure, A., Castets, A., & Flower, D. R. 2005, A&A, 442, 527

Martín-Pintado, J., de Vicente, P., Fuente, A., & Planesas, P. 1997, ApJ, 482, L45+

Martín-Pintado, J., de Vicente, P., Rodríguez-Fernández, N. J., Fuente, A., & Planesas, P. 2000, A&A, 356, L5

Martín-Pintado, J., Rizzo, J. R., de Vicente, P., Rodríguez-Fernández, N. J., & Fuente, A. 2001, ApJ, 548, L65

Matthews, H. E. & Sears, T. J. 1983, ApJ, 272, 149

McKellar, A. 1940, PASP, 52, 187

Menten, K. M., Walmsley, C. M., Henkel, C., & Wilson, T. L. 1988, A&A, 198, 253

Mestel, L. & Spitzer, Jr., L. 1956, MNRAS, 116, 503

Millar, T. J. 1993, The Chemistry of Hot Molecular Cores (Dust and Chemistry in Astronomy), 249–+

Minh, Y. C., Irvine, W. M., Ohishi, M., Ishikawa, S., Saito, S., & Kaifu, N. 1993, A&A, 267, 229

Minier, V., Ellingsen, S. P., Norris, R. P., & Booth, R. S. 2003, A&A, 403, 1095

Mizuno, A., Fukui, Y., Iwata, T., Nozawa, S., & Takano, T. 1990, ApJ, 356, 184

Morris, M., Palmer, P., & Zuckerman, B. 1980, ApJ, 237, 1

Mundy, L. G., Wootten, A., Wilking, B. A., Blake, G. A., & Sargent, A. I. 1992, ApJ, 385, 306

Mundy, L. G., Wootten, H. A., & Wilking, B. A. 1990, ApJ, 352, 159

Nagaoka, A., Watanabe, N., & Kouchi, A. 2005, ApJ, 624, L29

Nomura, H. & Millar, T. J. 2004, A&A, 414, 409

Nummelin, A., Bergman, P., Hjalmarson, Å., Friberg, P., Irvine, W. M., Millar, T. J., Ohishi, M., & Saito, S. 2000, ApJS, 128, 213

Ohashi, N., Hayashi, M., Ho, P. T. P., & Momose, M. 1997, ApJ, 475, 211

O'Linger, J., Wolf-Chase, G., Barsony, M., & Ward-Thompson, D. 1999, ApJ, 515, 696

Pagani, L., Pardo, J.-R., Apponi, A. J., Bacmann, A., & Cabrit, S. 2005, A&A, 429, 181

Peeters, Z., Rodgers, S. D., Charnley, S. B., Schriver-Mazzuoli, L., Schriver, A., Keane, J. V., & Ehrenfreund, P. 2006, A&A, 445, 197

Pineau des Forets, G., Roueff, E., Schilke, P., & Flower, D. R. 1993, MNRAS, 262, 915

Pohorille, A. 2002, Advances in Space Research, 30, 1509

Pratap, P., Dickens, J. E., Snell, R. L., Miralles, M. P., Bergin, E. A., Irvine, W. M., & Schloerb, F. P. 1997, ApJ, 486, 862

Reipurth, B., Rodríguez, L. F., Anglada, G., & Bally, J. 2002, AJ, 124, 1045

—. 2004, AJ, 127, 1736

Remijan, A. & Hollis, J. M. 2006, ApJ, in press

Requena-Torres, M. A., Martín-Pintado, J., Rodríguez-Franco, A., Martín, S., Rodríguez-Fernández, N. J., & de Vicente, P. 2006, A&A, in press

Roberts, H., Herbst, E., & Millar, T. J. 2003, ApJ, 591, L41

Rodgers, S. D. & Charnley, S. B. 2001, ApJ, 546, 324

—. 2003, ApJ, 585, 355

Rodríguez-Fernández, N. J., Martín-Pintado, J., de Vicente, P., Fuente, A., Hüttemeister, S., Wilson, T. L., & Kunze, D. 2000, A&A, 356, 695

Rodríguez-Fernández, N. J., Martín-Pintado, J., Fuente, A., & Wilson, T. L. 2004, A&A, 427, 217

Roser, J. E., Manicò, G., Pirronello, V., & Vidali, G. 2002, ApJ, 581, 276

Roueff, E., Lis, D. C., van der Tak, F. F. S., Gerin, M., & Goldsmith, P. F. 2005, A&A, 438, 585

Rowe, B. R., Dupeyrat, G., Marquette, J. B., Smith, D., Adams, N. G., & Ferguson, E. E. 1984, J. Chem. Phys., 80, 241

Sandell, G., Knee, L. B. G., Aspin, C., Robson, I. E., & Russell, A. P. G. 1994, A&A, 285, L1

Sandford, S. A., Allamandola, L. J., & Bernstein, M. P. 1998, in ASP Conf. Ser. 148: Origins, ed. C. E. Woodward, J. M. Shull, & H. A. Thronson, Jr., 392–+

Schilke, P., Benford, D. J., Hunter, T. R., Lis, D. C., & Phillips, T. G. 2001, ApJS, 132, 281

Schilke, P., Groesbeck, T. D., Blake, G. A., & Phillips, T. G. 1997, ApJS, 108, 301

Schöier, F. L., Jørgensen, J. K., van Dishoeck, E. F., & Blake, G. A. 2002, A&A, 390, 1001

—. 2004, A&A, 418, 185

Schutte, W. A., Boogert, A. C. A., Tielens, A. G. G. M., Whittet, D. C. B., Gerakines, P. A., Chiar, J. E., Ehrenfreund, P., Greenberg, J. M., van Dishoeck, E. F., & de Graauw, T. 1999, A&A, 343, 966

Shirley, Y. L., Evans, N. J., & Rawlings, J. M. C. 2002, ApJ, 575, 337

Shirley, Y. L., Evans, II, N. J., Rawlings, J. M. C., & Gregersen, E. M. 2000, ApJS, 131, 249

Shu, F. H. 1977, ApJ, 214, 488

Smith, I. W. M., Herbst, E., & Chang, Q. 2004, MNRAS, 350, 323

Sorrell, W. H. 2001, ApJ, 555, L129

Stark, R., Sandell, G., Beck, S. C., Hogerheijde, M. R., van Dishoeck, E. F., van der Wal, P., van der Tak, F. F. S., Schäfer, F., Melnick, G. J., Ashby, M. L. N., & de Lange, G. 2004, ApJ, 608, 341

Sutton, E. C., Blake, G. A., Masson, C. R., & Phillips, T. G. 1985, ApJS, 58, 341

Sutton, E. C., Peng, R., Danchi, W. C., Jaminet, P. A., Sandell, G., & Russell, A. P. G. 1995, ApJS, 97, 455

Tafalla, M., Myers, P. C., Caselli, P., Walmsley, C. M., & Comito, C. 2002, ApJ, 569, 815

Tamura, M., Ohashi, N., Hirano, N., Itoh, Y., & Moriarty-Schieven, G. H. 1996, AJ, 112, 2076

Terebey, S. & Padgett, D. L. 1997, in IAU Symp. 182: Herbig-Haro Flows and the Birth of Stars, ed. B. Reipurth & C. Bertout, 507–514

Thompson, M. A. & MacDonald, G. H. 1999, A&AS, 135, 531

Tielens, A. G. G. M. 1983, A&A, 119, 177

—. 2005, The Physics and Chemistry of the Interstellar Medium (The Physics and Chemistry of the Interstellar Medium, by A. G. G. M. Tielens, pp. . ISBN 0521826349. Cambridge, UK: Cambridge University Press, 2005.)

Tielens, A. G. G. M. & Allamandola, L. J. 1987, in ASSL Vol. 134: Interstellar Processes, ed. D. J. Hollenbach & H. A. Thronson, Jr., 397–469

Tielens, A. G. G. M. & Hagen, W. 1982, A&A, 114, 245

van der Tak, F. F. S., van Dishoeck, E. F., & Caselli, P. 2000a, A&A, 361, 327

van der Tak, F. F. S., van Dishoeck, E. F., Evans, N. J., & Blake, G. A. 2000b, ApJ, 537, 283

van Dishoeck, E. F., Blake, G. A., Jansen, D. J., & Groesbeck, T. D. 1995, ApJ, 447, 760

Vastel, C., Caselli, P., Ceccarelli, C., Phillips, T., Wiedner, M. C., Peng, R., Houde, M., & Dominik, C. 2006, ApJ, 645, 1198

Vastel, C., Phillips, T. G., & Yoshida, H. 2004, ApJ, 606, L127

Viti, S., Collings, M. P., Dever, J. W., McCoustra, M. R. S., & Williams, D. A. 2004, MNRAS, 354, 1141

Wakelam, V., Caselli, P., Ceccarelli, C., Herbst, E., & Castets, A. 2004, A&A, 422, 159

Wakelam, V., Selsis, F., Herbst, E., & Caselli, P. 2005, A&A, 444, 883

Walker, C. K., Carlstrom, J. E., & Bieging, J. H. 1993, ApJ, 402, 655

Walker, C. K., Lada, C. J., Young, E. T., Maloney, P. R., & Wilking, B. A. 1986, ApJ, 309, L47

Walker, C. K., Lada, C. J., Young, E. T., & Margulis, M. 1988, ApJ, 332, 335

Walmsley, C. M., Flower, D. R., & Pineau des Forêts, G. 2004, A&A, 418, 1035

Walmsley, C. M. & Schilke, P. 1993, Observations of Hot Molecular Cores (Dust and Chemistry in Astronomy), 37–+

Walsh, A. J., Burton, M. G., Hyland, A. R., & Robinson, G. 1998, MNRAS, 301, 640

Ward-Thompson, D., André, P., Crutcher, R., Johnstone, D., Onishi, T., & Wilson, C. 2006, in Protostars and Planets V

Ward-Thompson, D., Buckley, H. D., Greaves, J. S., Holland, W. S., & André, P. 1996, MNRAS, 281, L53

Watanabe, N., Shiraki, T., & Kouchi, A. 2003, ApJ, 588, L121

Whitworth, A. P., Bhattal, A. S., Francis, N., & Watkins, S. J. 1996, MNRAS, 283, 1061

Widicus Weaver, S. L., Kelley, M. J., & Blake, G. A. 2005, in IAU Symposium, ed. D. C. Lis, G. A. Blake, & E. Herbst, 180–+

Williams, D. A. 1993, Physical and Chemical Processes on Dust (Dust and Chemistry in Astronomy), 143–+

Wilner, D. J. & Welch, W. J. 1994, ApJ, 427, 898

Wootten, A. 1989, ApJ, 337, 858

Wootten, A., Evans, II, N. J., Snell, R., & vanden Bout, P. 1978, ApJ, 225, L143

Zhang, Q., Ho, P. T. P., & Wright, M. C. H. 2000, AJ, 119, 1345

Zhou, S. 1992, ApJ, 394, 204

—. 1995, ApJ, 442, 685

Appendix A
Nomenclature of complex organic molecules

Table A.1 Simple and complex organic molecules observed in hot cores.

Simple compounds	Common name	Complex compounds	Common name
CCH	Ethynyl	HCOOH	Formic acid
C_2H_2	Acetylene	C_2H_5OH	Ethanol
CH_3CCH	Propyne	CH_3CHO	Acetaldehyde
CH_4	Methane	$HCOOCH_3$	Methyl formate
CO	Carbon monoxide	CH_3COOH	Acetic acid
CN	Cyanide radical	CH_3OCH_3	Dimethyl ether
CS	Carbon monosulfide	CH_2CO	Ketene
CH_3OH^a	Methanol	$(CH_3)_2CO$	Acetone
H_2O^b	Water	CH_3CN^g	Methyl cyanide
H_2S^c	Hydrogen sulfide	C_2H_5CN	Ethyl cyanide
HC_3N	Cyanoacetylene	C_2H_3CN	Vinyl cyanide
HCN	Hydrogen cyanide	NH_2CHO	Formamide
HNC	Hydrogen isocyanide	CH_2OHCHO	Glycolaldehyde
HNCO	Isocyanic acid	$HOCH_2CH_2OH$	Ethylene glycol
H_2CO^d	Formaldehyde	CH_2CHCHO	Propenal
H_2CS	Thioformaldehyde	CH_3CH_2CHO	Propanal
OCS	Carbonyl sulfide	CH_3CONH_2	Acetamide
NH_3^e	Ammonia	c-H_2C_3O	Cyclopropenone
NO	Nitric oxide		
NS			
SO	Sulfur monoxide		
SO_2^f	Sulfur dioxide		
SiO	Silicon monoxide		

Isotopomers:
[a] $^{13}CH_3OH$, CH_3OD, CH_2DOH
[b] HDO, D_2O
[c] HDS
[d] D_2CO
[e] NH_2D, NHD_2
[f] $^{33}SO_2$
[g] $CH_3{}^{13}CN$

Appendix B
Hot corinos: description and physical parameters

B.1 IRAS16293–2422 (IRAS16923)

IRAS16293 is a multiple system of low-mass protostars located in the ρ Ophiucus molecular cloud, at a distance of 160 pc. It is composed of two main cores, A and B, identified from the two continuum peaks seen in the radio (Wootten 1989; Estalella et al. 1991; Remijan & Hollis 2006) and in the (sub)millimeter (Mundy et al. 1992; Walker et al. 1993; Bottinelli et al. 2004b; Kuan et al. 2004; Chandler et al. 2005). IRAS16293A is itself a multiple system with at least two components (Wootten 1989; Mundy et al. 1992; Chandler et al. 2005). A quadrupolar outflow is associated to the IRAS16293 system with a NE-SW outflow driven by source A and an E-W "fossil" outflow originating from source B (Walker et al. 1988; Mizuno et al. 1990; Walker et al. 1993; Stark et al. 2004).

B.2 NGC1333-IRAS4A (IRAS4A) and NGC1333-IRAS4B (IRAS4B)

IRAS4A and IRAS4B belong to the multiple system IRAS 4, located in the NGC1333 reflection nebula, in the Perseus cloud. IRAS4A and IRAS4B are separated by $30''$, and are located $11''$ and $17''$ respectively from the third component, IRAS4C (Looney et al. 2000; Reipurth et al. 2002). IRAS4A was itself resolved into two components with a separation of $1\farcs8$ (Lay et al. 1995; Reipurth et al. 2002; Looney et al. 2000). Looney et al. (2000) suggest that IRAS4B may also be a multiple stellar system.

Both IRAS4A and IRAS4B are associated with highly collimated molecular outflows with a dynamical age of a few thousand years, seen in CO, CS (Blake et al. 1995) and SiO (Lefloch et al. 1998). Infall motion was detected by Di Francesco et al. (2001) and Choi et al. (1999) with estimated accretion rates of 1.1×10^{-4} and 3.7×10^{-5} $M_\odot$ yr^{-1}, inner masses of 0.71 and 0.23 $M_\odot$ and ages of $\sim$6500 and $\sim$6200 yr for IRAS4A and IRAS4B respectively (see also Maret et al. 2002). Choi (2005) suggests multiple outflows in IRAS4A: a highly collimated one (that had previously been observed), running NE-SW, that would be driven by component A2 and a weaker one driven by A1, revealed by a red lobe south of this component.

B.3 NGC1333-IRAS2A (IRAS2A)

IRAS2A is part of a protobinary system and is separated by 30″ from its companion IRAS2B (Looney et al. 2000; Reipurth et al. 2002). Two CO bipolar outflows appear to originate within a few arcsec of IRAS2A: a highly collimated jet (also seen in HCN, SiO, SO, CS, and CH_3OH; Jørgensen et al. 2004) in the east-west direction and a large-scale outflow aligned NNE-SSW (Sandell et al. 1994; Knee & Sandell 2000).

B.4 L1448-MM and L1448-N

L1448-MM (also called L1448C) and L1448-N (or L1448 IRS3) are Class 0 protostars separated by 82″ in the Perseus molecular cloud. A third, less luminous protostar (L1448NW or L1448 IRS2) also lies in the vicinity, at 101″ and 16″ from L1448-MM and N respectively (O'Linger et al. 1999; Reipurth et al. 2002). see O'Linger et al. 1999; Barsony et al. 1998).

L1448-MM drives a powerful, high-velocity, highly collimated outflow seen in CO (Bachiller et al. 1990), SiO (Girart & Acord 2001) and CH_3OH (Jiménez-Serra et al. 2004).

L1448-N was observed as a binary (L1448-N(A) and L1448-N(B), separated by 7″) in the continuum at 2 and 6 cm, and a third component is seen at 2.7 mm, $\sim 20''$ away from both A and B (Looney et al. 2000, and references therein). Two distinct outflows are observed in L1448N, one powered by L1448N(A) and the other by L1448N(B) (Barsony et al. 1998). Barsony et al. (1998) also detect a bridge of dust emission linking L1448C to L1448N, which traces the surface where the L1448C and L1448N(A) outflows collide.

B.5 L1157-MM

The last object in the sample to be located in the Perseus molecular cloud A well-collimated CO bipolar outflow is seen in CH_3OH, H_2CO, HCN, CN, SO and SO_2 (Bachiller & Perez Gutierrez 1997), as well as in SiO and CS (Zhang et al. 2000). The outflow was found to precess (Gueth et al. 1996, 1998) and Plateau de Bure interferometric images of this source by Gueth et al. (1996) revealed the presence of two cavities which the authors explain as excavations by the propagation of large bow-shocks due to episodic events in the precessing jet.

B.6 L1527

L1527 is a well-studied Class 0 source in the Taurus molecular cloud complex. This is seen as a close (0.″2 separation) binary at 7 cm by Loinard et al. (2002). It drives a compact CO outflow oriented east-west and lying in the plane of the sky (Tamura et al. 1996). Moreover, Reipurth et al. (2004) observed a curving radio continuum jet a 3.6 cm, which could be the effect of two separate outflows produced by each of the binary component, or of rapidly changing outflow direction. There is also strong evidence for rotation in this source (e.g. Ohashi et al. 1997).

Table B.1 Characteristics of the sample of hot corinos (Adapted from Maret et al. 2004).

Source	RA (2000) $h\ m\ s$	Dec (2000) $^\circ\ '\ ''$	Cloud	Dist.[a] (pc)	$L_{\rm bol}$[b] ($L_\odot$)	$M_{\rm env}$[c] ($M_\odot$)	$L_{\rm smm}/L_{\rm bol}$[d] (%)	$T_{\rm bol}$[e] (K)	$R_{\rm 100K}$[f] (AU)
NGC1333–IRAS4A	03 29 10.3	+31 13 31	Perseus	220	6	2.3	5	34	53
NGC1333–IRAS4B	03 29 12.0	+31 13 09	Perseus	220	6	2.0	3	36	27
NGC1333–IRAS2A	03 28 55.4	+31 14 25	Perseus	220	16	1.7	$\lesssim$1	50	47
L1448-N	03 25 36.3	+30 45 15	Perseus	220	6	3.5	3	55	20
L1448-MM	03 25 38.8	+30 44 05	Perseus	220	5	0.9	2	60	20
L1527	04 39 53.9	+26 03 10	Taurus	140	2	0.9	0.7	60	20
L1157-MM	20 39 06.2	+31 13 31	Isolated	325	11	1.6	5	60	40
IRAS16293–2422	16 32 22.7	−24 38 32	ρ-Ophiucus	160	27	5.4	2	43	133

[a] Distance.
[b] Bolometric luminosity.
[c] Mass of the envelope.
[d] Submillimetric-to-bolometric luminosity ratio.
[e] Bolometric temperature.
[f] Radius where $T = 100\,{\rm K}$.

Table B.2 Physical parameters of the envelopes of hot corinos.

Source	r_i (AU)	$n(r_i)$ cm^{-3}	α	$r_{10\mathrm{K}}$ (AU)	Ref.
NGC1333–IRAS4A	66.7	1.1×10^{8}	1.5	1.5×10^{3a}	m02
	23.9	5.0×10^{9}	1.8	4.7×10^{3}	j02
NGC1333–IRAS4B	10.6	6.7×10^{8}	1.3	7.0×10^{3}	j02
NGC1333–IRAS2A	23.4	1.3×10^{9}	1.8	1.2×10^{4}	j02
L1448-N	10.0	4.9×10^{8}	1.2	7.0×10^{3}	m04
L1448-MM	9.0	5.4×10^{8}	1.4	8.1×10^{3}	j02
L1527	4.2	9.9×10^{6}	0.6	6.3×10^{3}	j02
L1157-MM	17.9	3.1×10^{9}	1.7	5.4×10^{3}	j02
IRAS16293–2422	66.7	2.4×10^{7}	1.5	4.0×10^{3a}	cht96
	32.1	2.3×10^{9}	1.7	8.0×10^{3}	s02

NOTE — $n = n(r_i) \times \left(\frac{r}{r_i}\right)^{-\alpha}$; $r_{10\mathrm{K}}$ is the radius where $T = 10$ K, except where noted.
[a] Radius where $T = 30$ K.
References: m02 = Maret et al. (2002), j02 = Jørgensen et al. (2002), m04 = Maret et al. (2004), cht96 = Ceccarelli et al. (1996), s02 = Schöier et al. (2002)

Appendix C
Spectroscopic parameters for the IRAM-30m observations

Table C.1 Transitions in the observed frequency ranges with the IRAM-30m for the targeted molecules and other species of interest.

Molecule	Frequency (GHz)	log(I)	E_{low} (cm^{-1})	g_{up}	Transition
		90 GHz			
$HCOOCH_3$-A	90156.4803	-4.8701	10.6618	15	$7_{2,5} - 6_{2,4}$
	90229.6286	-4.7840	10.9337	17	$8_{0,8} - 7_{0,7}$
$HCOOCH_3$-E	90145.6894	-4.8703	10.6742	15	$7_{2,5} - 6_{2,4}$
	90227.6052	-4.7840	10.9471	17	$8_{0,8} - 7_{0,7}$
HCOOH	90164.6280	-4.4792	13.3446	9	$4_{2,2} - 3_{2,1}$
C_2H_5OH	90117.6100	-4.7906	3.4925	9	$4_{1,4} - 3_{0,3}$
		98 GHz			
$HCOOCH_3$-A	98611.1703	-4.7752	15.6463	17	$8_{3,6} - 7_{3,5}$
	98682.6219	-4.8400	18.8698	17	$8_{4,5} - 7_{4,4}$
$HCOOCH_3$-E	98606.8055	-4.7758	15.6577	17	$8_{3,6} - 7_{3,5}$
	98711.8624	-4.8543	18.8768	17	$8_{4,5} - 7_{4,4}$
	98747.9796	-4.8540	18.8858	17	$8_{4,4} - 7_{4,3}$
$C_2H_5CN^a$	98523.8720	-3.7989	44.2506	23	$11_{6,*} - 10_{6,*}$
	98524.6720	-3.8919	54.2869	23	$11_{7,*} - 10_{7,*}$
	98532.0840	-4.0174	65.8601	23	$11_{8,*} - 10_{8,*}$
	98533.9870	-3.7283	35.7543	23	$11_{5,*} - 10_{5,*}$
	98544.1640	-4.1984	78.9669	23	$11_{9,*} - 10_{9,*}$
	98559.9270	-4.5086	93.6035	23	$11_{10,*} - 10_{10,*}$
	98564.9300	-3.6746	28.8014	23	$11_{4,8} - 10_{4,7}$
	98566.6150	-3.6746	28.8014	23	$11_{4,7} - 10_{4,6}$
	98610.2500	-3.6349	23.3943	23	$11_{3,9} - 10_{3,8}$
	98701.0700	-3.6341	23.3984	23	$11_{3,8} - 10_{3,7}$
C_2H_5OH	98585.0950	-4.2602	106.4977	31	$15_{1,15} - 15_{0,15}$
		110 GHz			
CH_3CN^b	110329.6080	-4.2473	133.3112	26	$6_{5,0} - 5_{5,0}$
	110348.9720	-3.8945	88.6466	26	$6_{4,0} - 5_{4,0}$
	110364.0840	-3.3907	53.8969	52	$6_{3,0} - 5_{3,0}$
	110374.8740	-3.5661	29.0700	26	$6_{2,0} - 5_{2,0}$
	110381.3459	-3.4961	14.1716	26	$6_{1,0} - 5_{1,0}$
	110383.4940	-3.5484	9.2052	22	$6_{0,0} - 5_{0,0}$
C_2H_5OH	110368.4950	-4.5516	59.7280	17	$8_{1,8} - 8_{0,8}$
		135 GHz			
HCOOH	135737.7000	-3.8897	20.1178	13	$6_{2,4} - 5_{2,3}$
CH_3CHO-A	135685.3490	-3.4196	19.8353	15	$7_{2,5} - 6_{2,4}$
C_2H_5OH	135664.8650	-4.2741	58.4366	17	$8_{0,8} - 7_{0,7}$
	135830.6410	-4.3119	51.7391	27	$13_{2,12} - 13_{1,13}$
		146 GHz			
CH_3OCH_3	146677.9635	-5.1331	10.2296	72	$4_{3,2_1} - 4_{2,3_1}$
	146684.7103	-5.1912	10.2294	45	$4_{3,2_0} - 4_{2,3_0}$
	146704.7162	-4.9872	2.8153	56	$3_{2,1_1} - 2_{1,2_1}$
	146707.1671	-5.1910	2.8150	35	$3_{2,1_0} - 2_{1,2_0}$
	146872.5451	-4.8712	13.3863	88	$5_{3,3_1} - 5_{2,4_1}$
	146877.3085	-5.2708	13.3861	33	$5_{3,3_0} - 5_{2,4_0}$
C_2H_5CN	146894.5240	-3.1045	40.1247	35	$17_{1,17} - 16_{1,16}$
C_2H_5OH	146707.2802	-4.4135	72.5945	21	$10_{2,9} - 10_{1,9}$
	146714.0944	-4.1501	63.4095	19	$9_{1,9} - 8_{1,8}$

Continued.

Molecule	Frequency (GHz)	log(I)	E_{low} (cm^{-1})	g_{up}	Transition
		223 GHz			
CH_3OCH_3	223200.0564	-4.9725	19.1811	34	$8_{2,7_2} - 7_{1,6_2}$
	223200.0647	-4.7964	19.1811	51	$8_{2,7_3} - 7_{1,6_3}$
	223202.2444	-4.3704	19.1809	136	$8_{2,7_1} - 7_{1,6_1}$
	223204.4281	-4.5745	19.1806	85	$8_{2,7_0} - 7_{1,6,0}$
C_2H_5CN	223385.3500	-2.6709	94.4441	53	$26_{1,26} - 25_{1,25}$
		226 GHz			
$HCOOCH_3$-A	226718.6880	-3.7282	75.9860	41	$20_{2,19} - 19_{2,18}$
	226778.7072	-3.7279	75.9812	41	$20_{1,19} - 19_{1,18}$
$HCOOCH_3$-E	226713.0600	-3.7282	75.9959	41	$20_{2,18} - 19_{2,18}$
	226773.1300	-3.7280	75.9911	41	$20_{3,18} - 19_{3,17}$
CH_3CHO-A	226589.5860	-2.7538	42.0021	25	$12_{0,12} - 11_{0,11}$
CH_3CHO-E	226850.5992	-4.1471	49.0674	23	$11_{3,8} - 11_{2,9}$
C_2H_5OH	226661.7010	-3.8625	27.9057	21	$10_{2,9} - 9_{1,8}$
		241 GHz			
HCOOH	241146.3283	-3.1242	40.7435	23	$11_{0,11} - 10_{0,10}$
CH_3OCH_3	240985.0778	-4.3627	10.2470	88	$5_{3,3_1} - 4_{2,2_1}$
	240989.9393	-4.7598	10.2468	33	$5_{3,3_0} - 4_{2,2_0}$
		257 GHz			
CH_3CN[b]	257482.7789	-2.2745	100.5247	116	$14_{3,0} - 13_{3,0}$
	257507.5609	-2.5123	75.7023	58	$14_{2,0} - 13_{2,0}$
	257522.4310	-2.5057	60.8067	54	$14_{1,0} - 13_{1,0}$
	257527.3857	-2.4931	55.8411	54	$14_{0,0} - 13_{0,0}$

NOTE — For CH_3OCH_3, the second subscript indicates the AA (0), EE (1), EA (2) or AE (3) states.
[a] A star in the subscript indicates that the transition is an unresolved doublet.
[b] All CH_3CN lines listed here are unresolved triplets.

Appendix D
Publications

Thesis-related publications

- "Hot corinos in NGC1333-IRAS 4B and IRAS 2A", **Bottinelli, S.**, Ceccarelli, C., Lefloch, B., Williams, J. P. 2006, A&A accepted
  Results published in this article are presented in Chapters 3 and 6.

- "Near-arcsecond resolution observations of the hot corino of the solar type protostar IRAS16293–2422", **Bottinelli, S.**, Ceccarelli, C., Neri, R., Williams, J. P., Caux, E., Cazaux, S., Lefloch, B., Maret, S., & Tielens, A. G. G. M. 2004, ApJ, 617, L69
  These observations can be found in Chapter 4.

- "Complex molecules in the hot core of the low-mass protostar NGC1333-IRAS 4A", **Bottinelli, S.**, Ceccarelli, C., Lefloch, B., Williams, J. P., Castets, A., Caux, E., Cazaux, S., Maret, S., Parise, B., & Tielens, A. G. G. M. 2004, ApJ, 615, 354
  See also Chapter 3

Other publications related to star-formation

- "Modeling the millimeter emission from the Cepheus A young stellar cluster: Evidence for large scale collapse", **Bottinelli, S.** & Williams, J. P. 2004, A&A, 421, 1113

- "Detection of cool dust around the G2V star HD 107146", Williams, J. P., Najita, J., Liu, M. C., **Bottinelli, S.**, Carpenter, J. M., Hillenbrand, L. A., Meyer, M. R., & Soderblom, D. R. 2004, ApJ, 604, 414

Astronomy & Astrophysics manuscript no. paper-low-mass
November 7, 2006

Hot corinos in NGC1333-IRAS4B and IRAS2A

S. Bottinelli[1,2], C. Ceccarelli[1], J. P. Williams[2], and B. Lefloch[1]

[1] Laboratoire d'Astrophysique de l'Observatoire de Grenoble, BP 53, 38041 Grenoble, Cedex 9, France.
e-mail: sbottine,ceccarel,lefloch@obs.ujf-grenoble.fr
[2] Institute for Astronomy, University of Hawai'i, 2680 Woodlawn Drive, Honolulu HI 96822, USA.
e-mail: jpw@ifa.hawaii.edu

Received ; Accepted October, 11 2006

ABSTRACT

Context. Complex organic molecules have been detected in massive hot cores for over two decades, and only recently in three hot corinos (the inner regions surrounding Sun-like protostars, where the dust temperature exceeds 100 K). Since hot corinos have sizes of ∼100 AU (i.e. of order the extent of the Solar System), it is particularly relevant to understand whether they are common and to identify the formation route(s) of complex organic molecules. Much has yet to be learned on this topic, since even recent models predicted it was not possible to form these molecules in low-mass protostars.
Aims. We aim to enlarge the number of known hot corinos and carry out a first comparative study with hot cores. The ultimate goal is to understand whether complex organic molecules form in the gas-phase or on grain surfaces, and what the possible key parameters are.
Methods. We observed millimeter rotational transitions of HCOOH, $HCOOCH_3$, CH_3OCH_3 CH_3CN and C_2H_5CN in a sample of low-mass protostars with the IRAM-30m. Using the rotational diagram method coupled with the information about the sources' structure, we calculate the abundances of the observed molecules. To interpret these abundances, we review the proposed formation processes of the above molecules.
Results. We report the detection of $HCOOCH_3$ and/or CH_3CN towards NGC1333-IRAS4B and NGC1333-IRAS2A. We find that abundance ratios of O-bearing molecules to methanol or formaldehyde in hot corinos are comparable and about unity, and are relatively (depending on how the ratios are determined) higher than those in hot cores and in Galactic Center clouds.
Conclusions. So far, complex organic molecules were detected in all the hot corinos where they were searched for, suggesting that it is a common phase for low-mass protostars. While some evidence point to grain-surface synthesis (either in the cold or warm-up phase) of these molecules (in particular for HCOOH and $HCOOCH_3$), the present data do not allow us to disregard gas-phase formation. More observational, laboratory and theoretical studies are required to improve our understanding of hot corinos.

Key words. ISM: abundances — ISM: molecules — stars: formation

1. Introduction

Many aspects of the formation of a solar-type stars have now been elucidated and, even though the details are much debated, there exists a widely accepted framework for it (see the volume Protostars and Planets V, for example Ceccarelli et al.; Ward-Thompson et al.; White et al.). Low-mass stars form inside molecular clouds from dense and cold condensations, called prestellar cores, which evolve into Class 0 and then Class I sources. In the latest phases, the newly born star is surrounded by a proto-planetary disk, which eventually may form planets.

Somewhat less understood, and therefore more argued, is the chemical evolution of matter from the molecular cloud to the proto-planetary phase, and then to planets (e.g. Ceccarelli et al. 2006). It is now acknowledged that, at the densities and temperatures typical of the centers of prestellar cores ($\geq 10^6$ cm^{-3} and $\leq$ 10 K respectively), heavy-element bearing molecules condense out onto dust grains, forming icy mantles. Very likely, hydrogenation and oxidation of small molecules and atoms (like CO, O, N, etc) occur on the grain surfaces, so that the mantles end up being composed mainly of water, interspersed with traces of formaldehyde, methanol, ammonia and possibly even more complex molecules. As material from the surrounding envelope starts accreting onto the central protostar, the increased radiation output heats up the surroundings. When and where the dust reaches the appropriate sublimation temperature of the ices (which depends on the exact composition of these ices), the grain mantles evaporate, injecting their components into the gas phase. These components can further react to form more complex molecules. The regions where the ice mantles sublimate (at $T_{dust} \gtrsim 100$ K) and where the emission from complex molecules (whether evaporated from the grain mantles or formed in the gas) originates, are called hot corinos (Ceccarelli 2004; Bottinelli et al. 2004a). The chemical composition of these hot corinos reflects both the heritage from the prestellar core phase and the reactions taking place in the warm gas. The result is a gas rich in complex organic molecules

Send offprint requests to: S. Bottinelli

(Cazaux et al. 2003), whose diversity is far from being fully explored and understood. Likely, we have discovered only the tip of the iceberg. Moreover, the story does not end here. Indeed, the fate of these complex organic molecules is almost totally unknown. Possibly they condense onto the grain surfaces again during the proto-planetary disk phase. Perhaps they are incorporated into the planetesimals forming the building-blocks of planets, or into comets and asteroids, in which case they may end up on newly formed planets as accretion proceeds. This picture is, at least partially, supported by the fact that some complex organic molecules are found both in hot corinos and in comets (e.g. methyl cyanide CH_3CN, methyl formate $HCOOCH_3$, and formic acid HCOOH; Ehrenfreund & Charnley 2000). For these reasons, the hot corino phase is not only interesting in itself, but it is a critical phase in the process of solar-type star formation.

In short, the molecular complexity in hot corinos is particularly relevant to molecular astrophysics and (exo)planetary science, but particularly unknown. Our ignorance can be summarized by this simple, multiple-part question: *which, why, where and how complex organic molecules are formed?* At present we are simply unable to answer this question for the following reasons. *(i)* We do not have a census of the complex organic molecules. We suspect that many complex molecules are present in the millimeter spectra of hot corinos, but the firm identification of a large molecule requires several lines from this molecule and can be hampered by the multitude of weak lines in the spectra (e.g. Combes et al. 1996; Ceccarelli et al. 2000c). *(ii)* We do not know why they form. The gas-grain models for hot cores (the high-mass analogs of hot corinos) predict that there is not enough time for hot corinos to form molecules because the gas falls rapidly towards the central forming star before any gas-phase reaction can lead to complex organic molecules (e.g. Schöier et al. 2002). *(iii)* We debate whether the observed complex molecules reside in the passive heated envelope (Ceccarelli et al. 2000a,b), in the hidden circumstellar disk (Jørgensen et al. 2005b), or in the interface between the outflow and the envelope (Chandler et al. 2005). *(iv)* Finally, we don't know how complex molecules form: in the gas-phase or on the grain surfaces, or both. Much of our ignorance stems from the too few hot corinos so far studied: IRAS16293–2422 (hereafter IRAS16293 Cazaux et al. 2003; Kuan et al. 2004; Bottinelli et al. 2004b; Remijan & Hollis 2006), NGC1333-IRAS4A (hereafter IRAS4A Bottinelli et al. 2004a), NGC1333-IRAS4B (hereafter IRAS4B Sakai et al. 2006) and NGC1333-IRAS2A (hereafter IRAS2A Jørgensen et al. 2005a).

In this paper, we present detections of complex organic molecules in two Class 0 hot corinos: $HCOOCH_3$ and CH_3CN in IRAS4B, and CH_3CN in IRAS2A. The article is organized as follows: details on the choice of sources are given in section 2, the observations are described in section 3 and results are presented and discussed in sections 4 and 5 respectively. Section 5 starts with a summary of the formation mechanisms of the complex molecules HCOOH, $HCOOCH_3$, CH_3OCH_3, CH_3CN and C_2H_5CN (A), followed by the analysis of our data (5.2 and 5.3) and ends with a comparison of hot corinos with hot cores (5.4) and with Galactic Center clouds (5.5). Finally, a summary and concluding remarks are given in section 6.

2. Source selection and background

We observed two Class 0 protostars, IRAS4B and IRAS2A, located in the Perseus complex, specifically in the NGC1333 cloud, whose distance is estimated to be 220 pc (Černis 1990). IRAS4B belongs to the multiple system IRAS4 and is located $\sim 30''$ and $\sim 17''$ from the other two components, IRAS4A and IRAS4C (Looney et al. 2000; Reipurth et al. 2002). It may be itself a multiple stellar system (Looney et al. 2000). Both IRAS4A and IRAS4B are associated with molecular outflows with a dynamical age of a few thousand years, seen in CO, CS (Blake et al. 1995) and SiO (Lefloch et al. 1998). IRAS2A is part of a protobinary system and is separated by $30''$ from its companion IRAS2B (Looney et al. 2000; Reipurth et al. 2002). Two CO bipolar outflows appear to originate within a few arcsec of IRAS2A: a highly collimated jet in the east-west direction and a large-scale outflow aligned NNE-SSW (Sandell et al. 1994; Knee & Sandell 2000).

IRAS4B and IRAS2A were selected from the sample studied in Maret et al. (2004, 2005) because they both are good hot corino candidates and because, due to their distance and luminosity, they are expected to have brighter lines compared to other Class 0 sources (e.g. from the André et al. 2000 sample). The candidacy relies upon the claim by Maret et al. (2004, 2005) for the presence, in both IRAS2A and IRAS4B, of a warm ($\gtrsim$ 100 K) inner region where grain mantles sublimate. The claim is based on the observed jumps in the abundances of formaldehyde and methanol: low abundances in the outer, cold envelope where formaldehyde and methanol are still frozen onto grain surfaces, and high abundances in the inner, warm envelope where the heat from the central object causes the desorption of formaldehyde and methanol into the gas-phase. Indeed, in the two sources where hot corinos have been so far detected, IRAS16293 (Cazaux et al. 2003) and IRAS4A (Bottinelli et al. 2004a), similar jumps in the formaldehyde and/or methanol abundances have also been claimed (Maret et al. 2004, 2005) , supporting the choice of our targets.

However, there is a noticeable difference in the extent of the hot corinos (54 to 266 AU, Maret et al. 2004) and in the jump sizes in all four sources. Indeed, according to Maret et al. (2005), methanol abundances show jumps of a factor 100 to 350 in all sources but IRAS4A, where the jump is lower than about a factor 15, whereas Maret et al. (2004) found formaldehyde abundance jumps of a factor 100 to 6000. Other authors have carried out analyses of methanol and formaldehyde in low-mass protostars (e.g. Schöier et al. 2002; Jørgensen et al. 2005b). In contrast with what found by Maret et al. (2004), Jørgensen et al. (2005b) claimed that no jump of formaldehyde abundance is required to model the line intensities in any of the sources except IRAS16293 (Schöier et al. 2002). However, like Maret et al. (2005), Jørgensen et al. (2005b) and Schöier et al. (2002) found a methanol abundance jump in IRAS4B, IRAS2A and IRAS16293, but not necessarily in IRAS4A. The

hot corino abundances of formaldehyde and methanol found by the two groups are summarized in Table 1. In the following we will adopt the Maret et al. (2004, 2005) framework, but we will also discuss the results in the light of the Jørgensen et al. (2005b) analysis.

In summary, the four hot corinos — IRAS16293, IRAS4A, IRAS4B and IRAS2A — form a sample of interestingly different sources, both because they span an apparent large range of formaldehyde and methanol abundances, and because the very existence of the abundance jumps is still debated. Hence, even though statistically small, this sample will permit a first assessment of how the presence and abundance of complex organic molecules in hot corinos depend on formaldehyde and methanol. Indeed, these two molecules are predicted to be among the most important parent ones (e.g. Caselli et al. 1993; Rodgers & Charnley 2001, 2003), but it is not always clear how they relate to the complex molecules (e.g. Horn et al. 2004).

3. Observations

The observations were carried out in June 2003 with the 30-meter telescope of the Institut de RadioAstronomie Millimétrique (IRAM)[1]. The positions used for pointing were (α, δ)(2000) = ($03^h29^m12\overset{s}{.}0$, 31°13′09″) for IRAS4B, and (α, δ)(2000) = ($03^h28^m55\overset{s}{.}4$, 31°14′35″) for IRAS2A.

Based on the observations of IRAS16293 by Cazaux et al. (2003), we targeted the following complex molecules: methyl formate, $HCOOCH_3$ (A and E), formic acid, HCOOH, dimethyl ether, CH_3OCH_3, methyl cyanide, CH_3CN, and ethyl cyanide, C_2H_5CN. Different telescope settings were used in order to include as many transitions as possible for each molecule (see Table 2). All lines were observed with a low resolution, 1 MHz filter bank of 4 × 256 channels split between different receivers, providing a velocity resolution of ∼ 3, 2, and 1 km s^{-1} at 3, 2, and 1 mm, respectively. Each receiver was simultaneously connected to a unit of the autocorrelator, with spectral resolutions of 20, 80 or 320 kHz and bandwidths between 40 and 240 MHz, equivalent to a (unsmoothed) velocity resolution of 0.1–0.4 km s^{-1} at 3, 2, and 1 mm. Typical system temperatures were 100–200 K, 180–250 K and 500–1500 K, at 3, 2 and 1 mm respectively.

Two observation modes were used: position switching with the OFF position at an offset of $\Delta\alpha = -100''$, $\Delta\delta = +300''$, and wobbler switching with a 110″ throw in azimuth. Pointing and focus were regularly checked using planets or strong quasars, providing a pointing accuracy of 3″. All intensities reported in this paper are expressed in units of main-beam brightness temperature. At 3, 2 and 1 mm, the angular resolution is 24, 16 and 10″ and the main beam efficiency is 76, 69 and 50%, respectively. Figure 1 shows the obtained spectra.

4. Results

Detected transitions have been identified using the JPL molecular line catalog (Pickett et al. 1998), the Cologne Database for Molecular Spectroscopy (Müller et al. 2001, 2005) and the National Institute of Standards and Technology (NIST) Recommended Rest Frequencies for Observed Interstellar Molecular Microwave Transitions (Lovas & Dragoset 2004). They are reported in Table 3.

We considered as good identifications only lines with a 3-σ detection and a V_{LSR}=7.0±0.4 km s^{-1}. We detected two of the five targeted molecules: 4 transitions for $HCOOCH_3$-A in IRAS4B and 5 and 6 transitions for CH_3CN in IRAS4B and IRAS2A respectively. We also have a possible detection for C_2H_5OH at 226.661 GHz in IRAS4B[2].

Note that no observations were made at 110 GHz for IRAS2A (see Table 2), and that the rms reached at 257 GHz for IRAS4B is too high to detect the CH_3CN transitions at this frequency, if the line ratios are similar to those in IRAS4A.

In order to derive rotational temperatures and beam-averaged column densities (see Table 4), we used the rotational diagram method (Fig. 2). For this analysis, we assumed that the emission from a given molecule is unresolved in the smallest beam in which a transition of that molecule was detected (θ_{min}, which is always ≥ 10″ — see columns 3 and 7 in Table 4). This is justified by the interferometric observations of IRAS16293–2422 (Bottinelli et al. 2004b; Kuan et al. 2004; Chandler et al. 2005), NGC1333-IRAS2A (Jørgensen et al. 2005a) and NGC1333-IRAS4A (Bottinelli et al. 2006), which show that the bulk of the emission occurs over a region $\lesssim 1''$. We therefore corrected the integrated intensities observed at lower frequencies for beam dilution with respect to θ_{min}. Then, the hot corino abundances were obtained by scaling the beam-averaged column densities to the sizes of the hot corinos (taken from Table 6 of Maret et al. 2004: 0.″25 for IRAS4B and 0.″43 for IRAS2A) and dividing by the hot corino H_2 column density. The latter was obtained from the density profiles derived by Jørgensen et al. (2002), based on single-dish observations of the dust continuum and radiative transfer calculations (see also Table 6 of Maret et al. 2004). This introduces an uncertainty in

Table 2. Observed frequencies and targeted molecules.

Frequency range (GHz)	Molecule	Frequencies (GHz)	rms (mK) IRAS4B	rms (mK) IRAS2A
90.07 – 90.32	$HCOOCH_3$-A	90.156, 90.229	7	2
	$HCOOCH_3$-E	90.145, 90.227	2, 7	2
	HCOOH	90.164	2	2
98.50 – 98.75	$HCOOCH_3$-A	98.611, 98.682	7, 2	3
	$HCOOCH_3$-E	98.606, 98.711	7, 2	3
	C_2H_5CN	98.610, 98.701	7, 2	3
110.29 – 110.43	CH_3CN	110.329 – 110.383	5	–
223.17 – 223.42	CH_3OCH_3	223.200 – 223.204	13	34
	C_2H_5CN	223.385	13	34
226.50 – 227.00	$HCOOCH_3$-A	226.718, 226.778	11	15
	$HCOOCH_3$-E	226.713, 226.773	11	15
257.35 – 257.55	CH_3CN	257.403 – 257.527	22	28

Note. – A dash indicates that no data were taken in the corresponding frequency range.

[1] IRAM is an international venture supported by INSU/CNRS (France), MPG (Germany) and IGN (Spain).

[2] This transition is not seen in NGC1333-IRAS4A. In this source, there is a tentative detection at 90.118 GHz (Bottinelli et al. 2004a) that has a lower energy (3.5 vs 28 cm^{-1}) but also lower line strength (log(I)=-4.8 vs -3.9).

Table 1. Hot corino abundances for formaldehyde ($X_{hc}(H_2CO)$) and methanol ($X_{hc}(CH_3OH)$).

Source	L_{bol}[a] ($L_\odot$)	$X_{hc}(H_2CO)$ Maret et al. (2004)	$X_{hc}(H_2CO)$ Jørgensen et al. (2005b)[b]	$X_{hc}(CH_3OH)$ Maret et al. (2005)	$X_{hc}(CH_3OH)$ Jørgensen et al. (2005b)[c]
IRAS16293–2422	27	1×10^{-7}	6×10^{-8}[d]	1×10^{-7}	1×10^{-7}
NGC1333-IRAS4A	6	2×10^{-8}	3×10^{-9}	$< 1\times10^{-8}$	$\leq 3.5\times10^{-9}$
NGC1333-IRAS4B	6	3×10^{-6}	1×10^{-8}	7×10^{-7}	9.5×10^{-8}
NGC1333-IRAS2A	16	2×10^{-7}	8×10^{-10}	3×10^{-7}	1.5×10^{-7}

[a] From Jørgensen et al. (2002).

[b] Note that except in IRAS16293 (Schöier et al. 2002), the formaldehyde abundances modeled by Jørgensen et al. (2005b) do not require any jump (see text for further details).

[c] Methanol abundances averaged over A- and E-types.

[d] From Schöier et al. (2002).

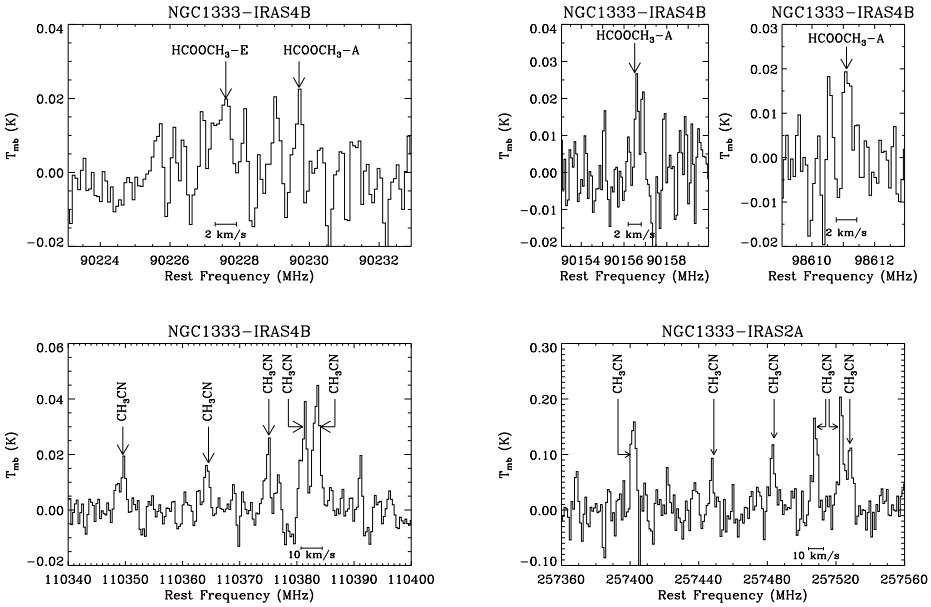

Fig. 1. Observed spectra towards IRAS4B and IRAS2A. The rms are 7 mK (top panels) and 5 and 28 mK (bottom panels, left to right); the spectral resolutions are 0.2, 0.3, 0.8 and 1.2 km s^{-1} at 90, 98, 110 and 257 GHz respectively. Detected transitions are (from left to right, top to bottom): $HCOOCH_3$-E ($8_{0,8} - 7_{0,7}$), $HCOOCH_3$-A ($8_{0,8} - 7_{0,7}$, $7_{2,5} - 6_{2,4}$, $8_{3,6} - 7_{3,5}$), CH_3CN ($6 - 4$, $K = 4, ...0$) and CH_3CN ($14 - 13$, $K = 5, ...0$). Unlabeled lines are unidentified.

the derived abundances, due to the uncertain sizes and H_2 column densities of the hot corinos, caused by the extrapolation from single-dish observations. However, abundance ratios are not affected by this uncertainty, unless different molecules are formed in different regions (see discussion in §5.2).

We make the following remarks about the results we obtain.

The rotational temperature of $HCOOCH_3$-A is poorly constrained due to the absence of points at higher energies.

More generally, some of the rotational temperatures are below 100 K. This could be due to non-LTE and/or line opacity effects.

We find that the derived CH_3CN abundance is consistent with the value obtained by Jørgensen et al. (2005b) for an inner ($T > 90$ K) region. Upper limits were calculated for the targeted molecules that were not detected: HCOOH and C_2H_5CN in both sources, $HCOOCH_3$-A in IRAS2A and CH_3OCH_3 in IRAS4B. The upper limits for the O-bearing molecules were derived using the rotational temperature derived for $HCOOCH_3$-A in IRAS4B, whereas the upper limits for N-bearing molecules were calculated assuming a rotational temperature equal to that of CH_3CN in each source. Finally, the CH_3OCH_3 abundance in IRAS2A was taken from Jørgensen et al. (2005a): the quoted abundance (3×10^{-8} in

Table 3. Molecular lines detected.

Molecule	Transition line	Frequency (MHz)	E_u[a] (cm^{-1})	T_{mb} (mK)	ΔV[b] (km s^{-1})	$\int T_{mb}dV$ (K km s^{-1})
		IRAS4B				
$HCOOCH_3$-A	$7_{2,5} - 6_{2,4}$	90156.5	13.7	26	0.6	0.017 ± 0.004
	$8_{0,8} - 7_{0,7}$	90229.7	13.9	23	0.5	0.013 ± 0.004
	$8_{3,6} - 7_{3,5}$	98611.1	18.9	21	0.7	0.016 ± 0.004
$HCOOCH_3$-E	$8_{0,8} - 7_{0,7}$	90227.8	14.0	18	1.8[d]	0.035 ± 0.005
CH_3CN[c]	$6_{4,0} - 5_{4,0}$	110349.7	92.3	18	2.3	0.045 ± 0.009
	$6_{3,0} - 5_{3,0}$	110364.6	57.6	17	2.8	0.049 ± 0.011
	$6_{2,0} - 5_{2,0}$	110375.1	32.8	24	2.5	0.062 ± 0.013
	$6_{1,0} - 5_{1,0}$	110381.5	17.9	33	3.4	0.119 ± 0.014
	$6_{0,0} - 5_{0,0}$	110383.6	12.9	42	3.8	0.171 ± 0.015
		IRAS2A				
CH_3CN[c]	$14_{5,0} - 13_{5,0}$	257403.6	188.5	169	3.8	0.692 ± 0.091
	$14_{4,0} - 13_{4,0}$	257448.9	143.9	111	1.6	0.190 ± 0.046
	$14_{3,0} - 13_{3,0}$	257482.7	109.1	113	3.4	0.413 ± 0.044
	$14_{2,0} - 13_{2,0}$	257507.9	84.3	145	2.7	0.411 ± 0.055
	$14_{1,0} - 13_{1,0}$	257522.5	69.4	198	3.1	0.662 ± 0.087
	$14_{0,0} - 13_{0,0}$	257527.4	64.4	115	3.8	0.470 ± 0.068

[a] Energy of the upper level of the transition.
[b] Width of the observed line.
[c] All the CH_3CN lines are unresolved triplets, except at 110349.7 MHz which is an unresolved doublet. The quoted signal is the integral over each triplet or doublet.
[d] This line of the E form of $HCOOCH_3$ has a width about three times as large as that of the corresponding transition of the A form, which could be due to the presence of some unknown transition(s) artificially increasing the width.

an inner, $T > 90$ K region) is consistent with the upper limit derived from our data ($x < 4.2 \times 10^{-7}$, also calculated using the rotational temperature derived for $HCOOCH_3$-A in IRAS4B). Jørgensen et al. (2005a) also report a tentative detection of $HCOOCH_3$ but do not give an estimate of the abundance of this molecule.

5. Discussion

In order to investigate whether the data provide information on the formation of complex molecules, it is necessary to know what the possible formation paths are. We therefore report in Appendix A the formation reactions found in the literature for the detected molecules, and we bring up some key points regarding these formation routes in §5.1. Since low-mass protostars were thought to have insufficient luminosity to develop a hot core-type region, we will then investigate the potential dependence of the complex molecules' abundances on the luminosity (§5.2). In section 5.3, we will analyze the hot corino data in view of the information given in section A and look at the differences with their massive counterparts and with Galactic Center clouds in sections 5.4 and 5.5, respectively.

5.1. Notes on the formation routes of complex organic molecules

For all the complex molecules considered here, we can see from Appendix A that grain-surface formation is a possible alternative to the "classical" gas-phase formation. In this classical view, an estimate of the formation and destruction timescales for CH_3OCH_3 indicates that destruction of this molecule is likely compensated by formation mechanisms (§A.5). Regarding grain-surfaces processes, it is usually implicitly assumed that they are taking place during the cold phase preceding the warm-up of the dust by the newly born star. However, as the protostar heats up, it is improbable that the dust temperature suddenly jumps from ∼10 to ∼100 K. Instead, it is more likely that the temperature "slowly" rises across the inner envelope, leading to a gradual heating of the grains (e.g. Viti et al. 2004; Garrod & Herbst 2006). The effect of this gradual temperature change on grain-surface and gas-phase chemistry can be quite substantial. Indeed, the modeling by Garrod & Herbst (2006) shows that gas-phase and grain-surface chemistries are strongly coupled during the warm-up phase: molecules formed on the grain can evaporate and affect the gas-phase chemistry whose products can re-accrete and in turn change the grain-surface chemistry.

Note that for some molecules, grain-surface formation is not only an alternative, but also apparently the only choice. This is the case for $HCOOCH_3$ and even more so for HCOOH since it has been detected in the ices of star forming regions (e.g. Schutte et al. 1999; Keane et al. 2001), as well as of quiescent molecular clouds (Knez et al. 2005). In particular, the detection of icy HCOOH in quiescent clouds would indicate, not only that HCOOH formation occurs on grain-surface, but also that it would pre-date the first phase of the star formation mechanism, supporting the theory of formation in the cold, rather than warm-up phase. Whether the

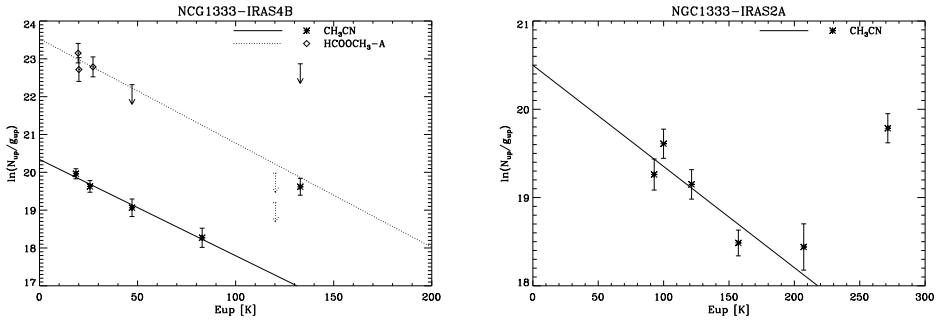

Fig. 2. Rotational diagrams of the detected molecules, corrected for beam dilution at lower frequencies. The arrows show the upper limits for undetected transitions. Lines represent the best fit to the data. Error bars are derived assuming a calibration uncertainty of 10% on top of the statistical error. The excess of emission of the CH_3CN transition at 270 K in IRAS2A and 135 K in IRAS4B is probably due to contamination from CH_3OH $18_{3,16} - 18_{2,17}$ and unknown line(s) respectively, and are not included in the fits.

Table 4. Results from the rotational diagrams and upper limits for IRAS4B and IRAS2A.

Molecule	IRAS4B				IRAS2A			
	T_{rot} (K)	θ_{min} ($''$)	N_{beam}[b] (cm^{-2})	X_{hc}[c]	T_{rot} (K)	θ_{min} ($''$)	N_{beam}[b] (cm^{-2})	X_{hc}[d]
$HCOOCH_3$-A	38^{+49}_{-35}	10	$(4.7 \pm 3.6)\times10^{13}$	$(1.1 \pm 0.8)\times10^{-6}$	[38]	10	$< 2.9 \times 10^{14}$	$< 6.7 \times 10^{-7}$
HCOOH	[38]	22	$< 1.0 \times 10^{13}$	$< 1.0 \times 10^{-6}$	[38]	25	$< 7.4 \times 10^{12}$	$< 1.2 \times 10^{-7}$
CH_3OCH_3	[38]	10	$< 6.8 \times 10^{13}$	$< 1.2 \times 10^{-6}$	[38]	10	$< 1.8 \times 10^{14}$	$< 4.2 \times 10^{-7}$
CH_3CN	39 ± 3	22	$(9.7 \pm 1.0)\times10^{11}$	$(9.5 \pm 0.2)\times10^{-8}$	87 ± 17	10	$(3.7 \pm 1.0)\times10^{12}$	$(8.7 \pm 2.4)\times10^{-9}$
C_2H_5CN	[39]	10	$< 4.2 \times 10^{13}$	$< 7.5 \times 10^{-7}$	[87]	10	$< 4.3 \times 10^{13}$	$< 1.0 \times 10^{-7}$

Note — When they could not be derived from a rotational diagram, temperatures have been assumed to be equal to that of $HCOOCH_3$ and CH_3CN for O-bearing and N-bearing molecules respectively. In this case, the values are shown in square brackets.
[a] Smallest beam size for which a transition was detected (see text for details).
[b] Column density averaged over θ_{min}.
[c] Abundance in the hot corino assuming an H_2 column density of $N(H_2) = 8.1 \times 10^{22}$ cm^{-2} and a hot corino size of 54 AU, i.e. 0.25$''$ at 220pc (From Maret et al. 2004).
[d] Abundance in the hot corino assuming an H_2 column density of $N(H_2) = 2.1 \times 10^{23}$ cm^{-2} and a hot corino size of 94 AU, i.e. 0.43$''$ at 220pc (From Maret et al. 2004).

other complex organic molecules could also follow the same pattern cannot be commented upon since, to our knowledge, no other complex molecule has been detected in ices. This is because, unfortunately, the infrared spectra of complex organic molecules are not well known in this medium. The difficulty in determining the presence of these molecules lies in the fact that they may produce only slight shifts and broadenings, and that the peak positions are characteristic of functional groups not molecular species (Tielens, priv. comm.). Hence, specific identifications are always somewhat ambiguous.

Overall, it also stands out from Appendix A that more experiments on thermal surface chemistry at low temperatures are needed to check the feasibility of the outlined reactions. Cosmic ray processing of icy grain mantles may also be able to produce complex molecules, but this process requires more quantitative modeling to compare with observations.

5.2. Luminosity dependence

As mentioned previously, before the discovery of a hot corino around IRAS16293, it was believed impossible to have chemically rich regions driven by gas-phase reactions following mantle evaporation around low-mass protostars. The argument was that, given the low luminosity of these objects, the regions where the ices sublimate would be so small that the gas crossing-time would be shorter than the time needed to form complex organic molecules in the gas-phase (e.g. Schöier et al. 2002). This is in fact not the case since several hot corinos have now been discovered (Cazaux et al. 2003; Bottinelli et al. 2004a; Jørgensen et al. 2005a, this work). But

the question remains regarding the impact of the luminosity on the abundances of complex organic molecules in hot corinos.

Table 5 lists the measured abundances and upper limits for the four hot corinos. In order to remove the uncertainty on the sizes of the hot corinos, we choose to look at abundance ratios, in particular with respect to formaldehyde and methanol since these molecules have been proposed to be the parent molecules for complex oxygen-bearing species, if they are formed in the gas-phase. These abundance ratios are plotted on Figure 3 as a function of the bolometric luminosity of the low-mass protostars. For information, the abundance ratio for CH_3CN is also plotted (C_2H_5CN was not included due to the number of upper limits), although formaldehyde and methanol are not thought to be the parent molecules of nitrogen-bearing species (see section A.4). Note that the abundance ratios of CH_3OCH_3 with respect to both H_2CO and CH_3OH in IRAS2A seem to be "outliers" compared to the other protostars and to other O-bearing molecules. However, recall that the CH_3OCH_3 abundance was taken from Jørgensen et al. (2005a) where it was derived from only one detected transition. Apart from the CH_3OCH_3 points and taking into account the uncertainties pertaining to abundance determination, we can see from Figure 3 that the abundance ratios of complex molecules with respect to H_2CO or CH_3OH do not depend on the luminosity, in the range $\sim 5 - 30$ $L_\odot$. Since the abundances of H_2CO or CH_3OH are not themselves a function of luminosity (see Maret et al. 2004, 2005), then *the absolute abundances of the complex species do not depend on the luminosity of the protostar*. Whatever the formation mechanism, either in the gas phase or on the grain surfaces, the efficiency in forming complex organic molecules is largely constant in the range of studied luminosities. Since the luminosity, together with the density, defines the radius at which ices sublimate, this also implies that this efficiency is rather constant in the inner 200 AUs or so of the studied sources, despite the different involved densities (from 10^6 to 10^9 cm^{-3}, Maret et al. 2004).

We also investigated the possible dependence of the abundance ratios on the ratio of submillimeter to bolometric luminosity, L_{smm}/L_{bol}, since it has been suggested as an indicator of evolutionary stage. We find that the abundance ratios do not depend on this parameter either. Maret et al. (2004) found an apparent anti-correlation between the inner abundance of H_2CO and L_{smm}/L_{bol} and proposed that this could be explained if L_{smm}/L_{bol} depends on the initial conditions of the protostars rather than their evolutionary stage. Indeed, more atomic hydrogen is available in less dense (i.e. with a higher L_{smm}/L_{bol}) environments, which leads to the formation of more H_2CO and CH_3OH. If we plot the inner CH_3OH abundance as a function of L_{smm}/L_{bol}, we also notice an apparent anti-correlation. Since the abundance ratios are roughly constant with different L_{smm}/L_{bol}, then the absolute abundances of complex molecules should also be anti-correlated with this parameter. Following a similar line of thought as Maret et al. (2004) and assuming that complex O-bearing molecules form on grain surfaces via H, O, OH and/or CH_3 additions, this anti-correlation could be indicative of these species being more readily available in less dense environments.

5.3. Dependence on methanol and formaldehyde hot corino abundances

Whether we consider gas-phase or grain-surface formation, CH_3OH and H_2CO appear as key molecules: in the first case, they have been suggested as parent molecules, in the second, they are known mantle constituents. It is therefore interesting to investigate the abundance ratios of complex molecules to CH_3OH and H_2CO as a function of CH_3OH and H_2CO abundances themselves. We plot these quantities for hot corinos in Figures 4 and 5 respectively. From these figures, we can see that:

(i) The complex molecules in hot corinos have comparable abundance ratios, apparently independent of the CH_3OH and H_2CO abundances.
(ii) These abundance ratios are close to unity.

The implications are:

- *In the case of gas-phase formation from methanol or formaldehyde:* (i) and (ii) mean that, in all the hot corinos, the formation of complex molecules uses up a significant fraction of the parent molecules sublimated from the mantles. However, gas-phase chemistry does not seem able to reproduce this behavior. For example, the collapsing envelope model of Rodgers & Charnley (2003; see also Rodgers & Charnley 2001) predicts CH_3OCH_3 to CH_3OH abundance ratios of only $10^{-2} - 10^{-1}$. Similarly, Rodgers & Charnley (2001) predicted $HCOOCH_3$ to CH_3OH abundance ratios $< 7 \times 10^{-3}$, and we now know that they used too high a formation rate coefficient for $HCOOCH_3$, so that the actual prediction should be even smaller (Horn et al. 2004). Therefore, either gas-phase models are not adequate, or complex molecules are not formed in the gas phase.
- *In the case of grain-surface formation:* (i) and (ii) show that complex molecules are as important mantle constituent as CH_3OH and H_2CO. Observations of solid HCOOH and CH_3OH along quiescent lines of sight by Knez et al. (2005) and in protostars (Keane et al. 2001) support this idea since the quoted HCOOH and CH_3OH abundances yield abundance ratios of order unity, as we find for the hot corinos. No observations of other complex molecules in the ices are available, but their presence cannot be excluded considering, as mentioned in section 5.1, the difficulty of identifying their signature in infrared spectra.

Note that gas-phase reactions proposed in section A.1 for the formation of HCOOH do not involve CH_3OH or H_2CO. Therefore the conclusion mentioned for gas-phase formation do not apply to this molecule, whereas the analysis regarding grain-surface formation is still valid.
Using the methanol abundances derived by Jørgensen et al. (2005b) does not change the shape of Figure 4 since their values are comparable to the ones derived by Maret et al. (2005). However, if we take formaldehyde abundances from Jørgensen

Table 5. Abundances of parent and daughter molecules in our sample of four low-mass protostars.

Molecule	IRAS16293	IRAS4A	IRAS4B	IRAS2A	Ref.
H_2CO	1×10^{-7}	2×10^{-8}	3×10^{-6}	2×10^{-7}	1,2,3
CH_3OH	1×10^{-7}	$< 1\times10^{-8}$	7×10^{-7}	3×10^{-7}	4
$HCOOCH_3$-A[a]	1.7×10^{-7}	3.4×10^{-8}	1.1×10^{-6}	$< 6.7\times10^{-7}$	5,2,6
HCOOH	6.2×10^{-8}	4.6×10^{-9}	$< 1.0\times10^{-6}$	$< 1.2\times10^{-7}$	5,2,6
CH_3OCH_3	2.4×10^{-7}	$< 2.8\times10^{-8}$	$< 1.2\times10^{-6}$	3.0×10^{-8}	5,2,6,7
CH_3CN	1.0×10^{-8}	1.6×10^{-9}	9.5×10^{-8}	8.7×10^{-9}	5,2,6
C_2H_5CN	1.2×10^{-8}	$< 1.2\times10^{-9}$	$< 7.5\times10^{-7}$	$< 1.0\times10^{-7}$	5,2,6

NOTE — Except for H_2CO and CH_3OH, for which Maret et al. (2004, 2005) took into account the effects of opacity to derive the abundances of these species, it was not possible to determine the optical thickness of the complex molecules' transitions, so that all the complex molecules' abundances should be considered as lower limits.

[a] We report here the abundances of the A form only of $HCOOCH_3$, for which we have the highest number of rotational diagrams. Note that the abundance of the E form is usually very close to that of the A form (from IRAS16293 and IRAS4A; Cazaux et al. 2003; Bottinelli et al. 2004a), so that the total $HCOOCH_3$ abundance would be twice that of the A form.

References – (1) Ceccarelli et al. (2000c). (2) Bottinelli et al. (2004a). (3) Maret et al. (2004). (4) Maret et al. (2005). (5) Cazaux et al. (2003). (6) This work. (7) Jørgensen et al. (2005a).

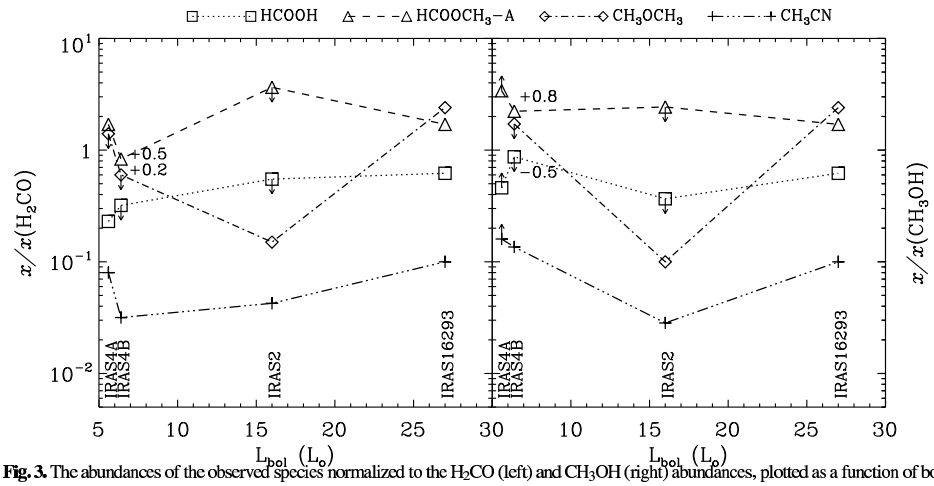

Fig. 3. The abundances of the observed species normalized to the H_2CO (left) and CH_3OH (right) abundances, plotted as a function of bolometric luminosity. Square, triangles, diamonds and plus signs represent HCOOH, $HCOOCH_3$, CH_3OCH_3 and CH_3CNrespectively. The abundance for CH_3OCH_3 in IRAS2A was taken from Jørgensen et al. (2005a) and is likely underestimated (see text). Note that we only have an upper limit on the CH_3OH abundance in the hot corino of IRAS4A, therefore, we did not plot the point corresponding to CH_3OCH_3 for which only an upper limit is available in that source. Also, we do not show C_2H_5CN since only upper limits are available in three of the four sources.

et al. (2005b), we notice that the abundance ratios are larger than those plotted in Figure 5 (as expected since Jørgensen et al. do not model any H_2CO abundance jump), and that the abundance ratios are scattered by up to two orders of magnitude.

Overall, in the Maret et al. (2004, 2005) framework, our data are consistent with either gas-phase or grain-surface formation of complex molecules in hot corinos, with nonetheless more support for the later route. However, other scenarios could be considered. For example, complex molecules could form in the ISM, deplete onto grain mantles during the accretion phase and desorb as the protostar heats up its environment. If this formation in the ISM were true, we should be able to observe their low-energy transitions in dark clouds or in the cold envelopes of the protostars. For example, Remijan & Hollis (2006) observed a transition of HCOOH with E_u=3.2 K around IRAS16293B for which the spatial distribution is around (and not peaking at) the position determined from the continuum. We cannot therefore rule out this theory, but more observations are needed to support it.

5.4. Comparison hot corinos – hot cores

Due to the physical differences between hot corinos and hot cores, comparing these two types of objects can potentially tell

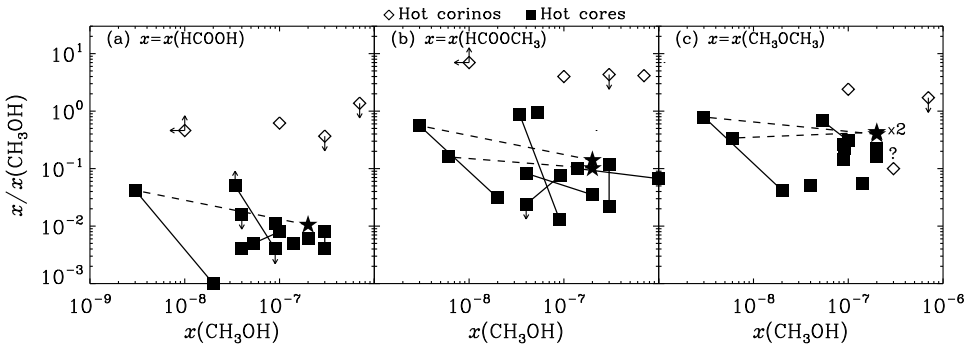

Fig. 4. Abundance ratios of complex O-bearing molecules to methanol, plotted as a function of the methanol abundance. Open diamonds represent hot corinos. Filled squares represent abundances ratios of hot cores, derived from beam-averaged column density analysis. Squares linked by a solid line represent abundance determinations from different authors (Gibb et al. 2000a and references therein, Ikeda et al. 2001). Stars represent the hot cores of SgrB2 (N) and (M), where an analysis of the methanol emission similar to what done in the hot corinos has been carried out (Nummelin et al. 2000). The dotted lines connect the SgrB2 (N) and (M) hot cores (stars) to the squares corresponding to the cold envelopes of these sources. See the text for further details. Note that panel (b) represents the total $HCOOCH_3$ abundances, that is twice the abundances of the A form quoted in Table 5. The point corresponding to CH_3OCH_3 in IRAS4A is not represented due to both CH_3OCH_3 and CH_3OH abundances being upper limits in this source. The question mark refers to the ratio in IRAS2A and indicates that the CH_3OCH_3 abundance is likely underestimated in this source (see Section5.2).

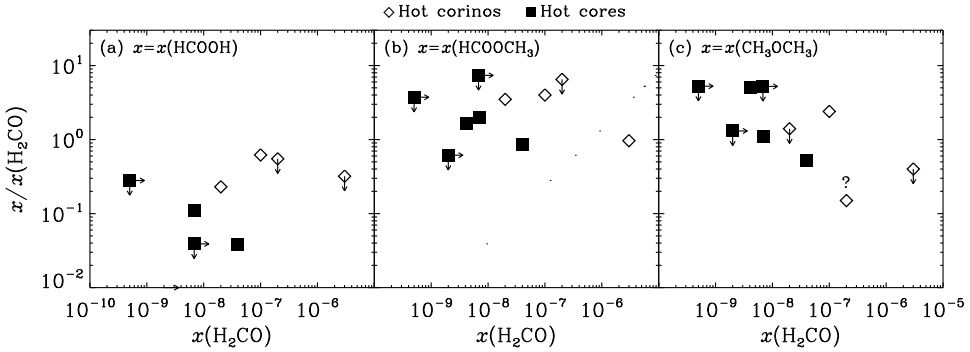

Fig. 5. Abundance ratios of complex O-bearing molecules to formaldehyde, plotted as a function of the formaldehyde abundance. Open diamonds represent hot corinos. Filled squares represent abundances ratios of hot cores, derived by beam-averaged column density analysis.

us a lot about the parameters influencing the formation and evolution of complex molecules. We therefore searched the literature for the relevant abundances in hot cores in order to calculate abundance ratios in these objects as well. To our knowledge, there are only four hot cores (Sgr B2(N), Orion hot core, Orion compact ridge and W3(H_2O)) for which data on all five O-bearing molecules studied here (H_2CO, CH_3OH, HCOOH, $HCOOCH_3$ and CH_3OCH_3) are available, but we can find another seven sources (Sgr B2(M), G327.30–0.60, G34.26+0.15, NGC6334(I), W51 e1/e2, G31.41+0.31 and G10.47+0.03) for which CH_3OH and at least two of the complex molecules molecules (HCOOH, $HCOOCH_3$ and CH_3OCH_3) have measured abundances. Data are taken from Gibb et al. (2000a) and references therein, and from Ikeda et al. (2001).

Figures 4 and 5 plot the abundance ratios of massive hot cores, as derived from the literature. A first thing to notice is that the abundance ratios in the massive hot cores have been derived by beam-averaged column densities, except for SgrB2 (N) and (M), where Nummelin et al. (2000) have carried out an analysis of the methanol emission similar to what has been done for the hot corinos, namely disentangling the hot core from the cold outer envelope contribution in the beam. For a given complex molecule, if a source was listed in both Gibb et al. (2000a) and Ikeda et al. (2001), then two abundance ratios were derived from the different authors. In this case,

the two values are reported in in Figure 4 and linked with a solid line. Disturbingly, they can differ by almost two orders of magnitude, and the cause of this discrepancy is unclear. In Figure 4, we also report the results obtained from the hot core + outer envelope analysis of CH_3OH emission in SgrB2 (N) and (M), to show the uncertainty associated with the different methods of abundance ratios' determinations. As can be seen, there is only a factor 4 difference in the abundance ratios if the hot core or the outer envelope abundance of methanol is used.

In principle, the different methods used to derive the abundance ratios in hot cores (beam-averaged column density) and corinos (full density and chemical structure analysis) may lead to such a different result that the comparison may be meaningless. However, while this would certainly be the case for the absolute values of the abundances, the abundance ratios suffer much less from the different methods, as shown by the "small" factor 4 in the SgrB2 (N) and (M) sources (Nummelin et al. 2000). In practice, the beam-averaged abundance ratios are very different from the reality only if the spatial distributions of the different molecules in the considered source are different, and/or if there is a large contribution from the outer envelope with respect to the hot core. While a direct measure of the molecular emission extent would require carrying out interferometric observations, the available data can give a good hint on where the emission originates from, by looking at the rotational temperature, $T_{\rm rot}$. As a matter of fact, the $T_{\rm rot}$ of the hot cores considered in this study (with the possible exception of the H_2CO and HCOOH) are implying that the emission is dominated indeed by the hot cores rather than the cold envelope (which may also be due to an observational bias, that is if the observed transitions are probing warm rather than cold gas). In this respect, therefore, we think that the comparison between hot corinos and hot cores shown in Figures 4 is reliable. There is, however, more uncertainty associated with the hot cores' abundance ratios reported in Figure 5, since H_2CO emission could have an important contribution from the cold envelope.

The abundance ratios with respect to CH_3OH and H_2CO were noticed to be roughly constant for hot corinos. Regarding hot cores, the ratios seem to decrease with increasing CH_3OH or H_2CO abundance, but the data are also consistent with a constant ratio with a larger scatter. In any case, it is clear from these figures that *the abundance ratios with respect to methanol in hot cores are lower than in hot corinos* by 1–2 orders of magnitude, whereas abundance ratios with respect to formaldehyde are comparable in hot corinos and hot cores. We also notice that the HCOOH abundance ratios in hot cores are about one order of magnitude lower than the $HCOOCH_3$ and CH_3OCH_3 abundance ratios, whereas they are lower by only about a factor four in hot corinos. For completeness, we considered how Figures 4 and 5 would change if we were to use beam-averaged abundances ratios in hot corinos, as in hot cores. In this case, abundance ratios in hot corinos would be smaller by a factor $\lesssim 10$: ratios for $HCOOCH_3$ and CH_3OCH_3 would become comparable in the two types of objects, while HCOOH ratios would still be larger in hot corinos than in hot cores. This is very likely due to the relative larger contribution of methanol and formaldehyde emission in the cold envelope in low mass with respect to high mass protostars. Indeed, high energy transitions are more easily detected in high than low mass protostars (e.g. Comito et al. 2005; Schilke et al. 2001, 1997; Blake et al. 1995), which support the above interpretation.

Whether considering beam-averaged ratios in all objects or not, Figures 4 (and to a lesser extent Figure 5) show that *hot corinos are not just scaled versions of hot cores* and that in fact, complex molecules are relatively more abundant in hot corinos than in hot cores. This conclusion would still be valid if we assume CH_3OH and H_2CO abundances from Jørgensen et al. (2005b) since, as mentioned in the previous section, the abundance ratios with respect to CH_3OH and H_2CO would be similar and higher respectively, so in any case, higher than the abundance ratios in massive hot cores.

A possible explanation for the difference between hot cores and hot corinos could lie in the grain mantle composition. Indeed, we already know that the levels of deuteration differ in these two types of objects, more specifically that extreme deuteration occurs in low-mass but not in high-mass protostars (e.g. Ceccarelli et al. 2006 and references therein). Moreover, Boogert et al. (2004) summarize the abundances of some mantle constituents (H_2O, CO, CO_2, CH_3OH, OCN^-) in two low-mass and high-mass embedded protostars and there also large differences can be seen. It would therefore not be surprising that this would also be the case for complex molecules if they formed on the grain surfaces. The reason could be, for example, that hot corinos are preceded by a longer cold phase during which grain-surface reactions are at play, so that complex molecules in hot cores would not have time to become an important grain-mantle constituent.
Alternatively, the difference in abundance ratios could be due to a difference in the chemistry, since this depends on environmental parameters such as the density and temperature of the gas. For example, the model of Rodgers & Charnley (2001) shows that the predicted abundances are different at 100 or 300 K. Also, considering for example the methyl formate, the gas-grain model in the warm-up phase presented in Garrod & Herbst (2006) shows that the gas-phase formation of this molecule is more efficient at low temperatures, and that the grain-surface pathway leads to higher abundances the longer the dust temperature remains in the $40 - 60$ K range. Either way, formation of complex molecules during the warm-up stage of the protostar would be more efficient in low- than in high-mass environments. However, observations performed towards Galactic Center clouds (see section 5.5) are acting against this theory since complex molecules are observed in these clouds although they are not subject to a warm-up phase. Finally, recall that all the proposed grain-surface formation routes of complex molecules involved UV or cosmic-ray processing. Hot cores/corinos are shielded from external UV radiation fields, but low-mass protostars, unlike massive ones, are known to be powerful X-ray sources (e.g. Feigelson & Montmerle 1999). X-rays have already been proposed to be the

reason for the presence of calcite in the low-mass protostars (Chiavassa et al. 2005; Ceccarelli et al. 2002b). In our case, X-rays emitted by Class 0 objects could provide the necessary energy to produce a large number of radicals and hence a large amount of complex molecules on the grain surfaces, thereby explaining the larger abundance ratios observed in hot corinos compared to hot cores.

5.5. Comparison with Galactic Center clouds

Hot cores/corinos are not the only objects where complex molecules have been observed. Indeed, Requena-Torres et al. (2006) have carried out a survey of complex O-bearing molecules in Galactic Center (GC) clouds. These clouds are known to possess a warm (> 100 K) and not too dense ($\sim 10^4$ cm^{-3}) gas (Hüttemeister et al. 1993; Rodríguez-Fernández et al. 2000; Ceccarelli et al. 2002a). This warm component is probably caused by shocks (e.g. Flower et al. 1995; Rodríguez-Fernández et al. 2004) arising from cloud-cloud collisions (Hüttemeister et al. 1993, 1998). These shocks are thought to be at the origin of the enhanced NH_3 (Flower et al. 1995), SiO (Martín-Pintado et al. 1997) and C_2H_5OH (Martín-Pintado et al. 2001) abundances.
Surprisingly enough, considering the very different physical environments between GC clouds and hot corinos, Requena-Torres et al. (2006) found, as we do in the present work for hot corinos, that the ratios of the abundances with respect to CH_3OH (which are comparable to those reported in Figure 4 for hot cores) are approximately constant and do not depend on the CH_3OH abundance. The authors conclude that the gas-phase abundances of the organic molecules they observed in GC clouds are likely due to the formation of these molecules on the grain surfaces and their release in the gas-phase from sputtering/erosion of the grain mantles by the shocks, as it is the case for ammonia, silicon oxide and ethanol.

Note that there is evidence for the presence of X-rays in these GC clouds (Martín-Pintado et al. 2000). These authors suggest that X-rays could contribute to the formation of molecules on grain surfaces and evaporate small dust grains. This theory adds some support to the possible role played by X-rays in the formation of complex organic molecules.

6. Conclusion

In this paper, we presented the detections of methyl formate and/or methyl cyanide in the low-mass protostars IRAS4B and IRAS2A, confirming the presence of a hot corino in their inner envelope. The conclusions arising from the analysis of these observations combined with data on the two other hot corinos (IRAS16293 and IRAS4A) are:

- *Hot corinos are a common phase in the formation of solar-type protostars* and complex organic molecules are ubiquitous in Class 0 protostars.
- The absolute abundances (i.e. with respect to H_2) of complex molecules in hot corinos do not depend on the bolometric luminosity.
- Abundance ratios of complex molecules' abundances to CH_3OH or H_2CO abundances ($x/x(CH_3OH)$ and $x/x(H_2CO)$ are of order unity and do not depend on CH_3OH nor H_2CO abundances, indicating that complex molecules form on grain surfaces or that gas-phase models have to be revised.

Furthermore, we compared hot corinos with massive hot cores. Keeping in mind the different methods of abundance determination used in the two types of objects, we found that $x/x(CH_3OH)$ and $x/x(H_2CO)$ in hot cores are relatively lower than in hot corinos showing that complex molecules are relatively more important in hot corinos, a difference that can be explained in the case of grain-surface synthesis.

Overall, although there is no absolute proof, there are circumstantial evidence for the formation of complex organic molecules on grain surfaces, either in the cold phase preceding the begin of the star formation process, or in the warm-up phase following the birth of the protostar. In this scenario, there is also a possibility that X-rays emitted by low-mass protostars participate in the formation of these complex molecules.

Finally, it clearly stands out from this work that not only more data (single-dish, interferometric and high-energy transitions) are needed, but also that laboratory studies of grain-surface reactions are necessary in order to answer of the question of which, why, where and how complex molecules are formed.

Acknowledgments. We wish to thank Miguel Requena-Torres and his co-authors, as well as Robin Garrod and Eric Herbst for communicating the results of their work prior to publication (at the time of submission).
We are also very grateful to Malcom Walmsley and the anonymous referee for their careful reading of the manuscript and for suggestions that helped to improve the paper.

References

Allen, M. & Robinson, G. W. 1977, ApJ, 212, 396
André, P., Ward-Thompson, D., & Barsony, M. 2000, Protostars and Planets IV, 59
Blake, G. A., Sandell, G., van Dishoeck, E. F., et al. 1995, ApJ, 441, 689
Blake, G. A., Sutton, E. C., Masson, C. R., & Phillips, T. G. 1987, ApJ, 315, 621
Boogert, A. C. A., Pontoppidan, K. M., Lahuis, F., et al. 2004, ApJS, 154, 359
Bottinelli, S., Ceccarelli, C., Lefloch, B., & Williams, J. P. 2006, A&A, submitted
Bottinelli, S., Ceccarelli, C., Lefloch, B., et al. 2004a, ApJ, 615, 354
Bottinelli, S., Ceccarelli, C., Neri, R., et al. 2004b, ApJ, 617, L69

Caselli, P., Hasegawa, T. I., & Herbst, E. 1993, ApJ, 408, 548
Cazaux, S., Tielens, A. G. G. M., Ceccarelli, C., et al. 2003, ApJ, 593, L51
Ceccarelli, C. 2004, in ASP Conf. Ser. 323: Star Formation in the Interstellar Medium: In Honor of David Hollenbach, 195–+
Ceccarelli, C., Baluteau, J.-P., Walmsley, M., et al. 2002a, A&A, 383, 603
Ceccarelli, C., Caselli, P., Herbst, E., Tielens, A. G. M. M., & Caux, E. 2006, in Protostars and Planets V
Ceccarelli, C., Castets, A., Caux, E., et al. 2000a, A&A, 355, 1129
Ceccarelli, C., Caux, E., Tielens, A. G. G. M., et al. 2002b, A&A, 395, L29
Ceccarelli, C., Hollenbach, D. J., & Tielens, A. G. G. M. 1996, ApJ, 471, 400
Ceccarelli, C., Loinard, L., Castets, A., Faure, A., & Lefloch, B. 2000b, A&A, 362, 1122
Ceccarelli, C., Loinard, L., Castets, A., Tielens, A. G. G. M., & Caux, E. 2000c, A&A, 357, L9
Černis, K. 1990, Ap&SS, 166, 315
Chandler, C. J., Brogan, C. L., Shirley, Y. L., & Loinard, L. 2005, ApJ, 632, 371
Charnley, S. B. & Rodgers, S. D. 2005, in IAU Symposium, 262–+
Charnley, S. B., Tielens, A. G. G. M., & Millar, T. J. 1992, ApJ, 399, L71
Charnley, S. B., Tielens, A. G. G. M., & Rodgers, S. D. 1997, ApJ, 482, L203+
Chiavassa, A., Ceccarelli, C., Tielens, A. G. G. M., Caux, E., & Maret, S. 2005, A&A, 432, 547
Combes, F., Q-Rieu, N., & Wlodarczak, G. 1996, A&A, 308, 618
Comito, C., Schilke, P., Phillips, T. G., et al. 2005, ApJS, 156, 127
Ehrenfreund, P. & Charnley, S. B. 2000, ARA&A, 38, 427
Feigelson, E. D. & Montmerle, T. 1999, ARA&A, 37, 363
Flower, D. R., Pineau des Forets, G., & Walmsley, C. M. 1995, A&A, 294, 815
Garrod, R. T. & Herbst, E. 2006, A&A, submitted
Gibb, E., Nummelin, A., Irvine, W. M., Whittet, D. C. B., & Bergman, P. 2000a, ApJ, 545, 309
Gibb, E. L., Whittet, D. C. B., Schutte, W. A., et al. 2000b, ApJ, 536, 347
Hasegawa, T. I. & Herbst, E. 1993, MNRAS, 261, 83
Herbst, E. 2005, J. Phys. Chem. A, 109, 4017
Horn, A., Møllendal, H., Sekiguchi, O., et al. 2004, ApJ, 611, 605
Hudson, R. L. & Moore, M. H. 1999, Icarus, 140, 451
Hüttemeister, S., Dahmen, G., Mauersberger, R., et al. 1998, A&A, 334, 646
Hüttemeister, S., Wilson, T. L., Bania, T. M., & Martín-Pintado, J. 1993, A&A, 280, 255
Ikeda, M., Ohishi, M., Nummelin, A., et al. 2001, ApJ, 560, 792
Irvine, W. M., Friberg, P., Kaifu, N., et al. 1990, A&A, 229, L9
Jørgensen, J. K., Bourke, T. L., Myers, P. C., et al. 2005a, ApJ, 632, 973
Jørgensen, J. K., Schöier, F. L., & van Dishoeck, E. F. 2002, A&A, 389, 908
Jørgensen, J. K., Schöier, F. L., & van Dishoeck, E. F. 2005b, A&A, 437, 501
Keane, J. V., Tielens, A. G. G. M., Boogert, A. C. A., Schutte, W. A., & Whittet, D. C. B. 2001, A&A, 376, 254
Knee, L. B. G. & Sandell, G. 2000, A&A, 361, 671
Knez, C., Boogert, A. C. A., Pontoppidan, K. M., et al. 2005, ApJ, 635, L145
Kuan, Y.-J., Huang, H.-C., Charnley, S. B., et al. 2004, ApJ, 616, L27
Lefloch, B., Castets, A., Cernicharo, J., & Loinard, L. 1998, ApJ, 504, L109+
Leung, C. M., Herbst, E., & Huebner, W. F. 1984, ApJS, 56, 231
Liu, S.-Y., Mehringer, D. M., & Snyder, L. E. 2001, ApJ, 552, 654
Liu, S.-Y. & Snyder, L. E. 1999, ApJ, 523, 683
Looney, L. W., Mundy, L. G., & Welch, W. J. 2000, ApJ, 529, 477
Lovas, F. J. & Dragoset, R. A. 2004, NIST Recommended Rest Frequencies for Observed Interstellar Molecular Microwave Transitions - 2002 Revision
Maret, S., Ceccarelli, C., Caux, E., et al. 2004, A&A, 416, 577
Maret, S., Ceccarelli, C., Tielens, A. G. G. M., et al. 2005, A&A, 442, 527
Martín-Pintado, J., de Vicente, P., Fuente, A., & Planesas, P. 1997, ApJ, 482, L45+
Martín-Pintado, J., de Vicente, P., Rodríguez-Fernández, N. J., Fuente, A., & Planesas, P. 2000, A&A, 356, L5
Martín-Pintado, J., Rizzo, J. R., de Vicente, P., Rodríguez-Fernández, N. J., & Fuente, A. 2001, ApJ, 548, L65
Müller, H. S. P., Schlöder, F., Stutzki, J., et al. 2005, in IAU Symposium, 30–+
Müller, H. S. P., Thorwirth, S., Roth, D. A., & Winnewisser, G. 2001, A&A, 370, L49
Nummelin, A., Bergman, P., Hjalmarson, Å., et al. 2000, ApJS, 128, 213
Peeters, Z., Rodgers, S. D., Charnley, S. B., et al. 2006, A&A, 445, 197
Pickett, H. M., Poynter, R. L., Cohen, E. A., et al. 1998, J. Quant. Spec. Radiat. Transf., 60, 883
Reipurth, B., Rodríguez, L. F., Anglada, G., & Bally, J. 2002, AJ, 124, 1045
Remijan, A. & Hollis, J. M. 2006, ApJ, in press
Requena-Torres, M. A., Martín-Pintado, J., Rodríguez-Franco, A., et al. 2006, A&A, in press
Rodgers, S. D. & Charnley, S. B. 2001, ApJ, 546, 324
Rodgers, S. D. & Charnley, S. B. 2003, ApJ, 585, 355
Rodríguez-Fernández, N. J., Martín-Pintado, J., de Vicente, P., et al. 2000, A&A, 356, 695
Rodríguez-Fernández, N. J., Martín-Pintado, J., Fuente, A., & Wilson, T. L. 2004, A&A, 427, 217
Rowe, B. R., Dupeyrat, G., Marquette, J. B., et al. 1984, J. Chem. Phys., 80, 241
Sakai, N., Sakai, T., & Yamamoto, S. 2006, PASJ, 58, L15
Sandell, G., Knee, L. B. G., Aspin, C., Robson, I. E., & Russell, A. P. G. 1994, A&A, 285, L1

Schilke, P., Benford, D. J., Hunter, T. R., Lis, D. C., & Phillips, T. G. 2001, ApJS, 132, 281
Schilke, P., Groesbeck, T. D., Blake, G. A., & Phillips, T. G. 1997, ApJS, 108, 301
Schöier, F. L., Jørgensen, J. K., van Dishoeck, E. F., & Blake, G. A. 2002, A&A, 390, 1001
Schutte, W. A., Boogert, A. C. A., Tielens, A. G. G. M., et al. 1999, A&A, 343, 966
Sorrell, W. H. 2001, ApJ, 555, L129
Stäuber, P., Doty, S. D., van Dishoeck, E. F., & Benz, A. O. 2005, A&A, 440, 949
Tielens, A. G. G. M. & Hagen, W. 1982, A&A, 114, 245
Viti, S., Collings, M. P., Dever, J. W., McCoustra, M. R. S., & Williams, D. A. 2004, MNRAS, 354, 1141
Ward-Thompson, D., André, P., Crutcher, R., et al. 2006, in Protostars and Planets V
White, R. J., Greene, T. P., Doppmann, G. W., Covey, K. R., & Hillenbrand, L. A. 2006, in Protostars and Planets V

Appendix A: Theories of complex molecules formation

In this Appendix, we review the different reactions that have been proposed for the formation of complex species. These reactions can occur in the gas-phase or on grain surfaces. Gas-phase reactions usually involve H_2CO or CH_3OH as precursors, or parents. These are known to form on grain surfaces (e.g. Tielens & Hagen 1982; Charnley et al. 1997) and evaporate in the gas-phase where they undergo further reaction to form more complex, or daughter, molecules. Grain-surface reactions generally consist in H or O additions and radical-radical reactions.

A.1. Formic acid

Both gas-phase and grain-surface processes have been proposed for the formation of HCOOH. In the gas-phase model of Leung et al. (1984), the precursor ion of HCOOH, $HCOOH_2^+$, is produced via the radiative association

$$H_2O + HCO^+ \rightarrow HCOOH_2^+ + h\nu \quad (A.1)$$

followed by dissociative electron recombination to produce HCOOH. But Irvine et al. (1990) mention that this reaction is believed not to occur due to a competitive exothermic reaction to form H_3O^+ and CO. Instead, they attribute the gas-phase formation of HCOOH via an ion-molecule reaction followed again by a dissociative electron recombination

$$CH_4 + O_2^+ \rightarrow HCOOH_2^+ + H \quad (A.2)$$
$$HCOOH_2^+ + e^- \rightarrow HCOOH + H \quad (A.3)$$

Reaction (A.2) has been measured in the laboratory and found to be quite rapid at low temperature (Rowe et al. 1984). Moreover, the calculated HCOOH abundance agrees with the values observed by Irvine et al. (1990) in the dark cloud L134 N.

On grain surfaces, Tielens & Hagen (1982) proposed the formation of HCOOH through successive additions of H, O, and H to solid-state CO:

$$CO \xrightarrow{+H} HCO \xrightarrow{+O} HCOO \xrightarrow{+H} HCOOH \quad (A.4)$$

However, radiolysis experiments (simulating the processing of interstellar ices by cosmic rays) by Hudson & Moore (1999) showed that HCOOH could form in H_2O–CO mixed ices via the following sequence:

$$H + CO \rightarrow HCO \quad (A.5)$$
$$HCO + OH \rightarrow HCOOH \quad (A.6)$$

The models of Hasegawa & Herbst (1993) are able to reproduce the abundances observed in massive hot cores for ages larger than $10^5 - 10^6$ yr. Finally, the grain-surface formation of HCOOH is supported by the interferometric observations of Sgr B2 and W51 by Liu et al. (2001), and would also be consistent with observations of this molecule in the ices surrounding the massive protostar W33A (Schutte et al. 1999; Gibb et al. 2000b).

A.2. Methyl formate

The commonly accepted formation path for $HCOOCH_3$ starts with the reaction between protonated methanol and formaldehyde to form protonated methyl formate and molecular hydrogen:

$$[CH_3OH_2]^+ + H_2CO \rightarrow [HC(OH)OCH_3]^+ + H_2 \quad (A.7)$$

followed by dissociative recombination of $[HC(OH)OCH_3]^+$ with electrons to form $HCOOCH_3$ (Blake et al. 1987). However, laboratory and theoretical work by Horn et al. (2004) indicates the existence of a very large activation energy for reaction (A.7), so that the later cannot lead to the formation of protonated methyl formate. Therefore, the formation of methyl formate in hot cores cannot occur via this reaction. Horn et al. searched for more favorable transitions between the reactants and products of reaction (A.7), but were unsuccessful. These authors also investigated reactions involving other abundant species in hot cores, such as protonated formaldehyde and CO. They show that none of the studied processes produces enough methyl formate to explain the observed abundances. However, they also state that one possibility for producing more methyl formate is that formic acid would be synthesized on grain surfaces and desorbed into the gas phase, in which case the reaction:

$$CH_3^+ + HCOOH \rightarrow HC(OH)OCH_3^+ + h\nu \quad (A.8)$$

would play a significant role.
The downfall is that Horn et al. (2004) find that even if HCOOH is injected with an abundance one order of magnitude higher than observed in OMC-1, their model still predicts a $HCOOCH_3$ abundance between one and two orders of magnitude below the observed value in this source. Overall, in the light of their work, Horn et al. conclude that no gas-phase route seem able to reproduce the observed abundances of

$HCOOCH_3$, and hence that this molecule should be produced, at least in part, on grain surfaces. As pointed out in section A.1, there is additional evidence in favor of HCOOH being synthesized on grain surfaces.

Two schemes for grain-surface formation of $HCOOCH_3$ have been proposed, but none of them has undergone laboratory investigation yet:

- Formation from precursors CO, O, C, and H landing on grain (Herbst 2005):

$$CO + H \rightarrow HCO \quad (A.9)$$

$$C \xrightarrow{+H} CH \xrightarrow{+H} CH_2 \xrightarrow{+H} CH_3 \xrightarrow{+O} CH_3O \quad (A.10)$$

$$CH_3O + HCO \rightarrow HCOOCH_3 \quad (A.11)$$

  Charnley & Rodgers (2005) mention that many radicals (like CH_3O and HCO) could form in close proximity via the hot secondary electron generated by the passage of a cosmic ray through the ice. In this case, it would ensue that radical-radical reactions such as (A.11) could occur efficiently.
- Sorrell (2001) proposed a model in which the photoprocessing of grain mantles by UV starlight creates a high concentration of radicals in the bulk interior of mantles. Grain-grain collisions then provide excess heat causing radical-radical reactions to occur and form large organic molecules. In this scheme, $HCOOCH_3$ would be produced from the reaction between the carboxyl acid (COOH) and the methyl group (CH_3) in the following way:

$$CO + OH \rightarrow COOH \text{ or } HCO + HCO \rightarrow COOH + O \quad (A.12)$$

$$CH \xrightarrow{+H} CH_2 \xrightarrow{+H} CH_3 \quad (A.13)$$

$$COOH + CH_3 \rightarrow HCOOCH_3. \quad (A.14)$$

  However, any grain-surface chemistry preceding the hot core/corino phase would occur in a very dense and highly visually extinct environment, hence well shielded from UV starlight. Therefore, such a UV photolysis of grains is unlikely to happen, as pointed out by Peeters et al. (2006). Nevertheless, the radical-radical reaction (A.14) could still be a possible formation path for $HCOOCH_3$ via cosmic ray processing.

A.3. Dimethyl ether

CH_3OCH_3 was proposed by Blake et al. (1987) to form in the gas-phase by methyl cation transfer to methanol, followed by electron dissociative recombination:

$$CH_3OH_2^+ + CH_3OH \rightarrow CH_3OCH_4^+ + H_2O \quad (A.15)$$

$$CH_3OCH_4^+ + e^- \rightarrow CH_3OCH_3 + H \quad (A.16)$$

Peeters et al. (2006) claim that their models support such a gas-phase route if the methanol abundance is of the order 10^{-6} or more, as it is the case for the OMC-1 hot core (recall that for hot corinos, $X(CH_3OH) \leq 3 \times 10^{-7}$). However, Ceccarelli et al. (2006) note that experimental measurements of the neutral products of dissociative recombination reactions show that two-body products such as in reaction (A.16) are often minor channels. Therefore, gas-phase formation of CH_3OCH_3 is plausible but not demonstrated.

On the grains, CH_3OCH_3 could be produced by a similar scheme as for $HCOOCH_3$, that is cosmic ray processing followed by the radical-radical reaction $CH_3 + CH_3O \rightarrow CH_3OCH_3$ (Allen & Robinson 1977). As in the case of $HCOOCH_3$, this reaction has not been validated by laboratory studies.

A.4. Methyl and ethyl cyanide

For completeness, we mention here the possible formation routes of these two molecules. However, we will not discuss them any further in this study, due to the lack of data on potential parents such as NH_3.

Two substantially different formation routes for CH_3CN have been proposed in the literature: either in the gas-phase or on grain surfaces.

- In the Rodgers & Charnley (2001) chemical model of massive hot cores, CH_3CN is synthesized from NH_3 in the following way: HCN is synthesized from the reaction between NH_3 and C^+ (yielding $HCNH^+$, reaction (A.17)), followed by electron recombination or proton transfer to ammonia (A.18). CH_3CN is then formed from the radiative association between the methyl ion and HCN (A.19), again followed by electron recombination (A.20):

$$NH_3 + C^+ \rightarrow HCNH^+ \quad (A.17)$$

$$HCNH^+ + e^- \rightarrow HCN + H \text{ or } HCNH^+ \rightarrow HCN + H^+ \quad (A.18)$$

$$CH_3^+ + HCN \rightarrow CH_3CNH^+ + h\nu \quad (A.19)$$

$$CH_3CNH^+ + e^- \rightarrow CH_3CN + H \quad (A.20)$$

  Comparisons between the results from this model and observations suggest that a grain-surface formation of CH_3CN is not required.

- On grain surfaces, CH_3CN can be formed by successive hydrogenation of C_2N or by recombination between CN and CH_3:
  - $C_2N \xrightarrow{+H} HCCN \xrightarrow{+H} CH_2CN \xrightarrow{+H} CH_3CN$. This set of reactions, used in Caselli et al. (1993), underestimates the CH_3CN abundance by a factor about 50 compared to the abundance observed in the Orion hot core. This could be explained by the fact that HCCN formation is in competition with C_3N formation and the former is indicated by the authors as a less important pathway.
  - $CN + CH_3 \rightarrow CH_3CN$ (Hasegawa & Herbst 1993), which yield a CH_3CN abundance in good agreement with the Orion hot core value for an age of 10^5 yr.

Regarding C_2H_5CN, some studies point towards grain-surface formation of this molecule by hydrogenation of HC_3N (Blake et al. 1987; Charnley et al. 1992; Caselli et al. 1993).

Observations by Liu & Snyder (1999) are consistent with this theory. However, the abundance ratio of CH_3CN to C_2H_5CN predicted by Caselli et al. (1993) is at least two orders of magnitude smaller than the ratio observed in hot cores and hot corinos. Therefore, it seems unlikely that both CH_3CN and C_2H_5CN form via the surface reactions proposed by Caselli et al. (1993).

A.5. Timescales for gas-phase processes

For the molecules for which no strong argument has been proposed against gas-phase formation, e.g. CH_3OCH_3, we can estimate a formation timescale from the slowest rate coefficient of the reactions involved. In general, for a reaction between reactants r_1 and r_2 yielding a product p, we have:

$$\frac{dn_p}{dt} = k_f\, n_{r_1}\, n_{r_2} \quad \text{(A.21)}$$

where k_f is the reaction rate coefficient in $cm^3\ s^{-1}$. In the event that $n_{r_1} >> n_{r_2}$ (which is the case for CH_3OCH_3, as we will see further down), we also have $n_{r_1} + n_p \sim n_{\rm tot}$, where $n_{\rm tot}$ is defined as $n_{r_1} + n_{r_2} + n_p$. Then,

$$\frac{dn_p}{dt} = k_f\,(n_{\rm tot} - n_p)\, n_{r_2} \quad \text{(A.22)}$$

$$= -k_f\, n_{r_2}\, n_p + k_f\, n_{\rm tot}\, n_{r_2} \quad \text{(A.23)}$$

$$= -\frac{1}{\tau_f}\, n_p + k_f\, n_{\rm tot}\, n_{r_2} \quad \text{(A.24)}$$

which has solution of the form $n_p(t) = C_1\ \exp[-t/\tau_f] + C_2$, where C_1 and C_2 are constants. The formation timescale is

$$\tau_f = (k_f\, n_{r_2})^{-1} \quad \text{(A.25)}$$

$$= (k_f\, n_{\rm H_2}\, x_{r_2})^{-1} \quad \text{(A.26)}$$

$$= \left(\frac{k_f}{10^{-10}}\right)^{-1} \left(\frac{n_{\rm H_2}}{10^8}\right)^{-1} \left(\frac{x_{r_2}}{10^{-10}}\right)^{-1} 3\times10^4\ \text{yr} \quad \text{(A.27)}$$

where $n_{\rm H_2}$ is the H_2 density in cm^{-3} and x_{r_2} is the abundance of r_2, the least abundant reactant.

For CH_3OCH_3, the slowest reaction is (A.15), which has a reaction rate of $1\times10^{-10}\ cm^3\ s^{-1}$ (from the gas-phase chemical network osu.2005[3]), and (predicted) $x_{r_2} = x_{CH_3OH_2^+} \sim (1-5)\times 10^{-10}$ (from Rodgers & Charnley 2003), which is much smaller than $x_{r_1} = x_{CH_3OCH_3} \gtrsim 1\times10^{-8}$ (from Table 5), hence justifying the derivation and use of Equation A.27. For our sources, $n_{\rm H_2} \sim 10^8 - 10^9\ cm^{-3}$, which yields $\tau_f = 6\times10^2 - 3\times10^4$ yr. Regarding the destruction of the studied species in the gas-phase, we expect ions such as H_3O^+, HCO^+ and H_3^+ to be the main destroyers of complex organic molecules during the hot corino phase, with H_3O^+ being the most important of the three due to the evaporation of water contained in the icy grain mantles (Ceccarelli et al. 1996; Rodgers & Charnley 2003). In this case, we have:

$$\frac{dn_p}{dt} = -k_d\, n_p\, n_{\rm H_3O^+} \quad \text{(A.28)}$$

$$= -\frac{1}{\tau_d}\, n_p \quad \text{(A.29)}$$

$$\Rightarrow n_p(t) = C_3\ \exp(-t/\tau_d) \quad \text{(A.30)}$$

where k_d is the destruction rate, τ_d is the destruction timescale and C_3 is a constant. Then,

$$\tau_d = (k_d\, n_{\rm H_3O^+})^{-1} \quad \text{(A.31)}$$

$$= (k_d\, n_{\rm H_2}\, x_{\rm H_3O^+})^{-1} \quad \text{(A.32)}$$

$$= \left(\frac{k_d}{10^{-10}}\right)^{-1} \left(\frac{n_{\rm H_2}}{10^8}\right)^{-1} \left(\frac{x_{\rm H_3O^+}}{10^{-10}}\right)^{-1} 3\times10^4\ \text{yr} \quad \text{(A.33)}$$

Destruction of CH_3OCH_3 by H_3O^+ has $k_d = 10^{-9}\ cm^3\ s^{-1}$ (osu.2005) and $x_{\rm H_3O^+} = 7\times10^{-11} - 5\times10^{-9}$ (from Ceccarelli et al. 1996 for the lowest value, and Rodgers & Charnley 2003 and Stäuber et al. 2005 for highest value), which yields $\tau_d = 6-4\times10^3$ yr. This is comparable to the mid-range of the formation scale. Moreover, as the protostar ages, its luminosity increases, causing the expansion of the evaporation front and the replenishment of the complex molecules, whether they are mantle species or whether they form from freshly evaporated CH_3OH and/or H_2CO. Therefore, the destruction by H_3O^+ is likely compensated by the evaporation or formation of more complex molecules.

[3] http://www.physics.ohio-state.edu/~eric/research.html

The Astrophysical Journal, 617:L69–L72, 2004 December 10

NEAR-ARCSECOND RESOLUTION OBSERVATIONS OF THE HOT CORINO OF THE SOLAR-TYPE PROTOSTAR IRAS 16293−2422[1]

S. Bottinelli,[2,3] C. Ceccarelli,[2] R. Neri,[4] J. P. Williams,[3] E. Caux,[5] S. Cazaux,[6]
B. Lefloch,[2] S. Maret,[2] and A. G. G. M. Tielens[7]
Received 2004 September 11; accepted 2004 October 25; published 2004 November 5

ABSTRACT

Complex organic molecules have previously been discovered in solar-type protostars, raising the questions of where and how they form in the envelope. Possible formation mechanisms include grain mantle evaporation, the interaction of the outflow with its surroundings, and/or the impact of UV/X-rays inside the cavities. In this Letter we present the first interferometric observations of two complex molecules, CH_3CN and $HCOOCH_3$, toward the solar-type protostar IRAS 16293−2422. The images show that the emission originates from two compact regions centered on the two components of the binary system. We discuss how these results favor the grain mantle evaporation scenario, and we investigate the implications of these observations for the chemical composition and physical and dynamical state of the two components.

Subject headings: ISM: abundances — ISM: individual (IRAS 16293−2422) — ISM: molecules — stars: formation

1. INTRODUCTION

Solar-type Class 0 protostars are characterized by being observable only at millimeter to far-infrared wavelengths. This is because the central forming stars are surrounded and obscured by massive envelopes, making them the coldest known protostars. Yet, the cold envelopes hide inner warm regions where the grain mantles, built during the precollapse phase, evaporate. Following gas-phase reactions between the evaporated mantle molecules (also called first-generation molecules), organic complex molecules (second-generation molecules) form in these regions. While this picture has now been widely accepted for massive protostars (see, e.g., Kurtz et al. 2000 and van Dishoeck & Blake 1998), it is only recently that evidence in support of parts of this scenario have been accumulated for low-mass protostars. Actually, so far the existence of inner warm regions with evaporated mantles in solar-type protostars has been argued indirectly from the sophisticated analysis of molecular multifrequency single-dish observations (Ceccarelli et al. 2000a, 2000b; Schöier et al. 2002; Maret et al. 2002, 2004; Doty et al. 2004). A survey on almost a dozen Class 0 sources has shown that, typically, the inner warm regions have sizes of a few tens of AU (Maret et al. 2004), i.e., the size of the solar nebula. Now that the existence of these regions has been demonstrated, the questions concerning their nature and chemical composition have become relevant because of the link to the formation of our own solar system. What is the inventory of organic molecules of such regions? What are their origin and evolution? In particular, could these molecules be incorporated into the planet-forming disks surrounding the protostars?

Based on theoretical arguments, no complex, second-generation molecules should have the time to form in solar-type protostars. The reason is that the gas crossing time of the warm regions is estimated to be much shorter ($\lesssim 10^3$ yr) than the predicted chemical formation time ($\gtrsim 10^4$ yr; Schöier et al. 2002). But our theories have some flaws, since complex organic molecules have been detected in the two (out of two) sources where they have been searched for: IRAS 16293−2422 (Cazaux et al. 2003) and NGC 1333 IRAS 4A (Bottinelli et al. 2004). We therefore may even doubt the basic prediction that those molecules originate in the warm inner regions of the envelopes! It is, for example, possible that the process that is responsible for the release in the gas phase of the mantle constituents is not the thermal evaporation but the interaction of the outflow with the surroundings, or even the interaction of UV/X-rays with the cavities excavated by the outflow (Schöier et al. 2002, 2004). Alternatively, the emission could come from disk surfaces that would have been heated by accretion shocks (Schöier et al. 2004). The proof that the complex organic molecules detected by Cazaux et al. (2003) and Bottinelli et al. (2004) originate from the inner warm regions (envelope or disk), called hot corinos (Ceccarelli 2004; Bottinelli et al. 2004), was still missing until today.

In this Letter we bring the missing proof and report interferometric observations of two complex, second-generation molecules, methyl cyanide and methyl formate, toward the prototype of the hot corinos, IRAS 16293−2422 (hereafter IRAS 16293).

2. OBSERVATIONS AND RESULTS

Observations of IRAS 16293 [$\alpha(2000) = 16^h32^m22\overset{s}{.}6$, $\delta(2000) = -24°28'33''$] were carried out at the IRAM Plateau de Bure Interferometer on 2004 February 1 and March 25 in the B and C configurations of the array. Five CH_3CN transitions at 110.4 GHz and four $HCOOCH_3$ transitions at 226.4 GHz were obtained simultaneously, along with the continuum emission at 3 and 1.3 mm. The receivers were tuned single sideband at 3 mm and double sideband (DSB) at 1.3 mm. The CH_3CN and $HCOOCH_3$ transitions were covered with two correlator units, each of 40 and 80 MHz bandwidth, respectively. Typical system temperatures were 250 K (upper sideband) at 3 mm

[1] Based on observations carried out with the IRAM Plateau de Bure Interferometer. IRAM is supported by INSU/CNRS (France), MPG (Germany), and IGN (Spain).
[2] Laboratoire d'Astrophysique de l'Observatoire de Grenoble, BP 53, 38041 Grenoble, Cedex 9, France; sbottine@obs.ujf-grenoble.fr, ceccarel@obs.ujf-grenoble.fr, lefloch@obs.ujf-grenoble.fr, maret@obs.ujf-grenoble.fr.
[3] Institute for Astronomy, University of Hawaii, 2680 Woodlawn Drive, Honolulu, HI 96822; jpw@ifa.hawaii.edu.
[4] Institut de Radioastronomie Millimétrique (IRAM), 300 rue de la Piscine, 38406 Saint Martin d'Hères, France; neri@iram.fr.
[5] Centre d'Etude Spatiale des Rayonnements, CNRS-UPS, 9 Avenue du Colonel Roche, BP 4346, 31028 Toulouse, Cedex 4, France; caux@cesr.fr.
[6] INAF, Osservatorio Astrofisico di Arcetri, Largo Enrico Fermi, 5 I-50125 Florence, Italy; cazaux@arcetri.astro.it.
[7] Kapteyn Astronomical Institute, P.O. Box 800, 9700 AV Groningen, Netherlands; tielens@astro.rug.nl.

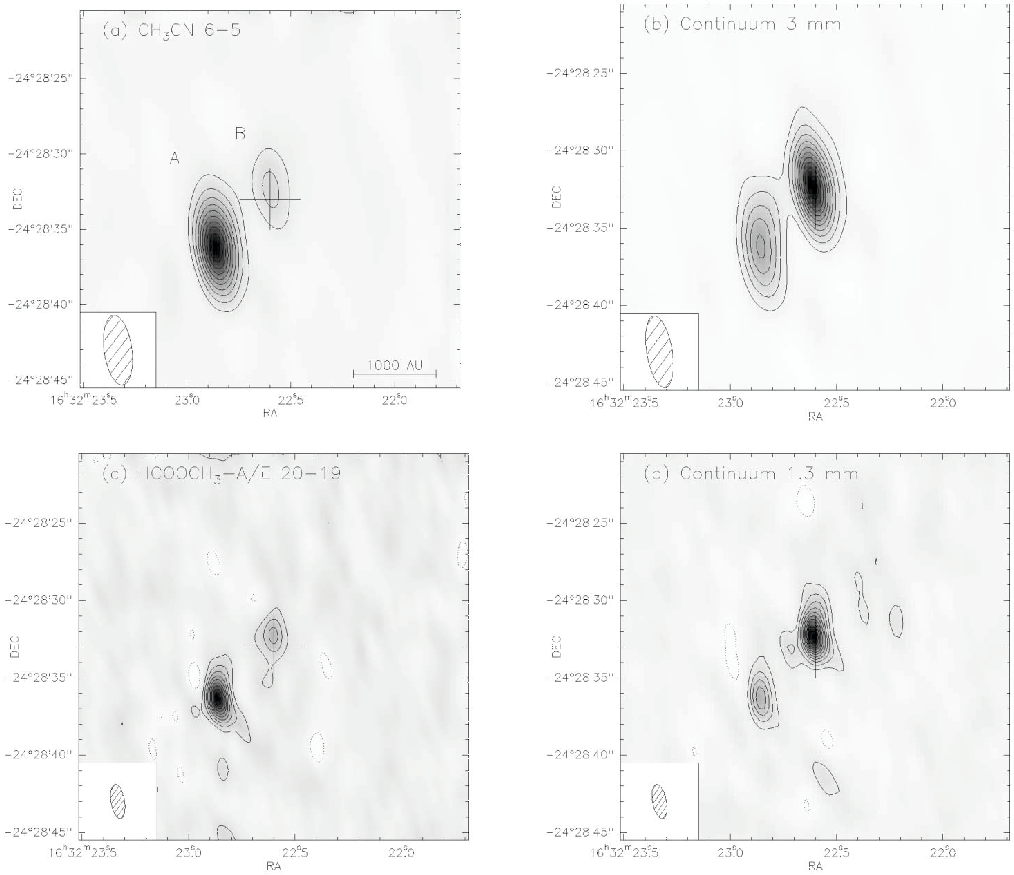

FIG. 1.—(*a*) Line map of CH_3CN, averaged over the five transitions listed in Table 1; the rms is 3 mJy beam^{-1}, and contours range from 15 to 150 mJy beam^{-1} in steps of 15 mJy beam^{-1}. (*b*) Continuum emission at 3 mm, with an rms of 3 mJy beam^{-1}; contour levels range from 20 to 220 mJy beam^{-1} in steps of 20 mJy beam^{-1}. (*c*) Line map of $HCOOCH_3$-*A* and -*E*, averaged over the four transitions listed in Table 1; the rms is 8 mJy beam^{-1}, and contour levels range from 20 to 200 mJy beam^{-1} in steps of 20 mJy beam^{-1}. (*d*) Continuum emission at 1.3 mm, with an rms of 15 mJy beam^{-1}; contour levels range from 50 to 600 mJy beam^{-1} in steps of 50 mJy beam^{-1}. Beam sizes are $4''.7 \times 1''.6$ and $2''.2 \times 0''.9$ at 3 and 1.3 mm, respectively. The cross indicates the pointing position (§ 2).

and 500 K (DSB) at 1.3 mm. Phase and amplitude calibrations were obtained by observing the nearby point sources 1514−241 and NRAO 530 every 20 minutes. The bandpass calibration was carried out on 3C 273 and 0851+202, and the absolute flux density scale was derived from MWC 349, 3C 345, and 0923+392. The data calibration was performed in the antenna-based manner, and uncertainties are less than 10% at 3 mm and less than 20% at 1.3 mm. Flux densities were obtained from visibilities using standard IRAM procedures. Continuum images were produced by averaging line-free channels. Line maps were obtained by cleaning line images after subtracting the continuum directly from the visibilities.

Figures 1*a* and 1*c* show the integrated line emission of CH_3CN and $HCOOCH_3$, averaged over all the transitions listed in Table 1 for each molecule. Note that the energy of the upper level of the CH_3CN transitions decreases with frequency but that maps averaged over each individual transition do not show any significant difference. This means that the emitting region does not depend on the energy of the transition, i.e., on the excitation conditions (but rather on a jump of the molecular abundances). Continuum emission at 3 and 1.3 mm is displayed in Figures 1*b* and 1*d*, respectively. These maps show two components that are spatially coincident with the centimeter-wavelength emission regions A and B mapped by Wootten (1989) and with the millimeter-wavelength emission regions MM1 and MM2 mapped by Mundy et al. (1990, 1992). As already noted in the previously mentioned works (see also Looney et al. 2000 and Schöier et al. 2004), the southeast region ("source A" or "MM1") is the weakest in the continuum but is the brightest in line emission. On the contrary, the northwest region ("source B" or "MM2") is the brightest in the continuum and weakest in line emission. Table 1 gives the intensities and sizes of the line and continuum emissions. Within

TABLE 1
LINE AND CONTINUUM EMISSION

MOLECULE	TRANSITION	E_{up}[a] (cm^{-1})	FREQUENCY (GHz) OR WAVELENGTH	(INTEGRATED) INTENSITY A	(INTEGRATED) INTENSITY B	SIZE[b] (arcsec) A	SIZE[b] (arcsec) B	ΔR.A., ΔDECL.[c] (arcsec) A	ΔR.A., ΔDECL.[c] (arcsec) B
CH_3CN	$6_{5,0}$–$5_{5,0}$	137.1	110.330	1.39(0.09)	0.51(0.06)	0.8(0.2)	<0.8	3.6, −3.3	−0.0, 1.1
	$6_{4,0}$–$5_{4,0}$	92.4	110.350	1.70(0.08)	0.38(0.06)	0.8(0.2)	<0.8	3.7, −3.2	−0.1, 0.7
	$6_{3,0}$–$5_{3,0}$	57.6	110.364	2.75(0.08)	0.67(0.05)	0.9(0.1)	<0.8	3.7, −3.2	+0.1,0.6
	$6_{2,0}$–$5_{2,0}$	32.8	110.375	2.56(0.08)	0.51(0.05)	1.2(0.1)	<0.8	3.6, −3.3	+0.1, 0.9
	$6_{1/0,0}$–$5_{1/0,0}$	17.9/12.9	110.381/110.383	5.26(0.10)	1.05(0.07)	0.9(0.1)	<0.8	3.6, −3.3	−0.0, 0.6
$HCOOCH_3$-*E*/*A*	$20_{2,19}$–$19_{2,18}$	83.5	226.713/226.718	6.44(0.41)	3.36(0.36)	1.4(0.2) × 0.7(0.1)	0.8(0.2)	3.6, −3.5	−0.1, 0.7
	$20_{1,19}$–$19_{1,18}$	83.5	226.773/226.778	11.13(0.49)	4.05(0.39)	1.6(0.1) × 0.8(0.1)	0.8(0.1)	3.7, −3.3	−0.0, 0.7
Continuum			3 mm	0.17	0.26	3.4 × 1.4	1.5 × 0.8	3.5, −2.9	+0.2, 0.7
			1.3 mm	0.77	1.02	3.7 × 1.2	1.5 × 0.8	3.5, −3.3	+0.2, 0.6

NOTE.—The line intensity is in units of Jy km s^{-1}, while the continuum is in Jy. Errors are given in parentheses.
[a] Energy of the upper level of the transition.
[b] FWHM of Gaussian fit.
[c] Relative peak position from the fit.

the errors, we recover all the line emission measured by the IRAM 30 m telescope (Cazaux et al. 2003).

Finally, the spectra at 1.3 mm of emission regions A and B are shown in Figure 2, assuming $V_{LSR} = 3.9$ (Fig. 2*a*) and 2.7 km s^{-1} (Fig. 2*b*), respectively (see discussion in the next section). Again, note that the sum of A and B (Fig. 2*c*) reproduces very well the features in the spectrum obtained at the IRAM 30 m telescope (Cazaux et al. 2003).

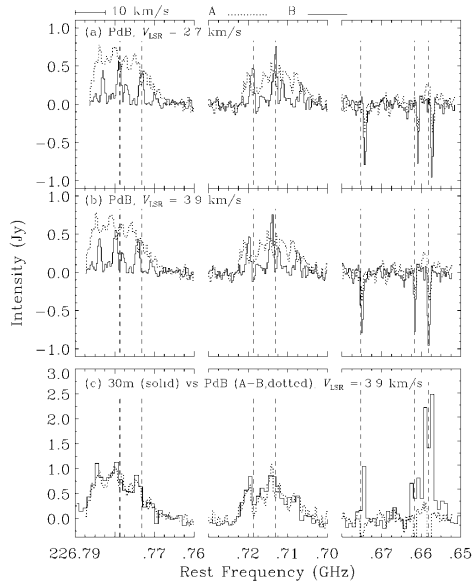

FIG. 2.—(*a*) Spectra at 1 mm averaged over the emission regions of sources A (*dotted line*) and B (*solid line*) and displayed for $V_{LSR} = 2.7$ km s^{-1}. The velocity resolution is 0.4 km s^{-1}, and the rms is 0.08 Jy for A and 0.06 Jy for B. (*b*) Same as (*a*), but with $V_{LSR} = 3.9$ km s^{-1}. (*c*) The solid line represents the spectrum obtained at the IRAM 30 m telescope (Cazaux et al. 2003) with a velocity resolution of 1.3 km s^{-1} and an rms of 0.11 Jy. Overlayed in dotted line is the sum of the Plateau de Bure (PdB) spectra of sources A and B (rms = 0.10 Jy). Vertical lines indicate the frequencies of $HCOOCH_3$ (*A* and *E*) lines (emission) and CN lines (absorption). *Right to left*: CN $2_{3/2,5/2}$–$1_{1/2,3/2}$, $2_{3/2,1/2}$–$1_{1/2,1/2}$, $2_{3/2,3/2}$–$1_{1/2,1/2}$, $HCOOCH_3$-*E* and -*A* $20_{2,19}$–$19_{2,18}$, $HCOOCH_3$-*E* and -*A* $20_{1,19}$–$19_{1,18}$.

3. DISCUSSION AND CONCLUSIONS

The most important result of the presented observations is that the complex molecules observed by Cazaux et al. (2003) originate in two compact regions, whose diameters are about 1.″5 (A) or less (B), as shown in Figure 1 (and Table 1). This goes along with the fact that the images do not show any evidence of emission associated with the molecular outflows seen at larger scales (see below for the discussion on the line profiles). Also, following the remark in § 1, the Plateau de Bure images do not reveal any evidence of emission from cavities excavated from the outflows either. Indeed, the cavities are typically ~20″ in size, located ~30″ away from the source along the ^{12}CO outflow (see, e.g., Arce & Sargent 2004), which would have been easily detected by the Plateau de Bure. The two regions where the molecular emission comes from are compact, and while source A is barely resolved in the 1 mm images,[8] source B is unresolved. The measured sizes (1.″5 at 160 pc corresponds to a radius of about 120 AU) are remarkably consistent with the emission coming from a region where the dust temperature exceeds 100 K in source A (150–200 AU, based on multifrequency single-dish observations; Ceccarelli et al. 2000a, 2000b; Schöier et al. 2002) and therefore, where the grain mantles evaporate. Thus, these observations support the basic prediction (from the modeling of the single-dish observations; Ceccarelli et al. 2000a, 2000b; Cazaux et al. 2003) that a hot corino with a radius of about 150 AU exists inside the cold envelope of IRAS 16293 and that in that region, complex molecules are formed because of grain mantle evaporation.

In addition to that, the Plateau de Bure observations confirm that the two sources A and B are different, as noted by previous authors (Wootten 1989; Mundy et al. 1990, 1992). They differ in line intensities and extent (Fig. 1), and this corresponds to a difference in their chemical composition. But, before discussing this point, it is necessary to address the second most striking difference in the two sources: their line profiles (Fig. 2). Source A has clearly broadened spectra (FWHM ~ 8 km s^{-1}), while source B shows apparently much narrower profiles (FWHM ~ 2 km s^{-1}). Furthermore, the lines of source B seem to peak at $V_{LSR} = 2.7$ km s^{-1}, whereas the parent cloud velocity is at $V_{LSR} = 3.9$ km s^{-1} (compatible with the spectra of source A, although given the broad profiles it is difficult to precisely determine the V_{LSR} of source A). Note that the cloud's V_{LSR} (3.9 km s^{-1}) is very nicely measured by the two CN absorption lines

[8] It is likely that the emission from source A originates in the disk around this source. A detailed study of this aspect is postponed to a forthcoming paper.

in the observed band[9] (Fig. 2). As said, no evidence of outflowing gas is seen in the images, and also the broad line profiles of source A are consistent with gas *infalling* toward an $\sim 1\ M_\odot$ object (Ceccarelli et al. 2000a, 2000b; Schöier et al. 2002). Therefore, both the images and line profiles of source A are fully consistent with the hot corino hypothesis.

The case of source B is less obvious: why does this source have narrower lines and why do they peak at 2.7 km s^{-1}? But is this true? A very careful look at the B spectra raises doubts. Indeed, all the B lines have a second small peak—sometimes at the limit of the noise—on the redshifted side of the spectrum. This second peak could indeed be part of the line itself, which would be strongly self-absorbed at $V_{\rm LSR} = 3.9$ km s^{-1}. If this is the case, the line widths of source B would be $\sim$ 4–6 km s^{-1} (Fig. 2), similar to the line widths measured toward source A. Note that the blue peak is expected to be brighter than the red peak in the case of optically thick lines from infalling gas (Leung & Brown 1977; Zhou 1992, 1995; Choi et al. 1995), so it would be consistent with the $\sim 1\ M_\odot$ hot corino hypothesis of source B too. This alternative explanation, optically thick lines in source B, is therefore very appealing and worth exploring in some detail. Using the LTE approximation, the required column densities for the CH_3CN and $HCOOCH_3$ lines to be optically thick are $N \sim 10^{16}$ cm^{-2} and $N \sim 10^{17}$ cm^{-2}, respectively. These values are about 1 order of magnitude larger than the column density derived in B from the emission lines, assuming that the lines are optically thin and LTE-populated and that the emission region fills up the Plateau de Bure synthesized beam (see below). Considering that the three adopted assumptions all underestimate the true column density, it is indeed possible, but not firmly established, that the lines in source B are optically thick. Unfortunately, "physical" considerations do not help either to distinguish between the two possible interpretations, optically thin or thick lines in source B. In the first case (B has $V_{\rm LSR} = 2.7$ km s^{-1} and FWHM ~ 2 km s^{-1}), source B would be less massive than A and would revolve around it at 1.2 km s^{-1} (multiplied by the inclination of the orbit), at a distance of 800 AU, which is fully consistent with $M_{\rm A} \sim 1\ M_\odot$ (unless the orbit is in the sky plane). In the second case (B also has $V_{\rm LSR} = 3.9$ km s^{-1} and FWHM $\sim$ 4–6 km s^{-1}), A and B have comparable masses (similar FWHM), but B is more compact. Future high-resolution observations of optically thin lines are hence required to definitely settle the question.

As said, the nature of source B affects the determination of the molecular abundances in this source and, hence, how much the chemical composition of the A and B hot corinos differ. Using the relation between column density and observed continuum flux density, and using a dust opacity κ_ν of 0.8 cm^2 g^{-1} at 1.3 mm and a dust temperature T_d of 40 K (e.g. Walker et al. 1986), we derive molecular hydrogen column densities from the 1.3 mm continuum emission equal to $N({\rm H_2}, {\rm A}) = 3.5 \times 10^{24}$ cm^{-2} in A and $N({\rm H_2}, {\rm B}) = 1.7 \times 10^{25}$ cm^{-2} in B (consistent with the values of Mundy et al. 1992).[10] Using these values and the CH_3CN total column densities derived from the rotational diagram method ($N_{\rm A} = 1.7 \times 10^{15}$ cm^{-2} and $N_{\rm B} = 3.9 \times 10^{14}$ cm^{-2}), we get CH_3CN abundances of 4.8×10^{-10} and 2.3×10^{-11} for A and B, respectively; i.e., CH_3CN is $\sim$20 times more abundant in A than in B. A rotational diagram could not be drawn for the $HCOOCH_3$ transitions as they have similar upper energy levels, but assuming $T_{\rm rot} \sim 60$ K (Cazaux et al. 2003) we get $HCOOCH_3$ column densities of $N_{\rm A} = 2.6 \times 10^{16}$ cm^{-2} and $N_{\rm B} = 8.4 \times 10^{15}$ cm^{-2}, i.e. $HCOOCH_3$ abundances of 7.5×10^{-9} and 4.9×10^{-10} for A and B, respectively, a factor 15 difference.[11] Note, however, that since B is unresolved in the line emission, and the lines could be optically thick (see above discussion), the molecular abundances quoted for B may be underestimated by about an order of magnitude (note also that the region of molecular emission could be more compact than the continuum emission region). Therefore, resolving the problem of the nature of the observed line emission in source B is crucial, not only for determining the dynamical state of this source but also for correctly assessing the difference in the chemical composition of sources A and B.

In summary, these interferometric observations with the Plateau de Bure show unambiguously that the observed complex organic molecules are emitted from two compact ($\leq$1.″5) regions, which is consistent with grain mantle evaporation. No indication was found in support of other formation mechanisms for these molecules. Two scenarios have been proposed to explain the observed differences in sources A and B. However, the available data are insufficient to fully understand how and why the two components differ in their dynamical and chemical state, and more interferometric observations (e.g., of optically thin lines) are needed in order to solve the issues raised in this Letter.

[9] The absorption originates in the foreground (envelope + cloud) cold gas, which absorbs the photons emitted in the hot corino regions (the CN emission component, being extended, is filtered out by the interferometric observations).

[10] We postpone the detailed analysis of the continuum emission to a forthcoming paper.

[11] Note that the abundances quoted in Cazaux et al. (2003) differ from those derived here because of the different estimate of the H_2 column density.

REFERENCES

Arce, H. G., & Sargent, A. I. 2004, ApJ, 612, 342
Bottinelli, S., et al. 2004, ApJ, 615, in press
Cazaux, S., Tielens, A. G. G. M., Ceccarelli, C., Castets, C. Wakelam, V., Caux, E., Parise, B., & Teyssier, D. 2003, ApJ, 593, L51
Ceccarelli, C. 2004, in ASP Conf. Ser. 323, Star Formaiton in the Interstellar Medium, ed. D. Johnstone, F. C. Adams, D. N. C. Lin, D. A. Neufeld, & E. C. Ostriker (San Francisco: ASP), in press
Ceccarelli, C., Castets, A., Caux, E., Hollenbach, D., Loinard, L., Molinari, S., & Tielens, A. G. G. M. 2000a, A&A, 355, 1129
Ceccarelli, C., Loinard, L., Castets, A., Tielens, A. G. G. M., & Caux, E. 2000b, A&A, 357, L9
Choi, M., Evans, N. J., II, Gregersen, E. M., & Wang, Y. 1995, ApJ, 448, 742
Doty, S. D., Schöier, F. L., & van Dishoeck, E. F. 2004, A&A, 418, 1021
Kurtz, S., Cesaroni, R., Churchwell, E., Hofner, P., & Walmsley, C. M. 2000, in Protostars and Planets IV, ed. V. Mannings, A. P. Boss, & S. S. Russell (Tucson: Univ. Arizona Press), 299
Leung, C. M., & Brown, R. L. 1977, ApJ, 214, L73
Looney, L. W., Mundy, L. G., & Welch, W. J. 2000, ApJ, 529, 477
Maret, S., Ceccarelli, C., Caux, E., Tielens, A. G. G. M., & Castets, A. 2002, A&A, 395, 573
Maret, S., et al. 2004, A&A, 416, 577
Mundy, L. G., Wootten, H. A., & Wilking, B. A. 1990, ApJ, 352, 159
Mundy, L. G., Wootten, A., Wilking, B. A., Blake, G. A., & Sargent, A. I. 1992, ApJ, 385, 306
Schöier, F. L., Jørgensen, J. K., van Dischoeck, E. F., & Blake, G. A. 2002, A&A, 390, 1001
———. 2004, A&A, 418, 185
van Dishoeck, E. F., & Blake, G. A. 1998, ARA&A, 36, 317
Walker, C. K., Lada, C. J., Young, E. T., Maloney, P. R., & Wilking, B. A. 1986, ApJ, 309, L47
Wootten, H. A. 1989, ApJ, 337, 858
Zhou, S. 1995, ApJ, 442, 685
———. 1992, ApJ, 394, 204

The Astrophysical Journal, 615:354–358, 2004 November 1

COMPLEX MOLECULES IN THE HOT CORE OF THE LOW-MASS PROTOSTAR NGC 1333 IRAS 4A

S. Bottinelli,[1,2] C. Ceccarelli,[1] B. Lefloch,[1] J. P. Williams,[2] A. Castets,[3] E. Caux,[4] S. Cazaux,[5] S. Maret,[1] B. Parise,[4] and A. G. G. M. Tielens[6]

Received 2004 June 2; accepted 2004 July 2

ABSTRACT

We report the detection of complex molecules ($HCOOCH_3$, HCOOH, and CH_3CN), signposts of a hot core–like region, toward the low-mass Class 0 source NGC 1333 IRAS 4A. This is the second low-mass protostar in which such complex molecules have been searched for and reported, the other source being IRAS 16293−2422. It is therefore likely that compact (a few tens of AU) regions of dense and warm gas, where the chemistry is dominated by the evaporation of grain mantles and where complex molecules are found, are common in low-mass Class 0 sources. Given that the chemical formation timescale is much shorter than the gas hot-core crossing time, it is not clear whether the reported complex molecules are formed on the grain surfaces (first-generation molecules) or in the warm gas by reactions involving the evaporated mantle constituents (second-generation molecules). We do not find evidence for large differences in the molecular abundances, normalized to the formaldehyde abundance, between the two solar-type protostars, suggesting perhaps a common origin.

Subject headings: ISM: abundances — ISM: individual (NGC 1333 IRAS 4A) — ISM: molecules — stars: formation

1. INTRODUCTION

There is strong support from the composition of cometary and meteoritic materials for the notion that the solar nebula, from which the planets formed, passed through a phase of warm, dense gas with a rich chemistry. While much observational effort has been dedicated to the study of such hot cores around massive protostars, hot cores around low-mass protostars have received little attention. Only very recently has the first hot core around a solar-type protostar been discovered, toward the typical Class 0 source IRAS 16293−2422 (hereafter IRAS 16293), exhibiting all characteristics of such regions: warm temperature (>100 K) and high density ($>10^7$ cm^{-3}; Ceccarelli et al. 2000a), high abundance of hydrides (CH_3OH, H_2CO, H_2O; Ceccarelli et al. 2000a, 2000b; Schöier et al. 2002), high deuteration levels (>10%; Ceccarelli et al. 1998, 2001; Parise et al. 2002; Roberts et al. 2002), and complex molecules ($HCOOCH_3$, HCOOH, CH_3OCH_3, CH_3CN, C_2H_5CN; Cazaux et al. 2003). The definition of "hot core" used for massive protostars implies the presence of a relatively large amount of warm and dense gas, along with a complex chemistry triggered by the grain mantle evaporation (e.g., Walmsley et al. 1992). In order to make clear that hot cores of low- and high-mass protostars are, however, substantially different in the amount of material involved, we use hereafter the term "hot corino" to identify the warm inner regions of the envelope surrounding the low-mass protostars.

The chemical composition of the (massive) hot cores is thought to reflect a variety of sequential processes (Walmsley et al. 1992; Charnley et al. 1992; Caselli et al. 1993; Charnley 1995; Rodgers & Charnley 2001, 2003). Specifically, in the precollapse cold cloud phase, simple molecules form on grain surfaces by hydrogenation of CO and other heavy elements (notable examples are H_2CO, CH_3OH, and H_2S). Upon heating by a newly formed star, these molecules, called "first-generation" or "parent" molecules, evaporate into the gas and undergo fast neutral-neutral and ion-neutral reactions producing complex organic molecules, i.e., "second-generation" or "daughter" molecules. The first part of this sequence (the formation of fully hydrogenated molecules on the grain surfaces) has been demonstrated to occur around low-mass protostars by studies of the multiply deuterated molecules formaldehyde (Ceccarelli et al. 1998; Bacmann et al. 2003), methanol (Parise et al. 2002, 2004), and sulfide (Vastel et al. 2003). Evaporation from grain mantles of these first-generation species (in particular H_2CO and CH_3OH) has been observed in IRAS 16293 (Ceccarelli et al. 2000b; Schöier et al. 2002) and in about a dozen low-mass protostars (Maret et al. 2004). However, since the timescale necessary to convert first-generation molecules into complex, second-generation molecules (around 10^4–10^5 yr; e.g., Charnley et al. 1992, 2001) is much longer than the transit time of the gas in the hot corinos (a few hundred years; e.g., Schöier et al. 2002), the formation in the gas of second-generation molecules seems improbable (e.g., Schöier et al. 2002). The detection of a high abundance of complex molecules in the hot core of IRAS 16293 (Cazaux et al. 2003) has evidently been a challenge to the simple theoretical sequence described above. The key question has shifted from "Is a hot core present in low-mass protostars?" to "What is the origin of the molecular complexity in these sources?" In particular, there may well be chemical pathways to complex molecules involving grain surface networks (e.g., Charnley 1995). In order to answer this question, more

[1] Laboratoire d'Astrophysique de l'Observatoire de Grenoble, BP 53, 38041 Grenoble, Cedex 9, France; sbottine@obs.ujf-grenoble.fr, ceccarel@obs.ujf-grenoble.fr, lefloch@obs.ujf-grenoble.fr, maret@obs.ujf-grenoble.fr.
[2] Institute for Astronomy, University of Hawai'i, 2680 Woodlawn Drive, Honolulu, HI 96822; jpw@ifa.hawaii.edu.
[3] Observatoire de Bordeaux, 2 Rue de l'Observatoire, BP 89, 33270 Floirac, France; castets@obs.u-bordeaux1.fr.
[4] Centre d'Etude Spatiale des Rayonnements, CNRS-UPS, 9 Avenue du Colonel Roche, BP 4346, 31028 Toulouse, Cedex 4, France; caux@cesr.fr, parise@cesr.fr.
[5] INAF, Osservatorio Astrofisico di Arcetri, Largo E. Fermi 5, I-50125 Firenze, Italy; cazaux@arcetri.astro.it.
[6] Kapteyn Astronomical Institute, P.O. Box 800, 9700 AV Groningen, Netherlands; tielens@astro.rug.nl.

observations of other low-mass protostars are necessary. This will allow the development of a solid observational framework within which we might search for clues to the formation of second-generation molecules. As remarked in previous studies, the question is far from being academic, since the molecules in the hot corinos constitute the material that will eventually form the protoplanetary disk and possibly the planets of the forming Sun-like star.

In this paper we present the first results of a survey we are carrying out on the sample of Class 0 sources studied by Maret et al. (2004). Here we report the detection of complex, second-generation molecules in NGC 1333 IRAS 4A (hereafter IRAS 4A), a well-known Class 0 protostar and a target of several studies of molecular emission (e.g., Blake et al. 1995). IRAS 4A is part of the binary system IRAS 4, located in the NGC 1333 reflection nebula in the Perseus cloud. It is separated by 31″ from the other component, IRAS 4B, and was itself resolved into two components with a separation of 2″ by Lay et al. (1995). The distance to the NGC 1333 cloud is uncertain (see, e.g., Maret et al. 2002), but assuming a value of 220 pc (derived by Černis 1990, for consistency with previous work), IRAS 4A has a luminosity of 6 $L_{\odot}$ and an envelope mass of 3.5 $M_{\odot}$ (Sandell et al. 1991). IRAS 4A is associated with a very highly collimated outflow detected in CO, CS, and SiO (Blake et al. 1995; Lefloch et al. 1998). Infall motion was detected by Di Francesco et al. (2001) and Choi et al. (1999) with an estimated accretion rate of 1.1×10^{-4} $M_{\odot}$ yr^{-1}, an inner mass of 0.7 $M_{\odot}$, and an age of ∼6500 yr (see also Maret et al. 2002).

2. OBSERVATIONS AND RESULTS

The observations were carried out in 2003 June with the IRAM 30 m telescope. The position used for pointing was $\alpha(2000) = 03^{h}29^{m}10\overset{s}{.}3$ and $\delta(2000) = 31^{\circ}13'31''$. Based on the observations of IRAS 16293 by Cazaux et al. (2003), we targeted the following complex molecules: methyl formate, $HCOOCH_3$ (A and E); formic acid, HCOOH; dimethyl ether, CH_3OCH_3; methyl cyanide, CH_3CN; and ethyl cyanide, C_2H_5CN. Different telescope settings were used in order to include as many transitions as possible for each molecule. All lines were observed with a low-resolution, 1 MHz filter bank of 4×256 channels split between different receivers, providing a velocity resolution of ∼3, 2, and 1 km s^{-1} at 3, 2, and 1 mm, respectively. Each receiver was simultaneously connected to a unit of the autocorrelator, with spectral resolutions of 20, 80, or 320 kHz and bandwidths between 40 and 240 MHz, equivalent to an (unsmoothed) velocity resolution range of 0.1–0.4 km s^{-1}. Typical system temperatures were 100–200 K, 180–250 K, and 500–1500 K, at 3, 2, and 1 mm, respectively.

Two observation modes were used: position switching with the off position at an offset of $\Delta\alpha = -100$, $\Delta\delta = +300$, and wobbler switching with a 110″ throw in azimuth. Pointing and focus were regularly checked using planets or strong quasars, providing a pointing accuracy of 3″. All intensities reported in this paper are expressed in units of main-beam brightness temperature. At 3, 2, and 1 mm, the angular resolution is 24″, 16″, and 10″, and the main-beam efficiency is 76%, 69%, and 50%, respectively.

Figure 1 shows two examples of the low-resolution spectra we obtained. Detected transitions have been identified using the JPL molecular line catalog (Pickett et al. 1998) and are reported in Table 1. We considered as good identifications only lines with a 3 σ detection and a $V_{LSR} = 6.8 \pm 0.3$ km s^{-1}. We detected three of the five targeted molecules: 10 transitions for $HCOOCH_3$ (A and E), 2 for HCOOH, and 9 for CH_3CN. We

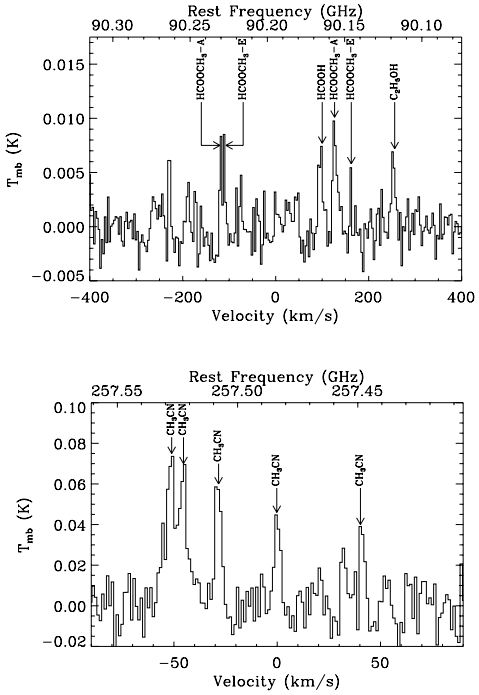

FIG. 1.—Two low-resolution spectra obtained during our observations of IRAS 4A. Lines that are not labeled are unidentified. The rms noise level is 2 mK (*top spectrum*) and 12 mK (*bottom spectrum*). The spectral resolution is 3.3 km s^{-1} (*top*) and 1.2 km s^{-1} (*bottom*). The V_{LSR} is 7.0 km s^{-1}. Known transitions are indicated but not all of them are detections, e.g., $HCOOCH_3$ at 90.145 GHz is not considered as such, but the upper limit derived from it is consistent with the rotational diagram of Fig. 2.

also have a possible detection for C_2H_5OH at 90.118 GHz; unfortunately, no other transition with a low enough energy and high enough Einstein coefficient was contained within the frequency ranges we observed to confirm the correct identification. No transitions of CH_3OCH_3 and C_2H_5CN were detected to a noise limit of 6 and 2 mK, respectively. All detected lines, with a few exceptions, have line widths ∼2−3 km s^{-1}, likely due to the presence of unresolved triplets or to the contamination of unidentified lines. In order to derive the rotational temperature and column density, we built rotational diagrams (Fig. 2) in which the observed fluxes were corrected for beam dilution, assuming a source size of 0.″5 (derived from a hot core radius of 53 AU and a distance of 220 pc, as found by Maret et al. 2004). The assumption that the complex molecules are confined to the hot corino is supported by a Plateau de Bure interferometric study of IRAS 16293, which shows localized emission in a region ∼1.″4 around the protostar (Bottinelli et al. 2004).

The rotational temperatures, total column densities, and abundances for the detected molecules are presented in Table 2. Note that the large errors in the HCOOH (this work) and CH_3OCH_3 (Cazaux et al. 2003) abundances are due to a poor constraint of the rotational temperature, and hence column

TABLE 1
Molecular Lines Detected toward IRAS 4A

Molecule	Transition Line	Frequency (MHz)	E_u[a] (cm^{-1})	δV[b] (km s^{-1})	ΔV[c] (km s^{-1})	T_{mb} (mK)	$\int T_{mb}\,dV$ (K km s^{-1})	rms[d] (mK)
$HCOOCH_3$-A	$7_{2,5}-6_{2,4}$	90156.5	13.7	0.5	1.5	22	0.036	5
	$8_{0,8}-7_{0,7}$	90229.7	13.9	0.5	2.5	16	0.041	5
	$8_{3,6}-7_{3,5}$	98611.1	18.9	0.2	1.2	28	0.036	7
	$8_{4,5}-7_{4,4}$	98682.8	22.2	1.9	4.2	95	0.042	2
$HCOOCH_3$-E	$7_{2,5}-6_{2,4}$	90145.7	13.7	0.5	1.3	14	0.019	5
	$8_{0,8}-7_{0,7}$	90227.8	14.0	0.5	3.1	16	0.055	5
	$8_{3,6}-7_{3,5}$	98607.8	18.9	0.9	3.8	13	0.054	4
	$8_{4,5}-7_{4,4}$	98711.7	22.2	0.2	1.4	22	0.034	7
	$20_{2,18}-19_{2,18}$	226713.1	83.6	0.8	1.0	89	0.099	26
	$20_{3,18}-19_{3,17}$	226773.3	83.6	0.8	2.1	54	0.121	19
HCOOH	$4_{2,2}-3_{2,1}$	90164.5	16.4	0.5	0.8	16	0.015	5
	$6_{2,4}-5_{2,3}$	135737.7	24.6	1.4	1.8	15	0.029	5
CH_3CN[e]	$6_{3,0}-5_{3,0}$	110364.6	57.6	0.8	5.1	20	0.110	6
	$6_{2,0}-5_{2,0}$	110375.1	32.8	0.8	2.3	46	0.112	6
	$6_{1,0}-5_{1,0}$	110381.5	17.9	0.8	3.4	67	0.241	6
	$6_{0,0}-5_{0,0}$	110383.6	12.9	0.8	4.3	76	0.347	6
	$14_{4,0}-13_{4,0}$	257448.9	143.9	1.2	3.3	40	0.141	12
	$14_{3,0}-13_{3,0}$	257482.7	109.1	0.4	2.6	53	0.150	19
	$14_{2,0}-13_{2,0}$	257507.9	84.3	0.4	3.1	59	0.195	19
	$14_{1,0}-13_{1,0}$	257522.5	69.4	0.4	2.2	74	0.172	19
	$14_{0,0}-13_{0,0}$	257527.4	64.4	1.2	3.8	68	0.274	12

[a] Energy of the upper level of the transition.
[b] Spectral resolution of the observation (when possible, the integrated intensity was derived from the high-resolution data).
[c] Width of the observed line.
[d] Computed over the line width.
[e] All the CH_3CN lines are (unresolved) triplets. The quoted signal is the integral over each triplet. Larger line widths could be due to the larger spacing between the components of the triplets.

density, of these two molecules, even though each molecule is clearly detected in each case.

3. DISCUSSION AND CONCLUSION

The most important result of the present work is the detection of complex molecules in the hot corino of IRAS 4A, the second Class 0 protostar in which those molecules have been searched for, after IRAS 16293 (Cazaux et al. 2003). This result demonstrates that as soon as a warm region is created in the center of the envelope of low-mass protostars, complex molecules are readily formed and/or injected on timescales lower than the estimated Class 0 source ages ($\sim 5\times10^4$ yr in IRAS 16293 and $\sim$6500 yr in IRAS 4A; e.g., Maret et al. 2002) and, most importantly, shorter than the transit time in the hot corinos. The latter is $\sim$400 and $\sim$120 yr in IRAS 16293 and IRAS 4A, respectively, based on the hot corino sizes quoted in Maret et al. (2004) and assuming free-falling gas.

We compare the measured composition of the hot corino of IRAS 4A to IRAS 16293 (Cazaux et al. 2003) and the massive hot core of OMC-1 (Sutton et al. 1995) in Table 2. Note that the latter abundances are derived from single-dish measurements with a 14″ beam, which encompasses several hot cores (Wright et al. 1996). Unfortunately, not all the molecules considered here have interferometric measurements available, so we can only use these 14″ beam-averaged estimates of the abundances.

The first remark is that the absolute abundances of the observed molecules are 1 order of magnitude smaller in IRAS 4A than in IRAS 16293, but their relative abundances with respect to H_2CO are quite similar, with the exception of methanol, which is underabundant with respect to H_2CO by about a factor of 10 in IRAS 4A (Fig. 3). There are two reasons to consider abundances with respect to formaldehyde. The first one is observational: while the IRAS 16293 hot core has now been imaged with the Plateau de Bure Interferometer (Bottinelli et al. 2004) and its size confirmed to be $\sim$1.″4, the IRAS 4A core size is only indirectly estimated from dust continuum single-dish (12″) observations to be 0.″5, and no interferometric observations are available yet with such a high resolution. So the IRAS 4A core size might be wrong by up to a factor of 3 (Maret et al. 2004) and the abundances by up to a factor of 10, i.e., the absolute abundances of IRAS 4A could be comparable to those of IRAS 16293. Using abundance ratios allows us to remove this size uncertainty. The second reason is theoretical: "standard" hot-core models predict that molecules like methyl formate or methyl cyanide are second-generation molecules formed in the warm gas from the evaporated grain mantle constituents (formaldehyde, ammonia, and methanol; e.g., Charnley et al. 1992; Caselli et al. 1993; Rodgers & Charnley 2003). It is therefore interesting to compare the abundances of the complex molecules to those of one of these supposed parent molecules. Formaldehyde was chosen because we only have an upper limit on the methanol abundance (S. Maret et al. 2004, in preparation), and no measurements of the ammonia abundance are available.

A possible interpretation for the similarity in the complex molecules' relative abundances, with respect to H_2CO and not with respect to CH_3OH, is that the former is the mother molecule of the observed O-bearing species, e.g., likely the case of $HCOOCH_3$ (Charnley et al. 1992), and that the chemical evolution timescale is shorter than the age of the youngest source. Charnley et al. (1992) also predict that methanol is the mother molecule of CH_3OCH_3, but we cannot say whether the available data confirm this hypothesis, since we only have an upper limit on the abundance of this molecule in IRAS 4A and

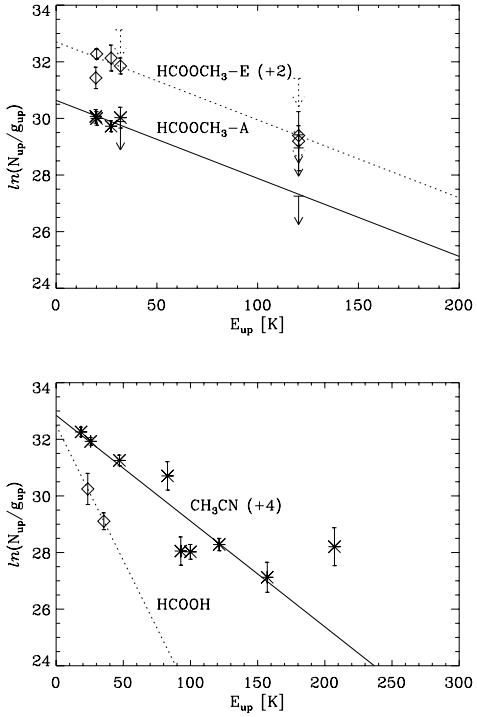

FIG. 2.—Rotational diagrams of the detected molecules, corrected for beam dilution. Arrows show the upper limits for the transitions that have not been detected, and lines represent the best fit to the data. *Top*: Asterisks and solid lines are associated with $HCOOCH_3$-A and diamonds and dotted lines with $HCOOCH_3$-E. *Bottom*: Asterisks and solid lines are associated with CH_3CN and diamonds and dotted lines with HCOOH. Error bars are derived assuming a calibration uncertainty of 10% on top of the statistical error. The excess of emission of the CH_3CN transition at 210 K is probably due to contamination from unknown line(s).

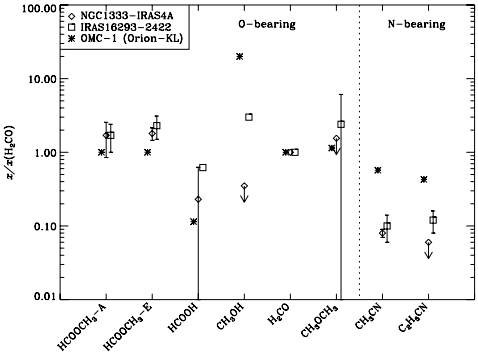

FIG. 3.—Abundances of the observed species (reported on the *x*-axis) normalized to the H_2CO abundances. Asterisks refer to the OMC-1 hot core, squares to the hot corino of IRAS 16293, and diamonds to the corino of IRAS 4A. Arrows represent upper limits in IRAS 4A derived from our observations. No errors were quoted by Cazaux et al. (2003) for the HCOOH abundance, which was determined from two transitions only and is rather uncertain.

a large error in IRAS 16293. Similarly, the N-bearing molecules CH_3CN and C_2H_5CN could both be daughters of the same mother molecule, probably ammonia. This would imply that the two sources have a similar ammonia mantle abundance. Alternatively, some or all of the reported molecules are possible mantle constituents themselves. This may be the case for formic acid, as predicted by Tielens & Hagen (1982) and suggested by the observational study by Liu et al. (2001). Moreover, the analysis of *Infrared Space Observatory* (*ISO*) absorption spectra toward the massive hot core W33A (e.g., Schutte et al. 1997) is consistent with the presence of solid formic acid and would also support the idea of this species being a mantle constituent. However, these considerations do not take into account the evolutionary state of the objects, and the fundamental question is: does the abundance of any of these complex molecules have anything to do with the age

TABLE 2
RESULTS FROM THE ROTATIONAL DIAGRAMS FOR IRAS 4A, IN COMPARISON WITH IRAS 16293 AND THE MASSIVE HOT CORE OMC-1

	IRAS 4A				
MOLECULE	T_{rot} (K)	N_{total} (cm^{-2})	X[a]	IRAS 16293[b] X	OMC-1[c] X
$HCOOCH_3$-A	36[d]	5.5 ± 2.7 E16	3.4 ± 1.7 E−8	1.7 ± 0.7 E−7	1 E−8
$HCOOCH_3$-E	36 ± 5	5.8 ± 1.1 E16	3.6 ± 0.7 E−8	2.3 ± 0.8 E−7	1 E−8
HCOOH	10 ± 6	7.3 ± 13.0 E15	4.6 ± 7.9 E−9	∼6.2 E−8	8 E−10
CH_3CN	27 ± 1	2.6 ± 0.3 E15	1.6 ± 0.2 E−9	1.0 ± 0.4 E−8	4 E−9
CH_3OH	...	...	≤7 E−9[e]	3 E−7	1 E−7
H_2CO	...	...	2 E−8[f]	1 E−7[g]	7 E−9
	Upper Limits				
CH_3OCH_3	36[d]	≤4.5 E16	≤2.8 E−8	2.4 ± 3.7 E−7	8 E−9
C_2H_5CN	27[h]	≤1.9 E15	≤1.2E−9	1.2 ± 0.4 E−8	3 E−9

[a] Assuming an H_2 column density in the hot corino of $N(H_2) = 1.6\times10^{24}$ cm^{-2} (from Maret et al. 2004).
[b] From Cazaux et al. (2003).
[c] From Sutton et al. (1995).
[d] T_{rot} assumed to be similar to the one derived for $HCOOCH_3$-E.
[e] From S. Maret et al. (in preparation).
[f] From Maret et al. (2004).
[g] From Ceccarelli et al. (2000b).
[h] T_{rot} assumed to be similar to the one derived for CH_3CN.

and/or evolutionary stage of the protostar, or is it dominated by the initial mantle composition? Evidently, two sources are not enough to answer this question, and observations of more low-mass sources are required.

Regarding the comparison with the massive hot core(s) in Orion, Figure 3 would suggest that, with respect to formaldehyde, there is a deficiency of methanol and of N-bearing complex molecules in the low-mass hot corinos. It is possible that these differences are mostly due to a different grain mantle composition, i.e., to a different precollapse density. However, recall that the abundance ratios of CH_3CN and CH_3OH in Figure 3 refer to the 14″ beam-averaged values around the OMC-1 hot core, which in fact includes several smaller cores (Wright et al. 1996). Therefore, in order to make precise comparisons, higher resolution observations of the OMC-1 hot core are needed. It is also worth noting that if we consider, for example, the measurements by Wright et al. (1996) in the compact ridge component (a region about 10″ away from the hot core central position, which is also a site of mantle evaporation and of active gas-phase chemistry; e.g., Charnley et al. 1992), the CH_3CN and CH_3OH abundance ratios with respect to H_2CO are (surprisingly) close to those found for the hot corinos of IRAS 16293 and IRAS 4A. Hence, interferometric observations of a larger number of massive hot cores are necessary to provide a significant comparison of the hot corinos with their high-mass counterparts.

In summary, although the present observations do not allow us to determine why and how complex molecules are formed, they do show that hot corinos, in the wide definition of chemically enriched regions, are a common property of solar-type protostars in the early stages. The evidence is that the types of complex molecules that are formed are determined primarily by the composition of the grain mantles. At this stage, it is not clear whether the evolutionary stage of the protostar plays any role at all, other than governing the presence and size of the mantle evaporation region.

REFERENCES

Bacmann, A., Lefloch, B., Ceccarelli, C., Steinacker, J., Castets, A., & Loinard, L. 2003, ApJ, 585, L55
Blake, G. A., Sandell, G., van Dishoeck, E. F., Groesbeck, T. D., Mundy, L. G., & Aspin, C. 1995, ApJ, 441, 689
Bottinelli, S., et al. 2004, ApJL, submitted
Caselli, P., Hasegawa, T. I., & Herbst, E. 1993, ApJ, 408, 548
Cazaux, S., Tielens, A. G. G. M., Ceccarelli, C., Castets, C., Wakelam, V., Caux, E., Parise, B., & Teyssier, D. 2003, ApJ, 593, L51
Ceccarelli, C., Castets, A., Caux, E., Hollenbach, D., Loinard, L., Molinari, S., & Tielens, A. G. G. M. 2000a, A&A, 355, 1129
Ceccarelli, C., Castets, A., Loinard, L., Caux, E., & Tielens, A. G. G. M. 1998, A&A, 338, L43
Ceccarelli, C., Loinard, L., Castets, A., Tielens, A. G. G. M., & Caux, E. 2000b, A&A, 357, L9
Ceccarelli, C., Loinard, L., Castets, A., Tielens, A. G. G. M., Caux, E., Lefloch, B., & Vastel, C. 2001, A&A, 372, 998
Černis, K. 1990, Ap&SS, 166, 315
Charnley, S. B. 1995, Ap&SS, 224, 251
Charnley, S. B., Rodgers, S. D., & Ehrenfreund, P. 2001, A&A, 378, 1024
Charnley, S. B., Tielens, A. G. G. M., & Millar, T. J. 1992, ApJ, 399, L71
Choi, M., Panis, J.-F., & Evans, N. J. 1999, ApJS, 122, 519
Di Francesco, J., Myers, P. C., Wilner, D. J., Ohashi, N., & Mardones, D. 2001, ApJ, 562, 770
Lay, O. P., Carlstrom, J. E., & Hills, R. E. 1995, ApJ, 452, L73
Lefloch, B., Castets, A., Cernicharo, J., & Loinard, L. 1998, ApJ, 504, L109
Liu, S.-Y., Mehringer, D. M., & Lewis, E. S. 2001, ApJ, 552, 654
Maret, S., Ceccarelli, C., Caux, E., Tielens, A. G. G. M., & Castets, A. 2002, A&A, 395, 573
Maret, S., et al. 2004, A&A, 416, 577
Parise, B., Castets, A., Herbst, E., Caux, E., Ceccarelli, C., Mukhopadhyay, I., & Tielens, A. G. G. M. 2004, A&A, 416, 159
Parise, B., et al. 2002, A&A, 393, L49
Pickett, H. M., Poynter, R. L., Cohen, E. A., Delitsky, M. L., Pearson, J. C., & Muller, H. S. P. 1998, J. Quant. Spectrosc. Radiat. Transfer, 60, 883
Roberts, H., Fuller, G. A., Millar, T. J., Hatchell, J., & Breckle, J. V. 2002, A&A, 381, 1026
Rodgers, S. D., & Charnley, S. B. 2001, ApJ, 546, 324
———. 2003, ApJ, 585, 355
Sandell, G., Aspin, C., Duncan, W. D., Russell, A. P. G., & Robson, E. I. 1991, ApJ, 376, L17
Schöier, F. L., Jørgensen, J. K., van Dischoeck, E. F., & Blake, G. A. 2002, A&A, 390, 1001
Schutte, W. A., Greenberg, J. M., van Dishoeck, E. F., Tielens, A. G. G. M., Boogert, A. C. A., & Whittet, D. C. B. 1997, Ap&SS, 255, 61
Sutton, E. C., Peng, R., Danchi, W. C., Jaminet, P. A., Sandell, G., & Russell, A. P. G. 1995, ApJS, 97, 455
Tielens, A. G. G. M., & Hagen, W. 1982, A&A, 114, 245
Vastel, C., Phillips, T. G., Ceccarelli, C., & Pearson, J. 2003, ApJ, 593, L97
Walmsley, C. M., Cesaroni, R., Churchwell, E., & Hofner, P. 1992, Astron. Gesellschaft Abstract Ser., 7, 93
Wright, M. C. H., Plambeck, R. L., & Wilner, D. J. 1996, ApJ, 469, 216

A&A 421, 1113–1119 (2004)
DOI: 10.1051/0004-6361:20035640

Astronomy & Astrophysics

Modeling the millimeter emission from the Cepheus A young stellar cluster: Evidence for large scale collapse

S. Bottinelli and J. P. Williams

Institute for Astronomy, University of Hawai'i, Honolulu, HI 96822, USA

Received 6 November 2003 / Accepted 8 April 2004

Abstract. Evidence for a large scale flow of low density gas onto the Cepheus A young stellar cluster is presented. Observations of K-band near-infrared and multi-transition CS and N_2H^+ millimeter line emission are shown in relation to a sub-millimeter map of the cool dust around the most embedded stars. The near-infrared emission is offset from the dust peak suggesting a shift in the location of star formation over the history of the core. The CS emission is concentrated toward the core center but N_2H^+ peaks in two main cores offset from the center, opposite to the chemistry observed in low mass cores. A starless core with strong CS but weak N_2H^+ emission is found toward the western edge of the region. The average CS(2–1) spectrum over the cluster forming core is asymmetrically self-absorbed suggesting infall. We analyze the large scale dynamics by applying a one-dimensional radiative transfer code to a model spherical core with constant temperature and linewidth, and a density profile measured from an archival 850 μm map of the region. The best fit model that matches the three CS profiles requires a low CS abundance in the core and an outer, infalling envelope with a low density and undepleted CS abundance. The integrated intensities of the two N_2H^+ lines is well matched with a constant N_2H^+ abundance. The envelope infall velocity is tightly constrained by the CS(2–1) asymmetry and is sub-sonic but the size of the infalling region is poorly determined. The picture of a high density center with depleted CS slowly accreting a low density outer envelope with normal CS abundance suggests that core growth occurs at least partially by the dissipation of turbulent support on large scales.

Key words. radio lines: ISM – stars: formation – ISM: kinematics and dynamics – ISM: molecules – ISM: abundances – radiative transfer

1. Introduction

Most stars, particularly massive stars, form in groups (e.g., Carpenter 2000). It is therefore essential to study cluster forming regions in order to understand more completely the way in which the majority of stars are formed. Isolated low mass star formation occurs via the nearly isothermal free-fall collapse of a dense molecular cloud core, followed by the evolutionary phases Class 0, I, II and III objects (e.g., Evans 1999). However, the applicability of this paradigm to the formation of massive stars is debated (Garay & Lizano 1999): for example, massive stars begin burning hydrogen and reach the main sequence while still accreting matter from the surrounding protostellar envelope and they can also develop strong winds, both of which will strongly affect the physical conditions, structure and chemistry of their surroundings. Due to the shape of the IMF and the fact that they evolve faster, massive protostars are rarer (and therefore more distant on average) than low mass protostars. Consequently fewer Class 0 massive protostar counterparts have been studied in detail. It is only recently that catalogs of high-mass protostellar objects have been made (e.g., Sridharan et al. 2002).

Send offprint requests to: S. Bottinelli,
e-mail: sandrine@ifa.hawaii.edu

The molecular cloud core Cepheus A East (hereafter Cep A) is a nearby site of massive star formation (Sargent 1977) located in the Cepheus OB association at a distance of 725 pc (Blauuw et al. 1959). The far-IR luminosity is $2.4 \times 10^4\ L_\odot$ (Evans et al. 1981), corresponding to a small cluster of B stars. Cep A harbors one of the first molecular bipolar outflow sources discovered (Rodríguez et al. 1980). Higher spatial resolution CO observations showed the outflow to be extremely complex, and it was termed quadrupolar (Torrelles et al. 1993). The fastest components of this outflow are bipolar and oriented northwest-southeast (Rodríguez et al. 1980), perpendicular to the low velocity CO structure. The slower and more extended component has been interpreted as the diverting and redirecting of the main outflow by the interaction with interstellar high-density gas, seen in NH_3 lines by Torrelles et al. (1993). Ultra compact H II regions and a diffuse thermal dust emission source have been identified from 20 μm maps and 6 cm low-resolution VLA observations by Beichman et al. (1979). Seven ionized hydrogen complexes lie in "strings" that form a "Y" tilted to the east (Hughes & Wouterloot 1984), the bifurcation point of which is coincident with the exciting source of the molecular outflow. A cluster of compact radio sources have been identified as pre-main-sequence stars by Hughes (1988) due to their variability and the presence of OH and H_2O maser

emission. From subsequent ammonia VLA observations, Torrelles et al. (1993) proposed that one of these radio sources, HW2, is a ∼10–20 $M_\odot$ protostar. The larger core surrounding the cluster has temperature 35 K and mass 200−300 $M_\odot$ (Moriarty-Schieven et al. 1991). On the basis of its protostellar content, high luminosity and low temperature, and following the bolometric temperature definition of Chen et al. (1995), the Cep A core may be considered a high mass Class 0 source.

In order to examine the properties of this young, massive cluster forming region, we obtained near-infrared and millimeter wavelength multi-transition CS and N_2H^+ data. The observations are discussed in Sect. 2. We derive the density profile from 850 μm continuum measurements and fit core-averaged spectra using a 1-D radiative transfer model in Sect. 3. Our results indicate large CS depletion in the central core and an outer undepleted accreting layer. We discuss these results and conclude in Sect. 4.

2. Observations

2.1. Millimeter data

Observations were made with the 10 antenna Berkeley-Illinois-Maryland array[1] (BIMA) for two 8 h tracks in CS(2–1) in April and May 1998 and one 8 h track in N_2H^+(1–0) in May 1998, all in C-array. A seven field hexagonal mosaic was made with phase center, $\alpha(2000) = 22^h56^m18\overset{s}{.}9, \delta(2000) = 62°01'42\overset{''}{.}6$. Amplitude and phase were calibrated using 5 min observations of 2322+509 interleaved with each 25 min integration on source. The calibrator flux was 0.66 ± 0.22 Jy based on observations of Uranus during the middle of each track. The correlator was configured with two sets of 256 channels at a bandwidth of 12.5 MHz (0.15 km s^{-1} per channel) in each sideband and a total continuum bandwidth of 800 MHz. Data reduction was carried out using standard procedures in the MIRIAD package. The final maps covered a hexagonal region ∼3.′5 × 3.′5 region at ∼9″ × 7″ resolution.

Complementary single-dish maps of the same lines were made at the Five College Radio Astronomy Observatory[2] (FCRAO) 14-m telescope in December 1999 using the SEQUOIA 16 beam array receiver and the FAAS backend consisting of 15 autocorrelation spectrometers with 1024 channels set to an effective resolution of 24 kHz (0.06 km s^{-1}). The CS and N_2H^+ lines were observed simultaneously in frequency switching mode. The pointing and focus were checked every three hours on nearby SiO maser sources. Third order baselines were removed from the data and spectra coadded using the CLASS package. The resolution of the data is 50″ and the final maps were Nyquist sampled over 8′ × 8′ centered on the BIMA phase center. A single spectrum of $C^{34}S$(2–1) was also taken toward the map center using the same setup.

The FCRAO data were combined with the BIMA data using maximum entropy deconvolution (using a gain for FCRAO at these frequencies of 43.7 Jy K^{-1}). The resulting maps show the large scale structure observed in the single-dish map at the ∼10″ resolution of the interferometer map. These maps have an rms noise of 0.2 and 0.4 K per 0.5 km s^{-1} channel, for CS (2–1) and N_2H^+ (1–0) respectively. All the flux is recovered in the combined map but features at intermediate scales, in the range 70″−100″, may be poorly represented (e.g., Williams et al. 2003).

Observations of CS(5–4), CS(7–6) and N_2H^+(3–2) were made at the Heinrich Hertz Telescope[3] (HHT) in November 1999. The data were taken using the SIS-230 and SIS-345 receivers and AOS backend (2048 channels, 48 kHz resolution) in on-the-fly (OTF) mode. Pointing and focus were checked using observations of Saturn and Orion IRc2. The final maps, made from several OTF maps in orthogonal scan directions, were coadded and first order baselines removed using the CLASS package. The resolution of the observations is 31″, 22″, and 27″ for CS(5–4), CS(7–6) and N_2H^+(3–2) respectively and the final maps covered 3.′5 × 3.′5, with an rms noise of 0.4 K per 0.5 km s^{-1} channel.

To compare the near-infrared and millimeter wavelength line data with the cool dust emission around the most embedded (Class 0 counterpart) stars in the cluster, we downloaded archival SCUBA observations taken on the James Clerk Maxwell Telescope in August 1997 and reduced them using the SURF package.

2.2. Infrared data

Cep A was observed on the University of Hawai'i 2.2 m telescope at the $f/10$ focus with QUIRC (QUick InfraRed Camera) in K band (2.200 μm) in July and August 2003. The plate scale of the telescope is 0.1886 arcsec pixel^{-1} and the field-of-view 193″ × 193″. The total on source integration time was 23.2 min. The average seeing was 1.″1 *FWHM*. The observations were carried out by taking alternate object and sky exposures. All frames were flat-fielded using a normalized incandescent light dome flat. Sky frames were obtained by computing the median of several sky exposures close in time to a given object frame. The sky frames were subtracted from the object frames. The individual images were registered and coadded to produce a single image. Unfortunately, the conditions were non-photometric but we conservatively estimate that we should be able to detect to a limiting magnitude of at least 19, which is 3.4 mag fainter than 2MASS.

3. Analysis

3.1. Continuum and line maps

Figure 1 shows contours of the 850 μm continuum emission overlaid on the grayscale K-band image. Note that for 35 K

[1] The BIMA array is operated with support from the National Science Foundation under grants AST-9981308 to UC Berkeley, AST-9981363 to U. Illinois, and AST-9981289 to U. Maryland.

[2] FCRAO is supported in part by the National Science Foundation under grant AST-0100793 and is operated with permission of the Metropolitan District Commission, Commonwealth of Massachusetts.

[3] The HHT is operated by the Submillimeter Telescope Observatory on behalf of Steward Observatory and the Max-Planck-Institut fuer Radioastronomie.

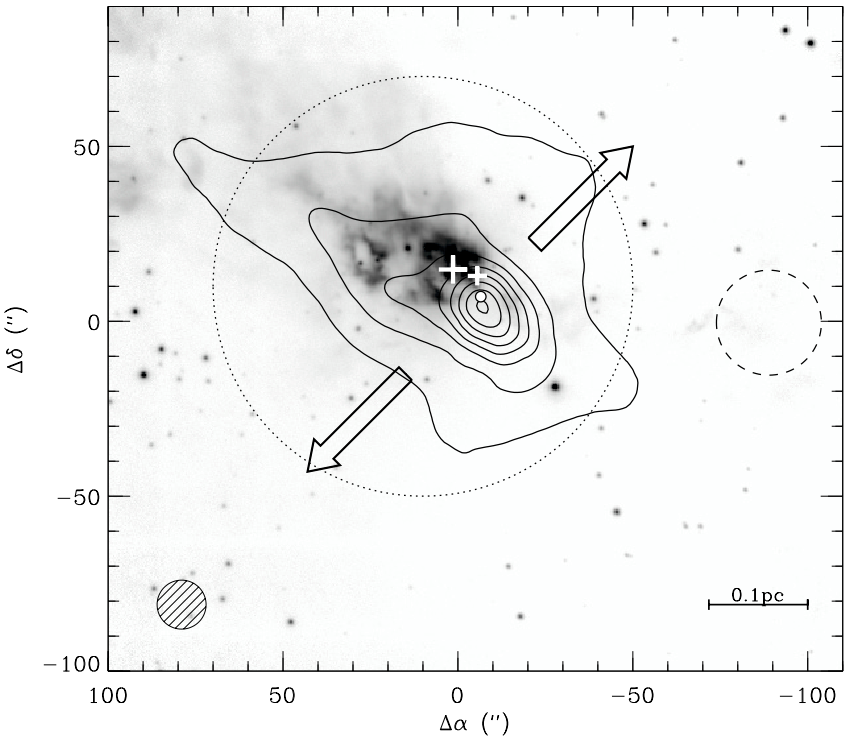

Fig. 1. Grayscale K-band image over-plotted with SCUBA 850 μm contours of Cep A showing the stellar and dust content. The central position is at $\alpha(2000) = 22^{\rm h}56^{\rm m}18\overset{\rm s}{.}9, \delta(2000) = 62°01'42\overset{''}{.}6$. The 850 μm contours start at 1 Jy beam^{-1} and increment by 2 Jy beam^{-1}. The large and small white plus signs show the location of the IRAS and MSX point sources respectively (each with a positional accuracy of less than 5″). The small white circle near the center of the map marks the location of the high mass protostar, HW2. The arrows show the direction of the bipolar CO outflow observed by Rodríguez et al. (1980). The dashed circle at the western edge of the map shows the location of the starless core seen in the CS maps and the dotted circle, centered at (10, 10) with diameter 2′ defines the region over which the spectral line averages were calculated.

dust and the SCUBA beamsize of 14″, 1 Jy beam^{-1} corresponds to a visual extinction, $A_{\rm V} = 24$, or an extinction at K-band, $A_K = 2.4$. The infrared nebulosity lies within the extended sub-millimeter emission ($A_K \sim 5-8$) but is offset from the peak. There is one IRAS and one MSX point source in the region, slightly offset from each other. The IRAS-HiRes 12 μm and MSX 10 μm emission are both associated with the near-infrared nebulosity, but the 60 μm IRAS-HiRes image peak is closer to the maximum of the 850 μm map, which traces the cooler dust. This suggests a spread in ages and location of star formation in Cep A, with the youngest protostars more deeply embedded in the core and invisible at near- and mid-infrared wavelengths.

Spectral line maps and their comparison with the dust emission are shown in Figs. 2 and 3. In each case the emission has been integrated over the full extent of the line, including all hyperfine components in the case of N_2H^+. Figure 2 shows the combined BIMA+FCRAO data at 10″ resolution. Figure 3 shows these maps and the higher transition data smoothed to a uniform resolution of 30″. Due to their high dipole moments, CS and N_2H^+ both trace high volume densities over a range, $n_{\rm H_2} \sim 10^4-10^6$ cm^{-3}, for these transitions. The complex structure apparent in the line maps contrasts with the relative simplicity of the dust continuum emission. The spatial distribution of N_2H^+ is similar to that of the ammonia (Torrelles et al. 1993) and generally follows the 850 μm continuum emission, but N_2H^+ is notably absent toward the core center where the CS is strongest. This behavior is opposite to the situation in low mass cores where N_2H^+ is more centrally concentrated than CS (Tafalla et al. 2002).

The maps also reveal an apparently starless core located ~90″ to the west of the bright 850 μm peak, indicated by a dashed circle in Fig. 1. The core is detected in CS(2–1) and (5–4) but has only very weak N_2H^+(1–0) emission (Fig. 2) and no stars are seen in the near-infrared image. This core is on the edge of the SCUBA map where there is extended emission but

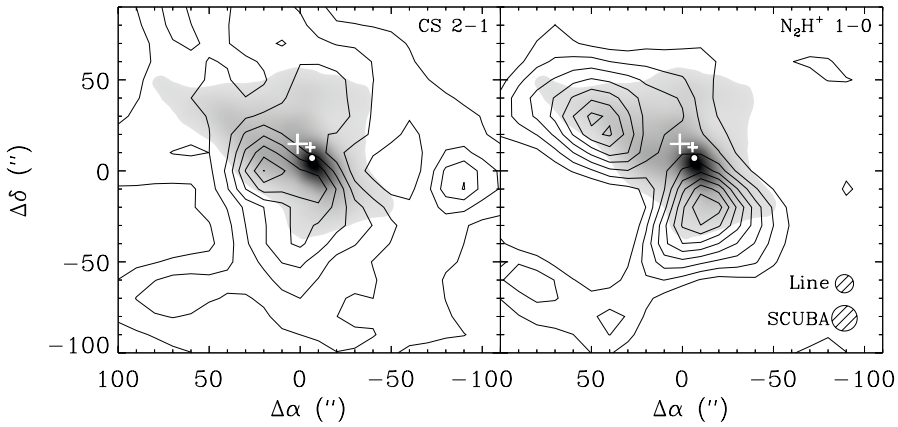

Fig. 2. Comparison of line and dust emission. The line maps have a resolution of 10″ and are contoured with starting levels and increments equal to 4.0 K km s^{-1} for CS (2–1) and 5.0 for N_2H^+ (1–0). The dust emission has a resolution of 14″ and is shown as a grayscale ranging from 1 to 15 Jy beam^{-1}. Symbols are as in Fig. 1.

no significant peak. The presence of CS (5–4) emission indicates large enough densities that we would expect to observe N_2H^+ emission, as in the large core. Since this emission is very weak, there must be a variation of abundances between the two cores. Potential reasons for the wide range of abundances throughout the region are discussed in Sect. 4.

3.2. Radiative transfer modeling

Our understanding of the structure and dynamics in Cep A is complicated by the small scale chemical variations within the core. Henceforth, we restrict attention to the large scale properties of the region as if observed with a 2′ Gaussian beam centered at offset (10, 10). The size and location of the averaging region was chosen so as to be broadly centered on the sub-millimeter continuum map but also to include the most prominent CS and N_2H^+ structures within the core. The averaging region is indicated on the continuum and line maps in Figs. 1 and 3. Averaged line profiles are displayed in Fig. 4. This figure also includes the line profile for $C^{34}S$(2–1). This isotopomer of CS, which is less abundant and therefore optically thinner, peaks near the same velocity as the dip in the average CS(2–1) spectrum. We therefore conclude that the two peaks in the latter are due to radiative effects (self-absorption) and not to two kinematically independent features along the line of sight. Although individual CS profiles show both blue- and red-shifted self-absorption that may be due to a mix of infall, outflow, and rotation (Di Francesco et al. 2001), the average CS(2–1) profile has a blue-shifted peak brighter than the red-shifted one, indicating that infall is the dominant effect on the scale of the core (Leung & Brown 1977).

In order to examine the properties of the large scale structure and dynamics, we modeled the core average line profiles using the radiative transfer code, ratran (Hogerheijde & van der Tak 2000). Collisional rate coefficients for CS are from Turner et al. (1992) and for N_2H^+ from Monteiro (1985, and references therein). From the brightness temperature of the N_2H^+ and assuming an excitation temperature equal to the dust temperature, 35 K, we estimate the optical depth of each hyperfine component to be less than 0.1. For the purposes of the modeling, therefore, we can ignore the complicated hyperfine structure (7 components at J = 1–0 and 45 at J = 3–2) and simply match the integrated intensity of each rotational transition.

The inputs to the radiative transfer model include the density, temperature, and velocity structure of the core and the abundances of each molecule. However, many parameters are constrained by related observations and results. The remaining free parameters, eight in all, were then varied so as to fit the profiles of each of the three CS transitions and the integrated intensity of the two N_2H^+ transitions.

3.2.1. Model inputs

The 850 μm map in Fig. 1 allows us to measure the column density profile of the core and thereby estimate the volume density. Since the radiative transfer model is one-dimensional, we approximated the density structure as a radial function by calculating the average flux in concentric elliptical annuli centered on the peak of the emission. The equivalent radii were defined as the geometric mean of the semi-major and semi-minor axes of each ellipse. The column density was determined by assuming a dust temperature of 35 K (Moriarty-Schieven et al. 1991) and a mass-opacity κ = 0.02 cm^2 g^{-1} (Ossenkopf & Henning 1994). The volume density was then derived by assuming a path length through the core equal to twice the equivalent radius. The resulting density profile was fit to a Plummer-like model,

$$n_{\mathrm{H_2}}(r) = n_0\left[1 + \left(\frac{r}{r_0}\right)^2\right]^{-\alpha/2},$$

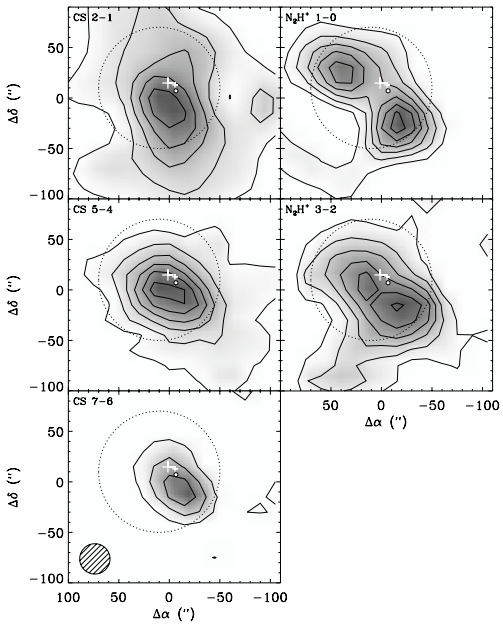

Fig. 3. Line maps of the Cepheus A core shown as grayscale with contours overlayed. Positions are given in offset coordinates with the same central position as Fig. 1. CS maps are shown in the left panels and N_2H^+ in the right. The maps have been smoothed to a uniform 30″ resolution. The contour starting levels and increments for each map are 4.0 K km s^{-1} (CS 2–1), 4.0 (CS 5–4), 1.5 (CS 7–6), 5.0 (N_2H^+ 1–0), and 3.0 (N_2H^+ 3–2). Note the isolated core in the CS(2–1) map ∼ 90″ west of center (see text for discussion). The 2′ diameter circle shows the region over which the data were averaged to analyze the large scale dynamics of the core, and symbols are as in Fig. 1.

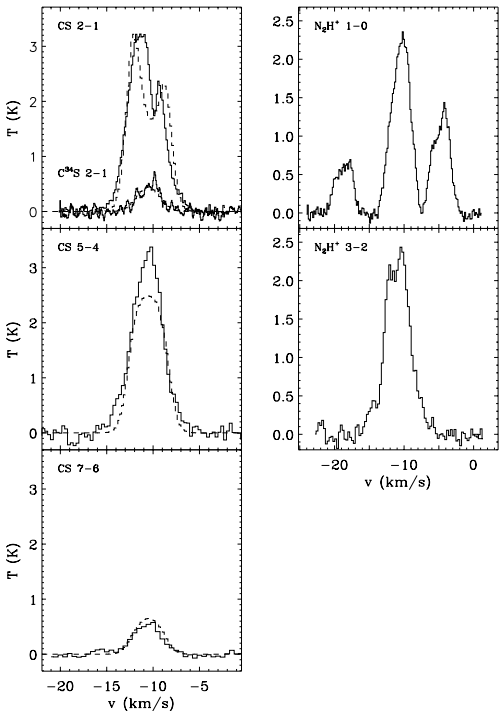

Fig. 4. Averages of CS and $C^{34}S$ (2–1) (*left*) and N_2H^+ (*right*) spectra over the central core region outlined by the circles in Figs. 1 and 3. The heavy solid lines show the observed data and the dashed line shows the modeled profiles for the CS lines. The multiple peaks in the N_2H^+ spectra is due to hyperfine structure which was not modeled (the fits matched only the integrated intensity of each rotational transition).

where $n_0 = 1.1 \times 10^7$ cm^{-3}, $r_0 = 0.02$ pc and $\alpha = 2.0$. The model discretizes this density profile over nine logarithmically spaced shells. Both measured and discretized density profiles are displayed in Fig. 5; there are no data points for radii smaller than 0.03 pc, the equivalent radius corresponding to a semi-minor axis of half the 850 μm beamsize, and for radii larger than 0.18 pc, which corresponds to the extent of the 850 μm map.

Additional inputs to the model include a temperature of 35 K, derived from a graybody fit to the SED (Moriarty-Schieven et al. 1991), and a systemic velocity and velocity dispersion derived from fitting the optically thin N_2H^+(1–0) line, $v_{\rm core} = -10.5$ km s^{-1} and $\sigma_{\rm core} = 1.2$ km s^{-1}, respectively. A constant temperature and velocity dispersion were adequate to model the core.

To model the observed self-absorption in the CS(2–1) line, we found that we required a low excitation (and therefore low density) and low velocity dispersion ($\sigma_{\rm env} = 1.1$ km s^{-1}) outer shell. The low velocity dispersion is required by the narrowness of the observed absorption dip. The overall model has 10 shells therefore, but it can effectively be considered as two layers; a power law core on the inside and a low density outer envelope. The free parameters in the model are the inner core cutoff radius, the size, density, velocity dispersion and relative velocity of the envelope and the molecular abundances in the core and envelope.

The values for the molecular abundances were guided by observations of other cores and theoretical models. In cold molecular cloud cores prior to star formation, the chemistry is dominated by low-temperature gas-phase ion-molecule and neutral-neutral reactions (van Dishoeck & Blake 1998). During the cold collapse phase, however, the density becomes so high that many molecules freeze onto grain surfaces. Tafalla et al. (1998) find that, in low mass star forming cores, the abundances of the tightly bound sulfur-bearing molecules such as CS begin to exhibit large depletions at densities in the range, $n_{\rm H_2} \sim 2{-}6 \times 10^4$ cm^{-3}. This behavior is in contrast to that of N_2H^+ which, due to the low binding energy of the precursor molecule N_2, depletes only at the highest densities

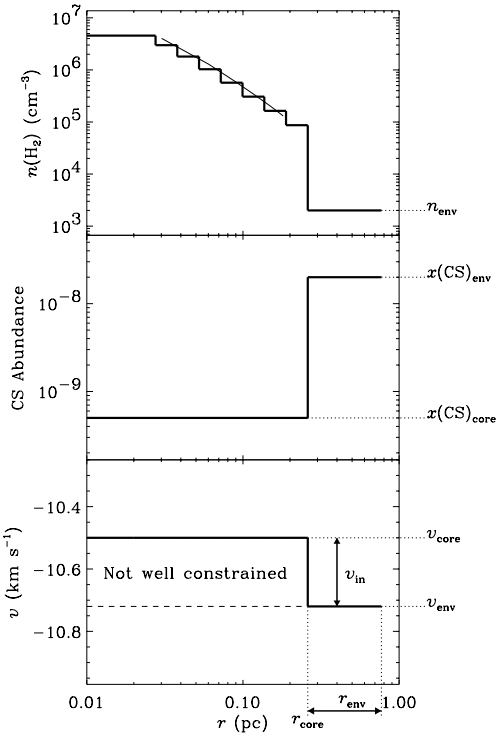

Fig. 5. Radial profiles of H_2 volume density, core-envelope CS abundance and velocity profiles used in the best fit model. Relative motions in the inner region, $r < r_{core}$, were not well constrained by the data. The thin solid line shows the H_2 density profile derived from the 850 μm data (see text).

(Bergin & Langer 1997). Based on these results, we assume a constant abundance of N_2H^+ but allow the CS abundance to vary. As we show later, we fit the data with a simple "jump" model where the CS is depleted in the inner dense core relative to a lower density outer envelope. This is a similar abundance profile to the detailed chemical modeling of the high mass star forming region, AFGL 2591, by Doty et al. (2002).

3.2.2. Model results

By varying the density, size and velocity of the envelope, and the CS abundance in the core and envelope, we were able to fit the integrated intensities of the three observed CS transitions to within 20% and reproduce the asymmetry in the (2–1) line reasonably well. The observed and model CS spectra are compared in Fig. 3. The parameters of the fit are tabulated in Table 1, where r_{core} is the inner core cut-off radius, r_{env}, n_{env} and $v_{in} = v_{env} - v_{core}$ are the size, density and relative velocity of the outer envelope, and $x(CS)_{core}$ and $x(CS)_{env}$ are the CS abundances in the core and the envelope

Table 1. Fit parameters.

Parameter	Value
r_{core}	0.26 pc
r_{env}	0.51 pc
n_{env}	2×10^3 cm^{-3}
σ_{env}	1.1 km s^{-1}
v_{in}	−0.22 km s^{-1}
$x(CS)_{core}$	5×10^{-10}
$x(CS)_{env}$	2×10^{-8}
$x(N_2H^+)$	3×10^{-11}

respectively. The density, velocity, and CS abundance profiles are graphed in Fig. 5 and annotated with the above parameters. Simultaneously, the N_2H^+ (1–0) and (3–2) integrated intensities were also matched: we found 8.1 and 9.5 K km s^{-1} respectively for the modeled values, whereas the observed values are 9.7 and 8.2 K km s^{-1} for the (1–0) and (3–2) transitions respectively. These results correspond to a match of 16 and 15% respectively. Finally, we also fitted the $C^{34}S$ (2–1) integrated intensity, using an abundance $x(C^{34}S) = x(CS)/30$. We found a modeled value of 1.4 K km s^{-1} which is within 8% of the observed value (1.5 K km s^{-1}).

Despite the good overall fit, some slight discrepancies remain. The observed CS(5–4) is stronger than the model by 20%. This may be due to calibration error or may reflect a more complex CS abundance profile in the core. The observed CS(2–1) profile is slightly narrower than the model spectrum, perhaps due to the constant linewidth assumption in the core (the velocity dispersion of cores is expected to decrease with radius, Larson 1981). A more refined model with additional parameters would fit the data more closely but probably not with greater significance.

Since the model reproduces the blue-red peak asymmetry in the CS(2–1) spectrum well we are confident that we have accurately measured the average infall speed of the envelope, $v_{in} = -0.22$ km s^{-1}. However, the size of the infalling region is not well determined because the average profiles of the higher transition CS lines are not self-absorbed and therefore relative motions of the higher density gas could not be constrained. Nevertheless, we were unable to model the spectra with a static outer shell and an inner collapse: no such set of parameters could reproduce the dip in the CS (2–1) spectrum. That is, our results indicate a *large scale collapse from the outside-in.*

4. Discussion and summary

The line observations reveal a complex chemistry in the core. The CS emission is concentrated toward the center near the peak of the 850 μm dust emission and the youngest, most embedded protostars. However, the N_2H^+ map shows two prominent cores offset on either side of the dust peak. The presence of CS and absence of N_2H^+ toward the star forming center of the core is likely due to the fact that neutral molecules released from the dust grains in the hotter region surrounding the protostars preferentially destroy ions such as N_2H^+ (Bergin 2000).

The maps also reveal a small starless core toward the west of the main core. The relatively strong CS and weak N_2H^+ emission toward this core suggests that it has only recently formed (Bergin & Langer 1997). Williams & Myers (1999) found a starless core with similar chemical properties in the Serpens NW cluster.

Despite the chemical complexities on small scales, the average CS(2–1) spectrum is asymmetrically self-absorbed suggesting large scale collapse. Using the Hogerheijde & van der Tak radiative transfer code, we fit the average CS and N_2H^+ spectra with a spherical model consisting of an inner region with a Plummer-like density profile measured from archival SCUBA 850 μm data with constant temperature and linewidth. The best fit model that matches the three CS profiles has a low CS abundance in the inner region and an outer, infalling envelope with a low density and higher CS abundance. The depletion toward the center matches chemical evolution model expectations (Bergin & Langer 1997) and the envelope CS abundance is similar to that in the extended ridge of Orion (van Dishoeck & Blake 1998). The fit also matched the integrated intensities of the two N_2H^+ spectra with a constant abundance similar to that found in B68 (Bergin et al. 2002). In practice the maps show that the N_2H^+ must deplete toward the core center (see also Doty et al. 2002) but we have not attempted to match the complicated small scale chemistry and our model fit for the N_2H^+ abundance should only be considered an average, weighted by column density, over the core.

The CS(2–1) self-absorption requires a large scale outside-in collapse. The velocity of the collapse could be accurately measured but the depth of the collapse region could not, due to the absence of self-absorption in the higher transition CS lines. At 0.22 km s^{-1}, the infall velocity is sub-sonic for a gas temperature of 35 K. The mass infall rate of the envelope can be estimated from the ratio of its mass, $M_{\rm env} = 240\ M_\odot$ determined from its size and density, and the time for the outer edge to reach the core center,

$$\dot{M}_{\rm in} = \frac{M_{\rm env} v_{\rm in}}{r_{\rm env} + r_{\rm core}} = 7 \times 10^{-5}\ M_\odot {\rm yr}^{-1}.$$

This may only be a lower limit to the total mass infall rate at the center if the inner region is also collapsing. Nevertheless, the envelope mass infall rate alone is more than an order of magnitude higher than typical mass infall rates for solar mass protostars (Zhou 1995).

Our data do not rule out inside-out collapse motions around individual protostars at higher densities on smaller size scales since the $\tau = 1$ surface of the CS(2–1) emission occurs at low densities and therefore at large scales. The multitude of sources, powerful outflows, and the complex chemistry would likely make an investigation of the small scale motions around individual protostars quite challenging.

On large scales, however, our picture is of a core with a Plummer-like density profile accreting low density gas subsonically. The CS abundance in the infalling envelope is similar to undepleted values in the ISM. The dissipation of turbulent support resulting in "cooling flows" may lead to core growth in this manner (Nakano 1998; Myers & Lazarian 1998; Williams & Myers 2000). The growing availability of dust continuum maps and multi-transition, multi-species line observations will lead to more refined structural and dynamical modeling and comparisons between different star forming environments in the future.

Acknowledgements. This work began when J.P.W. was a Jansky fellow and he thanks the NRAO for their support. The more recent analysis was supported by NSF grant AST-0324328. We thank Harold Butner for assistance with the observations at the Heinrich Hertz Telescope, Ted Bergin, Eric Herbst and Phil Myers for informative discussions, and the referee, Gary Fuller, for useful suggestions that improved the paper.

References

Beichman, C. A., Becklin, E. E., & Wynn-Williams, C. G. 1979, ApJ, 232, L47
Bergin, E. A., & Langer, W. D. 1997, ApJ, 486, 316
Bergin, E. A., Melnick, G. J., & Neufeld, D. A. 1998, ApJ, 499, 777
Bergin, E. A. 2000, in Astrochemistry: From Molecular Clouds to Planetary Systems, ed. Y. C. Minh, & E. F. van Dishoeck, Proc. IAU Symp., 197, 51
Bergin, E. A., Alves, J., Huard, T., & Lada, C. J. 2002, ApJ, 570, L101
Blauuw, A., Hiltner, W. A., & Johnson, H. L. 1959, ApJ, 130, 69
Carpenter, J. M. 2000, AJ, 120, 3139
Chen, H., Myers, P. C., Ladd, E. F., & Wood, D. O. S. 1995, ApJ, 445, 377
Di Francesco, J., Myers, P. C., Wilner, D. J., Ohashi, N., & Mardones, D. 2001, ApJ, 562, 770
Doty, S. D., van Dishoeck, E. F., van der Tak, F. F. S., & Boonman, A. M. S. 2002, A&A, 389, 446
Evans II, N. J., Becklin, E. E., Beichman, C., et al. 1981, ApJ, 244, 115
Evans II, N. J. 1999, ARA&A, 37, 311
Garay, G., & Lizano, S. 1999, PASP, 111, 1049
Hogerheijde, M. R., & van der Tak, F. F. S. 2000, A&A, 362, 697
Hughes, V. A., & Wouterloot, J. G. A. 1984, ApJ, 276, 204
Hughes, V. A. 1988, ApJ, 333, 788
Larson, R. B. 1981, MNRAS, 194, 809
Leung, C. M., & Brown, R. B. 1977, ApJ, 214, L73
Monteiro, T. S. 1985, MNRAS, 214, 419
Moriarty-Schieven, G. H., Snell, R. L., & Hughes, V. A. 1991, ApJ, 374, 169
Myers, P. C., & Lazarian, A. 1998, ApJ, 507, L160
Nakano, T. 1998, ApJ, 494, 587
Ossenkopf, V., & Henning, T. 1994, A&A, 291, 943
Rodríguez, L. F., Ho, P. T. P., & Moran, J. M. 1980, ApJ, 240, L149
Sargent, A. I. 1977, ApJ, 218, 736
Sridharan, T. K., Beuther, H., Schilke, P., Menten, K. M., & Wyrowski, F. 2002, ApJ, 566, 931
Tafalla, M., Mardones, D., Myers, P. C., et al. 1998, ApJ, 504, 900
Tafalla, M., Myers, P. C., Caselli, P., Walmsley, C. M., & Comito, C. 2002, ApJ, 569, 815
Torrelles, J. M., Verdes-Montenegro, L., Ho, P. T. P., Rodríguez, L. F., & Cantó, J. 1993, ApJ, 410, 202
Turner, B. E., Chan, K.-W., Green, S., & Lubowich, D. A. 1992, ApJ, 399, 114
van Dishoeck, E. F., & Blake, G. A. 1998, ARA&A, 36, 317
Williams, J. P., & Myers, P. C. 1999, ApJ, 518, L37
Williams, J. P., & Myers, P. C. 2000, ApJ, 537, 891
Williams, J. P., Plambeck, R. L., & Heyer, M. H. 2003, ApJ, 591, 1025
Zhou, S. 1995, ApJ, 442, 685

The Astrophysical Journal, 604:414–419, 2004 March 20

DETECTION OF COOL DUST AROUND THE G2 V STAR HD 107146

Jonathan P. Williams,[1] Joan Najita,[2] Michael C. Liu,[1,3] Sandrine Bottinelli,[1] John M. Carpenter,[4] Lynne A. Hillenbrand,[4] Michael R. Meyer,[5] and David R. Soderblom[6]

Received 2003 May 13; accepted 2003 December 1

ABSTRACT

We report the detection of dust emission at submillimeter wavelengths from HD 107146, a G2 V star with an age estimated to lie between 80 and 200 Myr. The emission is resolved at 450 μm with a size 300 AU $\times$ 210 AU. A fit to the spectral energy distribution gives a dust temperature of 51 K and a dust mass of 0.10 $M_{\oplus}$. No excess emission above the photosphere was detected at 18 μm, showing that there is very little warm dust and implying the presence of a large inner hole, at least 31 AU ($\sim$1″) in radius, around the star. The properties of this star-disk system are compared with similar observations of other systems. We also discuss prospects for future observations that may be able to determine whether the inner hole is maintained by the dynamical effect of an unseen orbiting companion.

Subject headings: circumstellar matter — planetary systems — stars: individual (HD 107146)

On-line material: color figure

1. INTRODUCTION

Protostellar disks dissipate over a period of several Myr as their constituent dust and gas either accrete onto the star, are dispersed by processes such as stellar winds and photoevaporation, or aggregate into planetesimals (Hollenbach, Yorke, & Johnstone 2000). Possible observational examples of disk systems in the process of dissipating are the "transitional disks," a thus far small class of objects that includes sources such as V819 Tau (Skrutskie et al. 1990), HR 4796A (Jura et al. 1993; Jayawardhana et al. 1998; Koerner et al. 1998; Schneider et al. 1999; Telesco et al. 2000), and HD 141569A (Weinberger et al. 1999; Augereau et al. 1999; Fisher et al. 2000).

Dramatic evidence for disk dispersal through planetesimal formation is the detection of numerous planets, and some planetary systems, around nearby stars (Marcy, Cochran, & Mayor 2000). Planetesimals are believed to grow into planets through collisional agglomeration. However, collisions between planetesimals are also expected to create a cascade of smaller particles, and in this way a relatively old circumstellar disk may regenerate its own dust.

Such second-generation dust was first detected around main-sequence stars by *IRAS* (Aumann et al. 1984). The *IRAS* results indicated that $\sim$15% of main-sequence stars possess dusty disks (Lagrange, Backman, & Artymowicz 2000), the brightest of which have been detected at submillimeter wavelengths (Zuckerman & Becklin 1993; Greaves et al. 1998; Sylvester, Dunkin, & Barlow 2001; see also Wyatt, Dent, & Greaves 2003). Submillimeter observations are useful because they place strong constraints on the dust mass of the disk, because of the low optical depth of dust grains in the submillimeter compared with their opacities at shorter wavelengths. Because of their small angular size and weak emission, only four debris disk systems have been spatially resolved at these wavelengths to date (Holland et al. 1998; Greaves et al. 1998). The maps of these systems show interesting asymmetries that have been interpreted as the dynamical signature of a planetary companion (Holland et al. 2003; Wilner et al. 2002; Greaves et al. 1998).

Although the majority of the well-studied debris (and transitional) disk systems surround early-type stars (Vega, Fomalhaut, β Pic, HR 4796A, and HD 141569A are all A stars), the expectation is that the process of disk dissipation and the regeneration of dust through planetesimal collisions is also a part of the evolutionary history of lower mass stars and, indeed, our own solar system. Thus, it is of considerable interest to identify debris disks associated with young solar-mass stars, since the detailed study of these objects can provide direct insight into the evolutionary history of our solar system. The ϵ Eri system ($d = 3.2$ pc) is one exciting example (Greaves et al. 1998; Hatzes et al. 2000). In this paper, we present submillimeter observations of a dusty disk around a close solar analog, the nearby young G2 V star HD 107146.

HD 107146 was first identified as an "excess dwarf" on the basis of *IRAS* colors by Silverstone (2000). We observed it as part of a program to provide ground-based support for the Formation and Evolution of Planetary Systems *Spitzer Space Telescope* Legacy program.[7] HD 107146 was selected for inclusion in the Legacy program based on its distance (28.5 pc; Perryman et al. 1997) and its high Ca II H and K index, $\log R'_{\rm HK} = -4.28$, which is indicative of youth. An age range can be estimated from its lithium equivalent width, 125 mÅ (Wichmann, Schmitt, & Hubrig 2003), which places it at the lower envelope of the 125 Myr Pleiades distribution

[1] Institute for Astronomy, University of Hawaii, 2680 Woodlawn Drive, Honolulu, HI 96822; jpw@ifa.hawaii.edu, mliu@ifa.hawaii.edu, sandrine@ifa.hawaii.edu.

[2] National Optical Astronomy Observatory, 950 North Cherry Avenue, Tucson, AZ 85719; najita@noao.edu.

[3] Hubble Fellow.

[4] Department of Astronomy and Astrophysics, MS 105-24, California Institute of Technology, 1201 East California Boulevard, Pasadena, CA 91125; jmc@astro.caltech.edu, lah@astro.caltech.edu.

[5] Steward Observatory, University of Arizona, 933 North Cherry Avenue, Tucson, AZ 85721; mmeyer@as.arizona.edu.

[6] Space Telescope Science Institute, 3700 San Martin Drive, Baltimore, MD 21218; drs@stsci.edu.

[7] Information concerning this program can be found at http://feps.as.arizona.edu.

(Soderblom et al. 1993) but above the distribution for the 250 Myr old M34 (Jones et al. 1997) at the effective temperature of a G2 V star. Wichmann et al. also show that its space motions are similar to those of the Pleiades moving group. Its X-ray luminosity, $L_X = 2 \times 10^{29}$ ergs s^{-1} (Voges et al. 1999), is again similar to those of solar-type Pleiades stars (Micela et al. 1999) but weaker than that of the average solar-type stars in the 80 Myr old α Per cluster (Prosser et al. 1996). Together, these indicators suggest an age for HD 107146 between 80 and 200 Myr. Its location in the H-R diagram is also consistent with this age range but allows for the possibility that it may be as young as 30 Myr if the star has just reached the main sequence.

Our observations, made at submillimeter and mid-IR wavelengths, are detailed in § 2. The results from the imaging and fits to the spectral energy distribution (SED) are presented in § 3. The SED shows clear evidence for a large inner hole, although the hole is too small to be resolved in the submillimeter maps presented here. In § 4, we compare the properties of the HD 107146 star-disk system to those of other debris and transitional disk systems. We also discuss prospects for future observations that may be able to determine whether the inner hole is maintained by the dynamical effect of an unseen orbiting companion.

2. OBSERVATIONS

HD 107146 was mapped using the Submillimeter Common-User Bolometric Array (SCUBA) at the James Clerk Maxwell Telescope (JCMT) on Mauna Kea, Hawaii, in dry, stable conditions during 2003 February 17–19. Precipitable water vapor levels were less than 0.5–1 mm during the observations and zenith optical depths ranged from 0.1 to 0.18 at 850 μm and from 0.4 to 0.85 at 450 μm. Observations were made simultaneously at 450 and 850 μm using a 64 point "jiggle" pattern to produce Nyquist-sampled images at each wavelength. Two maps were rejected in the reduction process because of an error in the telescope tracking software at high elevation (I. Coulson 2003, private communication). The final maps presented here are the median of 23 maps made at a range of image rotation angles on the array rebinned to a 1″ rectangular grid in equatorial coordinates. Pointing was checked between individual maps using Virgo A and 3C 273 and was accurate to an rms error of 2.″5. Calibration was carried out by observing the CRL 618 planetary nebula and bootstrapped to observations of Mars later in the night. Based on the gain variations from night to night, the calibration accuracy is estimated to be 20% at 850 μm and 30% at 450 μm. The total on-source integration time was 4.0 hr, and the noise in the final maps was 4 and 13 mJy beam^{-1} at 850 and 450 μm, respectively. The resulting peak signal-to-noise ratio is $\sim$7 in both maps, but the calibration uncertainty dominates the error in the absolute flux measurements.

We obtained mid-IR photometry of HD 107146 from the Keck II Telescope on Mauna Kea, Hawaii, using the facility instrument LWS. We observed the star on 2003 February 19 and 20 UT, using filters centered at 11.7 μm (10.5–12.9 μm) and 17.8 μm (17.3–18.2 μm). Contemporaneously and at similar airmasses, we observed the bright standard stars α CrB and μ UMa from Tokunaga (1988) for photometric calibration. Both nights were characterized by dry conditions, with an estimated 0.5–1.5 mm of precipitable water, as determined from sky dip measurements from the JCMT. Seeing conditions were poor and variable, leading to mid-IR images with 0.″4 to 0.″6 FWHM. Observations were conducted in the standard "chop/nod" mode, which involves switching between three sky positions using fast chopping of the secondary mirror and slower nodding of the telescope itself. This allows for effective subtraction of the very bright and variable thermal emission from the sky and telescope in the reduction process.

TABLE 1
Flux Measurements

λ (μm)	Flux (mJy)	Error (mJy)
11.7	175	10
17.8	85	8
450	130	40[a]
850	20	4[a]

[a] Calibration uncertainty.

HD 107146 was well detected in both filters, with a formal signal-to-noise ratio of less than 15 for the 17.6 μm data and less than 50 for the 11.7 μm data. However, the seeing conditions limited the photometric precision, because of varying image quality from the science target to the standard stars. These conditions also prevented any useful constraints on any extended mid-IR emission from HD 107146. Photometric errors were first determined from the scatter in measurements done with apertures scaled by the FWHM of the images. We then added in quadrature an error term to account for seeing mismatch (10 mJy at 11.7 μm; 8 mJy at 17.6 μm), estimated from analyzing curve-of-growth photometry for standard stars observed during the course of the entire night. The absolute flux calibration is based on the flux of Vega (α Lyr) compiled by Tokunaga (1988). The LWS and SCUBA fluxes are listed in Table 1.

3. RESULTS

The resulting maps of the emission at 450 and 850 μm are shown in Figure 1. There is a 2.″9 offset between the two maps, as measured by Gaussian fits to the data clipped at the FWHM level. The centroid of the emission is consistent with the stellar position to within 4.″4 (450 μm) and 1.″6 (850 μm). It is not clear how significant such small offsets are, given the relatively low signal-to-noise ratio in the data and the possibility of systematic pointing errors as large as 2.″5. No other source within this angular range of the star was apparent in the Digital Sky Survey, Two Micron All Sky Survey (2MASS), the Keck imaging at 11.7 and 17.8 μm, or the Faint Images of the Radio Sky at Twenty cm survey. In addition, Blain et al. (1999) predict 100–300 sources deg^{-2} with fluxes greater than 20 mJy at 850 μm, implying a probability less than 1.4×10^{-3} that an unrelated background object this bright would be found within 4.″4 of the star. Since the probability of unrelated submillimeter emission is very low, we assume that the SCUBA source is a disk associated with the star and discuss its properties in this context.

Allowing for pointing errors, the resolutions of the maps are 14.″5 at 850 μm and 8″ at 450 μm. The Gaussian fits give sizes of 15.″1 × 14.″9 and 13.″2 × 10.″9 (position angle −35°), respectively. The elongation at 450 μm is apparent at the half-power level and is therefore not due to the JCMT beam pattern, which shows significant noncircularity only at the 10% level. The slight extension in the 450 μm map is also

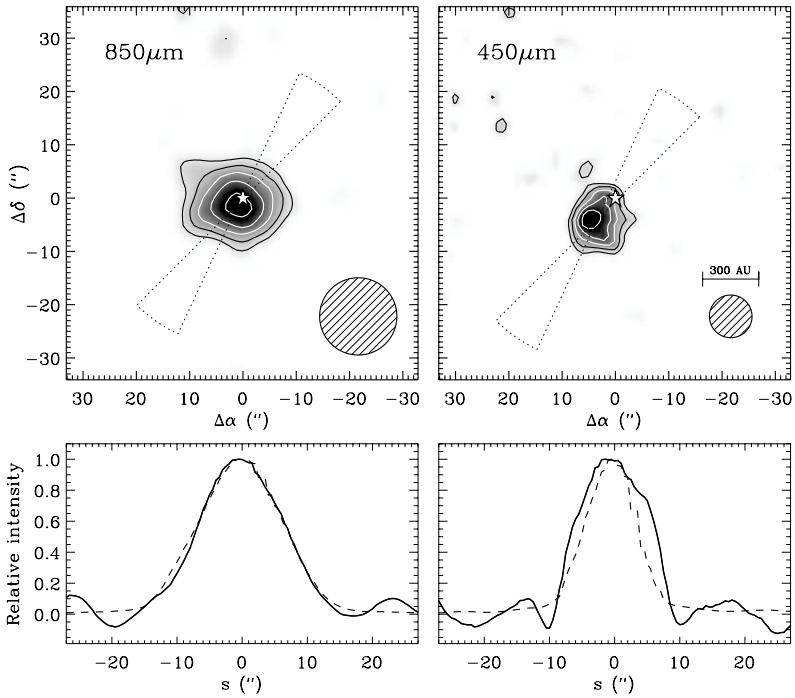

FIG. 1.—*Top*: SCUBA images of the dust emission around HD 107146. Coordinates are offset from the J2000.0 position of the star: epoch 2003.13, $\alpha = 12^{h}19^{m}6\overset{s}{.}46$, $\delta = 16^{\circ}32'53\overset{''}{.}4$, indicated by the star symbol. *Top left*: Emission at 850 μm. Contour levels begin at 2 σ and increment by σ, where $\sigma = 4$ mJy beam^{-1} is the noise in the map. The gray scale runs from 1 to 7 σ. *Top right*: Emission at 450 μm; contours begin at 3 σ and increment by σ, where $\sigma = 13$ mJy beam^{-1}. The gray scale runs from 2 to 8 σ. The beam sizes, 14″.5 at 850 μm and 8″ at 450 μm, are indicated by the hashed circles in the lower right corner of each figure. Inspection shows that the half-power point of the 450 μm image ($\sim$3.5 σ) is slightly greater than the beam size. Averaged cuts of the source and Mars are shown in the bottom panels for each wavelength. The cuts are centered on the peak of emission and averaged over position angles $-35^{\circ} \pm 10^{\circ}$, outlined by dotted lines in each image. The Mars profile is shown as the dashed line and is significantly narrower than that of HD 107146 in the higher resolution 450 μm image. [*See the electronic edition of the Journal for a color version of this figure.*]

seen in crosscuts through the image along the major axis. To increase the signal-to-noise ratio, an average crosscut over a range of position angles $-35^{\circ} \pm 10^{\circ}$ centered on the peak of emission is shown for each wavelength in the bottom panels of Figure 1. The same crosscut averaging, shown as dashed lines, was performed for a map of Mars, taken from the last night of observations, February 19, when the Martian diameter was 5″.7. We conclude that the disk around HD 107146 is marginally resolved at the 8″ resolution of the 450 μm data. Subtracting the beam size in quadrature from the Gaussian fit gives an angular size of 10″.5 × 7″.4 for the disk, corresponding to 300 AU × 210 AU.

The fluxes measured from the LWS and SCUBA observations are listed in Table 1. The SED of the source, from optical to submillimeter wavelengths, is plotted in Figure 2. The *UBVRI* photometry is from Landolt (1983), the near-IR fluxes in the *JHK* bands are from 2MASS, and the 10 μm point is from Palomar observations (Metchev, Hillenbrand, & Meyer 2004). *IRAS* fluxes were determined by color correcting the quoted values in the Faint Source catalog. The *IRAS* 12 μm flux is consistent with the Keck 11.7 μm observation and is not plotted. The stellar photosphere was fitted by a Kurucz model ($T_{\rm eff} = 5750$ K, $\log g = 4.5$, and solar metallicity) with a power-law extrapolation beyond 10 μm. Strong excess emission is apparent beyond 25 μm. In order to compare the properties of the excess with that detected from other debris disk systems, we fitted the disk SED using a single-temperature modified blackbody with emission efficiency $Q_{\lambda} = 1 - \exp\left[-(\lambda_0/\lambda)^{\beta}\right]$, which has asymptotic behavior: $Q_{\lambda} = 1$ for $\lambda \ll \lambda_0$ and $Q_{\lambda} = (\lambda/\lambda_0)^{\beta}$ for $\lambda \gg \lambda_0$. The critical wavelength, λ_0, was set to 100 μm for consistency with the assumptions made in previous analyses of debris disk SEDs (Dent et al. 2000; Wyatt et al. 2003).

The parameters of the modified blackbody fit were measured using a least-squares fit to the data. Errors were estimated via fits to multiple simulations of the dust excess SED. Simulated data points were drawn from a Gaussian distribution, with the mean and standard deviation as determined by the observed data. The resulting distributions of best-fit parameter values are $T = 51 \pm 4$ K and $\beta = 0.69 \pm 0.15$. Similarly low values of β are found for other disks around main-sequence stars (Dent et al. 2000). The dust mass, based on the fitted flux at

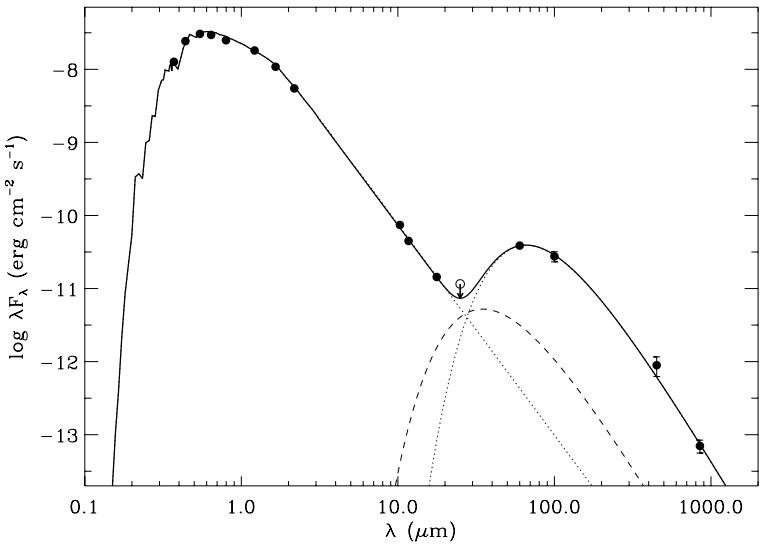

FIG. 2.—Optical to submillimeter SED of HD 107146. The open circle at 25 μm represents an upper limit from the *IRAS* Faint Source catalog. All other points represent detections, with error bars shown when the error exceeds the symbol size. The double-peaked distribution is modeled as the sum of a Kurucz model of the stellar spectrum and a modified blackbody fit to the points longward of 25 μm ($T = 51$ K, $M_d = 0.10\ M_\oplus$, $\beta = 0.7$). The individual contribution of each component is shown by the dotted lines and the sum of the two by the solid line. The dashed line shows the maximum allowable $T = 100$ K dust component that fits the constraint of the *IRAS* 25 μm upper limit. This component is not included in the overall fit shown by the solid line.

850 μm and assuming a dust mass absorption coefficient of $\kappa_{850} = 1.7$ cm^2 g^{-1}, is $M_d = 0.10 \pm 0.02\ M_\oplus$. This value of κ_{850} is chosen for consistency with Holland et al. (1998) and Greaves et al. (1998), but is on the high end of calculated values (Pollack et al. 1994). For the full range of $\kappa_{850} = 0.4$–1.7 cm^2 g^{-1} discussed in Pollack et al., the corresponding mass range is $M_d = 0.10$–$0.43\ M_\oplus$. As with all submillimeter observations, the inferred dust masses do not include a potentially dominant mass component that resides in larger bodies (grains and planetesimals) subtending a negligible solid angle. The mean parameter fit is shown in Figure 2.

The single-temperature fit is a simplification that is warranted by the small number of data points. Nevertheless, the large dip in the SED at 25 μm imposes a strong limit on the mass of warmer dust that may be present in the system. To illustrate this constraint, a $T = 100$ K, $\beta = 0.7$ modified blackbody component was added to the SED fit and increased until the *IRAS* 25 μm upper limit was exceeded. This maximum allowable contribution, which corresponds to a mass limit of $M_d(T = 100\ \mathrm{K}) = 7 \times 10^{-4}\ M_\oplus$, is shown in Figure 2 but was not included in the overall fit shown. The Keck 18 μm measurement tightly constrains the presence of still warmer dust to a 3 σ limit of $M_d(T = 200\ \mathrm{K}) < 3 \times 10^{-5}\ M_\oplus$.

The limits on dust cooler than 50 K are less stringent, since such dust emits less per unit mass and does so at longer wavelengths. The minimum grain temperature is 23 K for blackbody particles at the measured outer radius of the disk, 150 AU from the star. In practice, the effect of a range of cool dust temperatures is indistinguishable from changes in the wavelength dependence of the grain emissivity, parameterized by β. However, without changing the parameters of the fit in Figure 2, 0.13 $M_\oplus$ of 23 K dust can be added before the 850 μm 3 σ upper limit is exceeded. Thus, a significant fraction of the total dust mass may reside in cooler dust.

4. DISCUSSION AND SUMMARY

We have detected strong submillimeter excess emission from HD 107146, a G2 V star with an age estimated to lie in the range 80–200 Myr. Based on a fit to the SED of the system, the mass of the emitting dust is estimated to be 0.10 $M_\oplus$ or larger. We also find that the disk is marginally resolved at 450 μm. The constraints placed by these observations on the mass, temperature, and physical extent of the dust in the system are compared in Table 2 with the properties of other well-studied debris disk systems.

Four of the six stars in Table 2 are A stars, a probable bias due to the relatively high luminosity of these systems at far-IR and submillimeter wavelengths. Nevertheless, despite the range in central star masses and luminosities, the disks have similar properties and follow several trends. The HD 107146 disk is quite massive, comparable in mass to the β Pic disk. Although it lies noticeably above the trend of decreasing mass with age that is defined by HR 4796A, β Pic, Fomalhaut, and Vega (Holland et al. 1998), it is within the scatter in the mass-age relation found for larger samples of dust disks (Wyatt et al. 2003). The fractional dust luminosity (L_d/L_*) of HD 107146 is also large; it is half that of β Pic, more than 10 times that of Fomalhaut, and consistent with the trend of decreasing L_d/L_* with age (Spangler et al. 2001). Table 2 also indicates an apparent trend of decreasing outer disk radius with age. Perhaps this trend, admittedly of low statistical significance at

TABLE 2
PROPERTIES OF SPATIALLY RESOLVED SUBMILLIMETER DISKS AROUND CLASS V STARS

Source	Spectral Type	Age (Myr)	d (pc)	L_* ($L_\odot$)	L_d/L_* (10^{-5})	R_{in} (AU)	R_{out} (AU)	T_d (K)	M_d ($M_\oplus$)	References
HR 4796A.....	A0	3–10	67.1	21	500	~50	~200	110	0.250	1, 2, 3, 4
β Pic.....	A5	10–100	19.3	8.9	200	~20	210	85	0.096	5, 6, 7, 8
HD 107146	G2	80–200	28.5	1.1	120	>31	150	51	0.100	9
Fomalhaut.....	A3	100–300	7.7	13	10	60	160	40	0.018	5, 6, 7
Vega.....	A0	150–550	7.8	60	2	70	90	80	0.009	5, 6, 7, 10
ϵ Eri.....	K2	$\leq 10^3$	3.2	0.3	8	30	60	35	0.005	6, 7, 11

REFERENCES.—(1) Jura et al. 1998; (2) Jayawardhana et al. 1998; (3) Greaves, Mannings, & Holland 2000; (4) Schneider et al. 1999; (5) Holland et al. 1998; (6) Spangler et al. 2001; (7) Dent et al. 2000; (8) Lagage & Pantin 1994; Pantin, Lagage, & Artymowicz 1997; (9) this work; (10) Wilner et al. 2002; (11) Greaves et al. 1998.

present, will be verified when a larger number of debris disk systems have been spatially resolved.

We also find that the local minimum in the SED at 25 μm places a strong limit on the amount of warm dust in the HD 107146 disk, $M_d(T = 51\ \mathrm{K})/M_d(T = 100\ \mathrm{K}) \gtrsim 140$. This lack of warm dust implies that the disk does not extend all the way to the star. The dust temperature, and therefore the size of this inner hole, depends on the grain size distribution and optical properties. For grains that emit as blackbodies at 850 μm, 51 K dust would lie at 31 AU (Wyatt et al. 1999). This is a lower limit to the inner radius, since smaller grains could achieve this temperature at greater distances from the star. The other disks listed in Table 2 have inner holes of similar size, as determined from spatially resolved images in thermal emission or scattered light, and are comparable in size to the Kuiper Belt in our solar system.

Inner holes are not by themselves long lasting, because Poynting-Robertson drag will cause dust to spiral in from the outer disk onto the central star on ~10 Myr timescales. Such inward migration would be evident in the SED by the presence of warm dust (Jura et al. 1998). Thus, the existence of inner holes has been explained as a consequence of either the dynamical sweeping of an orbiting companion (e.g., Vega; Wilner et al. 2002) or the sublimation of icy grains (e.g., HR 4796A; Jura et al. 1998). Since water ice sublimates at temperatures greater than 100 K (Pollack et al. 1994), this explanation can not apply to the HD 107146 disk, where the shape of the SED places a strong limit on the mass of such warm dust. The alternative explanation, that the inner hole is dynamically maintained by a closely orbiting companion, would require a fairly low mass companion. The best current limit on the existence of close companions is from Palomar adaptive optics imaging by Metchev & Hillenbrand (2004), who found no companions at detection limits of 11.2, 11.7, and 15.2 in absolute K-band magnitude at angular separations of 0.″5, 1″, and 2″, respectively. The corresponding mass limits for an age of 100 Myr are approximately $30M_J$, $25M_J$, and $10M_J$ (Burrows et al. 1997).

While it has been well recognized that the dynamical sculpting of disks by orbiting companions can produce inner holes and ringlike structures, recent studies have shown that the migration of dust in the presence of a residual gas disk can also induce ringlike structures in the dust distribution. For example, Takeuchi & Artymowicz (2001) have shown that the dust structures seen in the HR 4796A and HD 141569A systems are qualitatively similar to those expected to result from the coupling between gas and dust in disks. However, orbiting companions may also induce significant departures from axisymmetry in the dust distribution (e.g., Liou & Zook 1999; Ozernoy et al. 2000; Quillen & Thorndike 2002; Moro-Martín & Malhotra 2002), whereas such nonaxisymmetric structures cannot be produced by dust migration. Thus, demonstrating the existence of asymmetries in the dust distribution, either in thermal emission or scattered light, as well as measuring the gas content of the HD 107146 disk, is needed to distinguish between these two possibilities.

At a distance of 28.5 pc, HD 107146 is relatively nearby. Compared to the other sources listed in Table 2, it is more distant than the debris disk systems that have been spatially resolved at submillimeter wavelengths (β Pic, Vega, Fomalhaut, and ϵ Eri), but it is at half the distance of HR 4796A. Since the HD 107146 disk is just resolved at the shortest operating wavelength of SCUBA, and the submillimeter excess is relatively bright, the Submillimeter Array should be able to map the morphology of the emitting dust in greater detail. Phase referencing will provide a more accurate absolute position, and such observations could determine whether the dust is distributed axisymmetrically (e.g., in a ring) or in a more asymmetric distribution. For example, these observations may confirm the marginal evidence for an offset between the stellar position and the peak of the 450 μm emission found in the observations presented here (Fig. 1). The offset, if real, may result from an asymmetric dust distribution, as has been found for several of the other debris disk systems in Table 2.

The dust disk asymmetry can also be addressed by imaging the disk in scattered light. The possibility of detecting scattered light from Vega-like stars is of great interest, given the few such systems that have been detected thus far, despite extensive deep surveys (e.g., Kalas & Jewitt 1996). Using the quantities listed in Table 2, we can make a rough estimate of the relative strengths of the scattered light from each disk. If we ignore the disk inclination and assume a similar dust grain size distribution and albedo, the scattering area will be proportional to M_d, and the flux of scattered light will be roughly proportional to $M_d L_*/R_{out}^2 d^2$, where d is the distance to the star and R_{out} is the physical extent of the disk. The factor of R_{out}^2 arises in this expression because grains of a given size located farther from the star intercept less starlight. Hence, the surface brightness of the disk will be proportional to $M_d L_*/R_{out}^4$. A potentially more relevant comparison is of the contrast between the expected surface brightness from the disk and the flux from the star, which is proportional to $M_d d^2/R_{out}^4$ (e.g., Jura et al. 1998). For the disk around HD 107146, the expected surface brightness of the scattered light is half that of the disk around β Pic, and the expected contrast is 9 times larger, suggesting that the scattered light from HD 107146

might not only be quite bright but might also stand out against the glare of the star. Given the low dust temperature deduced for the HD 107146 disk (<100 K), the grains are expected to be icy with a high albedo, which favors the detection of scattered light.

Nevertheless, there are significant uncertainties associated with this estimate. Detecting reflected light will be more challenging if the disk is face-on rather than edge-on. In addition, the submillimeter measurements from which M_d is derived are primarily sensitive to large grains ($\sim$100 μm), whereas the scattered-light observations will be particularly sensitive to much smaller grain sizes. Thus, scattered light from the HD 107146 disk will be weaker if the grain size distribution is significantly skewed to large grain sizes. Conversely, scattered-light measurements can help constrain the grain size distribution of the disk (e.g., Artymowicz, Burrows, & Paresce 1989).

Future spectroscopic observations of this disk with the *Spitzer Space Telescope*, particularly in the 30–40 μm range, will place additional constraints on the grain composition and size distribution (e.g., Wolf & Hillenbrand 2003). The *Spitzer Space Telescope* is also expected to discover many more disks over a large range of ages and stellar masses, with consequent improvements for our understanding of the formation and evolution of planetary systems.

We thank Anneila Sargent for counseling during an extended review process, Hervé Aussel, Remo Tilanus, Iain Coulson, and Randy Campbell for advice on instrumentation, Eric Mamajek for helpful discussions on the age of HD 107146, and Alan Tokunaga for making the Keck time available. We acknowledge support from NSF grant AST 03-24328 (J. P. W.), the Beatrice Watson Parrent Fellowship at the University of Hawaii and NASA grant HST-HF-01152.01 (M. C. L.), and NASA contract 1224768, administered through JPL (M. R. M., J. M. C., L. A. H.). This research has made use of the SIMBAD database.

REFERENCES

Artymowicz, P., Burrows, C., & Paresce, F. 1989, ApJ, 337, 494
Augereau, J. C., Lagrange, A. M., Moillet, D., & Menard, F. 1999, A&A, 350, L51
Aumann, H. H., et al. 1984, ApJ, 278, L23
Blain, A. W., Kneib, J.-P., Ivison, R. J., & Smail, I. 1999, ApJ, 512, L87
Burrows, A., et al. 1997, ApJ, 491, 856
Dent, W. R. F., Walker, H. J., Holland, W. S., & Greaves, J. S. 2000, MNRAS, 314, 702
Fisher, R. S., Telesco, C. M., Piña, R. K., Knacke, R. F., & Wyatt, M. C. 2000, ApJ, 532, L141
Greaves, J. S., Mannings, V., & Holland, W. S. 2000, Icarus, 143, 155
Greaves, J. S., et al. 1998, ApJ, 506, L133
Hatzes, A. P., et al. 2000, ApJ, 544, L145
Holland, W. S., et al. 1998, Nature, 392, 788
———. 2003, ApJ, 582, 1141
Hollenbach, D. J., Yorke, H. W., & Johnstone, D. 2000, in Protostars and Planets IV, ed. V. Mannings, A. P. Boss, & S. S. Russell (Tucson: Univ. Arizona Press), 401
Jayawardhana, R., Fisher, S., Hartmann, L., Telesco, C., Piña, R., & Fazio, G. 1998, ApJ, 503, L79
Jones, B. F., Fischer, D., Shetrone, M., & Soderblom, D. R. 1997, AJ, 114, 352
Jura, M., Malkan, M., White, R., Telesco, C., Piña, R., & Fisher, R. S. 1998, ApJ, 505, 897
Jura, M., Zuckerman, B., Becklin, E. E., & Smith, R. C. 1993, ApJ, 418, L37
Kalas, P., & Jewitt, D. 1996, AJ, 111, 1347
Koerner, D. W., Ressler, M. E., Werner, M. W., & Backman, D. E. 1998, ApJ, 503, L83
Lagage, P. O., & Pantin, E. 1994, Nature, 369, 628
Lagrange, A.-M., Backman, D. E., & Artymowicz, P. 2000, in Protostars and Planets IV, ed. V. Mannings, A. P. Boss, & S. S. Russell (Tucson: Univ. Arizona Press), 639
Landolt, A. U. 1983, AJ, 88, 853
Liou, J.-C., & Zook, H. A. 1999, AJ, 118, 580
Marcy, G. W., Cochran, W. D., & Mayor, M. 2000, in Protostars and Planets IV, ed. V. Mannings, A. P. Boss, & S. S. Russell (Tucson: Univ. Arizona Press), 1285
Metchev, S. A., & Hillenbrand, L. A. 2004, in ASP Conf. Ser. Debris Disks and the Formation of Planets, ed. L. Caroff & D. Backman (San Francisco: ASP), in press
Metchev, S. A., Hillenbrand, L. A., & Meyer, M. R. 2004, ApJ, 600, 436
Micela, G., Sciortino, S., Harnden, F. R., Kashyap, V., Rosner, R., Prosser, C. F., Damiani, F., Stauffer, J., & Caillault, J.-P. 1999, A&A, 341, 751
Moro-Martin, A., & Malhotra, R. 2002, AJ, 124, 2305
Ozernoy, L. M., Gorkavyi, N. N., Mather, J. C., & Taidakova, T. T. 2000, ApJ, 537, L147
Pantin, E., Lagage, P. O., & Artymowicz, P. 1997, A&A, 327, 1123
Perryman, M. A. C., et al. 1997, A&A, 323, L49
Pollack, J. B., Hollenbach, D., Beckwith, S., Simonelli, D. P., Roush, T., & Fong, W. 1994, ApJ, 421, 615
Prosser, C. F., Randich, S., Stauffer, J. R., Schmitt, J. H. M. M., & Simon, T. 1996, AJ, 112, 1570
Quillen, A. C., & Thorndike, S. 2002, ApJ, 578, L149
Schneider, G., et al. 1999, ApJ, 513, L127
Silverstone, M. 2000, Ph.D. thesis, UCLA
Skrutskie, M. F., Dutkevich, D., Strom, S. E., Edwards, S., Strom, K. M., & Shure, M. A. 1990, AJ, 99, 1187
Soderblom, D. R., Jones, B. F., Balachandran, S., Stauffer, J. R., Duncan, D. K., Fedele, S. B., & Hudon, J. D. 1993, AJ, 106, 1059
Spangler, C., Sargent, A. I., Silverstone, M. D., Becklin, E. E., & Zuckerman, B. 2001, ApJ, 555, 932
Sylvester, R. J., Dunkin, S. K., & Barlow, M. J. 2001, MNRAS, 327, 133
Takeuchi, T., & Artymowicz, P. 2001, ApJ, 557, 990
Telesco, C. M., et al. 2000, ApJ, 530, 329
Tokunaga, A. T. 1988, IRTF Photometry Manual (Honolulu: Univ. Hawaii Inst. Astron.)
Voges, W., et al. 1999, A&A, 349, 389
Weinberger, A. J., et al. 1999, ApJ, 525, L53
Wichmann, R., Schmitt, J. H. M. M., & Hubrig, S., 2003, A&A, 399, 983
Wilner, D. J., Holman, M. J., Kuchner, M. J., & Ho, P. T. P. 2002, ApJ, 569, L115
Wolf, S., & Hillenbrand, L. A. 2003, ApJ, 596, 603
Wyatt, M. C., Dent, W. R. F., & Greaves, J. S. 2003, MNRAS, 342, 876
Wyatt, M. C., Dermott, S. F., Telesco, C. M., Fisher, R. S., Grogan, K., Holmes, E. K., & Piña, R. K. 1999, ApJ, 527, 918
Zuckerman, B., & Becklin, E. E. 1993, ApJ, 414, 793

Résumé — L'un des buts majeurs de l'astrophysique est de comprendre la formation du Système Solaire. Les protoétoiles de faible masse étant de jeunes soleils, leur observation est le meilleur moyen d'étudier le processus de formation du Système Solaire. Dans ma thèse, je me suis concentrée sur les premières phases d'évolution de ces protoétoiles, les Classes 0. Des molécules organiques complexes ont été découvertes dans l'une d'entre elles, IRAS16293, démontrant l'existence d'un hot corino, région où les manteaux des grains subliment. Elles ont aussi été observées dans des comètes, soulevant la question de savoir si la chimie des Classes 0 affecte la composition du disque protoplanétaire formant les comètes et autres corps planétaires. Mais il faut d'abord savoir si les hot corinos sont omniprésents dans les Classes 0, ou si IRAS16293 est une exception. Ceci était le premier but de ma thèse. L'approche consistait principalement à chercher des molécules complexes dans trois Classes 0. J'ai ainsi découvert trois hot corinos de plus. Le second but était de contraindre la taille d'émission des molécules complexes grâce à l'interférométrie, taille que j'ai trouvée comparable à celle du Système Solaire. Enfin, j'ai confronté les voies de formation possibles des molécules complexes avec les résultats de mes observations pour essayer de distinguer si ces molécules se forment en phase gazeuse ou à la surface des grains. Mes données semblent favoriser le deuxième cas. De plus, la comparaison des hot corinos et de leurs homologues massifs (qui montre que les molécules complexes sont relativement plus abondantes dans les hot corinos), soutient également la formation à la surface des grains.

Mots clés: Formation stellaire — Etoiles de faible masse — Interférométrie — Astrochimie — Molécules pré-biotiques — Raies (sub)millimétriques — Abondances moléculaires — Continuum (sub) millimétrique

---

Abstract — One of the major goals of astrophysics is to understand the formation of our Solar System. Since low-mass protostars are young suns, their observation provides the best way to investigate the formation process of the Solar System. In my thesis, I focused on the first evolutionary phases of these protostars, the Class 0 objects. Complex organic molecules have been discovered in one of them, IRAS16293, proving the existence of a hot corino, the inner region of the protostellar envelope where the icy grain mantles sublimate. They have also been observed in comets, raising the question of whether the chemistry of Class 0 objects affects the composition of the protoplanetary disk material from which comets and other planetary bodies form. But it is first necessary to determine whether hot corinos are ubiquitous in Class 0 objects, or if IRAS16293 is an exception. This was the first goal of my thesis. The general approach was to search for complex organic molecules in three Class 0 objects. I thereby discovered three more hot corinos. The second goal was to constrain the size of emission of complex molecules via interferometric observations. I found this size to be of the order of the scale of the Solar System. Finally, I confronted the possible formation pathways of complex molecules with the results of my observations to try and discriminate between gas-phase and grain-surface formation. My data seem to favor the later type. Moreover, the comparison of hot corinos and their high-mass analogs (which shows that complex molecules are relatively more abundant in hot corinos), also support grain-surface synthesis.

Keywords: Star formation — Low-mass stars — Interferometry — Astrochemistry — Prebiotic molecules — (Sub)Millimeter lines — Molecular abundances — (Sub)Millemeter continuum